EJA

European Journal of Anatomy

Volume 26 - Number 1 January 2022

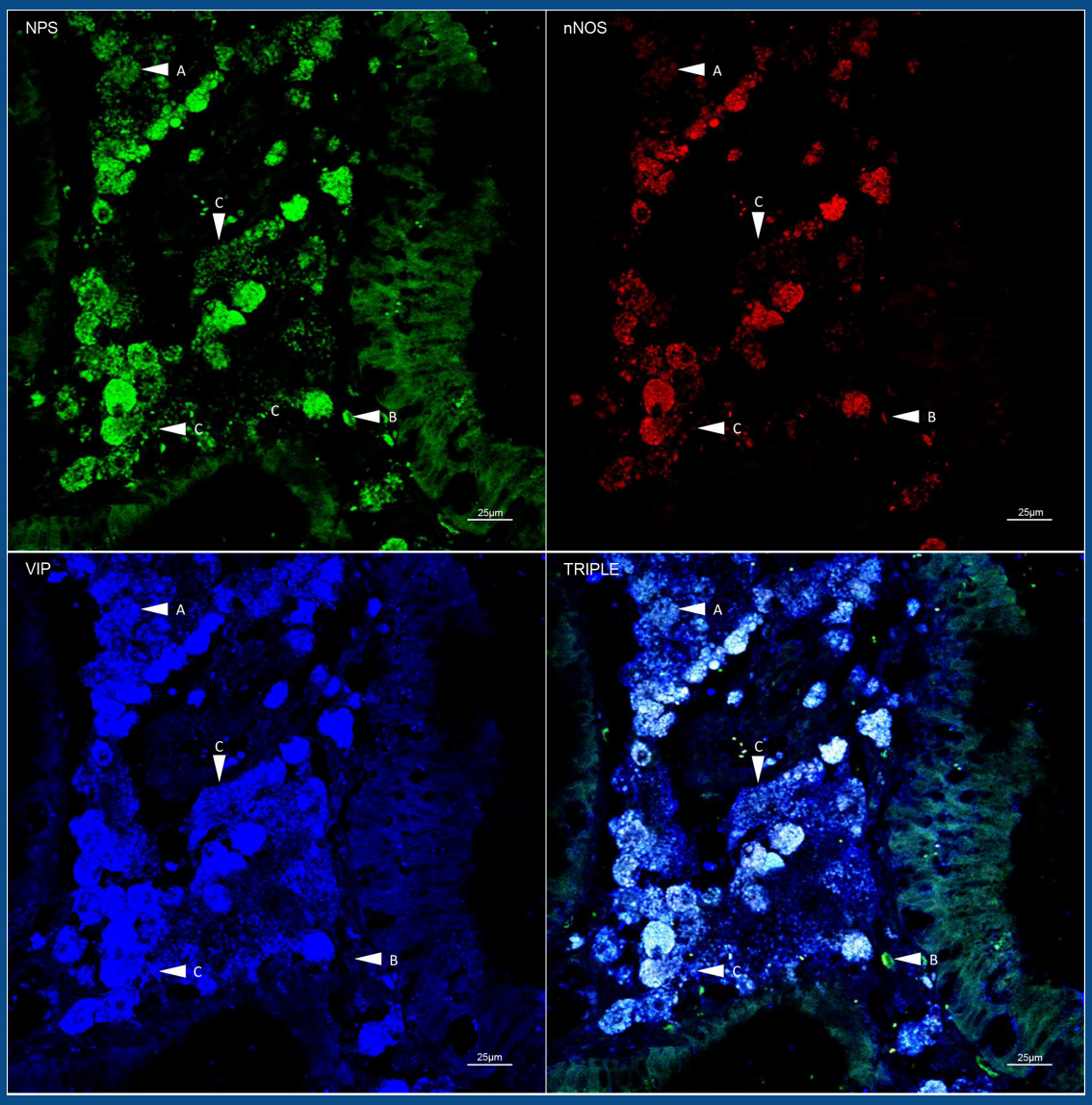

Indexed in:

CLARIVATE
- JCR:2020
- Q4 (21/23)
- I.F. J.C.I.: 0.19

DIALNET

EMBASE / Excerpta Medica

SCOPUS
- SJCR: 2020
- Q4 (31/39)
- I.F.: 0.162

Emerging Sources Citation Index

LATINDEX. Catálogo v1.0 (2002-2017)

Official Journal of the Spanish Society of Anatomy

www.eurjanat.com

EJA
European Journal of Anatomy
Volume 26 - Number 1 January 2022

CONTENTS

The coronary sinus and adjacent structures in human adult hearts: morphometrical cadaveric anatomy

Eugeniya G. Dmitrieva[1A, 2B], Anton A. Gaponov[1A], Sergey L. Khatsko[3B], Andrei A. Iakimov[1A, 2B]

[1] *Department of Human Anatomy*
[2] *Department of Medical Biochemistry and Biophysics*
[3] *Anatomical and Physiological Experimental Laboratory*
[A] *Ural State Medical University, Ekaterinburg, Russian Federation*
[B] *Ural Federal University, Ekaterinburg, Russian Federation*

SUMMARY

The aim of this study was to explore the anatomy and morphometry of the coronary sinus in hearts of adult humans, clarify position of the sinus to left atrium, left fibrous ring and adjacent arteries and describe topographic variants for adjacent anatomy of the coronary sinus in hearts of various types of coronary dominance. We studied 40 hearts weighing 200-420 g, obtained from patients who died from non-cardiac causes. We dissected 30 non-injected macroscopic specimens preserved into 4% PBS formalin to reveal and measure coronary sinus and neighboring coronary arteries. The rest 10 hearts we used for preparing histological slices from the points of the beginning of the sinus, in the middle, and near the "crux cordis". We measured large and small diameters, circumference, wall thickness of the coronary sinus, as well as explored relative position of the coronary sinus, adjacent arteries, left atrium and left fibrous ring.

The reference range of coronary sinus length was 33.76-48.4 mm. The median (Me) of the circumference of the coronary sinus increased from 13.87 mm at the beginning of the sinus to 23.99 mm at the "crux cordis". In some specimens, the cross section of the sinus looked flattened in the anteroposterior direction; in others, it appeared to be flattened basoapically. We distinguished two anatomical patterns of the coronary sinus: subepicardial and intramyocardial. The first we proposed to term myocardialless or, simply, "naked", and the second type we named muscularized. We proposed to divide the latter into partially and completely muscularized. Lack of adventitia between the myocardial sheet and tunica media of the coronary sinus allowed us to consider myocardial sleeves as an integral structure of the intramyocardial sinus wall. The wall thickness value of the coronary sinus at the point of origin, in the middle, and at the point of its turning anterosuperiorly toward the right atrium had no differences, but significantly depended on the myocardial cover and on the position of the

Corresponding author:
Andrei A. Iakimov, MD, PhD, Associate Professor. Department of Human Anatomy, Ural State Medical University, 20A Onufrieva street, Ekaterinburg, Russian Federation. Phone: +7 (904) 544 92 82. E-mail: andrei071997@gmail.com

Submitted: July 19, 2020. **Accepted:** July 9, 2021

https://doi.org/10.52083/BNUM8219

coronary sinus in the left atrioventricular sulcus. The distance from the sinus to the posterior wall of the left atrium was 0.15-7.66 mm (Me 0.91 mm); the distance to the left fibrous ring was 2.9-13.7 mm (Me 7.9 mm). We found four variants of topographic and anatomical relations of the sinus and its adjacent arteries. Commonly, arteries were located below the coronary sinus. The ranges of variability of morphometric values of the coronary sinus and neighboring structures may be considered as reference values of the anatomy of the coronary sinus in the normal human adult heart.

Key words: Gross anatomy – Heart – Cardiac veins – Coronary sinus – Coronary arteries – Left atrium

INTRODUCTION

Normal anatomy abounds of studies regarding cardiac morphology, but some structures of the heart still remain incompletely described. One structure that lacks detailed description is the coronary sinus (CS). CS is the greatest vein that drains venous blood from the most part of the cardiac walls. CS starts at the confluence point of the great cardiac vein and the oblique vein of the left atrium (LA), runs in the left posterior part of the atrioventricular groove, and opens into the right atrium. Clinically, CS is a cardiac structure, which is mainly the focus of interventional electrophysiological approaches, such as pacemaker lead placement for cardiac resynchronization therapy or radiofrequency ablation (Plass et al., 2008). Myocardial continuity from the right atrium through CS toward the posterior wall of LA may influence interatrial pacing and provide atrial fibrillation (Kasai et al., 2001; Habib et al., 2009). The coronary artery in the left posterior atrioventricular groove may cross the CS, and such anatomical pattern could represent an increased risk for compression of the artery after device implantation (Plass et al., 2008). The anatomical variants of relations of the left circumflex artery and the CS determine the safety of mitral annuloplasty as an occlusion of the artery, and its consequences might occur in some cases (Młynarski et al., 2013). Arguably, the most important clinical application is in the risk of compression of the neighboring artery, with the subsequent development of local myocardial ischemia. Being inserted into CS, a catheter may press the artery to the upper edge of the inferior wall of the left ventricle. The greatest risk of artery compression relates to the location of artery below or in front of the CS, between the CS, mitral annulus and the posterior wall of the LA (Sorgente et al., 2008). Thus, knowledge of the anatomy of the cardiac vessels and any variations are important for surgeons (Młynarski et al., 2013).

A multitude of studies, investigating various aspects of the morphology of CS, both provided new data and generated a lot of contradictions in describing of the morphology, morphometry and location of CS. Myocardial loops and sleeves over and around the CS have been described (Chauvin et al., 2000; Barcelo et al., 2004), but there is no clarity as to whether the myocardium is a layer of the sinus wall or should be considered as an element external to the CS. Morphometrical data of CS walls, with and without myocardial sleeves, are particularly lacking in literature. To our knowledge, there have been no detailed morphometric studies describing location of the CS of various patterns in relation to adjacent structures such as LA, left fibrous ring (LFR) and coronary arteries. The relationship of coronary dominance to various topographical forms of CS has not yet been evaluated. The aim of this study was to explore the anatomy and morphometry of the CS in hearts of adult humans, clarify the position of CS in relation to the left atrium, left fibrous ring and adjacent arteries, and describe topographic variants for adjacent anatomy of CS in hearts of various types of coronary dominance.

MATERIALS AND METHODS

Design of the study

The design of the study is a cross-sectional (transverse) observational, single blind (masked) study. Researchers who directly worked with the anatomical and histological material (E.G.D., A.A.G., S.L.K.) had no information about the anamnesis and personal data of the deceased persons.

Ethical Compliance

Anatomical material was obtained during the period 2017-2019 from the pathomorphological departments of the University clinics. Hearts belonged to the deceased whose bodies nobody claimed for burial, so we had no possibility for getting informed consent. The study project has been approved by the local ethics committee of the Ural State Medical University (Yekaterinburg, Russia).

We screened a total of 73 adult human hearts which have been obtained for criteria as follows. Inclusion criteria: 1) hearts obtained from cadavers that were not claimed for burial, 2) death from non-cardiac diseases, 3) normal left-sided position of the heart in the thorax, 4) heart weight 200-420 g. 17 hearts were excluded for the follow criteria: 1) abnormalities of cardiac chambers or septa (1 heart), 2) any evidence of previous cardiac surgery (2 hearts), 3) gross pathological changes of the heart or cardiac blood vessels (14 hearts). We randomly divided 56 selected hearts into two groups. The first group (n_1=30) were used for gross anatomic investigation. The other 26 hearts were screened histologically for any pathological processes in the heart wall. 16 hearts appeared to be unsuitable for normal anatomical study, mainly due to myocardial and perivascular fibrosis, or inflammatory. Thus, the group for microscopic investigation (n_2) included 10 hearts. Eventually, we studied a total of 40 hearts with the aim of this research. The specimens of both groups were immersed and preserved into 4% PBS formalin. The specimens for gross anatomy investigation were preliminary washed from blood clots. Before studying, the specimens of the first group were water-soaked for several days and dried at the air. Then we weighed the hearts used EJ-610 scales (A&D Co LTD, Japan). Following preliminary examination, epicardium and subepicardial fatty tissue were carefully removed to visualize the course of the CS, its tributaries, coronary arteries and their branches. With the caliper (precision 0.1 mm), we measured the length of the ventricular heart complex (VHC) from the apex of the heart to the origin of the aorta at the atrioventricular sulcus. The width of the VHC was evaluated as a maximum distance between the left and right pulmonary surfaces of the heart along atrioventricular sulcus (Fig. 1a, b). The term “ventricular heart complex” meant the part of the heart that included both ventricles, their lateral walls, the ventricular septum, as well as aortic and pulmonary roots. We used the specimens of the first subgroup also for exploring the relative position of the CS, its tributaries, and adjacent arteries which were found to be in the left

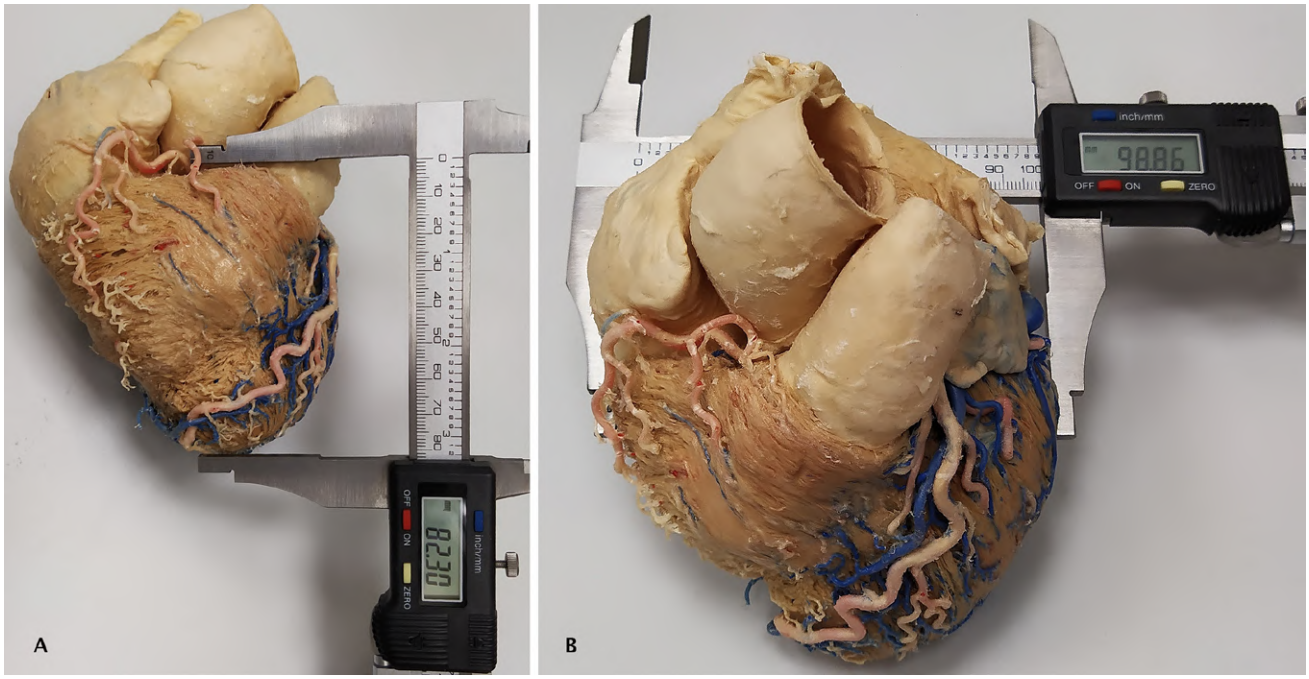

Fig. 1.- Morphometry of the length **(a)** and width **(b)** of the ventricular heart complex. Plastinated specimen used for demonstration of the method only.

posterior atrioventricular groove. We determined the type of ventricular coronary dominance (dominance of the right coronary artery, balanced circulation and dominance of the left coronary artery) based on the posterior interventricular branch belonging to the system of the left or right coronary artery (LCA, RCA).

We cut pieces of the heart for histologic study a) from the confluence of the great cardiac vein with the oblique vein of the LA (beginning of the CS), b) from the middle point of the CS length and 3) from the medial part of the CS immediately before its turning antero-superiorly towards the right atrium (Fig. 2). The fixed tissue blocks were washed with tap water, dehydrated through an ethyl alcohol series, cleared in xylene and embedded in paraffin. Sections of 5-7 μm thickness were made transverse to the axis of CS and stained with Ehrlich hematoxylin and eosin, as well as Van Gieson technique with aqueous picric acid solution and aqueous acid fuchsin solution. We have made a total of 60 histological specimens (20 from each location). Olympus CX31RTSF trinocular histological microscope (Japan) with TOUPCAM U31SPM18000KPA digital camera, and ADF Image Capture 4.7 (2019) software were used. Full histotopographic views were composed with the software option “stitching”. The thickness of the anterior, posterior, superior and inferior wall of the CS was measured in all of three places where the tissue pieces for histologic slices were taken from (the beginning, middle and medial part of the CS). We measured each wall three times: in the thinnest place, thickest place and in a section of medium thickness, and the results presented as the arithmetic mean of three measurements. In the presence of myocardial sleeves of the CS, we measured wall thickness from the CS endothelium to the inner layer of the sleeve (without myocardium), and then measured from the CS endothelium to outside surface of the sleeve (including the myocardium). In histotopograms, we measured large (maximal) and small (minimal) diameters between the opposite points of the CS endothelium. By means of the option “curve line”, we drew a line along the endothelium of the CS and the length of the line was considered as the circumference length. In order to compare the cross-sectional diameter of the CS with the data of other authors who considered the cross section of the CS to be round a priori, we applied the formula $L = 2\pi r$. For studying adjacent anatomy of the CS, we measured distances from the most external adventitial fibers of CS to those of the neighboring coronary artery, to the most external dense collagen fibers of the LFR, and

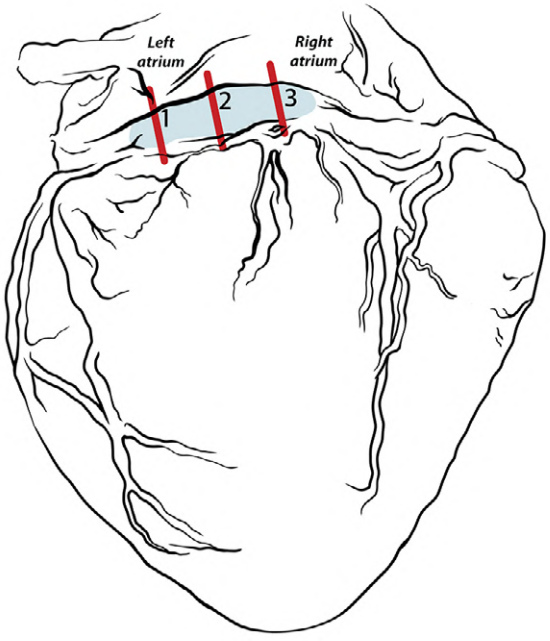

Fig. 2.- Sites for cutting heart tissue for histological sections. Red lines mark the incisions through the origin (1), middle (2) and pre-ending site (3) of the coronary sinus. *Posterior view.*

to the nearest point of the external myocardial layer of the posterior wall of the LA. Besides, we assessed the presence and number of arteries in the left part of the posterior atrioventricular groove, as well as location of the arteries relative to the CS.

We used the Statistica 13.0 (StatSoft Inc, USA) software. The distribution of values was evaluated using the Shapiro-Wilk test. If the distribution appeared to be abnormal at least in one of the compared groups, the results were presented as extreme values (minimum, maximum), percentiles (p25, p75), and medians (Me). For multiple comparisons, we used the Kruskal-Wallis H test. If the criterion revealed statistically significant differences, we proceeded to the pairwise comparison procedure with Mann-Whitney U-test. For the correlation analysis, the Spearman correlation coefficient (Rs) was used. The significance level α was 0.05 ($p<0.05$).

RESULTS

Anatomical parameters of the heart and coronary sinus

The Table 1 shows the values of the length and width of the VHC as well as the value of the heart weight. The length of the CS was found to range from 13.7 to 50 mm (Me 34.25). The length of the CS correlated with the width (Rs 0.38) and the length of the VHC (Rs 0.30). No correlation was found to be between the length of the CS and the heart weight (Rs 0.19).

We have distinguished CS for two groups: short (Me = 22.9 mm) and long (Me = 37 mm) sinuses (Fig. 3). Medians of those groups showed significant differences ($p<0.001$). Sinuses of various lengths differed in the number of tributaries: one posterior vein of the left ventricle flowed into short sinuses, and two or three of these veins opened into long ones. The middle cardiac vein was found to be the largest tributary of both short and long CS. This vein always opened into the CS shortly before its turning antero-superiorly toward the right atrium. Both diameters of CS as well as circumference of CS varied over a wide range (Table 2). The circumference of the CS was shorter ($U=23$, $p=0.045$) at its origin than at the "crux cordis", where CS turned toward the right atrium (Table 2).

In some specimens, the CS appeared to be flattened both in macroscopic specimens and histotopograms. One group of specimens showed the CS flattened in the anteroposterior direction. The large diameter of the CS was parallel to the posterior wall of the LA, and the anterior and

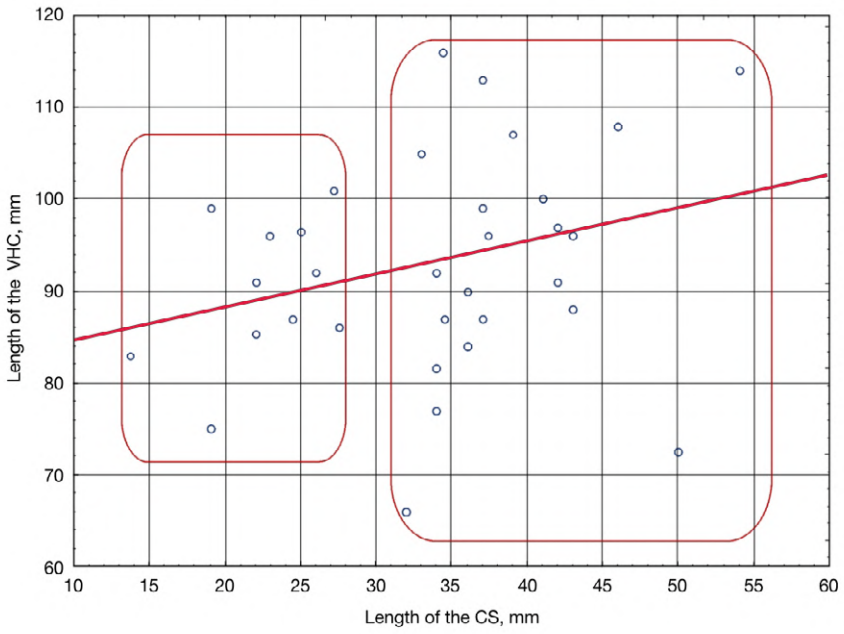

Fig. 3.- Length values of the short (left cluster) and long (right cluster) coronary sinuses (CS) and regression fit of the values on the length of the ventricular heart complex (VHC).

posterior walls were longer than the superior and inferior ones. Contrariwise, other sinuses seemed to lie in the coronary groove having been flattened in the superoinferior direction. The superior and inferior walls of those CS were the longest. The large diameter of such sinuses was perpendicular to the posterior wall of the LA (Fig. 4a, b).

When studying histotopograms, it was found that in most cases the CS partially or completely passed through the myocardial sleeves, which were formed by the myocardium of the posterior wall of the LA (Figs. 5, 6a, b). The absence of adventitia, which would separate the sleeve from the media, allowed to consider this structure, if any, as an integral part of the wall of the CS. Myocardial sleeves significantly affected the variability of the CS wall thickness (compare Fig. 7a and 7b). When comparing the CS wall thickness values, measured with sleeves, in three locations, differences in the thickness values of the anterior (H = 9.85; p = 0.007) and the posterior walls (H = 11.33; p = 0.004) were revealed. One group of specimens showed the myocardial sleeve surrounded the entire lateral half of the CS while the others found myocardium to be at the turning of the CS anterosuperiorly. The sleeve thickened the anterior wall in the middle of CS, and the posterior wall at the turning of the CS toward the right atrium. The thickness of the anterior wall increased on average 2.5 times: from 346μm at the origin of the CS to 875μm at its end (U = 6; p = 0.003). The thickness of the posterior wall throughout the CS increased 1.9 times: from 468 μm to 910 μm (U = 6; p = 0.003). Unlike anterior and posterior walls, nor superior neither inferior wall thickness changed significantly along the CS in the three locations.

We had measured four walls of the CS without sleeves in three locations, and we did not find to be significant differences in the thickness of the anterior (H = 0.44, p = 0.80), posterior (H = 0.66, p = 0.72), superior (H = 2.0, p = 0.37) and the inferior (H = 2.49, p = 0.29) walls. Also, no differences were found between the thicknesses of different walls of the CS within the same location (Fig. 7b). The absence of statistically significant differences allowed to combine these data to calculate medians and percentiles. The median wall thickness of the CS was 525 μm (p25-p75 = 364-839 μm).

Adjacent anatomy of the coronary sinus, left atrium, and the left fibrous ring

The distance from the CS to the LFR (Me = 7.9 mm) and to the myocardium of the LA posterior wall (Me = 0.91 mm) varied widely (Table 3). Heading down to the LFR, the posterior wall of the LA shifted forward moving more and more away from the CS. As a result, the distance from the CS to the LFR was greater than the distance from the CS to higher sections of the LA posterior wall. This

Table 1. Data of the heart measurements.

Parameter	Median	Extreme values
Weight of the heart, g	301	197; 419
Length of the VHC, mm	92	72; 113
Width of the VHC, mm	97	81; 121

VHC - ventricular heart complex

Table 2. Microanatomic morphometric parameters of the coronary sinus (CS), *mm.*

Place of measurement	Minimal diameter	Maximal diameter	Circumferential length
Origin of the CS	0.17 (0.02:3.80)	5.94 (3.16:7.70)	13.87* (7.46:29.63)
Middle point of the CS length	0.18 (0.02:1.53)	6.34 (3.64:15.48)	16.40 (7.63:35.00)
Turning of the CS from the av-groove anterosuperiorly toward the right atrium	0.76 (0.05:2.61)	9.13 (3.17:16.34)	23.99* (10.49:40.16)

(*) - p<.05

peculiarity of the CS with relation to LA and LFR, first of all, depended on the shape of the CS cross section and its orientation in the coronary groove (compare Fig. 4a and 4b). When comparing the distances at the beginning and in the middle of the CS, no differences were found either between the values of the distances from the CS to the LA (U = 36; p = 0.29) or between the values of the distances from the CS to the LFR (U = 42; p = 0.57). Hence, it follows that the anterior wall of the lateral half of the CS was always parallel to the posterior wall of the LA. The adjacent anatomy of the medial half of the CS, the atrial complex and the fibrous skeleton of the heart were more complicated. On its way to the opening into the right atrium, the medial part of the CS lay behind the postero-inferior portion of the posterior atrial groove, at the "crux cordis", which is the base of the inferior pyramidal space. Here, the posterior wall of the LA turned forward and inward, where it formed the left wall of that space, traditionally mistakenly referred to as the interatrial septum (Anderson et al., 2013). The posterior fragment of LFR also, following the posterior wall of the LA, was directed forward. As a result, no structures that could be attributed to the fibrous skeleton of the heart were revealed in front of the end section of the CS either by gross dissection or by studying histological specimens.

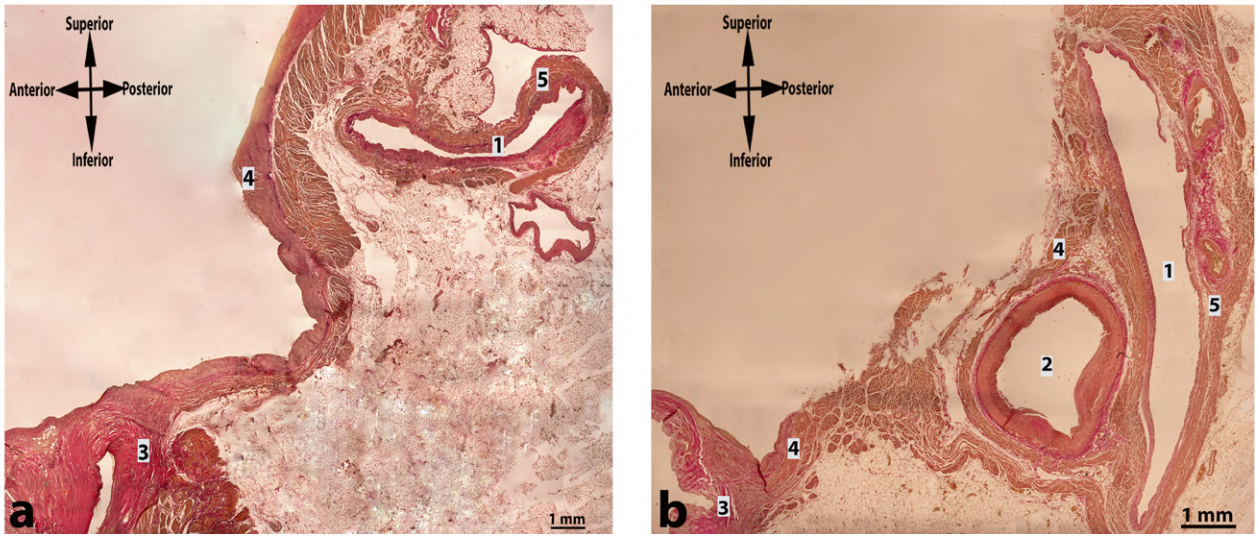

Fig. 4.- Anatomical patterns of the cross section of the coronary sinus (CS) in situ. **a –** the sinus is flattened in supero-inferior direction ("lying CS") **b –** the sinus is flattened in anteroposterior direction ("upright CS"). **1 –** coronary sinus, **2 –** coronary artery, **3 –** left fibrous ring, **4 –** posterior wall of the left atrium, **5 –** myocardial sleeve of the coronary sinus. Van Gieson, x 40.

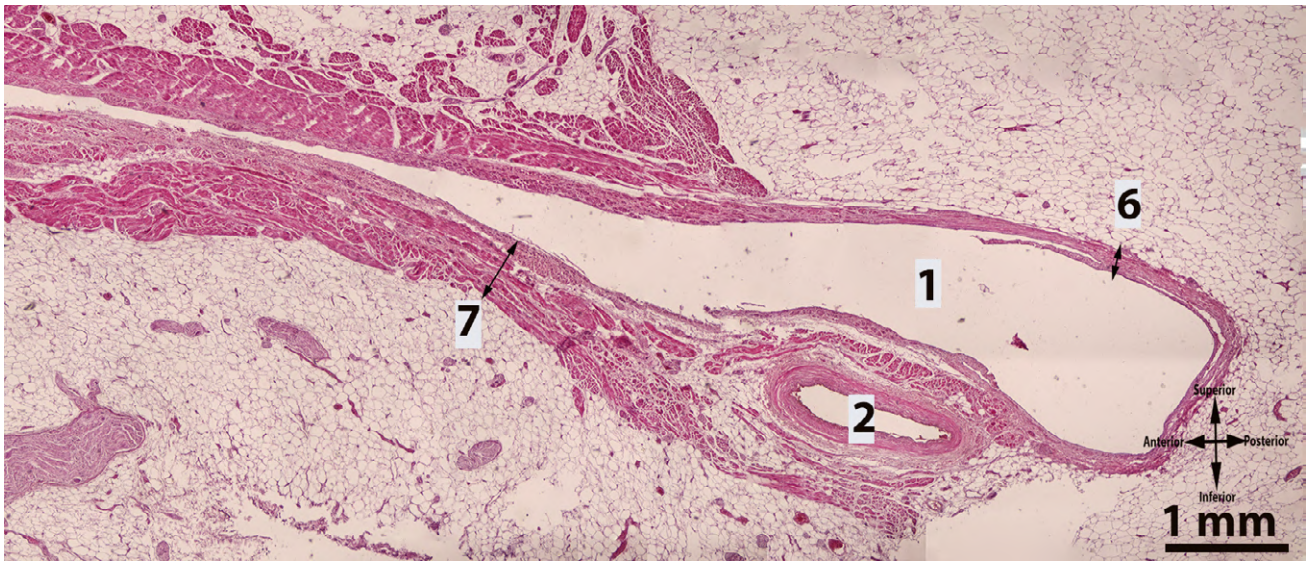

Fig. 5.- Partially muscularized coronary sinus. 1 – coronary sinus, 2 – coronary artery, 6 – coronary sinus wall without myocardial sleeve, 7 – coronary sinus wall with myocardial sleeve. Cross section. Hematoxylin & eosin staining, x 40. Scale bar = 1 mm.

Having passed behind the “crux”, the CS opened in the right atrium through its inferoposterior wall. It was noteworthy that in all cases, passing in the region of the “crux”, the CS bent forward, deviating from the atrioventricular groove by about 30-60°. As a rule, the place of bending coincided with the place where the middle cardiac vein opens into the CS.

Coronary sinus and adjacent arteries

The study of histological specimens showed that at the origin of the CS the arterial vessels closely adjoined to the CS in seven out of ten cases. In six specimens, the artery was located below (see Figs. 5, 6b), in one case the artery ran in front and was separated from the CS by 0.8 mm thick myocardial loop from the layer of the atrial myocardium (see Fig. 6a). Myocardial loops around the arteries near the CS were discovered in three hearts studied with histologic technique and in two hearts dissected and explored macroscopically. At the middle of the CS, the artery was located at the bottom of the CS in five specimens, posteriorly to the CS in three specimens, and ran in front of the CS in one heart. At the basis of the inferior pyramidal space (“crux”), arteries contiguous with the CS were found in seven specimens. In three hearts from those seven, arteries closely adjoined to the medial wall of the CS. When comparing the distances from the artery to the CS in its beginning, in the middle and near the “crux”, we have found no differences (H = 1.18; p = 0.55). The median of this distance was 0.73 mm (p25–p75 = 0.25–2,63 mm).

When studying CS and arteries on macroscopic specimens, we delineated four topographic variants for adjacent anatomy of these vessels (Fig. 8 a-d). In the first group of samples (10 of 30, 33.3%), the circumflex branch of the LCA continued into the left marginal artery and did not reach the CS, while the RCA or its circumflex branch came into contact with its anterior or inferior wall near the “crux” (Fig. 8a). In the second group (9 of 30, 30%), the left circumflex branch had the topography similar to the first group, while the terminal part of the RCA was adjacent to the CS throughout its entire length (Fig. 8b). In the third group, (4 of 30, 13.3%), the left circumflex artery was adjacent throughout the anterior or inferior wall of the CS (Fig. 8c). In the fourth group (7 of 30, 23.3%), both the left circumflex branch and the terminal part of the RCA ran closely to the anterior or inferior wall of the CS (Fig. 8d).

26 hearts showed right coronary dominance, two hearts showed left dominance, and the

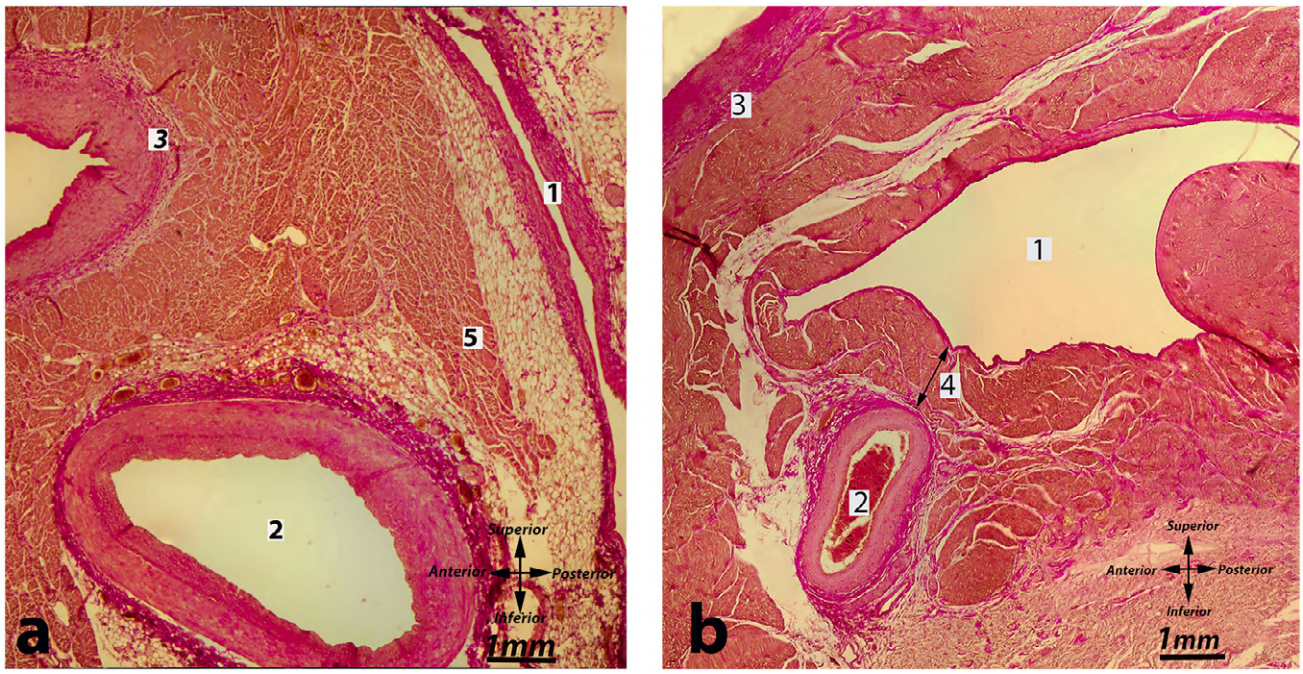

Fig. 6.- Anatomical variants of the coronary sinus (CS) wall. **a:** CS lies subepicardially and is flattened anteroposteriorly. **b:** CS lies intramyocardially. 1 – coronary sinus, 2 – coronary artery, 3 – posterior wall of the left atrium, 4 – myocardial sleeve of the CS, 5 – periarterial myocardial loop. Van Gieson staining, x 40. Scale bars = 1 mm.

remaining two hearts had balanced circulation. In the hearts with left coronary dominance and balanced circulation, the CS followed the circumflex branch of the LCA. In those with right coronary dominance, RCA was adjacent to the CS in 19 specimens (63.4%), which corresponded to the first and second variants of the adjacent anatomy of the blood vessel. In the remaining seven cases, the circumflex branch of the LCA and the RCA were adjacent to the initial and terminal parts of the CS. Thus, three variants of the vascular relationships of the CS were noted in right coronary dominance.

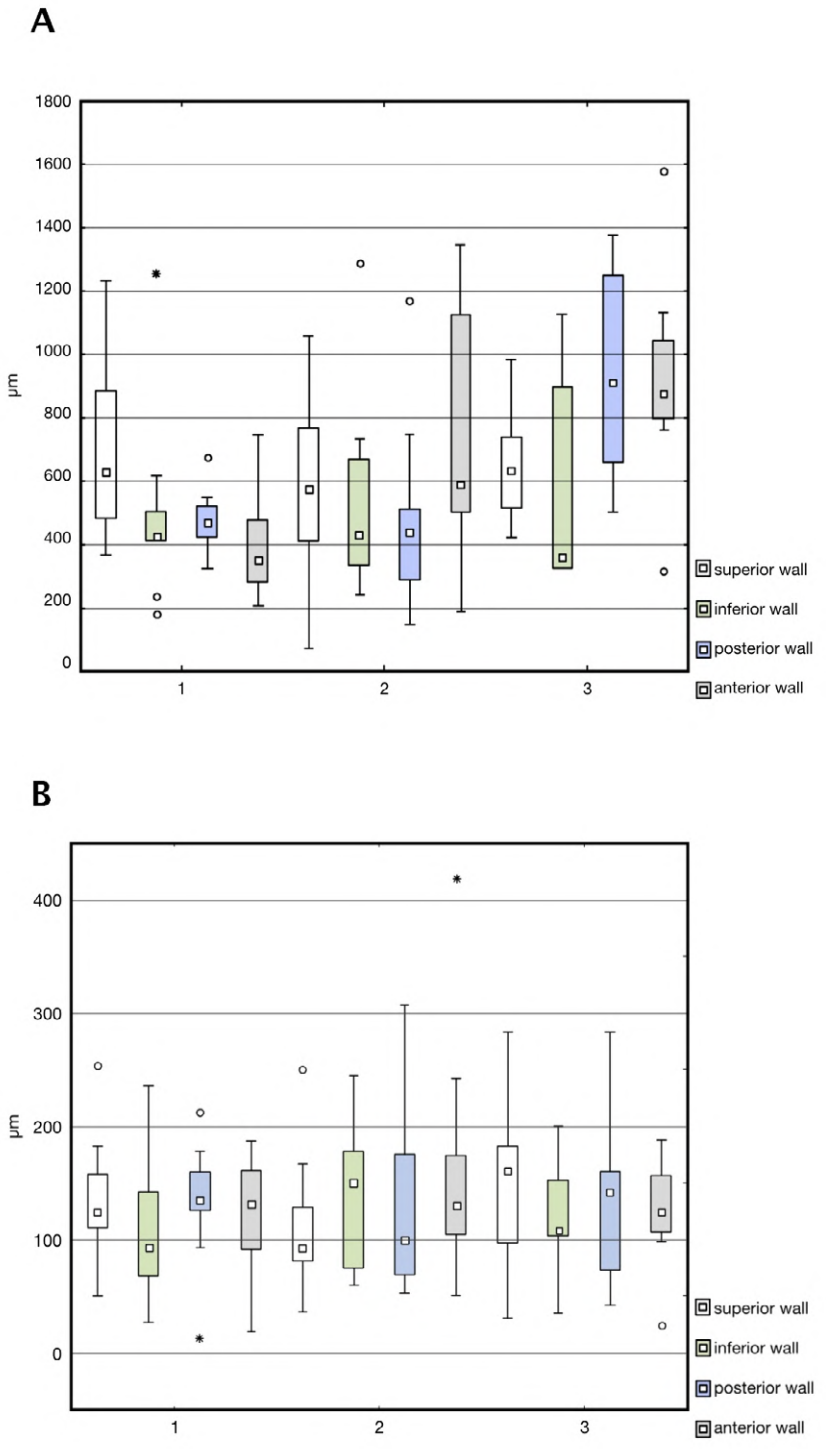

Fig. 7.- Thickness of the walls of the coronary sinus, measured with (A) and without (B) myocardial sleeve. Median. Box – p25-p75. Whiskers – extreme values.

Table 3. Distance from the coronary sinus (CS) to the left fibrous ring, and to the posterior wall of the left atrium, *mm.*

Place of measurement	Posterior wall of left atrium	Left fibrous ring
Beginning of the CS	1.57 (0.17:6.33)	18.21 (9.69:32.45)
Middle of the CS length	2.04 (0.10:7.31)	14.65 (3.51:25.37)

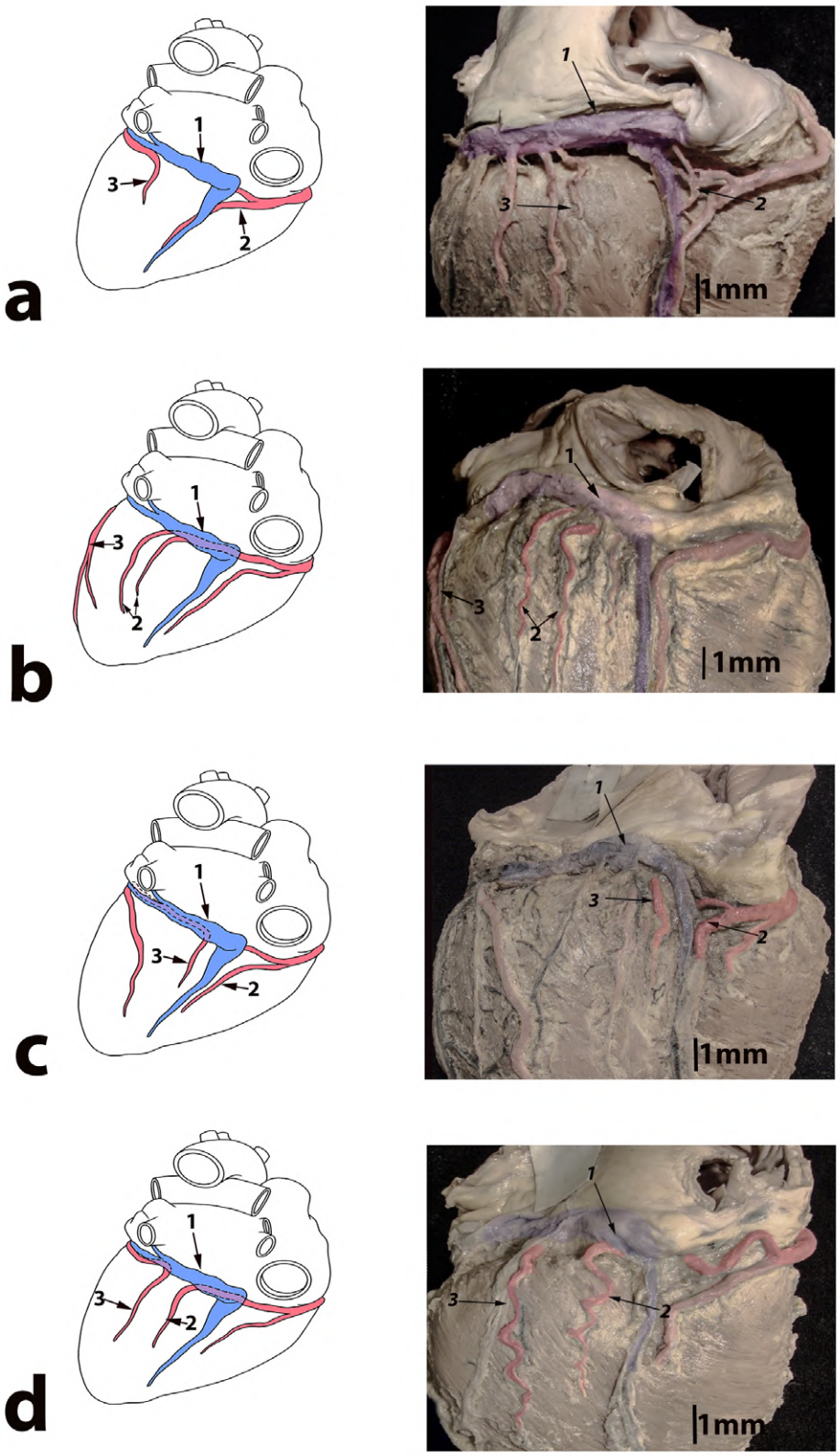

Fig. 8.- Topographical variants of the coronary sinus and coronary arteries. **a** – the 1st, **b** – the 2nd, **c** – the 3rd, **d** – 4th variant. Gross anatomical dissection of the non-injected vessels. We corrected colors of vascular images in the Photoshop photo editor. Blue showed the coronary sinus, red colored arteries from the systems of the right (2) and left (3) coronary arteries.

DISCUSSION

Morphometry of the coronary sinus

In this study, we have explored anatomy and morphometry of the CS in normal human hearts both gross- and micro-anatomically. We identified the relationship between the length of the CS and the length and width of the VHC. Macroscopically, we have measured the length of CS, outlined the range of the value and distinguished short and long sinuses. When studying the CS microscopically, we have distinguished two patterns of the CS transverse section.

Our study shows that the length of the CS has had weak correlation with both the length and width of the VHC. In black populations, Ominde et al. (2015) have measured the external length of the heart from the apex to the midpoint between the entry of left and right superior pulmonary veins and got resembling data. The researchers have also revealed that the length of CS showed a positive correlation with that of left atrioventricular groove in both males and females. According to most studies (table 4), the length of the CS varied from 20.5 to 63mm, the reference range of the average values of the CS length was 33.76– 48.4mm. Only one author has presented larger values (50-80 mm) (Fal'kovskiy, 2014). Taking into account that the author's experience in a large specialized clinical center, it can be assumed that Fal'kovskiy's data characterize the CS in the population of cardiologic patients, especially since there are reports in the literature about a longer CS in heart diseases than without them (Plass et al., 2008; Sun et al., 2012). Kagan et al. (2011) identified three groups of CS: 19.1% of specimens were long (60-82 mm), 65.4% were sinuses of medium length (30-59 mm) and 15.5% were short (16-29 mm). Sirajuddin et al. (2020) considered CS with a length of less than 20 mm as short. The sinuses with a length of over 60 mm, which were not found on our material, can be explained by cardiac pathology (Kagan et al., 2011). The differences in the lengths of the CS may be explained not only by the anatomical variability or heterogeneity of the selected groups, but also by a discrepancy for the beginning of the CS. The beginning of the CS is usually considered to be the confluence of the great cardiac vein and the oblique vein of the LA (Anderson et al., 2013; Chauvin et al., 2000; El-Maasarany et al., 2005;

Table 4. Length of the coronary sinus in human adults: reference values.

First author (year)	Methods	Number of observations	Length, mm	
			M ± SD	Min-max
El-Maasarany et al. (2005)	Cad	40	48,4±5,2	-----
Kosourov and Ivanov (2005)	Cad	200	-----	14–80
Sousa-Rodrigues et al. (2005)	Cad	26	40,3	27–54
Plass et al. (2008)	CT	26	108,9±18	------
Loukas et al. (2009)	Cad & CT	review	-----	20–50
Ballesteros et al. (2010)	Cad	68	25,96±6,34	------
Kagan et al. (2011)	CAG (v)	60	46±15,9	16–82
Sun et al. (2012)	CT	118	109±19	56–159
Manoranjitham et al. (2015)	Cad	30	54,98±12,2	------
Ominde et al. (2015)	Cad	74	39,55±5,32	------
Mehra et al. (2016)	Cad	40	35,35±4,43	20.9–39.6
Beegum et al. (2017)	Cad	50	38,22±8,6	20,5–58,8
Sharma et al. (2018)	Cad	30	33,76±5,36	26–48
Sirajuddin et al. (2019)	CT	review	-----	30–63
Our present data	Cad	30	34,25	13,7–50

Cad – cadaveric dissection, CT – in vivo computer tomography, CAG (v) – coronary angiography (venous phase).

Loukas et al., 2009; Sirajuddin et al., 2020), the orifice valve of the great cardiac vein (Vieussen's valve) is usually located there. Beegum et al. (2017) measured CS length from the opening of the oblique vein, and in its absence, from the Vieussen's valve; if the valve was not there, from the confluence of the great cardiac vein with the left marginal vein. Plass et al. (2008) and Sun et al. (2012) understood by CS the entire venous trunk located in the left atrioventricular groove, and this approach determined their data (see Table 4).

In the present study, the minimal and maximal diameters of CS varied over a wide range (Table 2). In order to compare our results with the data of other investigators, we presented mean diameter through the circumference using the formula $L = 2\pi r$ and the CS diameter varied from 2.4 to 12.8 mm (Me 5.1 mm). In the literature, the diameter of the CS varied from 5-10 mm (Fal'kovskiy, 2014) to 12 mm (Sirajuddin et al., 2020) or 16 mm (Loukas et al., 2009). In 63%, these values were in the range of 9-12 mm (Sharma et al., 2018). In a study performed on specimens injected with a hardening mass, the diameter of the CS was 8.87±1.48 mm (Sharma et al., 2018) and did not differ from the diameter of the CS, measured on macroscopic sections across the CS (9.3±5.3 mm) (El-Maasarany et al., 2005), as well as measured intravitally on computed tomograms (Plass et al., 2008). Beegum et al. (2017) found that the width of the CS was 4.25±1.4 mm at the origin, increased to 6.98±2.7 mm at the opening of the middle cardiac vein and reached maximum values (9.61±2.6 mm) in the mouth. Sousa-Rodrigues et al. (2005) have got the same results. The researchers appeared the average diameter of the CS increased from 6.34 mm to 9.28 mm from lateral to medial part. Our data of the CS' diameter calculated by means the circumference were lower than the values obtained by El-Maasarany et al. (2005) and Sharma et al. (2018), but in accordance with the results obtained by morphometry of total non-injected specimens (Sousa- Rodrigues et al., 2005, Beegum et al., 2017). With an injection, especially performed without pressure control, the CS could be expanded, and shrinkage of samples is inevitable in the preparation of histological specimens. Nevertheless, taking into account the range of variation of the diameter values, we tend to interpret the revealed differences not as the result of using various techniques, but, first of all, as individual structural features of the CS.

Some sinuses were found to be flattened apico-basally, and in cross-section they seemed to be upright in atrioventricular sulcus, and other CS appeared to lay in the sulcus (Fig. 4a, b). To our knowledge, the latter variant has not been described previously, whereas Jongbloed et al. (2005) have mentioned "upright" sinuses with the oval cross-sectional shape. A flattened sinus should not be considered an artifact for two reasons. First, all specimens were preserved under the same conditions, but some of them showed the CS flattened in superoinferior direction, and in others the CS appeared to be flattened anterior to posterior. Secondly, in microanatomical level, the microenvironment of the two variants of the flattened CS showed no signs of topographic displacement or deformity. Sinuses were uninjected and free of blood, so the obtained data on the cross-section shape of the CS we considered specific for systolic phase.

Myocardium of the coronary sinus

In this research, we found myocardial sheet within the wall of some sinuses. The striated muscle cuff of the CS was continuous with the left atrial myocardium. Lack of adventitia between the myocardial sheet and tunica media of CS allowed us to consider the sheet as a part of CS wall. Barcelo et al. (2004) delineated the external or free wall of the CS was made up of at least one thin layer of striated myocardial fibers. These fibers were usually seen to start at the level of the entrance of the oblique vein of Marshall. They enveloped the CS in its circumference as a muscular cuff or delicate net (Barcelo et al., 2004). Chauvin et al. (2000) investigated CS in ten human hearts and found a continuous cuff of cardiac striated muscle around the CS. Barcelo et al. (2004) and Chauvin et al. (2000) observed the myocardial coat of CS in every specimen. Our results showed intramyocardial CS as well as CS without myocardial sheet (compare Fig. 6a and Fig. 6b). To our mind, two microanatomical types of CS may be distinguished. The first we propose to term

myocardialless or, simply, "naked", and the second type we call muscularized. In turn, we propose to divide the latter into partially muscularized (Fig. 5) and completely muscularized (Fig. 6b). When analyzing from the origin to the turning of the CS, in our specimens the myocardium thickened the anterior and posterior wall of the CS, and did not change the thickness of the superior and inferior walls. The thickness of this muscular cuff varied between hearts (0.3 to 2.5 mm), and in 8 of the 10 hearts it was greater at the level of the ostium (1.35±0.7 mm) than at the other end (0.68±0.2 mm) (Chauvin et al., 2000). There were no muscle connections between the CS musculature and the left ventricular myocardium (Barcelo et al., 2004). Our data are in accordance with these observations.

Adjacent anatomy of the coronary sinus, left atrium and left fibrous ring

In our work, lateral half of the CS has been found to be closely to the LFR than its medial part. Mehra et al. (2016) mentioned that the CS was close to the posterior wall of the LA, but the researches did not study adjacent anatomy of those structures. It is known that the course of CS in the atrioventricular sulcus may not be strictly horizontal but may have one or two concavities due to thickening of the muscles of the left ventricular diaphragmatic wall (Fal'kovskiy, 2014). Commonly (49 of 50 cases), the CS laid in atrioventricular sulcus, which is consistent with our results, and only on one specimen the CS was 6.8 mm higher than the groove (Beegum et al., 2017). Meanwhile, in computed tomography of patients with mitral and aortic valve defects, a high position of the CS was observed in 61.4% (27 out of 44), in 17 cases out of 44 the CS ran parallel to LFR, located at the same level with the ring. Besides, the CS crossed this ring in six patients (Plass et al., 2008). The distance from the CS to LFR for mitral insufficiency and aortic malformations was 16±4.1 mm and 14.2±3.6 mm (p=0.69), respectively (Plass et al., 2008). Sorgente et al. (2008) showed that in vivo and in a large group of patients with normal ventricular function CS lied always behind the posterior wall of the LA at a significant distance from the mitral valvular annulus. In patients with normal dimension of left chambers, the researchers observed a large variability in the distance between CS and mitral annulus. When measuring the distances between CS, LFR and LA, we received a wide variance of the values too. In normal hearts, the distance from the CS to the area of attachment of the mural cusp of the mitral valve to LFR in adults usually varies from 5 to 15 mm (Anderson et al., 2013), which corresponds with our results. El-Maasarany et al. (2005) evaluated the smallest distance between the CS and LFR at the point of CS origin (9.1 mm), and the largest one at its mouth at the right atrium (11.6 mm). When comparing with these data, in our study, the median of this parameter is slightly smaller (7.9 mm), and the range of values is wider. The cross-sectional shape of the CS was considered as one of the factors determined these differences. Sinuses which appeared to be flattened in supero-inferior direction lied closely to the LFR than those flattened anteroposteriorly. The intensity of adipose tissue that separates the CS from the posterior wall of the LA can be considered as another factor. After studying the slices made along the CS, it was shown that as the CS approached the right atrium, the width of this fat compartment decreased: it was 1.47±1.29 mm in the proximal part, it was 0.95±0.74 mm in the middle of the CS, and it was 0.86±0.55 mm near the opening (Chauvin et al., 2000). However, when we compared the values of the distances from CS to LFR with these values, it was obvious that the adipose tissue of the coronary groove made an insignificant contribution to the variation of the distances. The third and, in our opinion, the main determine factor for both the gross structural variability and adjacent anatomy of the CS was its myocardial sheet.

Coronary sinus and adjacent arteries

In this work, we delineated four topographic types for the CS and adjacent arteries. These types have been described and painted earlier in Samoylova's atlas (Samoylova, 1970). When collating these types with the coronary dominance, we showed the first, second and fourth types in the hearts with the right coronary dominance. In the present study, when analyzing histotopograms

and macroscopic specimens, we found that the arteries were commonly located below the CS. Arteries adjoined CS in 78% of cadaveric studies (Ortale et al., 2001) and in 90% of patients (45 of 50) who underwent computed tomography (Plass et al., 2008). In 46% of cases, the CS came into contact with the final part of the RCA, in 32% it had a contact with the arterial branch from the LCA (Ortale et al., 2001). It is similar to our results. Mehra et al. (2016) found that in 23 of 40 hearts of human adults the circumflex artery was adjacent to the bottom of the terminal part of the great cardiac vein at the CS beginning, but the authors did not specify position of this artery in the remaining 17 hearts (Mehra et al., 2016). Sorgente et al. (2008) found circumflex artery to be located between CS and LFR in 77% of the patients, but in patients with severe mitral regurgitation CS crossed circumflex artery or marginal branch more frequently, in 97% of cases. Młynarski et al. (2013) retrospectively analyzed data for 320 patients from 64-slice computed tomography in order to evaluate the CS, circumflex artery and mitral annulus. The researchers found that the CS was usually above the mitral ring (75.9%), and the circumflex artery was commonly at the level of the posterior part of the ring. The pattern with the artery beneath the CS was also common in our specimens. We have met no hearts where coronary artery ran above the CS. Meanwhile, Kagan and Tyutyunnikova (2017) demonstrated an anatomical specimen with two arterial vessels located above the CS and ensheathing with myocardial loop (Fig. 3b in their article). At the origin of the CS, the circumflex branch of the LCA was located almost at the same frequency above (14 of 45 cases) and below CS (15 of 45 cases); in 16 cases these vessels ran parallel to each other (Plass et al., 2008). The CS crossed with the artery twice or thirds has been regarded as the most dangerous (Młynarski et al., 2013). Our research has not shown such adjacent anatomy.

In conclusion, this study has determined the normative values of the CS length, the values of the CS circumference, as well as the large and small diameters. By means of morphometry, we distinguished short and long CS. We described two variants of the cross-sectional shape of the CS. Some sinuses appeared to be flattened in the anteroposterior direction whereas the others seemed to be flattened supero-inferiorly. We distinguished two anatomical patterns of the coronary sinus: subepicardial and intramyocardial. The first we proposed to term myocardialless or, simply, “naked”, and the second type we named muscularized. We proposed to divide the latter into partially and completely muscularized. Myocardial sleeves we considered to be an integral structure of the intramyocardial CS wall. The results showed the direct dependence of the wall thickness of the CS on the majority of its myocardial cover. We delineated four topographic types for the CS and adjacent arteries, found wide range of variation in the distances from the CS to LA and LFR. The paper presented anatomical patterns of the morphometric adjacent anatomy for the CS that may expand such fundamental biomedical category as “anatomical normality” in cardiac morphology.

REFERENCES

ANDERSON RH, SPICER D, HLAVACEK AM, COOK AC, BACKER C (2013) Wilcox´s surgical anatomy of the heart, 4th ed. Cambridge University Press.

BALLESTEROS LE, RAMÍREZ LM, FORERO PL (2010) Study of the coronary sinus and its tributaries in Colombian subjects. *Rev Colomb Cardiol*, 17(1): 9-15 (in Spanish).

BEEGUM Z, RAJAN KUMAR S, RAVI KANT SH, NEELAM B (2017) Morphological and morphometric study of coronary sinus in North Indian population. *J Clin Diagn Res*, 11(9): AC15-AC19.

BARCELO A, DE LA FUENTE LM, STERTZER SH (2004) Anatomic and histologic review of the coronary sinus. *Int J Morphol*, 22(4): 331-338.

CHAUVIN M, SHAH DC, HAÏSSAGUERRE M, MARCELLIN L, BRECHENMACHER C (2000) The anatomic basis of connections between the coronary sinus musculature and the left atrium in humans. *Circulation*, 101(6): 647-653.

EL-MAASARANY S, FERRETT CG, FIRTH A, SHEPPARD M, HENEIN MY (2005) The coronary sinus conduit function: Anatomical study (relationship to adjacent structures). *Europace*, 7(5): 475-481.

FAL’KOVSKIY GE (2014) *Structure of the heart and anatomical bases of its function*. Bakulev Scientific Centre of Cardiovascular Surgery, Moscow. (in Russian).

HABIB A, LACHMAN N, CHRISTENSEN K.N, ASIRVATHAM SJ (2009) The anatomy of the coronary sinus venous system for the cardiac electrophysiologist. *Europace*, 11 (suppl 5): v15-v21.

JONGBLOED MR, LAMB HJ, BAX JJ, SCHUIJF JD, DE ROOS A, VAN DER WALL EE, SCHALIJ MJ (2005) Noninvasive visualization of the cardiac venous system using multislice computed tomography. *J Am Coll Cardiol*, 45: 749-753.

KAGAN II, BELYANIN VV, DEMIN AV (2011) Roentgenoanatomical differences of heart coronary sinus on data of intravital coronary angiography. *Morphol Newslett*, (3): 39-43 (in Russian).

KAGAN II, TYUTYUNNIKOVA NN (2017) Myocardial bridges and loops as an integral part of topography of heart coronary arteries and their branches. *Morfologiia*, 152(4): 27-31 (in Russian).

KOSOUROV AK, IVANOV VA (2005) Structural features of the heart coronary sinus in adult humans. *Morfologiia*, 128(6): 33-37 (in Russian).

LOUKAS M, BILINSKY S, BILINSKY E, EL-SEDFY A, ANDERSON RH (2009) Cardiac veins: A review of the literature. *Clin Anat*, 22(1): 129-145.

MANORANJITHAM R, SHALINI R, GOSAI SR, RAVI VC (2015) Morphological study of coronary sinus in human cadaveric hearts. *Int J Anat Res*, 3(3): 1415-1418.

MEHRA L, RAHEJA SH, AGARWAL S, RANI Y, KAUR K, TULI A (2016) Anatomical consideration and potential complications of coronary sinus catheterization. *J Clin Diagn Res*, 10(2): AC12-AC15.

MŁYNARSKI R, MŁYNARSKA A, SOSNOWSKI M (2013) Anatomical variants of left circumflex artery, coronary sinus and mitral valve can determine safety of percutaneous mitral annuloplasty. *Cardiol J*, 20(3): 235-240.

OMINDE BS, OLABU B, ONENG´O JA (2015) Length of coronary sinus in a black Kenyan population: correlation with heart length. *Anat J Africa*, 4(1): 488-495.

ORTALE JR, GABRIEL EA, IOST C, MÁRQUEZ CQ (2001) The anatomy of the coronary sinus and its tributaries. *Surg Radiol Anat*, 23: 15-21.

PLASS A, VALENTA I, GAEMPERLI O, KAUFMANN P, ALKADHI H, ZUND G, GRÜNENFELDER J, GENONI M (2008) Assessment of coronary sinus anatomy between normal and insufficient mitral valves by multi-slice computer tomography for mitral annuloplasty device implantation. *Eur J Cardiothorac Surg*, 33(4): 583-589.

SAMOYLOVA SV (1970) *Anatomy of the blood vessels of the heart*. Meditsina, Leningrad (in Russian).

SHARMA MK, SINGH J, SHARMA A, KAPOOR K, DEVINDER (2018) Morphology and morphometry of venous drainage system of heart: a retrospective cadaveric study. *Int J Cur Res Rev*, 10(10): 10-18.

SIRAJUDDIN A, CHEN MY, WHITE CS, ARAI AE (2020) Coronary venous anatomy and anomalies. *J Cardiovasc Comput Tomogr*, 14(1): 80-86.

SORGENTE A, TRUONG QA, CONCA C, SINGH JP, HOFFMANN U, FALETRA FF, KLERSY C, BHATIA R, PEDRAZZINI GB, PASOTTI E, MOCCETTI T, AURICCHIO A (2008) Influence of left atrial and ventricular volumes on the relation between mitral valve annulus and coronary sinus. *Am J Cardiol*, 102(7): 890-896.

SOUSA-RODRIGUES CF, ALCÂNTARA FS, OLAVE E (2005) Topografía y biometría del sistema venoso coronario y de sus tributaries. *Int J Morphol*, 23(2): 177-184 (in Spanish).

SUN JP, YANG XS, LAM YY, GARCIA MJ, YU CM (2012) Evaluation of coronary venous anatomy by multislice computed tomography. *World J Cardiovasc Surg*, 2(4): 91-95.

Neuropeptide S coexist with neuromodulators and presumptive neurotransmitter in the neurons of the ganglionated plexuses of the human gallbladder

Phillip Y.P. Jen[1], Fadi Al Akhrass[2], Harty Ashby[2], Noah Helphenstine[1], Nyla Gulley[1], Nicholas Bentley[1], Elizabeth Shepherd[1], Rachel Williams[1], Nathan Pray[3], Christina Al Akhrass[2], Akash Patel[1], Meera Singh[1]

[1] Department of Bio-Medical Science, University of Pikeville, Pikeville, Kentucky, United States of America

[2] Pikeville Medical Center, Pikeville, Kentucky, United States of America

[3] Kentucky College of Osteopathic Medicine, Pikeville, Kentucky, United States of America

SUMMARY

Indirect triple-labeling immunohistochemical techniques were used to identify the presence of neuropeptide serine (NPS), neuronal nitric oxide synthase (nNOS), vasoactive intestinal peptide (VIP), and neuropeptide Y (NPY) in the ganglionated plexuses of the human gallbladder.

The ganglionated plexuses examined in this report are composed of irregularly shaped neurons that inhabit the lamina propria and the muscularis propria. Most of the neurons of the lamina propria and muscularis were triple-labeled NPS, nNOS, and NPY. Moderate numbers of neurons in the lamina propria were immunopositive for NPS and nNOS (NPY negative). This same combination of immunopositivity was also seen in the muscularis. Inversely, only a few nerve cells were found to be NPS- and NPY-IR (nNOS negative) in both layers. A small population of the neurons in both layers was observed to possess singular positivity for nNOS-, NPS-, or NPY-IR.

Triple-labeled NPS-, nNOS- and VIP-IR neurons were often observed in all layers of the gallbladder but comparatively less frequently seen when compared to the previous combination. In the lamina propria, a modest number of nerve cells were NPS- and VIP-IR. A similar observation was made of the nerve cells in the muscularis. Of all the sections examined, coexisting NPS- and NOS-, or NOS- and VIP-IR neurons were not observed. Single-labeled VIP- or NPS-IR neurons were detected. However, no single labeled nNOS-IR neurons were ever seen. Our present research has demonstrated that NPS, along with many other neuropeptides and neurotransmitters, may play an essential role in the intrinsic regulation of the human gallbladder.

Corresponding author:
Dr. Phillip Jen. Armington Learning Center, 106, 147 Sycamore Street, Pikeville, Kentucky 41501, USA. Phone: (606) 218-5479. E-mail: phillipJen@upike.edu

Submitted: September 28, 2021. **Accepted:** November 5, 2021

https://doi.org/10.52083/RIGU3109

Key words: Immunohistochemistry – Triple-labeling – Gallbladder – Human – Neuropeptide S

INTRODUCTION

Named after its N-terminus serine residue, neuropeptide serine (NPS) is a 20 amino acid modulatory bioactive neuropeptide that has been identified in the brain, as well as the gastrointestinal tract of mammals (Xu et al., 2004). NPS targets neuropeptide S receptor (NPSR1, also named GPR154), a G protein-coupled to both Gs (Adenylyl cyclase) and Gq (phospholipase C), which increases cyclic adenosine monophosphate (cAMP) and intracellular calcium ions (Ca^{++}), respectively. (Reinscheid et al., 2005; Camilleri et al., 2010). In the amygdala tissue of rodents, NPS has also been reported to induce synthesis and phosphorylation of calcium/calmodulin-dependent kinase II (Grund and Neumann, 2018). The multiple mechanisms of action of NPS suggest that the NPS/NPSR system can potentially modulate various physiological and pathological functions.

In the central nervous system (CNS), NPS has been identified in nuclei of medial and lateral parabrachial nuclei, the Kölliker-Fuse nucleus, lateral lemniscus, locus coeruleus area, and the pontine central gray matter (Camillari et al., 2010; Adori et al., 2015). NPS has been found to promote both excitatory and inhibitory neurotransmitter pathways of the CNS, and reported to promote anxiolysis and panicolytic-like effects in rodents (Rizzi et al., 2008; Pulga et al., 2012), induces hyperlocomotion (Castro et al., 2009), inhibits food intake, promotes and regulate arousal, wakefulness, and anxiety in mammals, (Smith et al., 2006; Fedeli et al., 2009; Camilleri et al., 2010; Peng et al., 2010; Elphick et al., 2010; Saudi et al., 2015). Additionally, it has been reported that NPS may play an important role in the learning and memory process (Okamura et al., 2011).

In the gastrointestinal tract, studies have indicated that NPS and NPSR1 signaling triggers an increase in mRNA expression and subsequent production of various neuropeptides and hormones such as VIP, peptide YY, galanin, alpha polypeptides, tachykinin 1, neurotensin, cholecystokinin, and somatostatin. The release of these neuropeptides and hormones influences the motor and sensory disorders of the gastrointestinal tract (e.g., pain, gas, hastening of colonic transit, and urgency sensations), demonstrated by individuals suffering from irritable bowel syndrome (IBD) (Camilleri et al., 2010; Sundman et al., 2010). In a dose-dependent manner, NPS has also been reported to inhibit intestinal and colonic motility via nitric oxide neurons found in the myenteric plexus. In small concentrations, NPS increases myoelectric activity, and in greater concentrations, NPS decreases myoelectric activity. These observations are further supported, because many of the myenteric neurons demonstrated the coexistence of neuronal nitric oxide synthase (nNOS) and NPS. NPS has also been reported to increase mucosal permeability, although the mechanism of its actions is presently unknown (Saudi et al., 2015). Numerous studies have also shown that individuals suffering from inflammatory bowel disease (IBD) demonstrate multiple NPSR1 polymorphisms and higher mucosal epithelial immunoreactivity towards NPSR1 (D'Amato et al., 2007; Anedda et al., 2011).

Neuropeptide Y plays many important roles in physiological functions and is one of the most abundantly distributed neuropeptides in the CNS and the peripheral nervous system (PNS). In the CNS, NPY has been reported to trigger hypothermia, decrease energy expenditure, and possess an orexigenic effect (stimulate food intake). In the PNS, NPY has been reported to prompt mitogenesis and angiogenesis (Hwa et al., 1999; Tam et al., 2018). Studies have shown that the distribution of NPY-IR nerves and intramural ganglia, although plenteous, are rather organ and/or structural specific. For example, NPY has been reported in the adrenergic nerves, co-release with norepinephrine to trigger vasoconstriction. However, in the urinary bladder, NPY predominantly exists in cholinergic nerves and contributes to the contraction of the detrusor muscles (Iravani and Zar, 1994; Jen et al., 1995). On the other hand, in the gallbladder, NPY has been reported to have an inhibitory effect, and is involved in gallbladder smooth muscle relaxation and filling (Jansson et al., 1978; Uemura et al., 1997; Ballal Ding et al., 1991; Sand et al., 1993; De Giorgio et al., 1995; Sanford 1999; Jen et al., 2020).

Vasoactive intestinal peptide (VIP) is a 28-residue amino acid peptide first isolated in the porcine duodenum. It has been reported that VIP is widely distributed in both CNS and PNS, serving as a neurotransmitter and/or neuroendocrine releasing factor (Gonda et al., 1995; Umetsu et al., 2011; Iwasaki et al., 2019). Numerous studies have indicated that in the digestive tract, VIP in conjunction with nitric oxide (NO) triggers gastrointestinal smooth muscle relaxation, particularly at sphincters in the rat (Li and Rand, 1990). The close relationship between VIP and NO is further recognized by the reports that VIP is released from axonal terminals with enzymes of NO synthesis in the mammalian myenteric plexus (Björck et al., 1986; Gross and Pothoulakis, 2007). Research using animal models has indicated that VIP has been reported to trigger smooth muscle relaxation of the gallbladder and promote the secretion of epithelial cells (Jansson et al., 1978; Ballal and Sanford, 1999). For example, studies have indicated that VIP increases chloride (Cl^-) secretion in the porcine gallbladder (Yadav et al., 2011; Iwasaki et al., 2019). It has also been reported that VIP induces a potent relaxation of both basal and cholecystokinin-stimulated motor activity (Di Giorgio et al., 1995). It is interesting to note that the release of VIP is a local phenomenon isolated to the intrinsic neurons of the gallbladder wall in response to activation of adrenergic fibers in the vagus nerves (Dahlstrand et al., 1989, Balemba et al., 2004).

Although a few reports have targeted NPS in the gastrointestinal tract, no studies focused on their existence in the ganglionated plexuses in the human gallbladder. In the present study, triple-labeling immunohistochemistry was used to examine the coexistence of neuropeptide S (NPS) with neuronal nitric oxide synthase (nNOS), neuropeptide Y (NPY), and vasoactive intestinal peptide (VIP) in ganglionated plexus of the adult human gallbladder.

MATERIALS AND METHODS

Twenty-three (23) human gallbladder samples were obtained through contractual agreement and partnership with Pikeville Medical Center (PMC). These gallbladder samples were removed using laparoscopic cholecystectomy from patients suffering from gallbladder dysfunction with biliary colic as sequelae of their conditions. Of the 23 cases enrolled in the study, gallstones were found surgically in only 14 (60.87%) gallbladders, while all the cases (100%) demonstrated direct impact of the stones on the gallbladder walls, although no stones were found within the lumen of the organ. In these acalculus cholecystitis cases, the stones have most likely migrated into the cystic and common bile ducts.

Only seven gallbladders were collected from male patients; the remaining 16 samples were gathered from female patients. All patients were presented with chronic biliary colic (right upper quadrant abdominal pain and nausea exacerbated by fatty food). None of our patients had acute/chronic cholecystitis or pancreatitis. Most patients (91.3%) had normal white blood cell counts. All patients with available laboratory data had normal kidney function, platelet counts, thyroid function tests, lipid profile, and liver enzymes. All patients responded to surgical management with no postsurgical complications and remarkable clinical abdominal relief (Table 1).

General Morphology

The gallbladder lies in the gallbladder fossa on the visceral surface of the liver; this shallow fossa lies at the junction of the right and left liver (segments IVB and V). The hollow, pear-shaped gallbladder can hold up to 30-50 mL of bile, measuring 7–10 cm long and 4 cm in diameter. The gallbladder has three parts: the fundus, the body, and the neck. Peritoneum completely surrounds the fundus of the gallbladder and binds its body and neck to the liver. The hepatic surface of the gallbladder attaches to the liver by connective tissue of the fibrous capsule of the liver. The wall of the gallbladder consists of a mucosa composed of simple columnar epithelium and lamina propria, a thin muscularis with bundles of muscle fibers oriented in several directions, and an external adventitia or serosa. The lining epithelial cells of the gallbladder have prominent mitochondria, microvilli, and large intercellular spaces, all indicative of cells actively transporting water, for the purpose of concentrating bile. The

mechanism for which includes the activity of sodium cation (Na^+) pumps in the basolateral membranes followed by passive movement of water from the bile.

General histological examination of the 23 tissue samples reveals histopathological changes in the gallbladder mucosa due to cholelithiasis. In all the samples examined, the simple columnar cells of the epithelium have flattened to low columnar or high cuboidal-shaped cells, while many of these epithelial cells appear to possess vacuolated cytoplasm. The epithelium appears to be discontinuous and disrupted, while the apical microvilli, which are prevalent in healthy tissues, were not readily seen and/or simply missing in the tissues examined.

Immunohistochemistry

Tissues were obtained with the written consent of the patient. Specimens from each patient were collected and preserved using Zamboni's fixative solution. Samples were washed with phosphate-buffered saline (PBS) three times in ten-minute intervals using the New Brunswick Scientific Excella E24 Incubator Shaker. After washing, tissues were embedded onto the cryostat embedding mount using Sakura TissueTek® OCT Compound and Bright Cryospray 134A and flash frozen. Embedded tissues were then cut into 10 µm thick sections using the Bright OTF 5000 Cryostat and applied to gel-coated microscope slides. One from every ten prepared slides was selected for hematoxylin and eosin (H&E) staining. Once stained, the slides were dried, cleared, and mounted using Permount mounting medium. Remaining slides were stored at -80° C in a Helmer Scientific ultra-low temperature freezer.

Each H&E-stained slide was examined to reveal the location of the ganglionated plexus with intramural nerve cells. Once suitable sections were found, slides were then selected for triple labeling. Slides were washed for 10 minutes in blocking buffer (.05% Sodium Azide, 1.5% goat serum, 0.1% Triton, and 98.35% PBS). A barrier was drawn around tissue on slides with the Vector Laboratories® ImmEDGE™ Hydrophobic Barrier Pen to prevent antibodies from displacing during incubation.

Triple-labeling immunohistochemistry was performed on approximately twenty (20) selec-

Table 1. Patients' characteristics.

Patients' characteristics	Average findings
Age (years)	37.8 (23-59)
Sex, female	16/23 (69.57 %)
White blood cell count (NR: 3-11.3 k/µl)	8.7 (4.4-13.2)
Hemoglobin (NR: 10-16 g/dL)	14.08 (11.8-17.1)
Platelets (NR: 122-454 k/µl)	246.75 (180-285)
Alanine aminotransferase (ALT) (NR: 12-78 U/L)	29.33 (16-62)
Aspartate aminotransferase (AST) (NR: 15-37 U/L)	23.92 (11-93)
Total bilirubin (NR: 0.0-1.0 mg/dL)	0.67 (0.3-1.6)
Alkaline phosphatase (NR: 45-117 U/L)	75.71 (60-104)
Creatinine (NR: 0.6-1.3 mg/dL)	0.73 (0.5-0.9)
Albumin (NR: 3.4-5.0 g/dL)	3.73 (3.1-4.1)
Glucose (NR: 70-110 mg/dL)	111.83 (63-281)
Total cholesterol (NR: <200 mg/dL)	157.67 (118-165)
High-density lipoproteins (HDL) (NR: 40-59 mg/dL)	51.5 (42-55)
Low-density lipoprotein (LDL) (NR: <100 mg/dL)	85.97 (46-99)
Triglyceride (NR: <150 mg/dL)	98.33 (81-126)
Thyroid-stimulating hormone (TSH) (NR: 0.4-4.0 mIU/L)	3.64 (1.39-5.13))

NR: normal range.

ted sections from each of the 23 gallbladder specimens. The first group of staining involved antibodies targeting NPS, nNOS, and NPY. The second batch of tissues utilized antibodies targeting NPS, nNOS, and VIP.

Neuropeptide S (NPS rabbit; 1:1000; ABCAM) polyclonal antibodies were applied to the slide and left to incubate overnight (Table 2). All incubations were performed in a dark incubation slide box stored at 4oC in a Fisher Scientific general-purpose refrigerator. After incubation, slides were washed three times in ten-minute intervals with PBS using the Excella E24 incubator shaker. The secondary antibody, Biotinylated Anti-Rabbit IgG (H+L) (1:200; Vector Laboratories), was applied and left for four hours. Slides were again washed three times in ten-minute intervals with PBS. Fluorescein Avidin DCS (Cell Sorter Grade) (1:300; Vector Laboratories) was applied and left for three hours. The combination of the Anti-Rabbit IgG and the Fluorescein Avidin DCS was used to visualize the NPS polyclonal antibodies. Slides were again washed three times in ten-minute intervals with PBS using the Excella E24 incubator shaker.

Neuronal Nitric Oxide Synthase (nNOS) monoclonal antibody (mouse; 1:400, Thermo Fisher Scientific) was administered to slides and left overnight for incubation. Slides were again washed three times in ten-minute intervals with PBS (Table 2). To visualize the nNOS primary antibody, Donkey Anti-Mouse IgG Alexa Fluor 594 (1:200; Abcam) was applied and left to incubate for six hours. Slides were again washed three times in ten-minute intervals with PBS.

NPY polyclonal antibody (sheep; 1:500; Millipore) was applied to slides and left overnight to incubate (Table 2). Slides were again washed three times in ten-minute intervals with PBS. To visualize the NPY, slides were incubated with Donkey Anti-Sheep IgG H&L Alexa Fluor 405 (1:200; Abcam) for six hours. Slides were washed three times in ten-minute intervals with PBS before being mounted with a 50/50 PBS and glycerol solution.

VIP polyclonal antibodies (sheep; 1:1000; Abcam), was used on 23 cryo-sectioned gallbladder samples. These sections, affixed to gel-coated slides, were incubated overnight (Table 2). These slides were again washed three times in ten-minute intervals with PBS. Once the excess primary antibodies are removed, the slides were incubated with Donkey Anti-Sheep IgG H&L Alexa Fluor 405 (1:200; Abcam) for six hours. Again, the slides were washed three times in ten-minute intervals with PBS before being mounted with a 50/50 PBS and glycerol solution.

Analysis

Slides were viewed under an Olympus FluoView-FV1000 confocal microscope to determine the co-localization of the neurotransmitters (enzymes involved in neurotransmitter formation) and neuropeptides. All photomicrographs were taken at 400x magnification with 1x to 2x zoom.

RESULTS

The ganglionated plexuses of the human gallbladder examined in this report are composed of irregularly shaped neurons located in the lamina propria and the muscularis propria (ganglionated plexus of the adventitia are not reported). In our present study, immunofluorescent triple-labeling techniques were used to demonstrate the existence of neuropeptides and enzymes involved in neurotransmitter formation in the neurons of the ganglionated plexuses. Two sets of triple-labeling were used on the sectioned tissues: ① NPS, nNOS, and NPY; ② NPS, nNOS, and VIP.

Table 2. The characteristics of primary antibodies used in this experiment.

Antigen	Host Species	Antibody Type	Dilution	Supplier
NPS	Rabbit	Polyclonal	1:1000	ABCAM
NPY	Sheep	Polyclonal	1:500	Millipore
nNOS	Mouse	Monoclonal	1:400	Thermo Fisher
VIP	Sheep	Polyclonal	1:1000	ABCAM

Triple-labeled NPS, nNOS, and NPY were detected in most of the neurons examined in the ganglionated plexus of the lamina propria. To a much lesser extent, few neurons possess NPS- and nNOS-immunoreactivity, while remaining NPY-negative. In all the sections examined, only a few cells were seen to possess NPS and NPY without the presence of nNOS. Interestingly, a small population of the single positive nNOS-IR neurons was observed, while only a few cells exhibited singular immunopositivity for NPS or NPY (Fig. 1).

Similarly, in triple-labeled NPS, nNOS, NPY was frequently seen in the neurons of the muscularis. Few cells were observed to exhibit NPS-, nNOS-immunoreactivity without NPY-IR. Likewise, NPS-, NPY-IR neurons were rarely seen without demonstrating nNOS immunoreactivity. A moderate number of neurons showed nNOS and NPY immunoreactivity without being triple labeled with NPS. Like the cells of the ganglionated plexus in the lamina propria, single labeled nNOS and NPY were rarely observed in the smooth muscle layer, although neurons exhibiting single immunopositivity for NPS appear to be slightly more numerous (Fig. 2, Table 3).

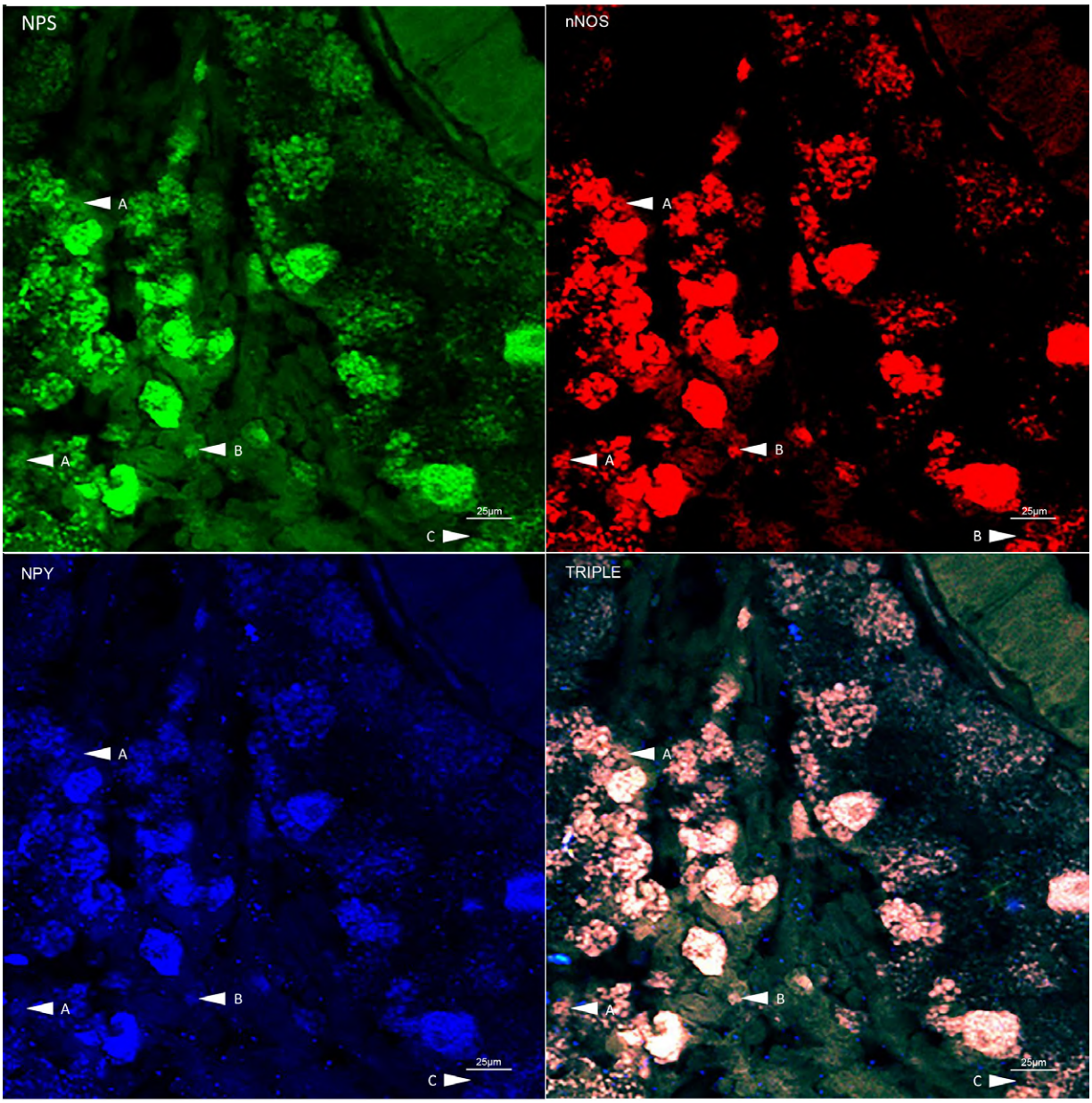

Fig. 1.- Photomicrographs showing that most of the neurons are triple-labeled with NPS, nNOS, and NPY in the gallbladder lamina propria. Arrow A indicates few cells that are singularly positive for nNOS, while arrows B and C show NPS and nNOS double-labeled neurons without NPY-IR. Scale bars = 25 µm.

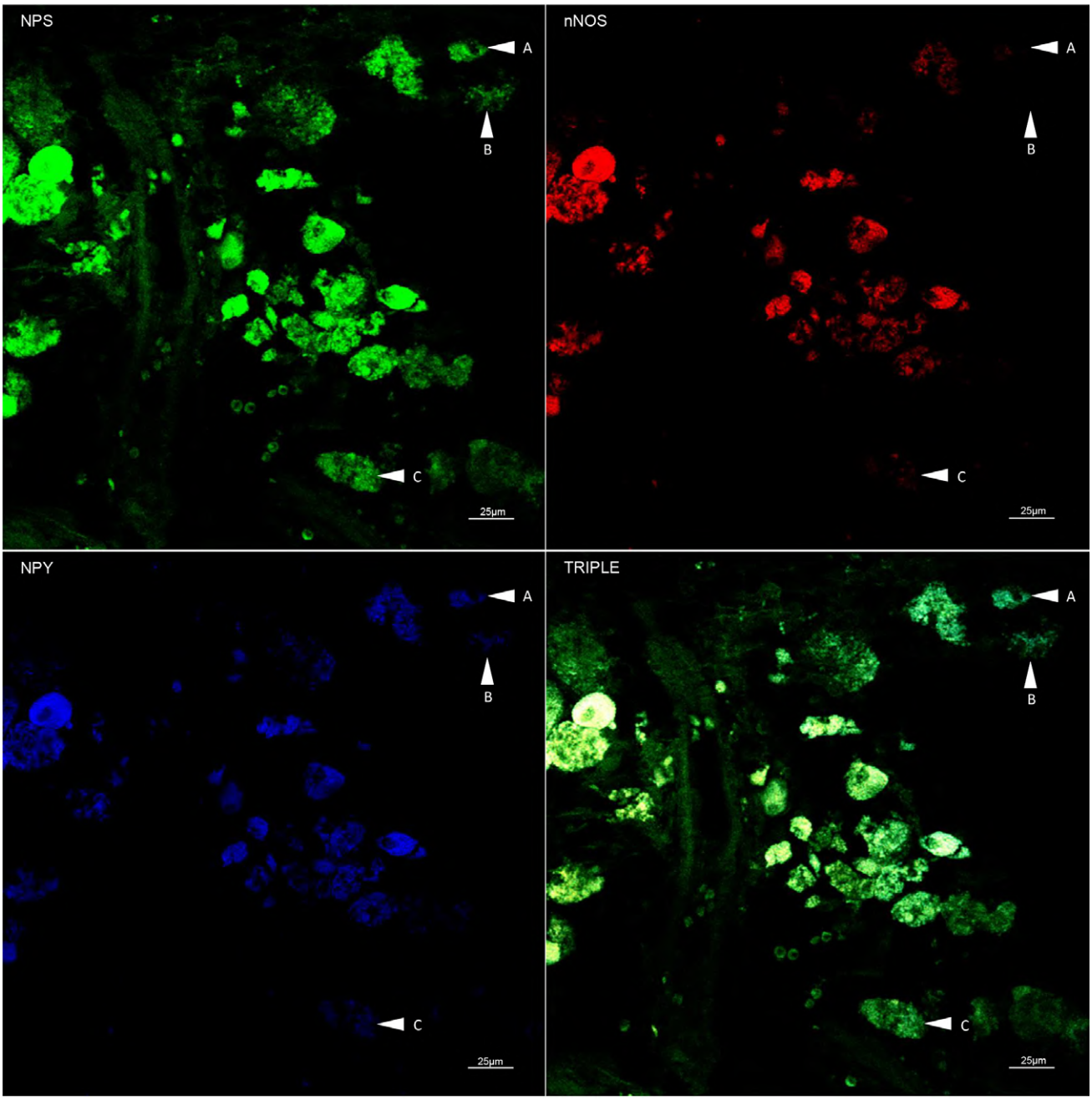

Fig. 2.- Triple-labeled ganglion found in the muscularis propria of the human gallbladder demonstrating immunopositivity for NPS, nNOS, and NPY. Most of the neurons were immunopositive for all three antibodies, a small subpopulation of nNOS-immunonegative neurons, while exhibiting NPS- and NPY-IR (arrow A). Arrow B demonstrates a nNOS-immunonegative neuron while being NPS- and weakly NPY-IR. Arrow C shows the first of the three cells that display single positivity for NPS without coexisting with NPY or nNOS. Scale bars = 25 µm.

Table 3. Estimated distribution of NPS, nNOS, and NPY in the ganglionated plexus of the human gallbladder. Please note: the estimate for individual existence or dual existence (single- or double-labeled) of neuropeptides and neurotransmitter synthesizing enzyme are part of the triple-labeled experiments. No single- or double-labeling experiments were performed.

Antibodies Used	Lamina Propria	Muscularis
NPS NOS NPY	+++	+++
NPS NOS	++	+
NPS NPY	+	+
NOS NPY	++	++
NPS	+	++
NOS	++	+
NPY	+	+

+++ High, ++ Moderate, + Sparse, - Not observed

Triple-labeled NPS, nNOS, and VIP were frequently detected in the neurons of the ganglionated plexus in the lamina propria. Only a moderate number of NPS- and VIP-IR neurons was seen without nNOS-immunoreactivity. Of all the sections examined, coexisting NPS- and NOS-, or NOS- and VIP-IR neurons were not observed. Nonetheless, moderate numbers of single labeled VIP- or NPS-IR neurons were detected. Of all the sections investigated, no single labeled nNOS-IR neurons were seen (Fig. 3). Likewise, in the ganglionated plexus of the muscularis, triple-labeled NPS, nNOS, and VIP were frequently detected. Only a small population of these neurons exhibited only NPS- and VIP-immunoreactivity, while no coexisting NPS- and NOS-IR combinations were ever seen. Modest numbers of neurons showed singularly VIP-immunoreactivity, while few neurons were single labeled NPS. Like the lamina propria, no single labeled nNOS-IR neurons were detected (Fig. 4, Table 4).

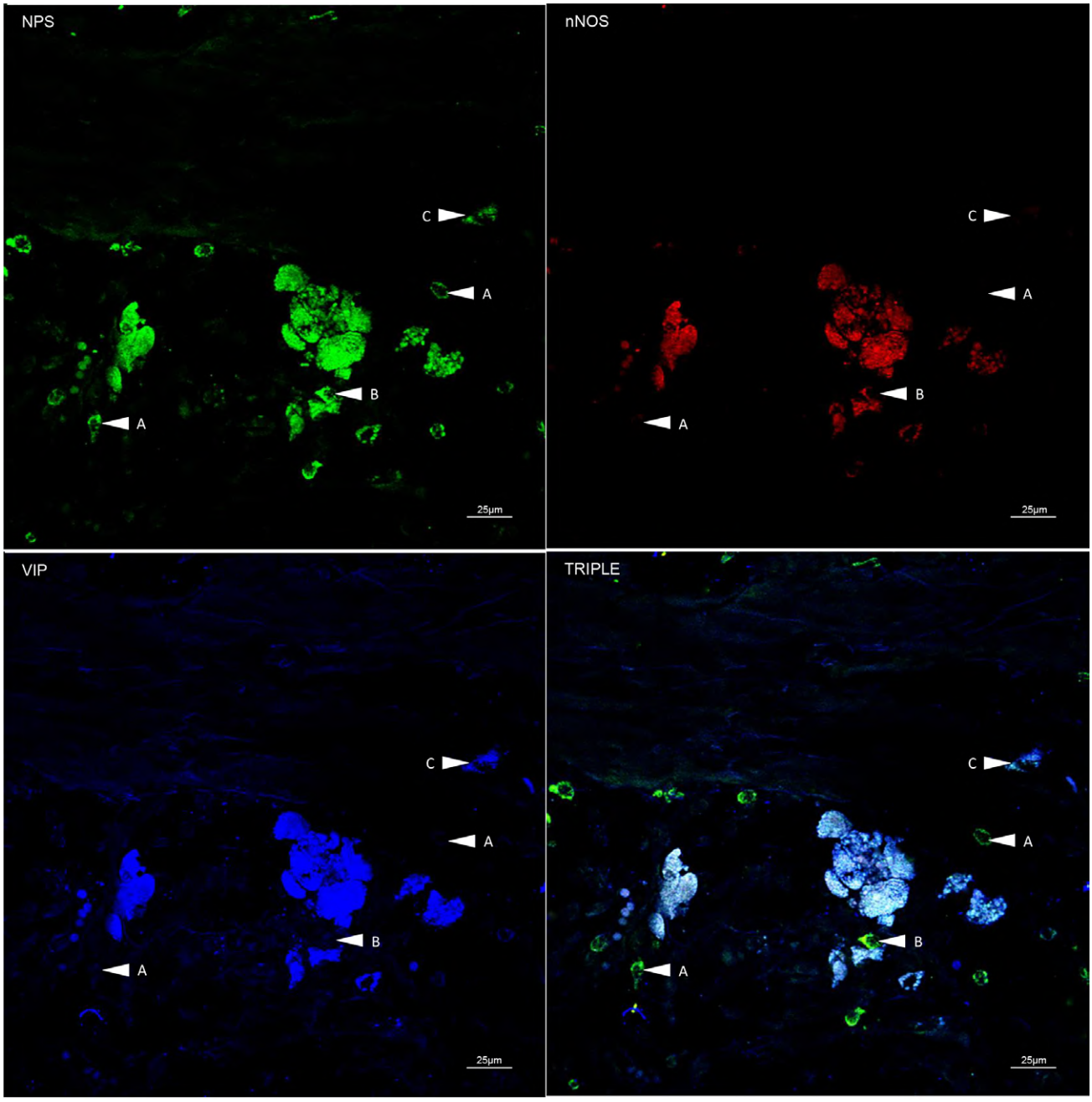

Fig. 3.- Most of the intrinsic neurons of the muscularis propria in the human gallbladder are immunopositive for all 3 antibodies, NPS, nNOS, and VIP. Arrow A shows neurons singularly positive for NPS. Arrow B indicates a neuron that is double positive for NPS and nNOS. Arrow C indicates a single cell that is immunopositive for NPS and NPY. Scale bars = 25 µm.

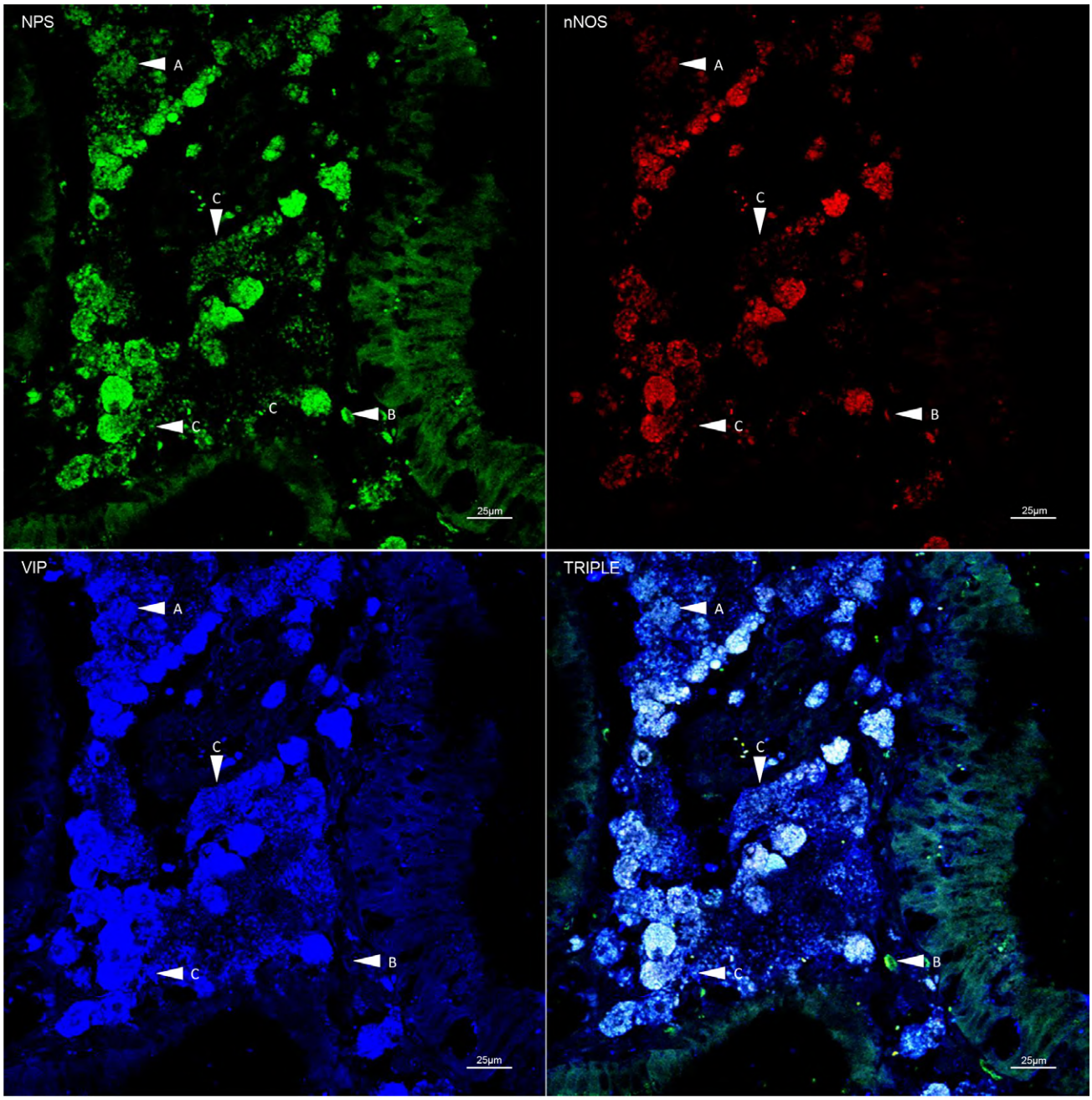

Fig. 4.- Majority of the intrinsic neurons of the gallbladder lamina propria demonstrates triple-labeled NPS, nNOS, and VIP. Arrow A demonstrates a small cluster of 3 neurons that are nNOS immunonegative, while displaying weak NPS- and strong VIP-immunoreactivity. Arrow B show a single immunopositivity for NPS and Arrow C displays single immunopositivity for VIP. It is interesting to note that nerve fibers immunopositive for NPS, nNOS and VIP are observed to loosely enfold the neurons. Scale bars = 25 µm.

Table 4. Estimated distribution of NPS, nNOS, and VIP in the ganglionated plexus of the human gallbladder.

Antibodies Used	Lamina Propria	Muscularis
NPS, NOS, VIP	+++	+++
NPS, NOS	-	-
NPS, VIP	++	+
NOS, VIP	-	-
VIP	++	++
NOS	-	-
NPS	++	+

+++ High, ++ Moderate, + Sparse, - Not observed

DISCUSSION

The human gallbladder's epithelial tissues and smooth musculature are regulated by ganglionated plexuses, which are derived from the same precursor neural crest cells that developed into the submucosal and myenteric plexus of the enteric nervous system (ENS). Although they originated from the same embryonic tissue, the ganglionated plexuses of the gallbladder display neurochemical and physiological characteristics that are distinct from the intrinsic nervous system of the gastrointestinal tract (Mawe et al., 1997).

The distribution of the intramural ganglionated plexus of the human gallbladder comprises an array of neurons distributed in the lamina propria and the muscularis. Although existing in two populations, the isolation of the individual ganglionated plexus appeared to be relatively random. Numerous researches have shown that the actions of these neurons are modulated by autonomic nerves (e.g., extrinsic sympathetic, parasympathetic), extrinsic sensory, duodenal neural inputs, bile acid influencing GPBAR1 and subsequent secretion of GLP-1 and -2 by L-cells (Li et al., 2011; Duboc et al., 2014; Yusta et al., 2017; Shapiro et al., 2018), and prompted by circulating hormones such as CCK, secretin, gastrin, FGF15/19, and pancreatic polypeptide (Mawe, 1998, 2000; Otsuki, 2000; Rehfeld, 2017; Kliewer and Mangelsdorf, 2016).

In our earlier study, we have reported that all the intrinsic neurons examined in the human gallbladder were observed to be ChAT-immunoreactive (-IR), although a spectrum of immunopositivity ranging from strong to weak was seen (Jen et al., 2020). In addition, these presumptive cholinergic neurons were seen coexisting with various neurochemicals. As reported previously, a large portion of these presumptive cholinergic neurons were also immunopositive for neuromedin U-8 (NMU-8), nNOS, and NPY.

In the present report, our analysis of triple-labeled sections demonstrated two distinct populations of intrinsic neurons. Clusters of neurons are found within the subepithelial layers; some appear to be closely aligned with the simple columnar cells of the epithelia. Scattered clusters of neurons are randomly detected within the smooth muscle layer of the gallbladder. Individual neurons were also detected; however, their appearance may be due to the orientation of the tissue and the particular tissue section examined. Interestingly, the distribution patterns of NPS, NPY, and nNOS appeared in most of the neurons examined. When combining the result of our previous studies with the present, we can safely assume that many of these triple-labeled neurons are also immunopositive for NMU-8. Unfortunately, the monoclonal antiserum for NMU-8 was not available at this present time, and their coexistence will have to be elucidated on a future date.

It is believed that the neurochemical contents of gallbladder neurons are to provide fine control to the organ's motility and regulate epithelial function (Peterson et al., 1993; De Giorgio et al., 1995; Talmage et al., 1996; Uemura et al., 1997). For example, muscularis propria nNOS-IR neurons are believed to play an inhibitory role in the musculature of the gallbladder, which, in turn, affects the filling process of the gallbladder. It has been reported that this filling process involves receptive relaxation, a neurologically controlled process, which increases the volume without causing a rise in intraluminal pressure (Cole et al., 1987; Mourelle et al., 1993). On the other hand, the nNOS-IR subepithelial neurons positive may be involved in the regulation of epithelial secretions (Uemura et al., 1997; Parkman et al., 1997; Greaves et al., 1998) and/or epithelial absorption of water and electrolytes that concentrates bile containing hydrophobic bile salts (Cole et al., 1987; Behar, 2013).

According to Saudi and collaborators, NPS closely associates with nNOS in the gastrointestinal tract by inhibiting small intestine and colonic motility in patients suffering from IBD. Their study demonstrated that the effect of NPS was abolished with pretreatment of L-NAME (NG-Nitro- l-Arginine Methyl Ester), a non-selective nitric oxide synthase (NOS) inhibitor; thereby concluding NPS action through NO in the myenteric plexus. Additional pretreatment of Tetrodotoxin (TTX), a sodium channel blocker,

also inhibited NPS-induced effects, suggesting NPS acts through neurological mechanisms (Saudi et al., 2015). To correlate with our present research, the high frequency that NPS and nNOS coexist among the neurons of the ganglionated plexus in the muscularis may suggest a similar mechanism of action in the human gallbladder, although additional research is required to confirm this observation.

Saudi and collaborators also showed that intravenous injection of NPS caused an increase in intestinal mucosal permeability in rodents through an unknown mechanism(s). A subsequent study demonstrated that intravenously treated rats displayed a reduction of basal duodenal bicarbonate secretion and net fluid secretion from the mucosa (Saudi and Sjöblom, 2017). Our results have found that NPS-IR neurons were frequently observed in the ganglionated plexus of the lamina propria. This observation may indicate a similar means could be utilized in controlling the functions of the gallbladder epithelium. Nonetheless, the exact mechanism that NPS functions in the lamina propria will require further elucidation.

Studies have shown that NPY and VIP frequently coexist in the ganglionated plexus of the human gallbladder and, through animal models, have also indicated that both of these neuropeptides are inhibitory and are involved in gallbladder smooth muscle relaxation and filling (De Giorgio et al., 1995; Jansson et al., 1978; Uemura et al., 1997; Ballal and Sanford 1999). In the lamina propria, VIP promotes the secretion of epithelial cells (Jansson et al., 1978; Ballal and Sanford, 1999), and their functions in controlling the epithelial cells are well documented. However, the function of NPY within the ganglionated plexus of the lamina propria will require additional examination.

Our results have shown that triple-labeled NPS, nNOS, and NPY were frequently observed among the neurons of the ganglionated plexus, while similar but less frequent observations were made for NPS, nNOS, and VIP. These triple existence of neuropeptide and presumptive neurotransmitter shown in the present study, coupled with the various neuropeptides and presumptive neurotransmitter markers examined in the previous study (e.g., NMU-8 and ChAT), indicates the versatile nature of the intramural neurons and their innervational effects on the smooth musculature and epithelial secretions (Jen et al., 2020).

In conclusion, our present study has shown that the intrinsic innervational patterns of the human gallbladder are complex, containing several immunohistochemically distinct populations based on their content of neurotransmitter-synthesizing enzyme and neuropeptides. Our report, in conjunction with the previous publication, has demonstrated that numerous inhibitory and excitatory neuropeptides and neurotransmitter (presumptive) coexist with excitatory cholinergic neurons of the gallbladder ganglionated plexus. Additional investigations will be required to illuminate the exact mechanism of their cooperative functions in the human gallbladder (Jen et al., 2020).

ACKNOWLEDGEMENTS

This research was partially funded by Colonel Lee B. Ledford Scholarship from Appalachian College Association. The authors would like to express our most profound appreciation to Meghna and Sanya Bhatnager for their laboratory assistance. Dr. Oma Morgan and Dr. Jennifer Dugan for their expert guidance. We would also like to thank Pikeville Medical Center, Mr. Erich E. Blackburn, and the University of Pikeville for their inter-institutional cooperation. Finally, the authors sincerely thank those who donated their bodies to science so that anatomical research and teaching could be performed. Results from such research can potentially increase scientific knowledge and can improve patient care. Therefore, these donors and their families deserve our highest respect.

REFERENCES

ADORI C, BARDE S, BOGDANOVIC N, UHLÉN, REINSCHEID RR, KOVACS GG, HÖKFELT (2015) Neuropeptide S- and Neuropeptide S receptor-expressing neuron populations in the human pons. *Front Neuroanat*, 9: 126.

ANEDDA F, ZUCCHELLI M, SCHEPIS D, HELLQUIST A, CORRADO L, D'ALFONSO S, ACHOUR A, MCINERNEY G, BERTORELLO A, LÖDAL M, BEFRITS R, BJÖRK J, BRESSO F, TÖKVIST L, HALFVARSON J, KERE J, D'ALMATO M (2011) Multiple polymorphisms affect expression and function of the neuropeptide S receptor (NPSR1). *PLoS One*, 6: e29523.

BALEMBIA OB, SALTER MJ, MAWE GM (2004) Innervation of the extrahepatic biliary tract. *Anat Rec A Discov Mol Cell Evol Biol*, 280(1): 836-847.

BALLAL MAG, SANFORD PA (1999) The physiology of the biliary tree. Motility of the gallbladder - Part 1. *Saudi J Gastroenterol*, 5(3): 93-105.

BEHAR J (2013) Physiology and pathophysiology of the biliary tract: the gallbladder and sphincter of Oddi – a review (2013) *ISRN Physiology*, 1-15.

BJÖRCK S, FAHRENKRUG J, JIVEGÅRD, SVANVIK (1986) Release of immunoreactive vasoactive intestinal peptide (VIP) from the gallbladder in response to vagal stimulation. *Acta Physiol Scand*, 128(4): 639-642.

CAMILLERI M, CARLSON P, ZINSMEISTER AR, MCKINZIE S, BUSCIGLIO I, BURTON D, ZUCCHELLI M, D'AMATO M (2010) Neuropeptide S receptor induces neuropeptide expression and associates with intermediate phenotypes of functional gastrointestinal disorders. *Gastroenterology*, 138: 98-107.

CASTRO AA, MORETTI, CASAGRANDE TS, MARTINELLO C, PETRONIHO F, STECKERT AV, GUERRINI R, CALO G, DAL PIZZOL F, QUEVEDO J, GAVIOLI EC (2009) Neuropeptide S produces hyperlocomotion and prevents oxidative stress damage in the mouse brain: A comparative study with amphetamine and diazepam. *Pharmacol Biochem Behav***,** 91(4): 636-642.

COLE MJ, SCOTT RB, SHAFFER EA (1987) Gallbladder pressure, compliance and hysteresis during cyclic volume change. *Can J Physiol Pharmacol*, 65: 2124-2130.

DAHLSTRAND C, DAHLSTRÖM, AHLMAN H (1989) Adrenergic and VIP-ergic relaxatory mechanisms of the feline extrahepatic biliary tree. *J Autonom Nerv Syst*, 26(2): 97-106.

D'AMATO M, BRUCE S, BRESSO F, ZUCCHELLI M, EZER S, PULKKNEN V, LINDGREN C, ASTEGIANO M, RIZZETTE M, GIOCHETTI P, REIGLER G, SOSTEGNI R, DAPERNO M, D'ALFONSO S, MOMIGLIANO-RICHIARDI P, TÖKVIST L, PUOLAKKAINEN P, LAPPALAINEN M, PAAVOLA-SAKKI P, HALME L, FÄKKILÄ M, TURUNEN U, KONTULA K, LÖFBERG R, PETTERSSON S, KERE J (2007) Neuropeptide S receptor 1 gene polymorphism is associated with susceptibility to inflammatory bowel disease. *Gastroenterology*, 133: 808-817.

DE GIORGIO R, ZITTEL TT, PARODI JE, BECKER JM, BRUNICARDI FC, GO VLW, BRECHA NC, STERNINI C (1995) Peptide immunoreactivities in the ganglionated plexuses and nerve fibers innervating the human gallbladder. *J Auton Nerv Syst*, 51(1): 37-47.

DING WG, FUJIMURA M, MORI A, TOOYAMA I, KIMURA H (1991) Light and electron microscopy of neuropeptide Y-containing nerves in human liver, gallbladder, and pancreas. *Gastroenterology*, 101: 1054-1059.

DUBOC H, TACHÉ Y, HOFMANN AF (2014) The bile acid TGR5 membrane receptor: From basic research to clinical application. *Dig Liver Dis*, 46(4): 302-312.

ELPHICK MR (2010) NG peptides: a novel family of neurophysin-associated neuropeptides. *Gene*, 458: 20-26.

FEDELI A, BRACONI S, ECONOMIDOU D, CANNELLA N, KALLUPI M, GUERRINI R, CALO G, CIFANI C, MASSI M, CICCOCIOPPO R (2009) The paraventricular nucleus of the hypothalamus is a neuroanatomical substrate for the inhibition of palatable food intake by neuropeptide S. *Eur J Neurosci*, 30: 1594-1602.

GONDA T, AKIYOSHI H, ICHIHARA K (1995) Hyperplastic innervation of vasoactive intestinal peptide in human gallbladder with cholelithiasis. *Histol Histopathol*, 10: 669-672.

GREAVES R, MILLER J, O'DONNELL L, MCLEAN A, FARTHING MJ (1998) Effect of the nitric oxide donor, glyceryl trinitrate, on human gall bladder motility. *Gut*, 42(3): 410-413.

GROSS KJ, POTHOULAKIS NC (2007) Role of neuropeptides in inflammatory Bowel disease. *Inflamm Bowel Dis*, 13(7): 918-932.

GRUND T, NEUMANN ID (2018) Brain neuropeptide S: via GPCR activation to a powerful neuromodulator of socio-emotional behaviors. *Cell Tissue Res*, 375(1): 123-132.

HWA JJ, WITTEN MB, WILLIAMS P, GHIBAUDI L, GAO J, SALISBURY BG, MULLINS D, HAMUD F, STRADER CD, PARKER EM (1999) Activation of the NPY Y5 receptor regulates both feeding and energy expenditure. *Am J Physiol Regul Integr Comp Physiol*, 277(5): R1428- R143.

IRAVANI MM, ZAR MA (1994) Neuropeptide Y in rat detrusor and its effect on nerve-mediated and acetylcholine-evoked contractions. *Br J Pharmacol*, 113(1): 95-102.

IWASAKI M, AKIBA Y, KAUNITZ JD (2019) Recent advances in vasoactive intestinal peptide physiology and pathophysiology: focus on the gastrointestinal system. *F1000 Faculty Rev*, 8: 1629.

JANSSON R, STEEN G, SVANVIK J (1978) Effect of intravenous vasoactive intestinal peptide (VIP) on gallbladder function in the cat. *Gastroenterology*, 75: 47-50.

JEN PYP, DIXON JS, GOSLING JA (1995) Immunohistochemical localization of neuromarkers and neuropeptides in human fetal and neonatal urinary bladder. *Brit J Urol*, 75: 230-235.

JEN PYP, AL AKHRASS F, PRAY N, DAY C, DE OLIVEIRA LM, ASHBY H, ABDALLAH L, COLLINS K, BOSSE-JOSEPH D (2020) Immunohistochemical characteristics of ganglionated plexuses in the human gallbladder. *Eur J Anat*, 24(1): 17-29.

KLIEWER SA, MANGELSDORF DJ (2015) Bile acids as hormones: The FXR-FGF15/19 pathway. *Dig Dis*, 33(3): 327-331.

LI T, HOLMSTROM SR, KIR S, UMETANI K, SCHMIDT DR, KLIEWER SA, MANGELSDORF DJ (2011) The G protein-coupled bile acid receptor, TGR5, stimulates gallbladder filling. *Mol Endocrinol*, 25(6): 1066-1071.

LI CG, RAND MJ (1990) Nitric oxide and vasoactive intestinal polypeptide mediate non-adrenergic, non-cholinergic inhibitory transmission to smooth muscle of the rat gastric fundus. *Eur J Pharmacol*, 191: 303-309.

MAWE GM (1998) Nerves and hormones interact to control gallbladder function. *News Physiol Sci*, 13(2): 84-90.

MAWE G, TALMAGE EK, CORNBROOKS EB, GOKIN A, ZHANG L, JENNINGS L (1997) Innervation of the gallbladder: Structure, neurochemical coding, and physiological properties of guinea pig gallbladder ganglia. *Microsc Res Tech*, 39: 1-13.

MOURELLE M, GUARNER F, MOLERO X, MONCADA S, MALAGELADA J-R (1993) Regulation of gall bladder motility by the arginine nitric oxide pathway in guinea pigs. *Gut*, 34: 911-915.

OKAMURA N, GARAU C, DUNANGDAO DM, CLARK SD, JÜNGLING K, PAPE HC, REINSCHEID RK (2011) Neuropeptide S enhances memory during the consolidation phase and interacts with noradrenergic systems in the brain. *Neuropsychopharmacology*, 36: 744-752.

OTSUKI M (2000) Pathophysiological role of cholecystokinin in humans. *J Gastroenterol Hepatol*, 15: 71-83.

PARKMAN HP, PAGANO AP, MARTIN JS, RYAN JP (1997) Electric field stimulation-induced guinea pig gallbladder contractions: role of calcium channels in acetylcholine release. *Digest Dis Sci*, 42(9): 1919-1925.

PETERSEN KU, GOERGEN R, HÖFKEN F, MACHEREY HJ, SPRAKTIES G (1993) Electrogenic bicarbonate secretion in gallbladder: induction by barium via neuronal, possibly VIP-ergic pathways. *Naunyn Schmiedebergs Arch Pharmacol*, 348(5): 526-535.

PENG YL, HAN RW, CHANG M, ZHANG L, ZHANG RS, LI W, HAN Y-F, WANG R (2010) Central neuropeptide S inhibits food intake in mice through activation of neuropeptide S receptor. *Peptides*, 31: 2259-2263.

PILGA A, RUZZA C, RIZZI A, GUERRINI R, CALO G (2012) Anxiolytic- and panicolytic-like effects of Neuropeptide S in the mouse elevated T-maze. *Eur J Neurosci*, 36: 3531-3537.

REHFELD JF (2017) Cholecystokinin - from local gut hormone to ubiquitous messenger. *Front Endocrinol*, 8(47): 1-8.

REINSCHEID RK, XU YL, OKAMURA N, ZENG J, CHUNG S, PAI R, WANG Z, CIVELLI O (2005) Pharmacological characterization of human and murine neuropeptide S receptor variants. *J Pharmacol Exp Ther*, 315: 1338-1345.

RIZZI A, VERGURA R, MARZOLA G, RUZZA C, GUERRINI R, SALVADORI S, REGOLI D, CALO G (2008) Neuropeptide S is a stimulatory anxiolytic agent: a behavioural study in mice. *Br J Pharmacol*, 154(2): 471-479.

SAND J, TAINIO H, NORDBACK I (1993) Neuropeptides in pig sphincter of Oddi, bile duct, gallbladder, and duodenum. *Digest Dis Sci*, 38(4): 694-700.

SAUDI WSW, HALIM A, RUDHOLM-FELDREICH T, GILLBERG L, ROSENQVIST E, TENGHOLM A, SUNDBOM M, KARLBOM U, NÄSLUND E, WEBB D-L, SJÖBLOM M, HELLSTRÖM XPM (2015) Neuropeptide S inhibits gastrointestinal motility and increases mucosal permeability through nitric oxide. *Am J Physiol Gastrointest Liver Physiol,* 309: G625-G634.

SAUDI WSW, SJÖBLOM M (2017) Neuropeptide S reduces duodenal bicarbonate secretion and ethanol-induced increases in duodenal motility in rats. *PLoS ONE*, 12: e0175312.

SHAPIRO H, KOLODZIEJCZYK AA, HALSTUCH D, ELINAV E (2018) Bile acids in glucose metabolism in health and disease. *J Exp Med*, 215(2): 383-396.

SMITH KL, PATTERSON M, DHILLO WS, PATEL SR, SEMJONOUS NM, GARDINER JV, GHATEI MA, BLOOM SR (2006) Neuropeptide S stimulates the hypothalamic-pituitary-adrenal axis and inhibits food intake. *Endocrinology*, 147: 3510-3518.

SUNDMAN L, SAARIALHO-KERE U, VENDELIN J, LINDFORS K, ASSADI G, KAUKINEN K, WESTERHOLM-ORMIO M, SAVILAHTI E, MÄKI M, ALENIUS H, D'AMATO M, PILKKINEN V, KERE J, SAAVALAINEN P (2010) Neuropeptide S receptor 1 expression in the intestine and skin--putative role in peptide hormone secretion. *Neurogastroenterol Motil*, 22(1): 79-87.

TALMAGE EK, POULIOT WA, SCHEMANN M, MAWE GM (1996) Structure and chemical coding of human, canine and opossum gallbladder ganglia. *Cell Tissue Res*, 284(2): 289-302.

TAN CMJ, GREEN P, TAPOULAL N, LEWANDOWSKI AJ, LEESON P, HERRING N (2018) The role of neuropeptide Y in cardiovascular health and disease. *Front Physiol*, 9: 1281.

UEMURA S, POMPOLO S, FURNESS JB, HARDY KJ (1997) Nitric oxide synthase in neurons of the human gallbladder and its colocalization with neuropeptides. *J Gastroenterol Hepatol*, 12(3): 257-265.

UMETSU Y, TENNO T, GODA N, MASAHIRO S, IKEGAMI T, HIROAKI H (2011) Structural difference of vasoactive intestinal peptide in two distinct membrane-mimicking environments. *Biochim Biophys Acta,* 1814(5): 724-730.

XU Y-L, REINSCHEID RK, HUITRON-RESENDIZ S, CLARK SD, WANG Z, LIN SH, BRUCHER FA, ZENG J, LY NK, HENRIKSEN SJ, DE LECEA L, CIVELLI O (2004) Neuropeptide S: a neuropeptide promoting arousal and anxiolytic-like effects. *Neuron*, 43(4): 487-497.

YADAV M, HUANG MC, GOETXL EJ (2011) VPAC1 (vasoactive intestinal peptide (VIP) receptor type 1) G protein-coupled receptor mediation of VIP enhancement of murine experimental colitis. *Cell Immunol*, 267(2): 124-132.

YUSTA B, MATTHEWS D, FLOCK GB, USSHER JR, LAVOIE B, MAWE GM DRUCKER DJ (2017) Glucagon-like peptide-2 promotes gallbladder refilling via a TGR5-independent, GLP-2R-dependent pathway. *Mol Metab*, 6: 503-511.

Surgical anatomy of the tricuspid valve

Santiago Cubas[1,2], Alejandra Garretano[1], Ricardo Robaina[1], Leticia Vázquez[1], Andrés Berke[1], Víctor Dayan[2]

[1] *Department of Anatomy, Faculty of Medicine, University of the Republic of Uruguay, Montevideo, Uruguay*
[2] *Cardiovascular Center, University of the Republic of Uruguay, Montevideo, Uruguay*

SUMMARY

The aim of this study was to describe danger zones between the tricuspid annulus and the coronary sinus and the right coronary artery to be considered during tricuspid interventions. Methods: 36 hearts from human adult corpses were dissected. We measured the distance between the middle third of the anterosuperior (anterior) leaflet to the right coronary artery (distance 1), between the anteroinferior (anteroposterior) commissure to right coronary artery (distance 2), between the middle third of inferior (posterior) leaflet to the right coronary artery (distance 3) and between the middle third of the septal leaflet to the ostium of the coronary sinus (distance 4). Distances were compared between right and left coronary dominance. The average distance 1 was 5,32 mm (1-11 mm), the average distance 2 was 3,07 mm (0.5-7 mm), the average distance 3 was 2,53 mm (0.5-12 mm) and the average distance 4 was 8,55 mm (2.5-18 mm). 31 hearts had right dominance, 4 left dominance and 1 co-dominance. We found no statistically significant differences between hearts with right and left coronary dominance at either D1 (5.26±2.55 mm vs 6.62±1.80 mm, p=0.213) or D4 (8.55±3.91 mm vs 11.62±0.95 mm, p=0.064). The highest risk area of injuring the right coronary artery corresponds to the posterior annulus (distance 3). In hearts with left dominance, tricuspid annulus has a safer distance to the right coronary artery and coronary sinus and therefore may present a lower risk of right coronary artery involvement in surgical and endovascular procedures.

Key words: Right coronary artery – Tricuspid valve – Tricuspid annulus

INTRODUCTION

Tricuspid valve (TV) disease can manifest itself in three different ways: stenosis, primary regurgitation, and secondary regurgitation. Secondary tricuspid regurgitation (TR) is the most common tricuspid valve pathology and responds to right ventricular (RV) dysfunction due to pressure or volume overload in the presence of structurally normal leaflets. Most patients who undergo tricuspid valve interventions do so during concomitant mitral or aortic valve intervention or myocardial revascularization (Vassileva et al., 2012).

Although surgery is still the gold standard for tricuspid valve corrective treatment, interventional procedures are currently under way for high-risk patients (Campelo et al., 2017). In order to avoid the inherent risks in these procedures, it is essential to achieve a comprehensive knowledge of the anatomy of the valve and its main relationships, mainly with the

Corresponding author:
Santiago Cubas. Luis B. Cavia 2883/001, Montevideo, Uruguay. Phone: +59899981355. E-mail: cubassantiago@hotmail.com

Submitted: September 24, 2021. **Accepted:** November 11, 2021

https://doi.org/10.52083/QOAI6106

atrioventricular node (NAV), right coronary artery (RCA) and the ostium of the coronary sinus (CS).

Our aim was to describe zones of proximity (and danger) between the tricuspid annulus and the CS and the RCA in order to consider during tricuspid interventions.

MATERIALS AND METHODS

Anatomical approach

The material used to carry out this work was donated under a written consent to the Department of Anatomy.

An observational descriptive anatomical study was performed using 36 hearts from human adult corpses previously fixed in formaldehyde solution. The age of the corpses was in the range from sixty-five to seventy-five. The donors were patients without cardiac pathology. We excluded from the sample any donors with cardiac pathologies.

The chest was approached through a bilateral para-median lateral thoracotomy, and the cardiopulmonary block was subsequently removed. An inverted "T" pericardiotomy was performed. The heart was released after sectioning of the intrapericardial pulmonary veins, vena cava, and supra-aortic vessels. Once the heart was released, the right atrium was approached through a right cava-cava atriotomy, and the incision was extended parallel to the tricuspid ring. Location and branches of the RCA were identified.

Measurements were taken from the atrial side of the middle third of the anterosuperior (anterior) leaflet, the anteroinferior (anteroposterior) commissure, the middle third of the inferior (posterior) leaflet and the middle third of the septal valve (Fig. 1).

The following distances were recorded: 1) Distance 1 (D1) – shortest distance from the

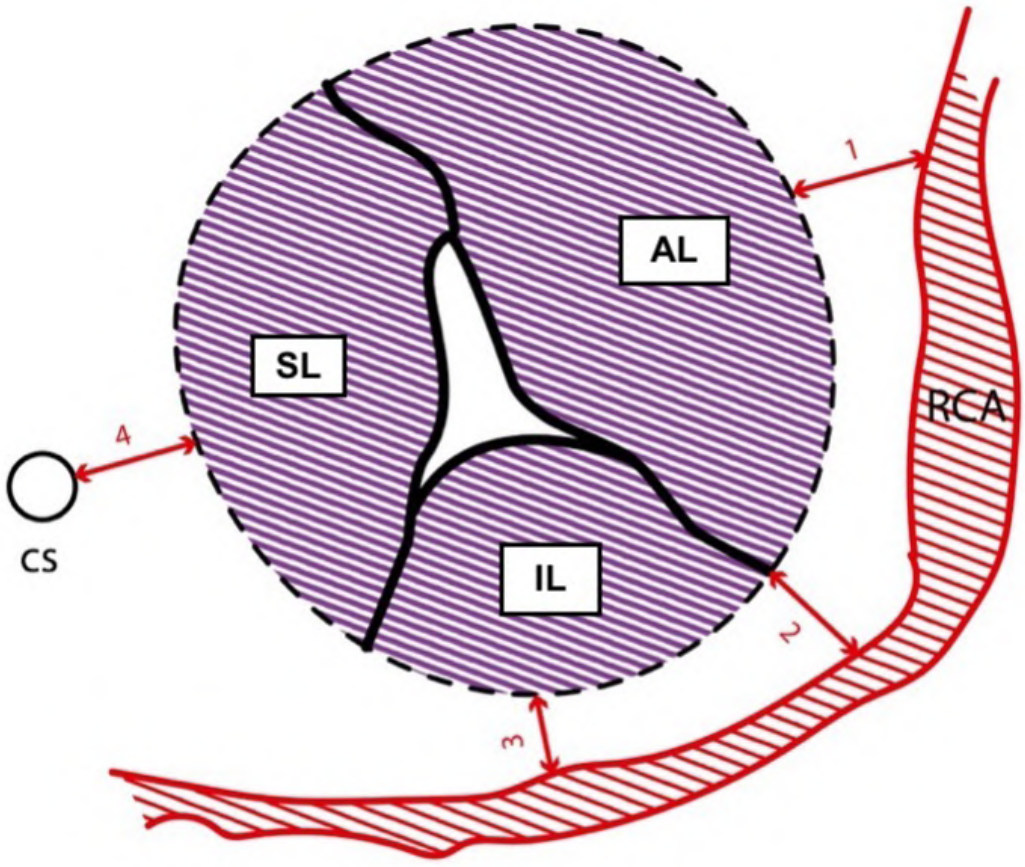

Fig. 1.- Schematic representation of the tricuspid valve (atrial view) in relation with the right coronary artery, and the coronary sinus. SL: Septal Leaflet. AL: Anterosuperior Leaflet. IL: Inferior Leaflet. CS: Coronary Sinus. RCA: Right Coronary Artery. 1: distance 1. 2: distance 2. 3: distance 3. 4: distance 4.

middle third of the anterosuperior leaflet to the RCA; 2) Distance 2 (D2) – shortest distance from the anteroinferior commissure to the RCA; 3) Distance 3 (D3) – shortest distance from the middle third of the inferior leaflet to the RCA; 4) Distance 4 (D4) – shortest distance from the middle third of the septal leaflet to the ostium of the coronary sinus (Figs. 1, 2 and 3).

Coronary dominance was defined as the coronary artery which gave rise to the posterior descending artery (Knaapen et al., 2013). In hearts with left dominance, it was not possible to take the measurement in relation to the anteroinferior commissure and inferior leaflet (Distance 2 and Distance 3).

Distances were compared in specimens with left and right coronary dominance using Mann-Whitney U test.

All measurements were made with a numerical millimeter caliper and by the same observer. Continuous variables were expressed as mean, range (minimum-maximum) and standard deviation (SD). Categorical variables as absolute numbers and %. P-value < 0.05 was considered significant.

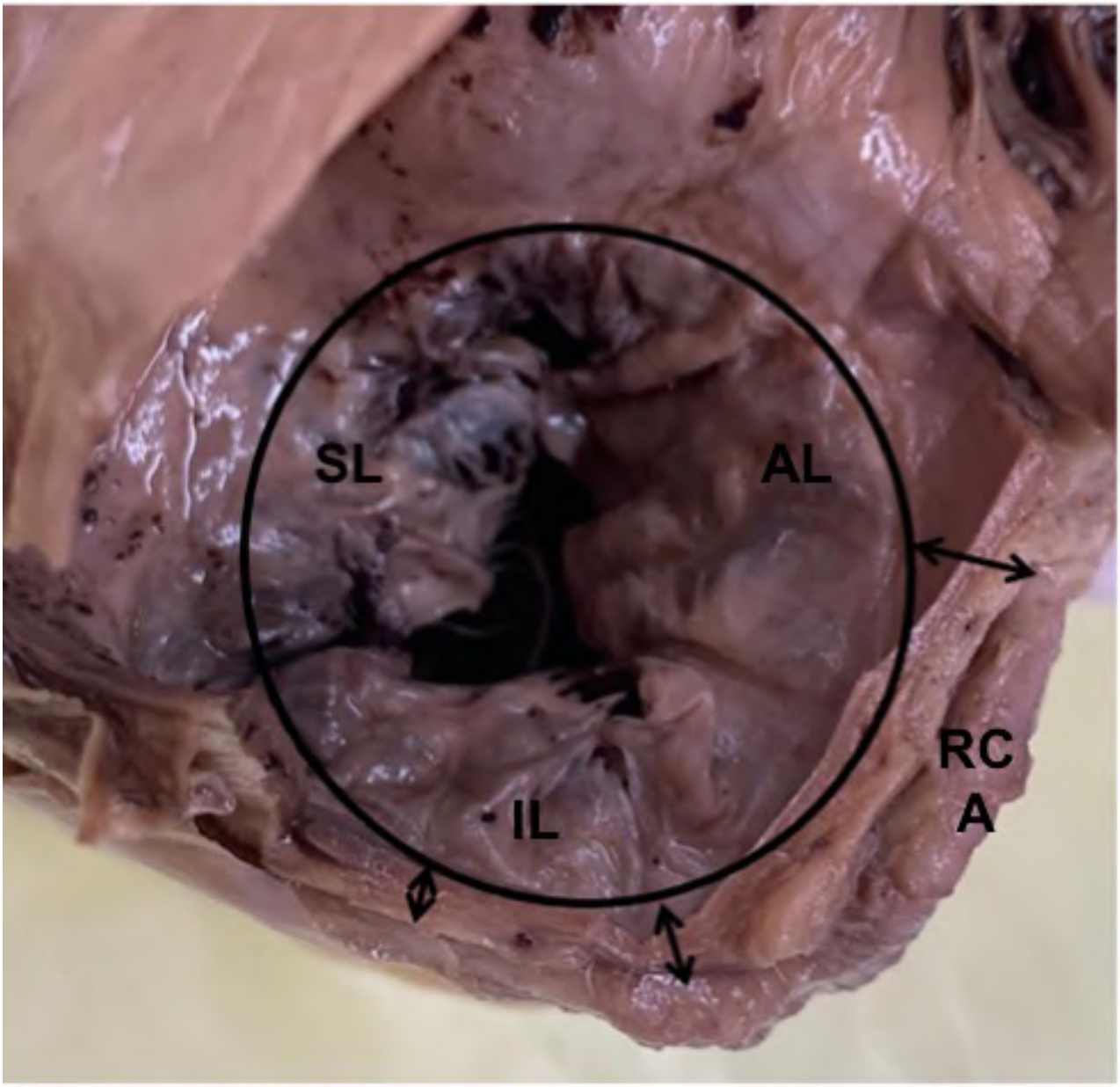

Fig. 2.- Atrial view of the tricuspid valve. SL: Septal Leaflet. AL: Anterosuperior Leaflet. IL: Inferior Leaflet. Arrows indicate the points of measure between the annulus to the right coronary artery.

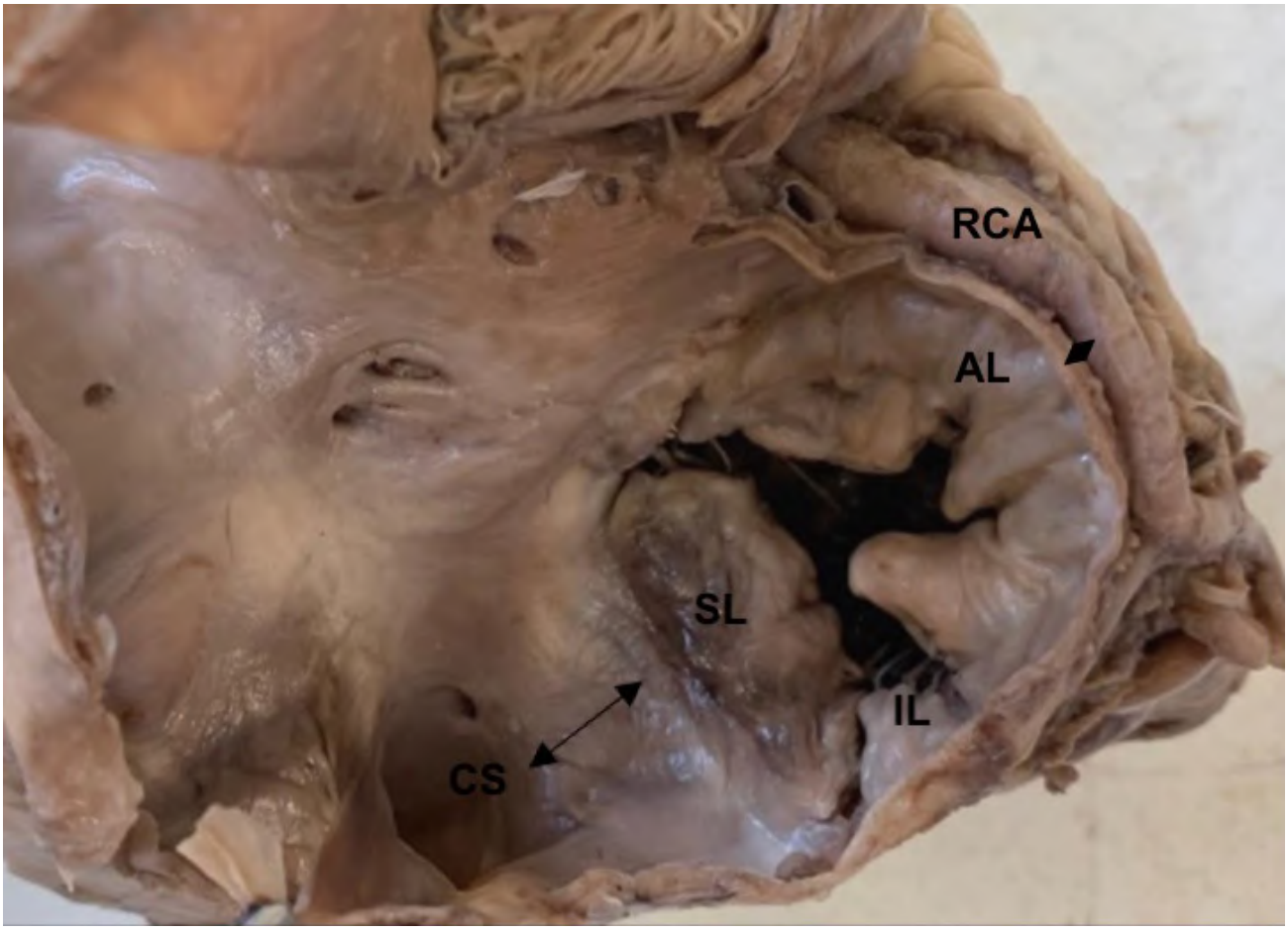

Fig. 3.- Atrial view of the tricuspid valve in cadaveric piece. Pattern of Left dominance. SL: Septal Leaflet. AL: Anterosuperior Leaflet. IL: Inferior Leaflet. CS: Coronary Sinus. RCA: Right Coronary Artery. Arrows indicate the points of measure between the annulus to the Coronary Sinus, and the annulus to Right Coronary Artery.

RESULTS

Of the 36 hearts, 31 presented right dominance (86.1%), 4 left dominance (11.1%) and 1 codominance (2.8%).

Mean D1 was 5.32 mm (1-11 mm), D2 was 3.07 mm (0.5-7 mm), D3 was 2.53 mm (0.5-12 mm) and D4 was 8.81 mm (2.5-18 mm) (Table 1).

In hearts with right coronary dominance, mean D1 was 5.26 mm (1-11 mm) and standard deviation (SD) was 2.55, D2 was 3.06 mm (0.5-7 mm) and SD was 1.66, D3 was 2.53 mm (0.5-12 mm) and SD was 2.26, D4 was 8.55 mm (2.5-18 mm) and SD was 3.9 (Fig. 4).

In hearts with left coronary dominance, mean D1 was 6.62 mm (4-8 mm) and SD was 1.80, D2 and D3 was not possible to obtain in this dominance pattern. Mean D4 was 11.62 mm (11-13 mm) and SD was 0.95 (Fig. 4).

In the only case of codominance, mean D1 was 2 mm, D2 was 3.5 mm, D3 was not possible to obtain in this dominance pattern. Mean D4 was 5.5 mm.

We found no statistically significant differences between hearts with right and left coronary dominance at either D1 (5.26±2.55 mm vs 6.62±1.80 mm, p=0.213) or D4 (8.55±3.91 mm vs 11.62±0.95 mm, p=0.064) (Table 2).

DISCUSSION

Tricuspid regurgitation (TR) is one of the most common manifestations of valvular heart disease (VHD) and may affect 65-85% of the population.

Primary TR implies pathology of the tricuspid valve (TV) complex and may be of rheumatic, degenerative, congenital, infectious, traumatic, or iatrogenic (usually secondary to pace- maker leads) origin. Secondary (or functional) TR is the most prevalent tricuspid pathology and related to right ventricular (RV) dilatation and/

or dysfunction, annular dilatation, and leaflet tethering, which are, in turn, usually secondary to left-sided VHD (especially affecting the mitral valve), atrial fibrillation or pulmonary hypertension (Antunes et al., 2017).

The TV annulus is part of the fibrous skeleton of the heart and has important anatomical relationships with the atrioventricular node, the RCA and with the ostium of the CS. A profound and extensive knowledge of its relations is imperative for anyone intervening on the TV in order to avoid serious complications. Our investigation has shown that the area of greatest risk for injury to the RCA is at the anterior-inferior commissure as well as the middle of the inferior leaflet. Using a clockwise system, with 0 corresponding to half of the anterior annulus, the area of greatest risk for injuring the RCA is the zone between 4 and 6 o'clock (Figs. 5 and 6). This risk might be higher for patients with right coronary dominance.

The relationship of the RCA with the annulus acquires importance for the surgical and interventional approach of the TV. The RCA runs through the right atrioventricular sulcus and gives rise to the posterior descending artery in 85-90% of cases (Knaapen et al., 2013) (right dominance). It has been described that, in right dominance, the RCA has closer relationship with the tricuspid annulus but there is limited information regarding the minimum safety distance (Dahou et al., 2019).

Table 1. Distance between the tricuspid annulus and the right coronary artery and coronary sinus (n=31).

	N	Mean	Minimum	Maximum	SD
Distance 1 (mm)	36	5,32	1,00	11,00	2,52
Distance 2 (mm)	32	3,07	,50	7,00	1,64
Distance 3 (mm)	31	2,53	,50	12,00	2,26
Distance 4 (mm)	36	8,81	2,50	18,00	3,80

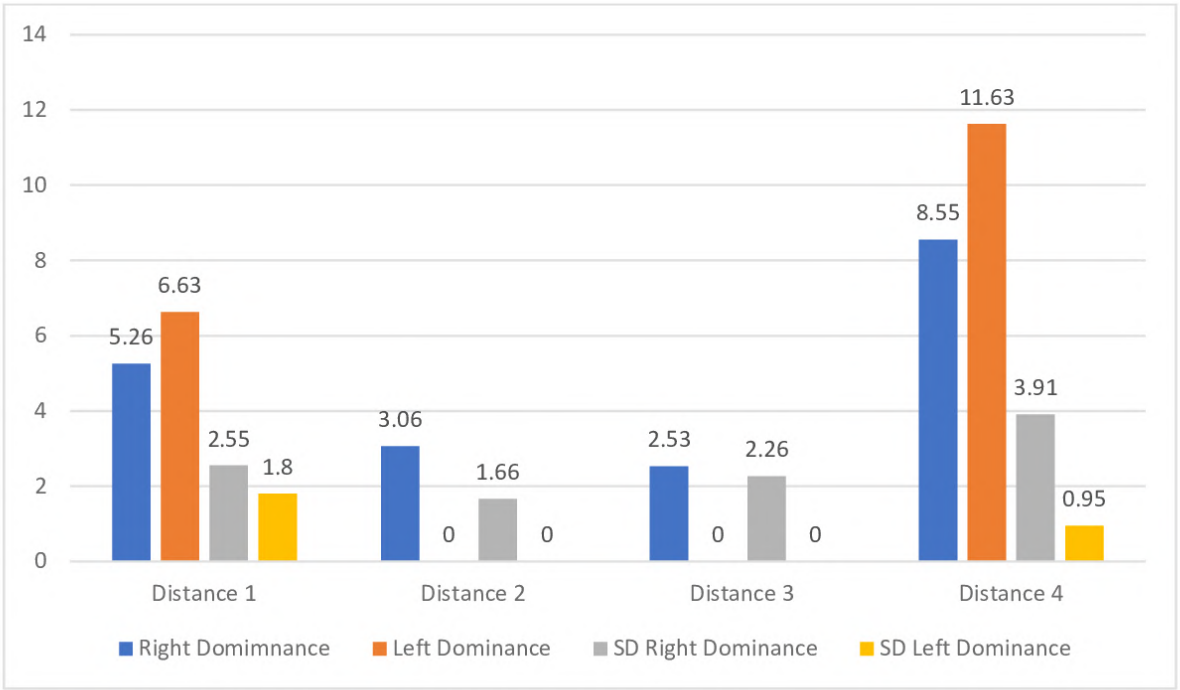

Fig. 4.- Mean distance (in millimeters and standard deviation) between the tricuspid annulus and right coronary artery (RCA), and coronary sinus. Distance 1: distance of the middle third of anterosuperior leaflet to RCA. Distance 2: distance of the anterior-inferior commissure to RCA. Distance 3: distance of the middle third of inferior leaflet to RCA. Distance 4: distance of the middle third of septal leaflet to CS.

Table 2. Distance comparison between hearts with right and left dominance (n=35).

	Right (n=31)	Left (n=4)	p
Distance 1 (mm)(SD)	5.26 (2.55)	6.62 (1.80)	0.213
	6.62	1.80	
Distance 4 (mm)(SD)	8.55 (3.91)	11.62 (0.95)	0.064
	11.62	.95	

When the heart has a left dominance, the RCA is smaller because it supplies a smaller proportion of myocardial tissue and has a shorter course. In our study, 86.1% of dissected hearts presented right dominance, 11.1% left dominance and 2.8% co-dominance, which were similar to other series (Angelini et al., 2002; Knaapen et al., 2013). We found that when there is left dominance, the RCA ends early and therefore has no relationship to the inferior leaflet.

Dahou et al. (2019) describes that the distance of the RCA at the proximal level is relatively distant from the tricuspid annulus, and gradually approaches the endocardial surface, acquiring at a lower level a distance of less than 3 mm. Sellke and Ruel (2019) mentions that the RCA runs through the AV groove from the anterior to the posterior annulus, and may be injured by deep stitches at the level of the annulus.

Data derived from previous anatomical studies and evaluations performed with computed tomography (CT) are very similar to our results. Buzzatti et al. (2018), using 44 normal human hearts, reported that the RCA had an average

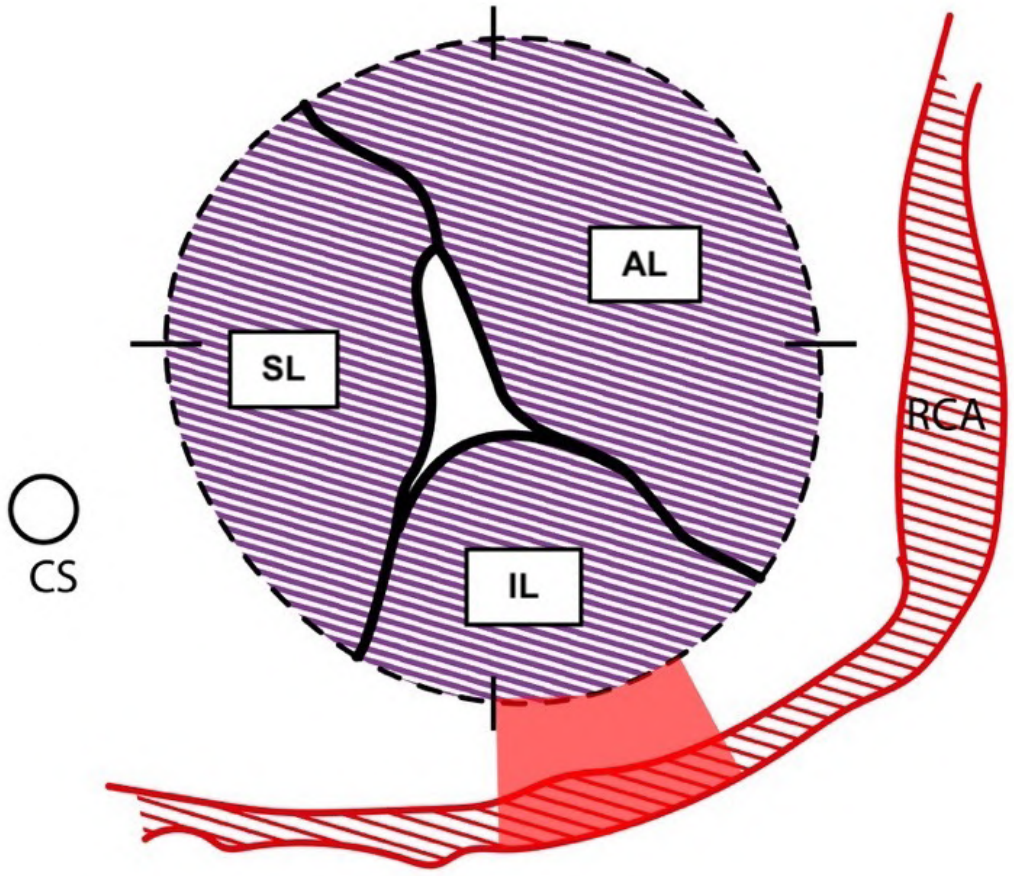

Fig. 5.- Schematic representation of the tricuspid valve of (atrial view) in relation with the right coronary artery, and the coronary sinus. Clockwise system, with the clock being the tricuspid ring, and 0 o'clock half of the anterior annulus. SL: Septal Leaflet. AL: Anterosuperior Leaflet. IL: Inferior Leaflet. CS: Coronary Sinus. RCA: Right Coronary Artery. Red zone, the greatest risk area.

distance to the tricuspid annulus, which was greatest at the anterosuperior leaflet (6.8 mm) and shortest at the posterior annulus (2.1 mm). Van Rosendael et al. (2017) evaluated 250 patients with CT and reported a distance from the RCA to the anterosuperior leaflet of the tricuspid valve of 8.8±4.5 mm and to the inferior leaflet 3.6±3.4 mm.

Antunes et al. (2017) describe the management of the tricuspid valve regurgitation. They specify the surgical techniques, and describe that, in annuloplasty techniques, sutures must be placed in the annulus, 1-2 mm beyond the leaflet hinge line to avoid the adjacent aortic valve and right coronary artery, and the last sutures should be placed in the anteroseptal commissure (right fibrous trigone) and in the middle of the septal annulus to avoid injury to the bundle of His. They describe that in the tricuspid valve replacement accurate prosthesis sizing is essential to prevent distortion of the right coronary artery.

Schofer et al. (2015) report the first human transcatheter tricuspid valve repair with a Mitralign system. They do a plication of the annulus and bicuspidizing the tricuspid valve at the level of the postero-anterior commissure. They consider that the position of the radiofrecuency wire to carry out this procedure must be positioned

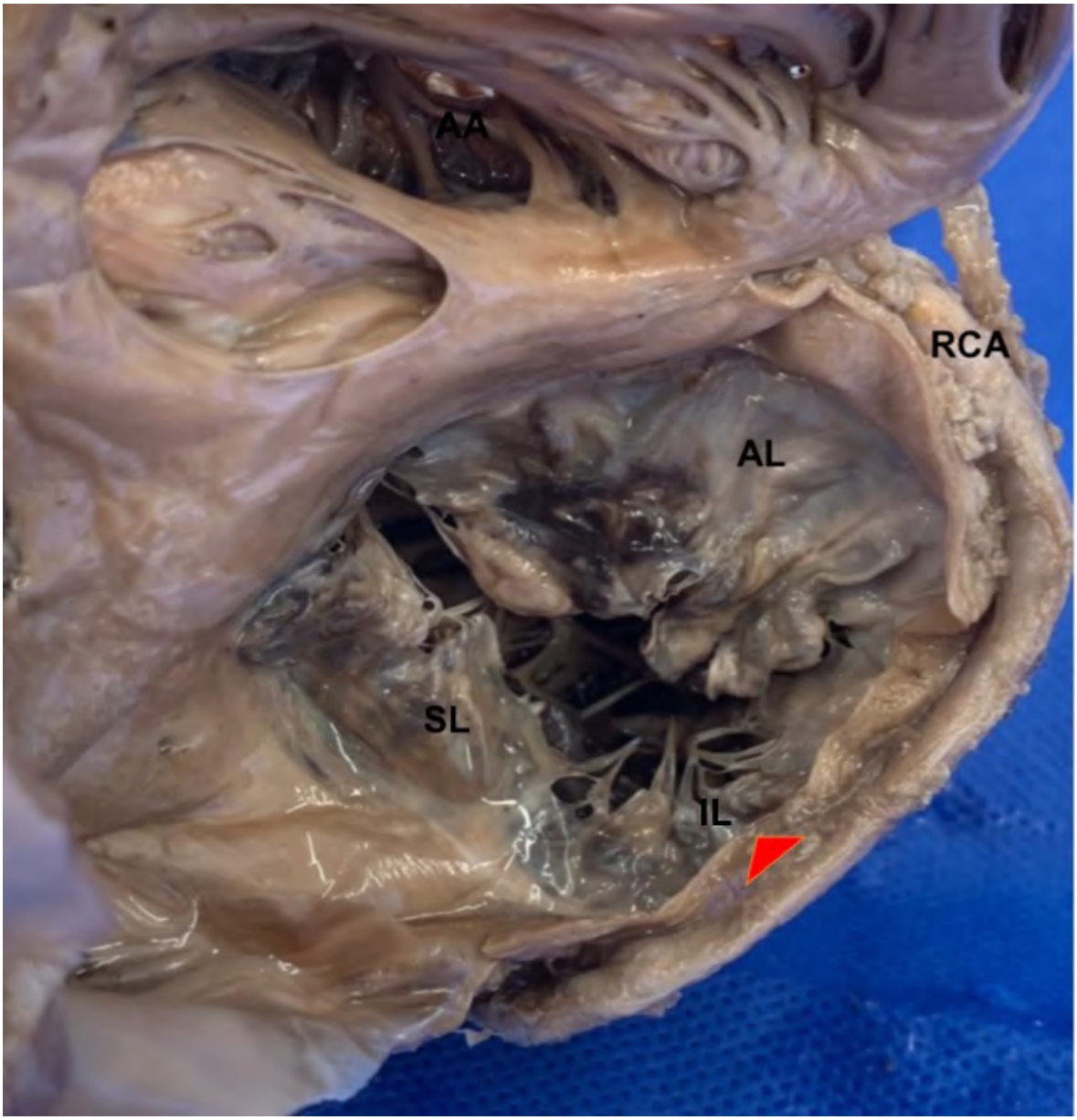

Fig. 6.- Atrial view of the tricuspid valve. Pattern of Right dominance. SL: Septal Leaflet. AL: Anterosuperior Leaflet. IL: Inferior Leaflet. AA: Atrial Appendage. RCA: Right Coronary Artery. Red triangle represents the greatest risk area.

2-5mm from the base of the leaflet and within the annulus directed toward the right atrium to avoid the right coronary artery perforation.

Taramasso et al. (2019), in the International TriValve Registry, report that 312 patients with severe or greater symptomatic tricuspid regurgitation (TR) underwent transcatheter tricuspid valve intervention (TTVI). Thirty-day mortality was 3.6%, and the mayor adverse events at 30 days were 10.3%, including 2 acute myocardial infarctions requiring right coronary artery stenting (0.7%). They do not specify whether this was because of compromise or distortion of the right coronary artery.

Iatrogenic damage to the RCA is a rare complication that has serious consequences if not diagnosed and treated early. RCA may be damaged directly during surgery when placing sutures in the tricuspid annulus or indirectly by tightening the tissues located in its closeness. In patients with right coronary dominance, RCA lesions are more frequent at the mid-distal level (Gotor et al., 2018). As we have shown, it is at this point where the artery has its closest relationship with the annulus.

Díez-Villanueva et al. (2014) reviewed their experience regarding direct injury to the RCA related to TV repair in patients with functional TR. Between 2005 and 2012, 499 patients underwent TV surgery, and repair techniques were performed in 450. Direct injury to the RCA complicated 4 of those 450 repair operations. All the patients had critical or sub-occlusive stenosis at the level of the mid or distal portions of the RCA. Díez-Villanueva et al. (2014) comment that the distance between the RCA and the endocardium is particularly small in those areas closest to the tricuspid annulus, especially in the cavotricuspid isthmus in the lower right atrium, with a distance less than 5 mm in over 80% of patients. They define a danger zone at the level of the anteroposterior commissure, and risk of RCA occlusion may be minimized by using semirigid rings, applying fewer sutures along the posterior annulus, and avoiding applying the stitches to the atrial wall.

The topography of the iatrogenic damage of the RCA is concordant with our results, in which the shortest distance of the RCA to the annulus is in the posterior annulus.

We did not find any reference regarding injury to the coronary sinus during interventional procedures on the TV (Taramasso et al., 2019). Nonetheless, there are few patients in whom TV devices have been implanted percutaneously, which could explain the scarcity of this report. According to our data, the distance between the TV annulus and the CS is quite safe in hearts with left dominance. In hearts with right dominance, this distance is shorter and therefore might represent an issue to consider during TV intervention planning.

Limitations

Measurements were performed on formaldehyde fixed hearts, which dehydrates the tissues and can determine alterations in the measurements with respect to fresh or living tissues. We must also consider that the measurements taken were analyzed only in the transversal plane, with no measurements of the ring being made to the RCA in the vertical plane. We were not able to identify the sex of each of the samples (cadaveric samples are not identified), and therefore our data do not allow to consider differences between males and females.

CONCLUSIONS

Anatomic relationships of the TV annulus with the RCA and CS are important in order to avoid its injury during interventional procedures. The highest risk area of injuring the RCA corresponds to the posterior annulus. TV annulus in hearts with left dominance have a safer distance to the RCA and CS and therefore may present a lower risk of RCA involvement in surgical and endovascular procedures. The anatomical knowledge of the tricuspid valve and its relationships are essential to reduce complications during surgical and endovascular procedures.

ACKNOWLEDGEMENTS

The authors express special recognition to all who in life decide to donate their body to our faculty, for teaching and research of Anatomy.

REFERENCES

ANGELINI P, VELASCO JA, FLAMM S (2002) Coronary anomalies: incidence, pathophysiology, and clinical relevance. *Circulation,* 105: 2449-2454.

ANTUNES MJ, RODRÍGUEZ-PALOMARES J, PRENDERGAST B, DE BONIS M, ROSENHEK R, AL-ATTAR N, BARILI F, CASSELMAN F, FOLLIGUET T, IUNG B, LANCELLOTTI P, MUNERETTO C, OBADIA JF, PIERARD L, SUWALSKI P, ZAMORANO P (2017) Management of tricuspid valve regurgitation: Position statement of the European Society of Cardiology Working Groups of Cardiovascular Surgery and Valvular Heart Disease. *Eur J Cardiothorac Surg*, 52(6): 1022-1030.

BUZZATTI N, DE BONIS M, MOAT N (2018) Anatomy of the tricuspid valve, pathophysiology of functional tricuspid regurgitation, and implications for percutaneous therapies. *Interv Cardiol Clin,* 7: 1-11.

CAMPELO F, LAIREZ O, CARRIÉ D (2017) Tratamientos percutáneos de la valvulopatía tricuspídea: una nueva esperanza para la válvula olvidada. *Rev Esp Cardiol,* 70(10): 856-866.

DAHOU A, LEVIN D, REISMAN M, HAHN RT (2019) Anatomy and physiology of the tricuspid valve. *JACC Cardiovas Imaging,* 12: 458-468.

DÍEZ-VILLANUEVA P, GUTIÉRREZ-IBANES E, CUERPO-CABALLERO G, SANZ-RUIZ R, ABEYTUA M, SORIANO J, Sarnago F, Elízaga J, González-Pinto A, Fernández-Avilés F (2014) Direct injury to right coronary artery in patients undergoing tricuspid annuloplasty. *Ann Thorac Surg,* 97: 1300-1305.

GOTOR CA, CENTENO JE, PÉREZ E, LÓPEZ MJ, CORTINA JM (2018) Iatrogenic occlusion of the right coronary artery during tricuspid valve replacement. *Rev Colomb Cardiol,* 26: 296-299.

KNAAPEN M, KOCH AH, KOCH C, KOCH KT, LI X, VAN ROOIJ PC, TIJSSEN JGP, PETERS RJ, VAN DER WAL AC, DAMMAN P, DE WINTER RJ (2013) Prevalence of left and balanced coronary arterial dominance decreases with increasing age of patients at autopsy. A postmortem coronary angiograms study. *Cardiovas Pathol,* 22(1): 49-53.

SCHOFER J, BIJUKLIC K, TIBURTIUS C, HANSEN L, GRPPTHUIS A, HAHN R (2015) First-human transcatheter tricuspid valve repair in a patient with severely regurgitant tricuspid valve. *J Am Coll Cardiol,* 65: 1190-1195.

SELLKE F, RUEL M (2019) Tricuspid valve operation. In: Elmistekawy E, Mesana TG (eds). *Atlas of Cardiac Surgical techniques,* 2nd edition. Russell Gabbedy, Philadelphia, USA, pp 384-405.

TARAMASSO M, ALESSANDRINI H, LATIB A, ASAMI M, ATTINGER-TOLLER A, BIASCO L, et al. (2019) Outcomes after current transcatheter tricuspid valve intervention. Mid-term results from the international trivalve registry. *JACC: Cardiovascular Intervention,* 12(2): 155-165. doi: 10.1016/j.jcin.2018.10.022.

VAN ROSENDAEL PJ, KAMPERIDIS V, KONG WK, VAN ROSENDAEL AR, VAN DER KLEY F, AJMONE N, DELGADO V, BAX JJ (2017) Computed tomography for planning transcatheter tricuspid valve therapy. *Eur Heart J*, 38(9): 665-674.

VASSILEVA CM, SHABOSKY J, BOLEY T, MARKWELL S, HAZELRIGG S (2012) Tricuspid valve surgery: the past 10 years from the Nationwide Inpatient Sample (NIS) database. *J Thorac Cardiovasc Surg,* 143(5): 1043-1049.

Applications of Sumach extract in reduction of male reproductive parameters damages following morphine administration through down-regulated apoptotic genes, antioxidants regulation, and inflammatory markers suppression

Ahmad Shabanizadeh[1], Shiva Roshankhah[2], Amir Abdolmaleki[2], Mohammad Reza Salahshoor[2]

[1] *Department of Anatomical Sciences, School of Medicine, Immunology of Infectious Diseases Research Center, Rafsanjan University of Medical Sciences, Rafsanjan, Iran*

[2] *Department of Anatomical Sciences, Medical School, Kermanshah University of Medical Sciences, Kermanshah, Iran*

SUMMARY

Morphine (MO), a psychoactive member of opium family, causes free radicals' accumulation in cells. *Sumach* (SU) is a medicinal plant with antioxidative activities. This study was designed to assess the probable ameliorative effects and alteration of apoptotic genes expression after SU extract administration on testopathy caused by chronic MO contamination. Sixty-four male rats were divided into 8 groups: 1, normal; 2, MO; 3, 200 mg/kg SU; 4, 400 mg/kg SU; 5, 800 mg/kg SU; 6, MO + 200 mg/kg SU; 7, MO + 400 mg/kg SU; and 8. MO + 800 mg/kg SU. All intraperitoneal injections of MO (10 mg/kg) were applied on the first day of the experiment, and SU extract was also treated orally (through a nasogastric tube) on the other 2-28 days. Apoptotic genes expression (*P53*, *Bcl2* and *caspase-3*) and inflammatory cytokines were measured by Real-Time PCR and ELISA techniques, respectively. Also, total antioxidant capacity (TAC) and male reproductive parameters were detected quantitatively. In MO group, significant detrimental changes of testes (including all investigated parameters) were detected in comparison with the normal group ($P < 0.01$), but genes expression of P53 and caspase-3 and inflammatory cytokine showed a significant incremental trend. In *SU* (200, 400, and 800 mg/kg) and *SU* (200, 400, and 800 mg/kg) + MO treated groups, all values were accelerated significantly in comparison with MO group ($P<0.01$), but genes expression of P53 and caspase-3, along with inflammatory cytokine indices, were down-regulated. Totally, therapeutic effects of SU extract were approved biochemically and histologically to scavenge MO impacts.

Key words: *Sumach* – Male reproductive – Morphine – Apoptosis – Inflammation – Antioxidant

Corresponding author:
Dr. Mohammad Reza Salahshoor, PhD. Department of Anatomical Sciences, Medical School, Kermanshah University of Medical Sciences, Kermanshah, Iran. Phone: 0098-09188360349. E-mail: reza.salahshoor@yahoo.com Orcid: 0000-0001-5362-9935

Submitted: December 11, 2020. **Accepted:** November 15, 2021

https://doi.org/10.52083/OFOO2669

INTRODUCTION

Typically, MO is used as an opiate for acute pain medication by direct effects on the nervous system (Jalili et al., 2016). Ward et al. (2020), scientifically proved that opioids could accelerate free radical production in the body to an unhealthy state, which leads to widespread cell death. Mainly, MO is detected as an opioid with damaging consequences on the male sexual system. These adverse effects included hypogonadism, histopathological transitions, and severe sexual hormonal imbalances (Karami et al., 2019). MO disrupts regular spermatogenesis and pituitary-hypothalamic testicular axis (Roshankhah et al., 2017). Apart from demolition effects on either sexual system, apoptosis was also observed on non-sexual cells, including neurons and hepatocytes (Jabari et al., 2019). Chronic consumption of MO can lead to aggregation of free radicals. Regarding MO administration, produced ROS neglect the three-dimensional DNA molecule and membrane organelles (Famitafreshi et al., 2020). In these cases, the intervention of the immune function to stand detrimental effects is often in a slow reaction. Also, there is no absolute therapeutic protection against such irreversible disorders. In this situation, utilization of plant-based antioxidants with lesser side-effects becomes a safe and healthy procedure (Jalili et al., 2019a).

SU is an herb with antioxidant features belonging to *Anacardiaceae* family. This plant generally grows in the mountainous regions of Iran (Gharaei et al., 2013). In traditional medicine, the SU is hired to cure insect bites, hemorrhoids, and colic pain (Shabbir et al., 2012). Anwer et al. (2013), confirmed that the SU is high in tannins and flavonoids as critical sources of antioxidant. Multiple literatures have indicated the hypoglycemic, antitumor, and antioxidant activities of Flavonoids (González et al., 2011). Based on the theoretical hypotheses, hydroalcoholic products of SU improves enzymatic efficacy of cellular antioxidants, including catalase and superoxide dismutase (Ahangarpour al., 2014).

According to the physiology of reproductive system components, any minor changes in structure or role of this organ could cause considerable disruptive results, such as lost fertility or full infertility conditions (Schilit et al., 2020). As was suggested in the previous study, infertility can be seen in more than 50% directly related to men's origins (Ho et al., 2020). Free radicals invade unsaturated fatty acids in cell membranes and trigger intracellular alkylation of protein molecules. They could also provoke necrosis via various mechanisms, including membranous lipid peroxidation and cytoplasmic partial removal of necessary enzymes (Tremellen et al., 2008). Reactive oxygen species (ROS) could arrest cell cycle leading to programmed cell death. Outcomes of this alteration can be more severe in poor-proliferating cells such as spermatozoa (Jalili et al., 2014; Ellis et al., 2016). Although MO administration is extremely common in medications and its adverse reactions on male sexual operation is authorized, also due to the antioxidant quality of SU to eliminate free radicals, this experiment was intended to investigate the potential therapeutic properties of SU on male rat reproductive dysfunction during MO administration.

MATERIALS AND METHODS

SU seed extraction method

Fresh SU plants were obtained from the local grocery (Javanrood town, Kermanshah, Iran). A botanist (Department of Pharmacognosy, Faculty of Pharmacy, Hamadan Medical Sciences University, Hamadan, Iran, voucher specimen NO. PCT-2037) identified the accuracy of the plant. An automatic grinder was also used to grind dried seeds. Then hydroalcoholic compound was constructed as follows: 300 gr of SU powder was dissolved in 1300 mL of concentrated mixture of water-ethanol. The solution was allowed to stay for 2 days at room temperature and purified by the use of filter paper; then the centrifugation was accompanied (4000 rpm, 15 min). The extract was preserved for potential administration at 37^{O}C after withdrawal of supernatant (Ahangarpour et al., 2014).

Phytochemical analysis

Semi-quantitative phytochemical analysis was used based on standard protocols (Treas and Evans, 1989). Ethanol (80%) was percolated

with 5 gr of SU powder. Vaporization was then established. TLC on silica gel Merck 60F245 (thickness 0.2 mm) was recruited to identify in 80% of ethanol extract; Liebermann-Burchard as a reagent and hexane/ethyl acetate; 1:1 as a mobile layer for terpenes and sterols (color range was produced after 10 min at 100° C sprayed plate heating) were also provided. Classical acid/base separation strategies were also established and examined in chloroform/methanol/ammonia solution by TLC as a solvent method for alkaloids. Then, patches were observed by applying Dragendorff 's reagent spry method. TLC was formed in 4:1:5 (top layer) n-butanol/acetic acid/water for flavonoid recognition, and 1% aluminum chloride solution in methanol (under UV, 366 nm) for spot representation. Tannin and saponin recognition was applied by adding 1% gelatin solution and froth analysis separately. In methanol, anthraquinones and phlobatannins were also reported by 10% potassium hydroxide solution (Roshankhah et al., 2020).

Antioxidant capacity assessment by 2,2, dipheny l,1, picrylhydrazyl (DPPH)

DPPH-free radical assay was used to assess antioxidant levels. In reaction among DPPH and an antioxidant agent which provide hydrogen, the DPPH is modified into a reduced state. Color adjustment (deep violet to pale yellow) is recorded using a spectrophotometer. DPPH (200 µl) was added to each dilution. During a half-hour in dark incubation, its emission was documented (517 nm). As a positive control, butylated hydroxytoluene (BHT, a typical antioxidant) with equal concentration was hired. The following method was used for the scavenging of free radicals; AA%= [A0-A1 / A0]100 (A0; DPPH absorption, A1; butylated hydroxytoluene and SU absorption) (Hosseinipour et al., 2019).

Animals

The University's animal house was considered as a center of animal training. Sixty-four male Wistar rats (200-230 gm) were collected. All typical environment requirements were equipped, including 12:12 hour light/dark period and 22 ± 2°C. This experimental approach was authorized by the ethical committee of the Kermanshah University of Medical Sciences and implemented in line with the National Institution of Health Guide for Laboratory Animals (IR.KUMS.REC.1397.500).

Design and settings

Sixty-four male Wistar rats were randomly divided into 8 groups (8 rats in each group). The first group (normal) handled with normal saline (resemble experimental groups in quantity (orally); the second group (MO) was handled as an established procedure (injection of 10 mg/kg on first day, followed by 20 mg/kg/day on 2-28 days); the third to fifth groups (SU) were handled with doses of 200, 400 and 800 mg/kg daily for 28 consecutive days; the sixth to eighth groups (MO+SU) were handled with MO followed by daily specific doses of 200, 400 and 800 mg/kg of SU (days 1–28). Oral (nasogastric tube) and injection procedures were handled for SU and MO administration, respectively. MO was treated from 9:45 AM to 10 AM (Ahangarpour et al., 2014; Jalili et al., 2016).

Sperm sample preparation

At the end of the procedure, the animals were anesthetized by intraperitoneal injection of ketamine HCl (100 mg/kg) and Xylazine (70 mg/kg). Blood samples were aspirated by subxiphoid pathway. Samples were placed for 20 min at atmospheric pressure and temperature. They were centrifuged for 10 min at 300 g. For biochemical study, purified blood serum was placed at -70 °C refrigerator. DMEMF12/FBS5% culture medium was used for scrotum dissection. Right testes were used for biochemical assays, and the left were fixed for histopathological evaluations in 10% formalin. A warmed petri dish (37 °C) comprising 10 ml Hank's balanced salt solution was also used for dissection of caudal portion of both samples. Dissolved sperms were used in order to assess sperm parameters (400x) (Roshahnkhah et al., 2017).

Histopathological methods

The left sample was immersed in standard saline and fixed in formaldehyde (10%) for 48 h (right specimen was used for biochemical studies). Five-micrometer cuts of the left testis

were processed using a microtome and stained with hematoxylin and eosin. Histological and GLH morphometric evaluations were treated under light microscopy and recorded by a Motic camera.

Sperm viability

Eosin penetrated into cells to discriminate between destroyed sperm cells and living ones. 20µl of condensed semen was diluted with the same quantity of eosin staining. 2-5 min later, half of the mixture was moved to a neobar slide culture to determine live (no pink) and dead (cytoplasm-pink) samples (40x). 100 sperm cells were included (from each sample) in 10 imaging fields. Eventually, sperm ratio was reported (Roshankhah et al., 2017).

Progressive sperm motility assessment

Only progressive movement was regarded as healthy and appropriate sperm motility according to the WHO recommendation (2010). 100 µl sperm storage was imposed on a slide field (Jalili et al., 2014).

Sperm count

400 µL suspension (sperm) was dissolved in formaldehyde fixative (Sigma; USA) to evaluate sperm count. 15 µL of sample was mounted on a hemocytometer. After 20 minutes, the steady cells were monitored and measured per 250 minor hemocytometer quadrangles (40x magnification). Semen concentration (per mm^3) equated to the sperm count (Jalili et al., 2016).

Morphology of sperm cells

Phenotype of sperms was selected based on sperm in right cauda epididymis. For morphology assessments, an aliquot of each specimen was used. Later, for a closer evaluation, a light microscope (400x) was employed through Eosin/nigrosine staining. Overall, 500 spermatozoa were counted on each slide (5000 in each group) (Roshankhah et al., 2017).

GLH morphology evaluation

Fixed testicular samples were handled for these histological assessments through standard tissue processing, including dehydration, clearing and embedding. Hematoxylin and eosin stained the 5-µm slices. At least 30 frameworks were prepared. GLH evaluation was applied using a Motic camera (Jalili et al., 2016).

Strategy of plasma ferric reduction capacity (FRAP)

In the FRAP approach, the possible capacity of blood plasma to regain ferric ions is stately as a serum TAC index. This procedure required Fe^{III} ions. Blue stain was developed when the acid-pH Fe^{III}-TPTZ was converted into Fe^{III}. Absorption occurred at 500 nm wavelength. TAC levels were also plotted via the default iron sulfate concentration curve (Jalili et al., 2019b).

Sexual hormones examination

Serum and frozen specimens were used for hormonal assessment. ELISA (Abcam 107555, USA) method examined serum testosterone levels (Jalili et al., 2016).

Real-time PCR

Real-time PCR was used to examine the gene expression of caspase-3, Bcl2 and p53 [Table 1]. The testis specimen was suspended in liquid

Table 1. Real-time PCR primers.

Primer ID	Primer sequences
GAPDH	F: 50- AAGCTCATTTCCTGGTATG-30 R: 50- CTGCCACAAGAACTAGAGA-30
p53	F:50-AGAGACCGCCGTACAGAAGA-30 R:50-GCATGGGCATCCTTTAACTC-30
caspase-3	F: 50-ATGGCGAAATGGAGATGAATA-30 R: 50-ACTGCCCATGATGGTTCTGTG-30
Bax	50-TGG GATGCCTTTGTGGAACT-30 R:50-GCATGGGCATCCTTTAACTC-30

nitrogen and stored at -80 °C in a freezer. RNA was extracted with a RNeasy kit (Qiagen), and DNA samples were prepared with a DNase kit (Qiagen). cDNA was developed using cDNA Synthesis Kit (Fermentas). Gene expression rate was calculated using the Maxima SYBR Green (Fermentas) approach (Esfandiari et al., 2014).

RESULTS

Phytochemical screening of SU

Pharmacologically, the product was formulated in 9-Octadecenoic acid (Z), methyl ester, Dodecanoic acid, Saponins, and tannins. Natural herbal products were also measured, including flavonoids, Phlobatannins, Anthraquinones, and Phlobatannins (Table 2).

Table 2. Phytochemical screening of hydroalcholic extracts of SU.

Phytochemical tests	Extract
Saponins	++
Flavonoids	++
Alkaloids	+
Tannins	++
Anthraquinones	+
Phlobatannins	+
9-Octadecenoic acid (Z), methyl ester	++
Dodecanoic acid	++

+ Mild presence, ++ Strong presence, SU: Sumach

Inflammatory cytokines assessments

Interleukin 1 beta (IL-1β) (Abcam Cambridge, UK) and tumor necrosis factor-alpha (TNFα) (Abcam, Cambridge, UK) of testis samples were analyzed using ELISA approach. RIPA (Abcam, Cambridge, UK) lysed full testis proteins and centrifuged at 15,000 g for 30 min. 1:20 supernatants/dilutions ratio was implanted into covered microplates with antibodies to provoke enzyme-substrate interaction. Standard solutions for drawing standard curves were also hired. ELISA kits explored the protein levels in supernatant divisions. Absorbance percentage was measured at 450 nm (Jalili et al., 2019b).

Statistical evaluation

Kruskal–Wallis was used to assess data normality and variance homogeneity at significance of 0.05. Both data analyzes were conducted using SPSS Statistics ver. 16 (SPSS Inc., Chicago, IL, USA). Variance analysis (ANOVA) was used. Mean ± standard error of mean and $P<0.05$ were considered to be statistically significant.

Sperm viability, motility, count, and morphology

MO, due to the inhibitory aspects, limited viability, progressive motility, and count of sperms, and even substantially improved typical morphology to pathological form compared to normal category ($P < 0.01$). Compared to standard group, SU displayed no significant alterations in SU (200, 400, and 800 mg/kg) groups ($P > 0.05$). Furthermore, these parameters were significantly enhanced in both SU (200, 400 and 800 mg/kg) and MO + SU (200, 400 and 800 mg/kg) groups compared to MO group (Table 3).

GLH

MO diminished GLH value in the MO group more than the normal group ($P < 0.01$). SU had no significant effects on SU group compared to the control group ($P > 0.05$). In SU (200, 400 and 800 mg/kg) and MO+SU (200, 400 and 800 mg/kg) groups, the GLH value was slightly higher than in the MO group ($P < 0.01$) (Fig. 1). Figure 2 demonstrated the GLH histopathological characteristics.

Table 3. Effect of SU and MO on sperm parameters (n=8).

Groups	Mean of sperm count (106)	Sperm progressive motility (%)	Sperm viability (%)	Normal sperm morphology (%)
Normal	93.36±4.64	33.36±3.10	91.36±6.8	82.64±4.62
MO	41.08±3.59*	5.39±0.33*	35.65±3.35*	31.83±2.11*
SU 200mg/kg	92.64±6.78†	31.34±3.61†	92.71±5.18†	81.04±3.09†
SU 400 mg/kg	94.82±6.77†	35.28±4.71†	90.03±5.94†	78.41±4.64†
SU 800 mg/kg	93.66±3.91†	33.12±4.34†	89.66±6.20†	83.64±6.71†
MO+SU 200 mg/kg	64.71±3.34¶	15.36±2.82¶	62.71±3.14¶	59.71±3.32†
MO+SU 400 mg/kg	59.55±4.85¶	12.81±3.43¶	60.38±4.72¶	59.91±4.02†
MO+SU 800 mg/kg	58.01±3.40¶	12.69±2.02¶	48.71±3.22¶	48.09±4.19†

Data presentation as mean ± SEM. * P < 0.01 compared to the normal group. † P < 0.01 compared to MO group. ¶ P < 0.01 compared to the MO group. MO: Morphine, SU: *Sumach*.

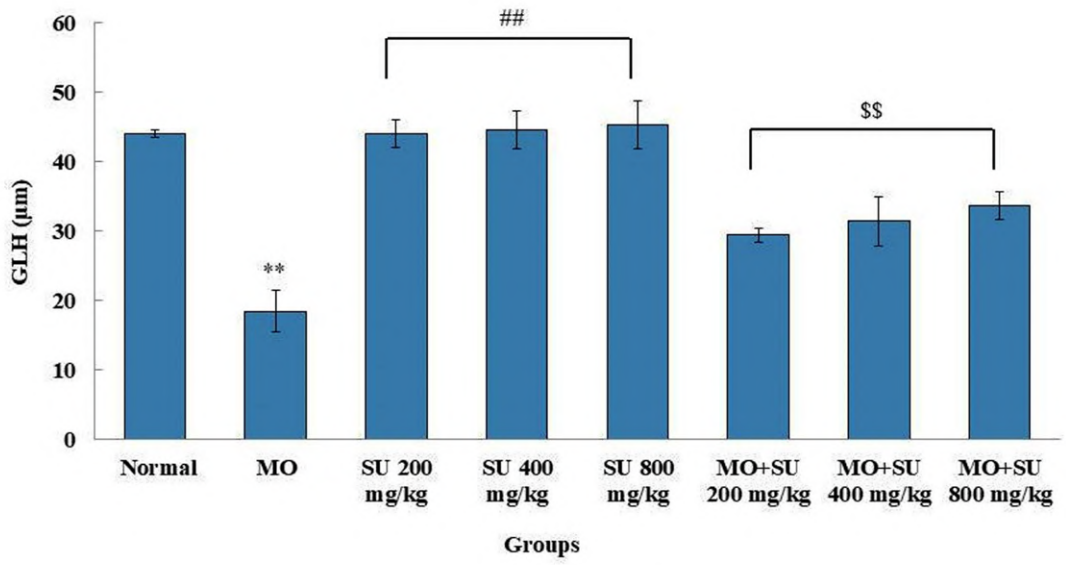

Fig. 1.- Comparison of GLH in all groups. **Significant reduction in MO group than normal group (P < 0.01). ## Significant differences in SU (200, 400 and 800 mg/kg) groups than MO group (P < 0.01). $$ Significant alteration in SU (200, 400 and 800 mg/kg) + MO groups than MO group (P < 0.01). MO: Morphine, SU: Sumach, GLH: Germinal layer height.

TAC

MO reduced TAC serum concentrations in the MO group in comparison with the normal group (P < 0.01). Also, SU elevated TAC levels in both SU ((200, 400 and 800 mg/kg) and MO + SU (200, 400 and 800 mg/kg) groups in comparison with the MO group (P < 0.01) (Fig. 3).

Testosterone levels

MO substantially decreased testosterone levels in the MO group in comparison with the normal group (P < 0.01). There were no significant biochemical differences in the SU group if compared to the normal group (P > 0.05). Similarly, testosterone in both SU (200, 400 and 800 mg/kg) and MO + SU (200, 400 and 800 mg/kg) groups displayed slightly higher amounts than MO (P < 0.01) (Fig. 4).

Gene expression rates

Up-regulated modifications of apoptotic p53 and caspase-3 genes and down-regulated differences of Bcl2 gene in MO-treated animals were identified as significant (P < 0.01). Similarly, a significant down-regulation of p53 and caspase-3 genes and up-regulated Bcl2 apoptotic gene were characterized in all SU doses and MO+SU (200, 400 and 800 mg/kg) groups than MO group (Fig. 5).

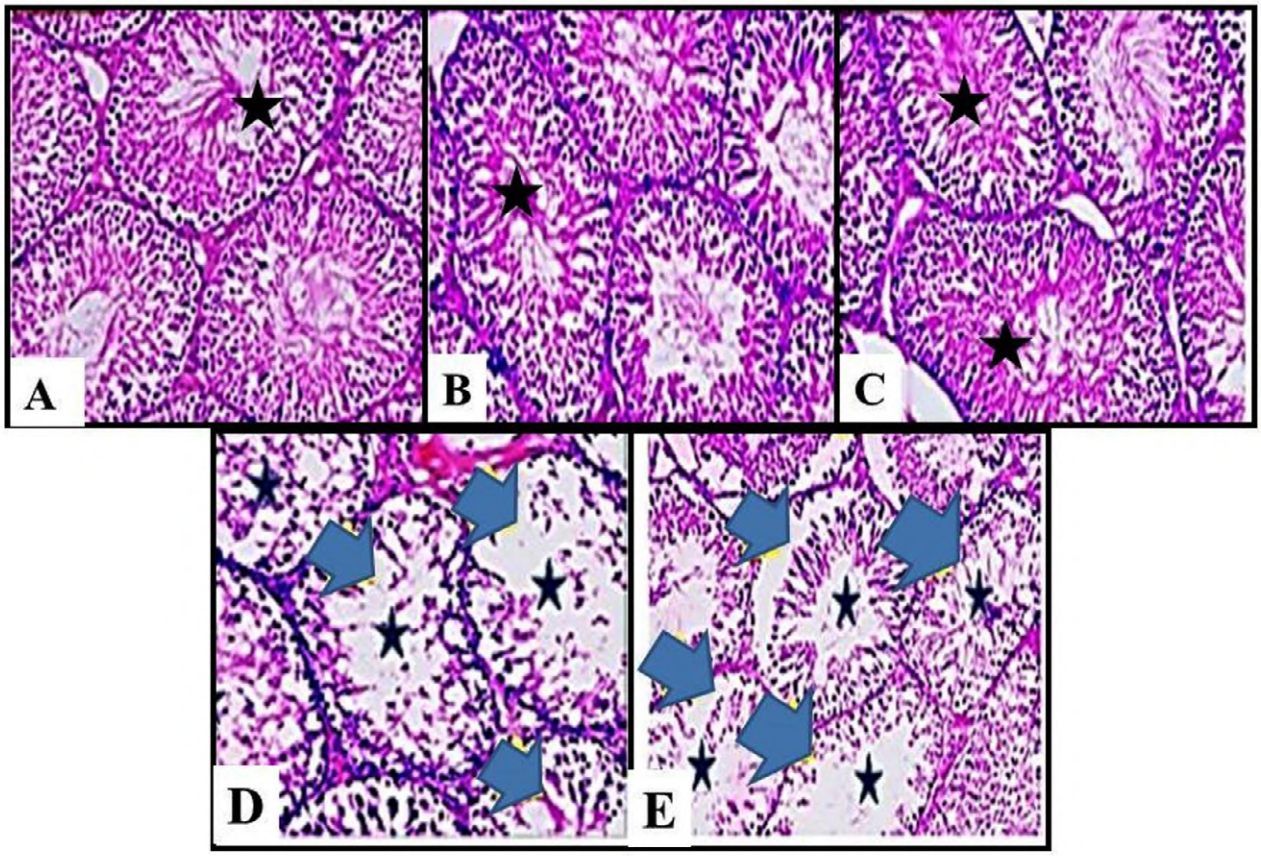

Fig. 2.- Effects of MO and SU on GLH value (×40). Healthy GLH structure was detected in groups of **A** (normal), **B** (SU, 800 mg/kg) and **C** (SU + MO, 800 mg/kg). A decreased level in GLH and sperm cells within the seminiferous tubule was observed in MO groups (**D** and **E**). Blue arrows indicated GLH value (decreased in GLH and irregularities in morphology of seminiferous tubule margin); and stars indicate sperm cells. MO: Morphine, SU: *Sumach*, GLH: Germinal layer height.

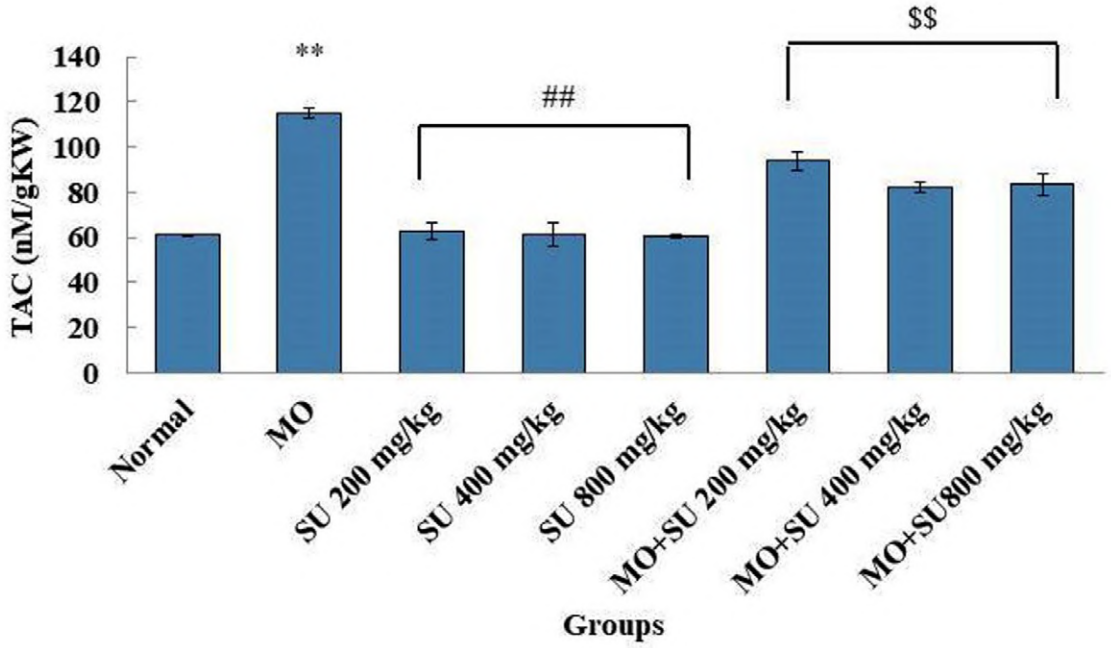

Fig. 3.- Comparison of TAC among treatment groups. **Significant reduction in MO group compared to normal group ($P < 0.01$). ##Significant increase in SU (200, 400 and 800 mg/kg) groups compared to MO group ($P < 0.01$). $$ Significant increase in SU (200, 400 and 800 mg/kg) + MO groups compared to MO group ($P < 0.01$). MO: Morphine, SU: Sumach.

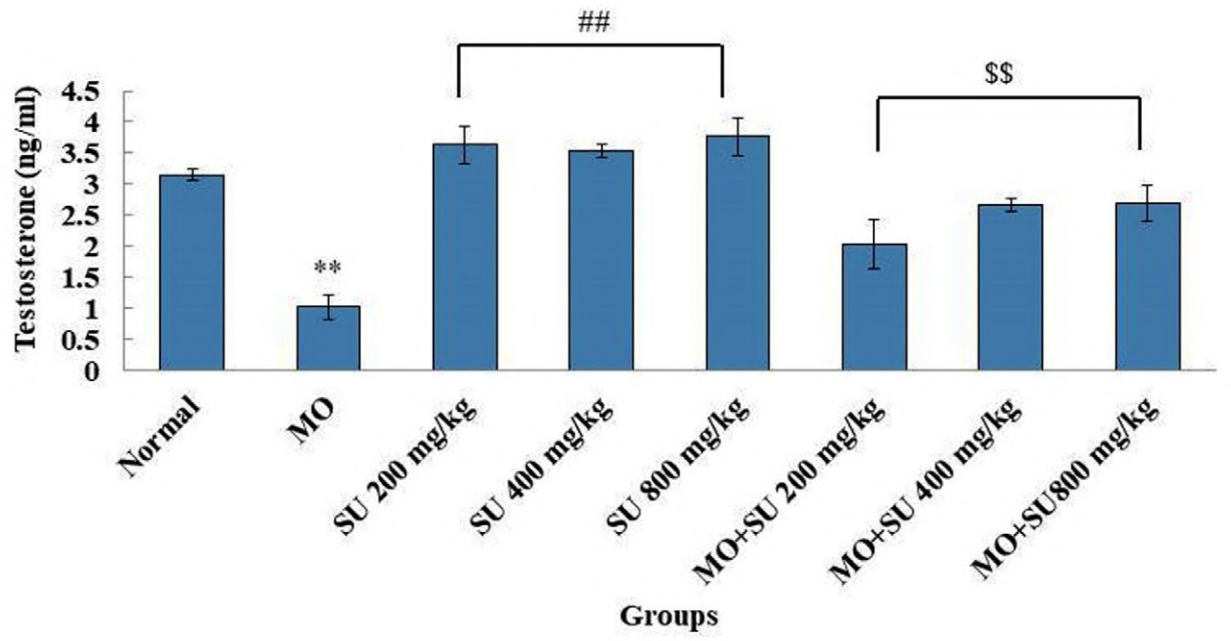

Fig. 4.- Comparison of testosterone hormone levels among treatment groups. **Significant decrease in MO group compared to normal group ($P < 0.01$). ## Significant increase in SU (200, 400 and 800 mg/kg) groups compared to MO group ($P < 0.01$). $$ Significant increase in SU (200, 400 and 800 mg/kg) + MO groups compared to MO group ($P < 0.01$). MO: Morphine, SU: Sumach.

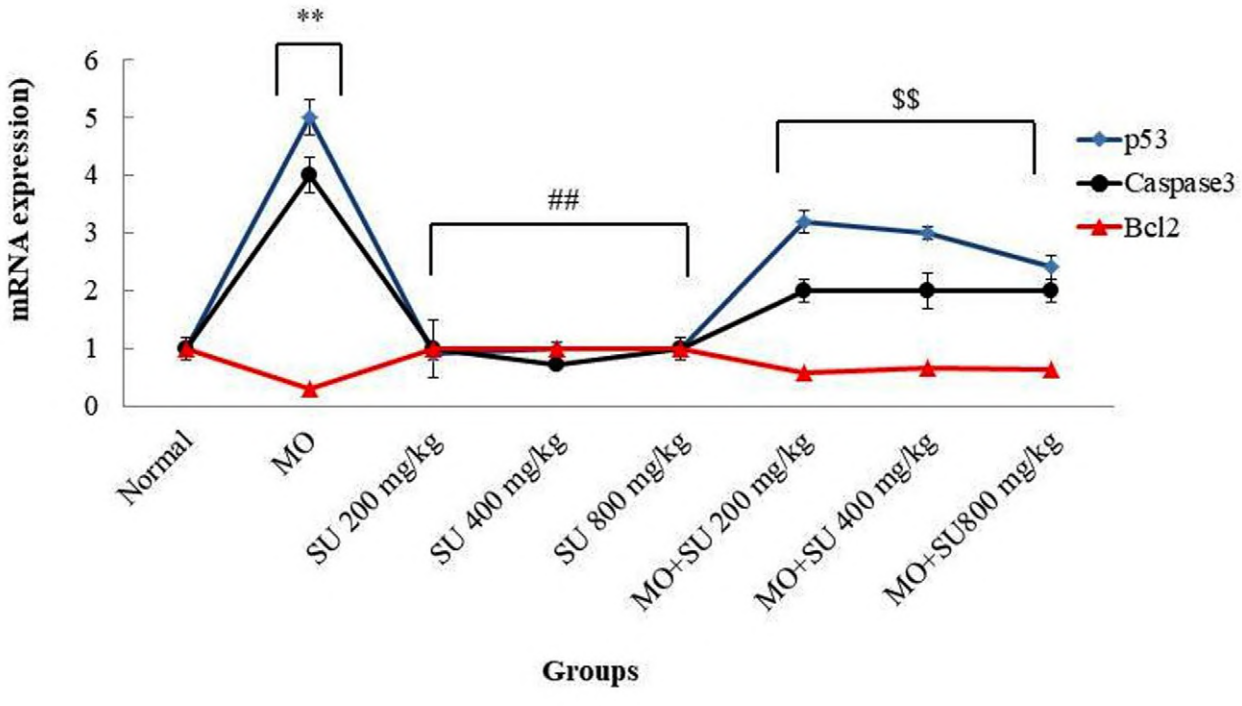

Fig. 5.- Effects of SU on Caspase 3, p53 and Bcl2 genes expression in normal, MO, and SU (200, 400 and 800 mg/kg) groups. ** Statistically significant ($P < 0.01$) between MO and normal groups. ## Statistically significant ($P < 0.01$) between SU and MO groups. $$ Significant increase in SU (200, 400 and 800 mg/kg) + MO groups compared to MO group ($P < 0.01$). MO: Morphine, SU: *Sumach.*

Inflammatory cytokines

In the morphine group, the inflammatory cytokines were elevated significantly if compared to the normal group ($P < 0.01$). No significant variations were observed in inflammatory cytokines in all SU groups, which remained similar to the normal group ($P > 0.05$). Subsequently, multiple doses of SU (200, 400 and 800 mg/kg) in SU and MO+SU (200, 400 and 800 mg/kg) groups exhibited a significant reduction in inflammatory cytokines compared to the MO group ($P < 0.01$) (Table 4).

According to the results of this study, there was no significant relationship between various increasing doses of SU and its effects on sperm parameters compared to the MO group. Besides, all doses of SU increased the quality of sperm parameters compared to the MO group. It is noteworthy to state that in the present study, the MO group was compared with the control group, and also the SU+MO groups was compared with MO group. All doses of SU in this group improved the quantity of sperm parameters. This phenomenon suggested that the therapeutic effects of SU are not related to dose. Previous studies on acceleration of sperm parameters using other antioxidant plants and morphine showed similar results (Jalili et al., 2016; Salahshoor et al., 2018).

Table 4. Effects of MO and SU on testicular levels of TNFα and IL-1β (n=8 for each group).

Groups	TNFα (pg/ml)	IL-1β (pg/ml)
Normal	75.88±4.2	102.44±9.0
MO	162.34±9.1*	222.34±11.4*
SU 200 mg/kg	70.71±5.3†	99.82±6.4†
SU 400 mg/kg	68.08±4.8†	103.71±9.3†
SU 800 mg/kg	72.64±4.9†	101.34±8.0†
MO+SU 200 mg/kg	110.82±8.3¶	141.83±7.5¶
MO+SU 400 mg/kg	109.64±9.2¶	133.73±10.7¶
MO+SU 800 mg/kg	99.78±3.4¶	130.83±8.3¶

Data presentation as mean ± SEM. * $P < 0.01$ compared to the normal group. † $P < 0.01$ compared to MO group. ¶ $P < 0.01$ compared to the MO group. MO: Morphine, SU: *Sumach*.

Hydro-alcoholic extract of SU with antioxidant efficacy

SU extract demonstrated higher antioxidant capacity in comparison to the standard value of butylates hydroxytoluene (Fig. 6).

DISCUSSION

MO administration creates free radicals which damage male reproductive system leading to minimized sperm parameters index. This harmful transition refers to oxidative characteristics of MO. As suggested previously, the harmful effects of MO could be decreased if it is administered with an antioxidant substance. According to extensive application of MO in medical interventions, the objective of this project was to prevent detrimental symptoms of MO on male reproductive system through an herbal antioxidant.

SU has varied benefits from conventional to modern medical sciences. This herb was first known for its abundance in the Western regions of Iran and usage in conventional medicine. Yet, the physiological functions of SU to relieve oxidative effects of MO is now uncertain. Based on the findings of this analysis, SU repelled MO's oxidative impact on sperm parameters. As we know, the male reproductive system is amongst the most important organs affected by free radicals of MO implementation. Furthermore, the SU seems to have inhibition effects on oxidative stress induced by other opioids. Based on significant statistical findings, medical MO intervention could decrease detrimental effects on total serum

antioxidant potential and fertility indices. MO also increased the levels of inflammatory cytokines and apoptotic genes expression (P53 and Caspase 3) in spermatogenic cell lines. Moreover, hydro-alcoholic extract of SU increased TAC levels and reproduction parameters in MO+SU (200, 400 and 800 mg/kg) groups by its antioxidant capabilities. In medical researches, MO is recognized as an effective promoter of oxidative stress production, especially in testes. Oxidative stress in reproductive organs induces mitochondrial ROS deposition, lipid peroxidation, and enzyme activity limitation (Jalili et al., 2019a). Tuerxun et al. (2019), in an experimental research, show that MO can stimulate hepatocarcinogenesis process in male rats.

TAC serum levels are considered a guideline for antioxidant levels. In this report, this value was decreased significantly. Whole genetic structures are vulnerable to ROS attacks, including nuclear DNA, mitochondrial DNA, and different cytoplasmic RNA classes. In ROS attack, the vital cellular and mitochondrial activities can also be interrupted, particularly in germ cells (Barroso et al., 2000). Instability of spermatogenesis and cellular and molecular processes could contribute to subfertility or infertility conditions (Houston et al., 2018). As such, all types of spermatogenic lines become vulnerable to free radicals' attacks (Leisegang et al., 2017). Parallel to our analysis, in an analytical study performed by Khan et al. (2013), it was concluded that MO could theoretically trigger the abnormal ROS level in cells. They reported that deformity, motility, and numbers of sperm cells are affected. Testosterone serum levels were also declined. In the primary ROS attack, the membrane was affected by lipid peroxidation. Also, ROS attacked to protective enzymes in sperm cytoplasm is reported. A large amount of cytoplasm was discarded in spermatogenesis, contributing to a weakened immune system. During ROS attack, Ca^{2+} channels in smooth endoplasmic retinaculum (SER) is also interrupted. This mechanism reduced sperm motility (Roshankhah et al., 2020). Non-motile sperms often report a decreased glutathione amount in their cytoplasm (Gomez et al., 1998).

Medical evidence has shown that every type of fatty acid oxidation induced by ROS attack can lead to reduced progressive sperm motility (Jalili et al., 2016). As described in the experimental research by Jalili et al. (2014), nicotine-induced oxidative stress can decrease sperm count, fertility index, testosterone level, and sperm motility. SU (200, 400 and 800 mg/kg) and MO+SU (200, 400 and 800 mg/kg) groups displayed a dramatic improvement in sperm parameters if compared to MO group, suggesting antioxidant effects of SU (Kosar et al.,

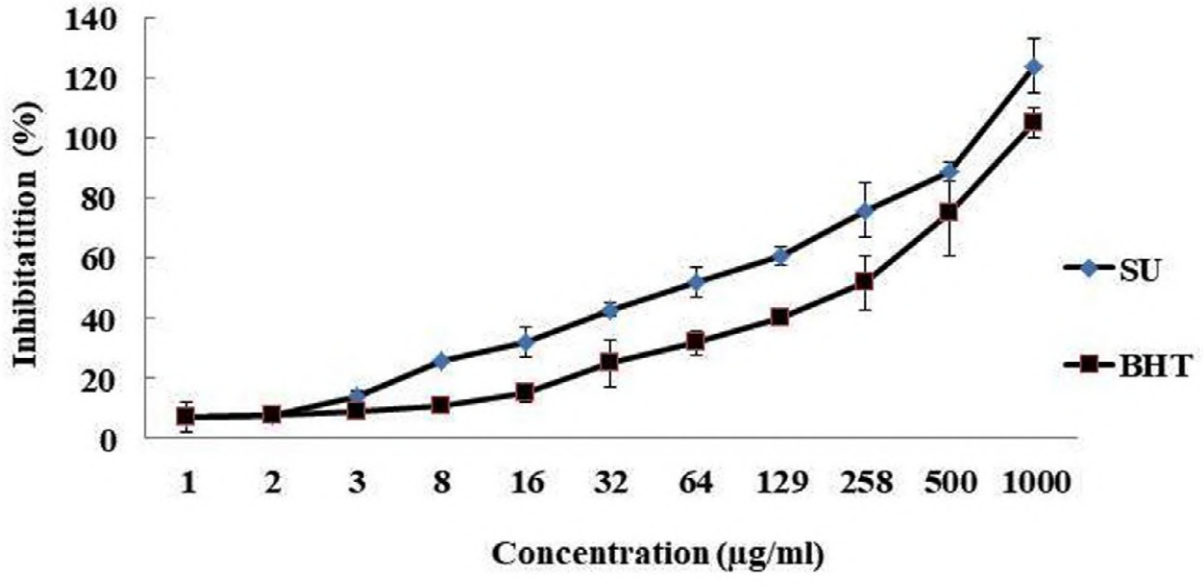

Fig. 6.- Antioxidant activities of different dilutions of hydro-alcoholic extract of SU in comparison with Butylate hydroxytoluene. SU: *Sumach*.

2008). Biochemical composition of semen fluid suggested the existence of a strong antioxidant mechanism which compensates for this system's deficiency in sperm with low cytoplasm content (Jalili et al., 2016). In relation to the findings of this research, Ahangarpour et al. (2014), also found that sperm parameters can be elevated in diabetic mice. Salimi et al. (2015), have reported that SU has antioxidant properties on diabetic animals induced by Streptozotocin. SU could disable receptor-alpha co-activator mechanism. This phenomenon triggers adenosine monophosphate protein kinase, and regulate mitochondrial activity (Kahale et al., 2015). TAC levels were higher in SU (200, 400 and 800 mg/kg) and SU (200, 400 and 800 mg/kg) + MO groups. In this research, following SU prescription, TAC levels were elevated showing anti-lipid peroxidation and antioxidant effects of SU. Testosterone and GLH levels were also decreased in MO group. Moreover, following implementation of SU (in SU (200, 400 and 800 mg/kg) and MO+SU (200, 400 and 800 mg/kg) groups), the GLH index appears to increase level, presumably based on the presence of Saponins and Flavonoids (Nozza et al., 2020). MO infiltration into intracellular cell-matrix can lead to damage of genetic material, induction of lipid peroxidation, and enzyme deformation (such as superoxide and hydrogen peroxide) (Jalil et ali., 2014). These biological changes, along with alteration of morphological feature,s could cause seminiferous tubules and apoptosis atrophy in specialized cells from germ cells, Sertoli cells, to Leydig cells (Roshankhah et al., 2020). Elevated blood flow is often recorded due to the SU administration (Ahangarpour et al., 2014). Cytochrome-c channels release cellular tumor antigen p53 to regulate the activities of key pro-apoptotic factors, including Bax, caspases, and endonucleases (Li et al., 2020). MO up-regulates these variables. Based on their intrinsic structure, the cells can escape from oxidants, but this aspect is significantly diminished by the presence of MO (Maher et al., 2020). In spermatogenesis, the apoptotic Fas/FasL cascade is widely used. However, in impaired testes, the caspase-3 and cytochrome-c expression could elevate the apoptotic rate (Wang et al., 2012). As Ibrahim et al. (2019), revealed the same results, the MO up-regulated caspase-3 genes and apoptosis frequencies.

MO increased expression of inflammatory factors. Experimental animal studies showed a strong link towards NO levels and inflammatory factors in lipopolysaccharide-induced lung damage (Somasundaram et al., 2020). In allergic rhinitis conditions, the concentrations of pro-inflammatory cytokine were diminished after SU prescription (Gharaei et al., 2020). There is a typical significant correlation among NO, TLRs, and inflammatory cytokines. However, critical role of cell lines in intercellular relationship between certain TLR and pro-inflammatory cytokine cannot be dismissed during inflammation. Equally, we expected a decent positive association between NO and TNFα expression in MO-induced testicular inflammation, and IL-1β, while SU reduced these dysfunctions and irregularities. These outcomes were exacerbated in the report by Jalili and colleagues. They established a relationship between TNFα and IL-6 in Acacetin-induced preventive cascade via antioxidants control in subsequent ischemia-reperfusion hepatitis (Roshankhah et al., 2020). The current study is valuable to describe either the IL-1β interaction or this dependency in MO administration and SU inflammation rescue.

CONCLUSION

In this research, SU amplified male infertility or subfertility triggered by MO contact. SU elevated TAC serum level, inflammatory cytokine and testosterone, changed impaired sperm parameters to physiological type, and arrested p53 and Caspase 3 gene expression. Thus, SU can improve the fertility rate or regain male infertility status dependent on natural antioxidants. Besides, further studies on animal models are required to achieve in-depth definitive proof of the molecular relationship between SU and MO, contributing to male reproductive degradation.

ACKNOWLEDGEMENTS

We gratefully acknowledge the Research Council of Kermanshah University of Medical Sciences for the financial support.

REFERENCES

ANWER T, SHARMA M, KHAN G, IQBAL M, ALI MS, ALAM MS, SAFHI MM, GUPTA N (2013) Rhus coriaria ameliorates insulin resistance in non-insulin-dependent diabetes mellitus (NIDDM) rats. *Acta Pol Pharm*, 70: 861-867.

AHANGARPOUR A, OROOJAN AA, HEIDARI H, EHSAN G, RASHIDI NOOSHABADI MR (2014) Effects of hydro-alcoholic extract of Rhus coriaria (Sumac) seeds on reproductive complications of nicotinamide-streptozotocin induced type-2 diabetes in male mice. *World J Men's Health*, 32: 151-158.

BARROSO G, MORSHEDI M, OEHNINGER S (2000) Analysis of DNA fragmentation, plasma membrane translocation of phosphatidylserine and oxidative stress in human spermatozoa. *Hum Reprod*, 15: 1338-1344.

ESFANDIARI E, ROSHANKHAH S, MARDANI M, HASHEMIBENI B, NAGHSH E, KAZEMI M, SALAHSHOOR M (2014) The effect of high frequency electric field on enhancement of chondrogenesis in human adipose-derived stem cells. *Iran J Basic Med Sci*, 17: 571-576.

ELLIS A, GRACE PM, WIESELER J, FAVRET J, SPRINGER K, SKARDA B, AYALA M, HUTCHINSON MR, FALCI S, RICE KC, MAIER SF (2016) Morphine amplifies mechanical allodynia via TLR4 in a rat model of spinal cord injury. *Brain Behav Immun*, 58: 348-356.

FAMITAFRESHI H, KARIMIAN M (2020) Reduction of anxiety level is associated with an oxidative-stress imbalance in the hippocampus in morphine administration period in male rats. *J Addict Dis*, 38: 1-7.

GHARAEI A, SHAFIE M, MIRDAR HARIJANI J, HASANEIN P, ARSHADI A (2020) Immune responses and haematological parameters changes of rainbow trout (Oncorhynchus mykiss) under effects of dietary administration of Sumac (*Rhus coriaria* L.). *J Agr Sci Tech*, 22: 173-186.

GHARAEI A, KHAJEH M, GHAFFARI M, CHOOPANI A (2013) Iranian Rhus coriaria (sumac) essential oils extraction. *TEOP*, 16: 270-273.

GONZÁLEZ R, BALLESTER I, LÓPEZ-POSADAS R, SUÁREZ MD, ZARZUELO A, MARTINEZ-AUGUSTIN O, MEDINA FS (2011) Effects of flavonoids and other polyphenols on inflammation. *Crit Rev Food Sci Nutr*, 51: 331-362.

GOMEZ E, IRVINE D, AITKEN R (1998) Evaluation of a spectrophotometric assay for the measurement of malondialdehyde and 4-hydroxyalkenals in human spermatozoa: relationships with semen quality and sperm function. *Int J Androl*, 21: 81-94.

HO TT, LE MT, TRUONG QV, NGUYEN VQ, CAO NT (2020) Psychological burden in couples with infertility and its association with sexual dysfunction. *Sexual Dis*, 38: 1-8.

HOSSEINIPOUR M, GOODARZI N, BAKHTIARI M (2019) Protective efficiency of Ashrasi date palm hydro-alcoholic extract against diabetes-induced testicular toxicity: A biochemical and stereological study. *Andrologia*, 51: e13420.

HOUSTON BJ, NIXON B, MARTIN JH, DE IULIIS GN, TRIGG NA, BROMFIELD EG, MCEWAN KE, AITKEN RJ (2018) Heat exposure induces oxidative stress and DNA damage in the male germ line. *Biol Reprod*, 98: 593-606.

IBRAHIM MA, SALAH-ELDIN AE (2019) Chronic addiction to tramadol and withdrawal effect on the spermatogenesis and testicular tissues in adult male albino rats. *Pharmacology*, 103: 202-211.

JABARI J, GHAFFARIFAR F, HORTON J, DALIMI A, SHARIFI Z (2019) Evaluation of morphine with imiquimod as opioid growth factor receptor or nalmefene as opioid blocking drug on leishmaniasis caused by leishmania major in vitro. *Iran J Parasitol*, 14: 394-406.

JALILI C, KHANI F, SALAHSHOOR MR, ROSHANKHAH SH (2014) Protective effect of curcumin against nicotine-induced damage on reproductive parameters in male mice. *Int J Morphol*, 32: 844-849.

JALILI C, AHMADI S, ROSHANKHAH S, SALAHSHOOR M (2016) Preventing effect of Genistein on reproductive parameter and serum nitric oxide levels in morphine-treated mice. *Int J Reprod BioMed*, 14: 95-102.

JALILI C, ROSHANKHAH S, JALALI A, SALAHSHOOR MR (2019a) Hepatoprotective activity of royal jelly on mercuric chloride–induced damage model in rats. *J Rep Pharma Sci*, 8: 181-187.

JALILI C, AKHSHI N, RAISSI F, SHIRAVI A, ALVANI A, VAEZI G, NEDAEI SE, GHANBARI A (2019b) Acacetin alleviates hepatitis following renal ischemia–reperfusion male Balb/C mice by antioxidants regulation and inflammatory markers suppression. *J Invest Surg*, 31: 1-8.

KHAN S, TELANG A, MALIK J (2013) Arsenic-induced oxidative stress, apoptosis and alterations in testicular steroidogenesis and spermatogenesis in Wistar rats: ameliorative effect of curcumin. *Wudpecker J Pharm Pharmocol*, 2: 33-48.

KOSAR M, BOZAN B, TEMELLI F, BASER KH (2007) Antioxidant activity and phenolic composition of sumac (Rhus coriaria L.) extracts. *Food Chem*, 103: 952-959.

KAHALE KH, TRANCHANT C, PAKZAD S, FARHAT AG (2015) Effect of sumac spice, Turkish coffee and yerba mate tea on the postprandial glycemic response to Lebanese mankoucheh. *Nutr Food Sci*, 11: 22-31.

KARAMI M, JAFARPOUR M, JALALI NADOUSHAN M (2019) Interaction of sulpiride with morphine in induction of male rat infertility. *J Basic Clin Pathophysiol*, 7: 6-11.

LI L, HAN X, GAO Y, DIAO Q, XIAO Y (2020) Ethanol extract of Gynura bicolor (GB) protects against UVB-induced photodamage of skin by inhibiting P53-mediated Bcl-2/BAX/Caspase-3 apoptosis pathway. *Arch Dermatol Res*, 312: 41-49.

LEISEGANG K, HENKEL R, AGARWAL A (2017) Redox regulation of fertility in aging male and the role of antioxidants: a savior or stressor. *Curr Pharm Design*, 23: 4438-4450.

MAHER DP, WALIA D, HELLER NM (2020) Morphine decreases the function of primary human natural killer cells by both TLR4 and opioid receptor signaling. *Brain Behav Immun*, 83: 298-302.

NOZZA E, MELZI G, MARABINI L, MARINOVICH M, PIAZZA S, KHALILPOUR S, DELL'AGLI M, SANGIOVANNI E (2020) Rhus coriaria L. fruit extract prevents UV-A-induced genotoxicity and oxidative injury in human microvascular endothelial cells. *Antioxidants*, 9: 292-299.

ROSHANKHAH SH, SALAHSHOOR MR, ARYANFAR S, JALILI F, SOHRABIL M, JALILI C (2017) Effects of curcumin on sperm parameters abnormalities induced by morphine in rat. *J Med Biomed Sci*, 6: 1-10.

ROSHANKHAH S, GHOLAMI MR, SALAHSHOOR MR (2020) Evaluation of male infertility treatment following Rhus coriaria extract administration on rats exposed to morphine. *Mol Biol Rep*, 23: 1-9.

SALIMI Z, ESKANDARY A, HEADARI R, NEJATI V, MORADI M, KALHORI Z (2015) Antioxidant effect of aqueous extract of sumac (Rhus coriaria L.) in the alloxan-induced diabetic rats. *Indian J Physiol Pharmacol*, 59: 87-93.

SHABBIR A (2012) Rhus coriaria linn, a plant of medicinal, nutritional and industrial importance: a review. *J Anim Plant Sci*, 22: 505-512.

SCHILIT SL, MENON S, FRIEDRICH C, KAMMIN T, WILCH E, HANSCOM C, JIANG S, KLIESCH S, TALKOWSKI ME, TÜTTELMANN F, MACQUEEN AJ (2020) SYCP2 translocation-mediated dysregulation and frameshift variants cause human male infertility. *J Hum Genet*, 106: 41-57.

SOMASUNDARAM V, GILMORE AC, BASUDHAR D, PALMIERI EM, SCHEIBLIN DA, HEINZ WF, CHENG RY, RIDNOUR LA, ALTAN-BONNET G, LOCKETT SJ, MCVICAR DW (2020) Inducible nitric oxide synthase-derived extracellular nitric oxide flux regulates proinflammatory responses at the single cell level. *Redox boil*, 28: 354-361.

SALAHSHOOR MR, HAGHJOO M, ROSHANKHAH S, MAKALANI F, JALILI C (2018) Effect of thymoquinone on reproductive parameter in morphine-treated male mice. *Adv Biomed Res*, 7: 212-219.

TUERXUN H, CUI J (2019) The dual effect of morphine on tumor development. *Clin Transl Oncol*, 21: 695-701.

TREMELLEN K (2008) Oxidative stress and male infertility; a clinical perspective. *Hum Reprod Update*, 14: 243-258.

WANG DH, HU JR, WANG LY, HU YJ, TAN FQ, ZHOU H, SHAO JZ, YANG WX (2012) The apoptotic function analysis of p53, Apaf1, Caspase3 and Caspase7 during the spermatogenesis of the Chinese fire-bellied newt Cynops orientalis. *PloS One*, 7: 145-151.

WARD P, MOSS HG, BROWN TR, KALIVAS P, JENKINS DD (2020) N-acetylcysteine mitigates acute opioid withdrawal behaviors and CNS oxidative stress in neonatal rats. *Pediatr Res*, 14: 1-9.

Possible protective role of L-thyroxin on the parotid gland of adult male albino rat in carbimazole induced hypothyroidism: histological, histomorphometry and ultrastructural study

Shaimaa A.R. Mostafa

Department of Anatomy and Embryology, Fayoum University, Egypt

SUMMARY

This study was carried out to throw more light on the histological, biochemical and immunohistochemical changes in the parotid gland of the adult male albino rat, following oral administration of Carbimazole and possible protective role of Levothyroxine sodium (L-Thyroxin). Fifty-five adult male albino rats (Sprague Dawley) were used. They were divided into four groups and eleven subgroups; five rats each; Animals were sacrificed and parotid specimens were processed for light and electron microscopic examination. Administration of Carbimazole resulted in significant damage in the parotid, which was more obvious with longer duration; most of the serous acini had irregular outlines, widely separated with narrow lumen and cytoplasmic vacuoles. Some acinar cells contained irregular, pyknotic or hyperchromatic nuclei. The interlobular and striated ducts appeared disrupted and dilated with cellular infiltration. Oral administration of L-Thyroxin significantly improves histological changes, expression of B cell lymphocyte (Bcl-2) and decrease collagen in Mallory-stained sections as were confirmed statistically. Induction of L-Thyroxin resulted in significant mitigating effects on damage of parotid gland. The results indicate that thyroid hormones administration causes parotid gland adaptation by augmenting endogenous antioxidants and protects rat parotid gland from oxidative stress associated with carbimazole-induced hypothyroidism and parotid gland atrophy.

Keywords: Thyroid hormones – Rat – Apoptosis – Carbimazole – Bcl-2

INTRODUCTION

Thyroid hormones (THs) are essential for physiological functions of almost all body tissues. They regulate reproductive functions, heart rate, body temperature, gastrointestinal motility and emotional stability. In addition, they control the metabolism of proteins, lipids and carbohydrates. Disruptions of thyroid function may produce

Corresponding author:
Shaimaa A.R. Mostafa. Department of Anatomy and Embryology, Fayoum University, Egypt. Phone: 01223698241. E-mail: Sar12@fayoum.edu.eg

Submitted: June 10, 2021. **Accepted:** November 15, 2021
Not final proof's revision by the authors
https://doi.org/10.52083/BGEK9578

various subclinical or clinical manifestations (Lamfon, 2014). THs are known to set the cellular basal metabolic rate, and are considered major regulators of energy metabolism, mitochondrial activity and biogenesi, oxygen consumption and active oxygen metabolism (Bhanja and Chainy, 2010). Thus, one of the most important functions performed by THs is the tight regulation of cellular oxygen consumption and consequent generation of reactive oxygen species (ROS) in several tissues (Petrulea et al., 2009), which can be attacked by the ROS for the initiation of lipid peroxidation (Vaidya et al., 2008). Hypothyroidism is one of the most common thyroid disorders, and may be congenital or acquired (Porth et al., 2004). It may result from dysfunction of the thyroid gland itself, impairment in mechanisms that control THs formation, or complications during treatment of hyperthyroidism. In humans, the hypothyroid state is a complex hormonal dysfunction rather than a single hormonal defect (Oncu et al., 2004), manifested largely by a reversible slowing down of all body functions (Dong, 2004).

Apart from general metabolic disturbance, impairment of THs production causes serious intellectual and behavioral abnormalities that may affect patient's daily functioning and result in additional stress and depression. Hypothyroid state led to increased levels of total cholesterol, low density lipoproteins and apolipoprotein B (El- Bassouny, 2012). It had been previously shown that THs increased the synthesis and mobilization of triglyceraldehydes stored in adipose tissue and lipoprotein-lipase activity (Pucci et al., 2000). Hypothyroidism is characterized by low metabolic rate resulting in adverse effect on many organs (Kiernan, 2015). Most of hypothyroid patients suffer from decreased gastrointestinal tract motility, malabsorption, loss of appetite and enlarged tongue (Rajab et al., 2017). It had been suggested that the parotid, the submandibular and in particular the sublingual glands were discernibly enlarged and served as a useful clue in the diagnosis of hypothyroidism (Fulop, 1989).

Apoptosis is a distinct process of cell death that is responsible for deletion of aged, injured and altered cells in normal and in certain specific pathologies like neoplasia. Indeed, the proper regulation of apoptosis is important in many aspects of life including development, homeostasis and disease biology (Khalawi et al., 2013). Bcl-2 family proteins are the regulators of apoptosis. Bcl-2 proteins have critical roles in normal cell physiology related to neuronal activity, autophagy, calcium handling, mitochondrial dynamics, energetics and other processes of normal healthy cells (Basanez and Hardwick, 2008). Bcl-2 family proteins consist of interacting partners includes inhibitors (anti- apoptotic) and inducers (pro apoptotic) of cell death. Together they regulate and mediate the process by which mitochondria contribute to cell death known as the intrinsic apoptosis pathway. This pathway is required for normal embryonic development and for preventing cancer (Basanez and Hardwick, 2008), so in the current work, immunohistochemical expression of Bcl-2 was performed. Hypothyroidism results in lower expression of Bcl-2 along with a high level of expression of Bax. These results suggest that THs promotes the expression of Bcl-2 genes, thus preventing apoptosis of early differentiating cells. However, under hypothyroid conditions, the downregulation of the anti-apoptotic Bcl-2 gene shifts the balance towards extensive apoptosis.

MATERIALS AND METHODS

Chemicals

Carbimazole (Neomercazol): is an antithyroid drug; obtained from Chemical Industries Development Co., Egypt; in a tablet form; each tablet contains 5mg. The tablet was crushed, dissolved in saline (1 ml/kg., bw) and given to the rats using gastric tube in a dose of 0.05 mg/Kg, bw. daily (Dakine et al., 2000).

Levothyroxine sodium (L-Thyroxin): is a thyroxin hormone analogue, was obtained from Glaxo Welcome Co., Egypt, in a tablet form. Each tablet contains 50 µg. Each tablet was crushed and dissolved in saline (1 ml/kg, bw) and was administered in a dose of 10 µg/100g bw, orally using gastric tube daily (Dakine et al., 2000).

Animals

Fifty-five adult male albino rats of Sprague Dawley strain, ageing 5-6 months, weighing 200-250 g. each, were used in the present study. They were obtained from the animal house, Faculty of Medicine, Cairo University. They were housed in cages (5 rats per cage). All animals were kept in clean, properly ventilated cages, exposed to regular light cycles of 12/12-10/14 hours light and dark with room temperature range for rat housing between 20 and 26ºC, and were supplied with food and water ad libitum. Ethical Committee Permission number is: cu III f 1 19. The rats were divided randomly into four groups and eleven subgroups as follows:

Group I (normal control): The rats in this group were divided into three subgroups of five rats each as follows: Group Ia: Normal control group; the rats did not receive any medications for three successive 3 weeks and were then sacrificed. Group Ib: Normal control group; the rats did not receive any medications for six successive weeks and were then sacrificed. Group Ic: Normal control group; the rats did not receive any medications for nine successive weeks and were then sacrificed.

Group II (sham control): The rats in this group were divided into three subgroups of five rats each as follows: Group IIa: the rats were given normal saline orally by gastric tube for three successive weeks, and were then sacrificed. Group IIb: the rats were given normal saline orally by gastric tube for six successive weeks, and were then sacrificed. Group IIc: the rats were given normal saline orally by gastric tube for nine successive weeks, and were then sacrificed.

Group III (medical hypothyroidism group): The rats in this group were divided into three subgroups of five rats each as follows: Group IIIa (medical Hypothyroidism, short duration): the rats in this group were given Carbimazole orally by gastric tube in a dose of 0.05 mg/kg daily for three successive weeks, and then they were sacrificed 24 hours after the last dose (Dakine et al., 2000). Group IIIb (medical Hypothyroidism, long duration): the rats in this group were given Carbimazole daily for six successive weeks, and then they were sacrificed 24 hours after the last dose. Group IIIc (medical Hypothyroidism, recovery group): the rats of this group were given Carbimazole orally daily for six successive weeks then were left without any medication for another 3 weeks, and then they were sacrificed.

Group IV (L-Thyroxine supplemented group): The rats in this group were divided into two subgroups as follows: Group IVb (L-Thyroxine supplemented group, short duration): the rats in this group were given Carbimazole orally daily for three successive weeks then L-Thyroxine was given orally in a dose of (10 µg/100g bw) daily for another three successive weeks (El-Bassouny, 2012), then they were sacrificed 24 hours after the last dose of L-Thyroxine. Group IVc (L-Thyroxine supplemented group, long duration): the rats in this group were given carbimazole orally daily for six successive weeks, thereafter L-Thyroxine was given orally daily for three successive weeks (Dakine et al., 2000). The rats were then sacrificed after the last dose of L-Thyroxine.

At the end of the allowed experimental period for each group, the rats were sacrificed (without euthanasia, cervical decapitation method was used). Blood samples were rapidly collected from rat tail and used for biochemical examinations. The parotid glands were extracted from all animals and then prepared for histological study (light and electron microscopic study).

Biochemical investigations

The mean serum T3, T4 and TSH were measured in each group. This was done in the Biochemistry Department, Faculty of medicine, Cairo University (El-Wakf et al., 2009).

Tissue preparation for histological study

Light microscopic study: specimens were fixed in formol saline and were processed for paraffin sections of 5 µm-thick stained with (Bancroft and Gamble, 2008): (a) Hematoxylin and Eosin (Avwioro. 2010), to observe the parotid gland architecture; (b) Mallory's trichrome stain (Ross and Michael, 2011), to evaluate the collagen fibers; (c) Immunohistochemical Study (Bcl-2) (Kiernan, 2015) were carried out using the avidin biotin peroxidase system for localization of Bcl-2 protein.

Morphometric study

This was carried out by using Leica Qwin 500 Image Analyzer Computer System. The percentage of the area of collagen tissue fibers in Mallory trichrome stained sections and Immunohistochemical optical density were examined.

Statistical analysis

The data obtained (serum total T3, serum total T4, serum TSH) and area percent of collagen for all groups were expressed as means ($\bar{X}$) and standard deviations (SD) and subjected to statistical analysis using one-way analysis of variance (ANOVA) for comparison between the different groups (more than two groups). The level $P \leq 0.05$ was considered the cut-off value for significance. All statistical analysis was done using the (SPSS) version 18 packages.

RESULTS

Histological results

Groups I and II: Light microscopic examination showed no observable difference in the histological findings between the normal and the sham control groups were noticed; sections of the parotid gland were composed of several lobes of different sizes. Each lobe comprised several lobules; consisted of numerous serous acini, lying close to one other and were separated by a fine network of an inter-acinar connective tissue. Each serous acinus was composed of cuboidal cells with basal rounded nuclei and narrow lumina with homogenous acidophilic cytoplasm (Fig. 1A, 1B). The striated ducts were lined by columnar cells with central rounded nuclei (Fig. 1A). Excretory interlobular ducts were present within the interlobular connective tissue, with wide irregular lumina and lined with pseudo stratified columnar epithelium (Fig. 1A, 1B). Blood vessels were seen in the connective tissue septa (Fig. 1A, 1B). Mallory's trichrome stained sections demonstrated a thin layer of collagen fibers present around the serous acini, blood vessels and the ducts (Fig. 2A, 2B). Immunohistochemical stained sections showed strong immune reaction for Bcl-2 in the cytoplasm of parotid cells (Fig. 3A, 3B). Electron microscopic examination of parotid gland sections of the control group showed serous acini with basal euchromatic nuclei and prominent nucleoli. Their cytoplasm presented many electron-lucent secretory granules (Fig. 4A, 4B). The nuclei of the acinar cells were surrounded by extensive rough endoplasmic reticulum (Fig. 4A).

Group IIIa: Hematoxylin and eosin-stained sections showed degenerative change in the form of some of serous acini which showed irregular outlines and were widely separated. Some acinar cells had deeply stained nuclei. Other acini appeared normal. Extravasated blood and cellular infiltration were also found in the interstitial space. The interlobular ducts and striated ducts appeared disrupted and dilated (Fig. 1C). Mallory's trichrome stained sections revealed apparently increased collagen fibers deposition in between lobules and around blood vessels (Fig. 2C). Immunohistochemical stained sections showed moderate expression of Bcl-2 protein in the cytoplasm of parotid gland cells and ducts (Fig. 3C) indicating damage caused by the drug. Electron microscopic examination showed condensed heterochromatic nucleus of the acinar cells, dilated rough endoplasmic reticulum and multiple cytoplasmic vacuolations; swollen mitochondria were seen and the rough endoplasmic reticulum was markedly dilated. Also, normal mitochondria with intact cristeal appearance could be detected (Fig. 4C). Group IIIb: Hematoxylin and eosin-stained sections showed marked degenerative changes than group IIIa; most of serous acini were atrophic with indistinct outline with mononuclear cellular infiltration. The cell cytoplasm was not uniformly stained and showed clear unstained vacuolar spaces. Dilated and congested blood vessels were also seen. Dilated irregular intercalated ducts were seen (Fig. 1D). Mallory's trichrome stained sections revealed extensive collagen fibers deposition more than group III a in between lobules and around blood vessels (Fig. 2D), indicating more destruction with longer duration. Immunohistochemical stained sections showed moderate (Fig. 3D) expression of Bcl-2 protein in the cytoplasm of parotid gland cells and ducts indicating more damage caused with longer duration. Electron microscopic

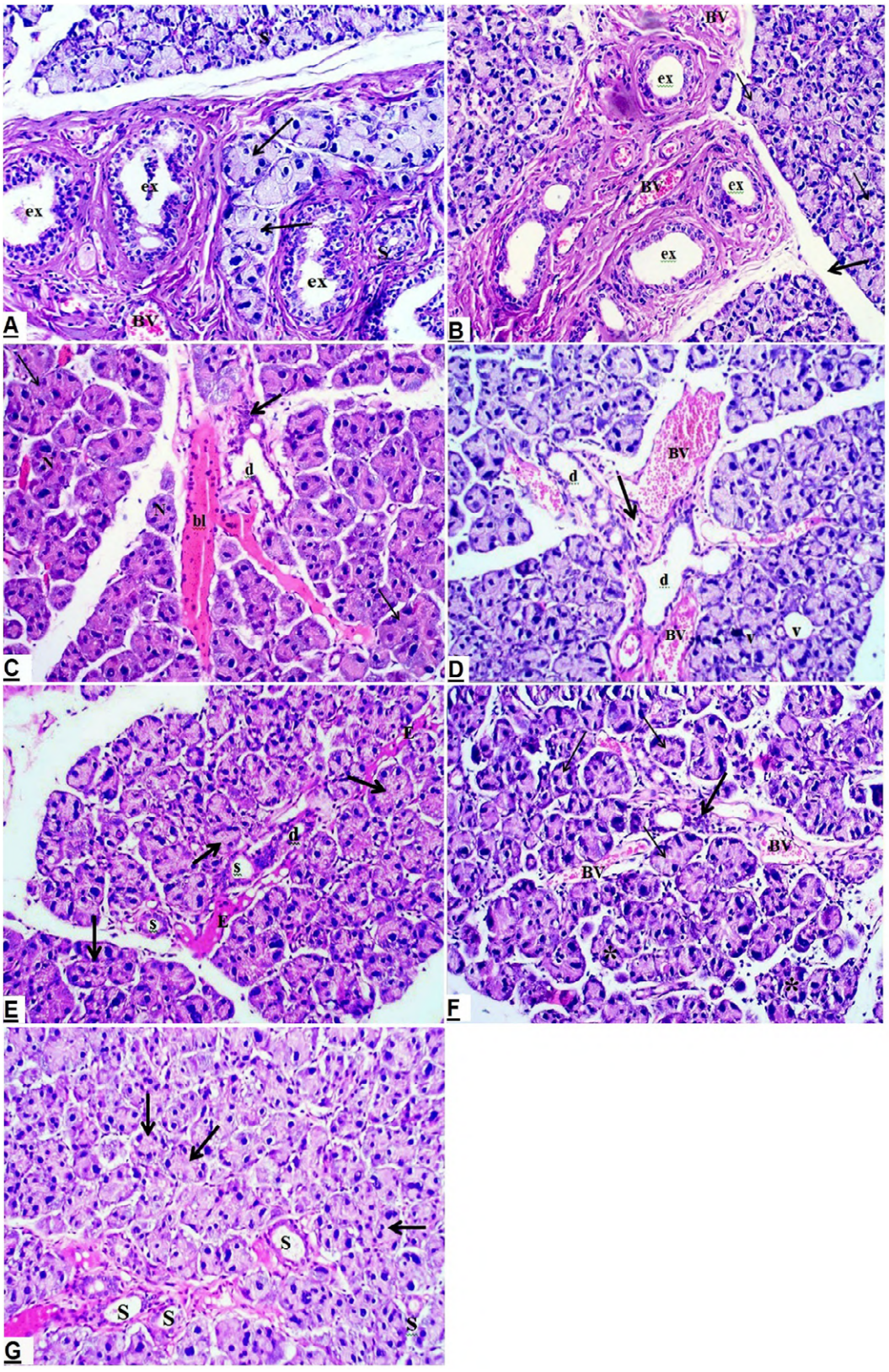

Fig. 1.- Sections of the parotid gland. **A**. group I showing normal serous acini (arrows) lined with cuboidal cells, striated duct(s) has rounded narrow lumen surrounded by simple columnar cells, excretory interlobular ducts (ex) have wide irregular lumina; lined with pseudo stratified columnar epithelium. Blood vessels (BV) are seen in the connective tissue septa; **B**. group II showing normal serous acini (thin arrows) composed of cuboidal cells with basal rounded nuclei and narrow lumens. Thin connective tissue septa in between the lobules (thick arrow) are seen rich in blood vessels (BV) and excretory interlobular ducts (ex) have wide irregular lumina; lined with pseudo stratified columnar epithelium; **C**. group IIIa showing the acini with irregular outlines (thin arrows). The cells of these acini contain darkly stained nuclei and others appear normal (N). Dilated intercalated duct (d), inflammatory cellular infiltration (thick arrow) and extravasated blood (bl) are seen; **D**. group IIIb showing cytoplasmic vacuoles (V) in the serous acini. Dilated irregular intercalated ducts (d), inflammatory cellular infiltration (thick arrow), and dilated congested blood vessels (BV) are seen. **E.** group IIIc showing apparently normal acini (arrows), striated ducts (s) and intercalated ducts (d). Interstitial hemorrhagic exudate (E) is present. **F**. group IVb showing serous acini regaining their normal architecture (thin arrows), others are irregular (star). Blood vessels (BV) are normal but inflammatory cells (thick arrow) could be detected. **G.** group IVc showing the serous acini restoring their normal architecture (arrows) and apparently normal striated ducts(S). Hematoxylin & Eosin, x200.

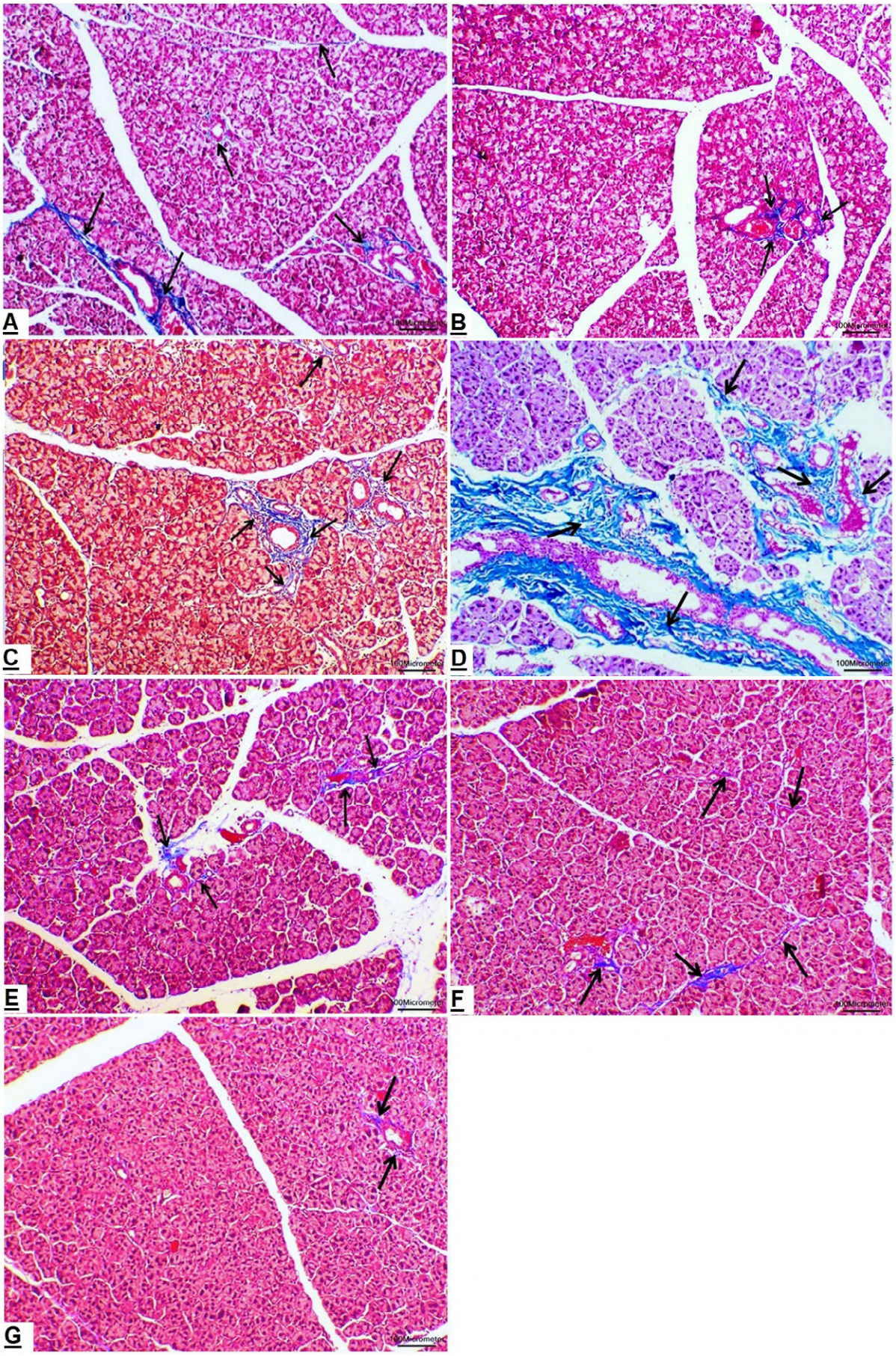

Fig. 2.- Sections of the parotid gland. **A**. showing thin layer of collagen fibers in between the lobules, around blood vessels and the ducts (arrows); **B**. thin layer of collagen fibers around blood vessels and the ducts (arrows); **C.** increased collagen fibers deposition in between lobules and around blood vessels (arrows); **D**. collagen fibers deposition in wide areas between the lobules and around blood vessels (arrows); **E**. minimal amount of collagen fibers (arrows) in between the acini and around blood vessels. **F** and **G.** minimal amount of collagen fibers in between the lobules and around blood vessels (arrows). Mallory T, x100.

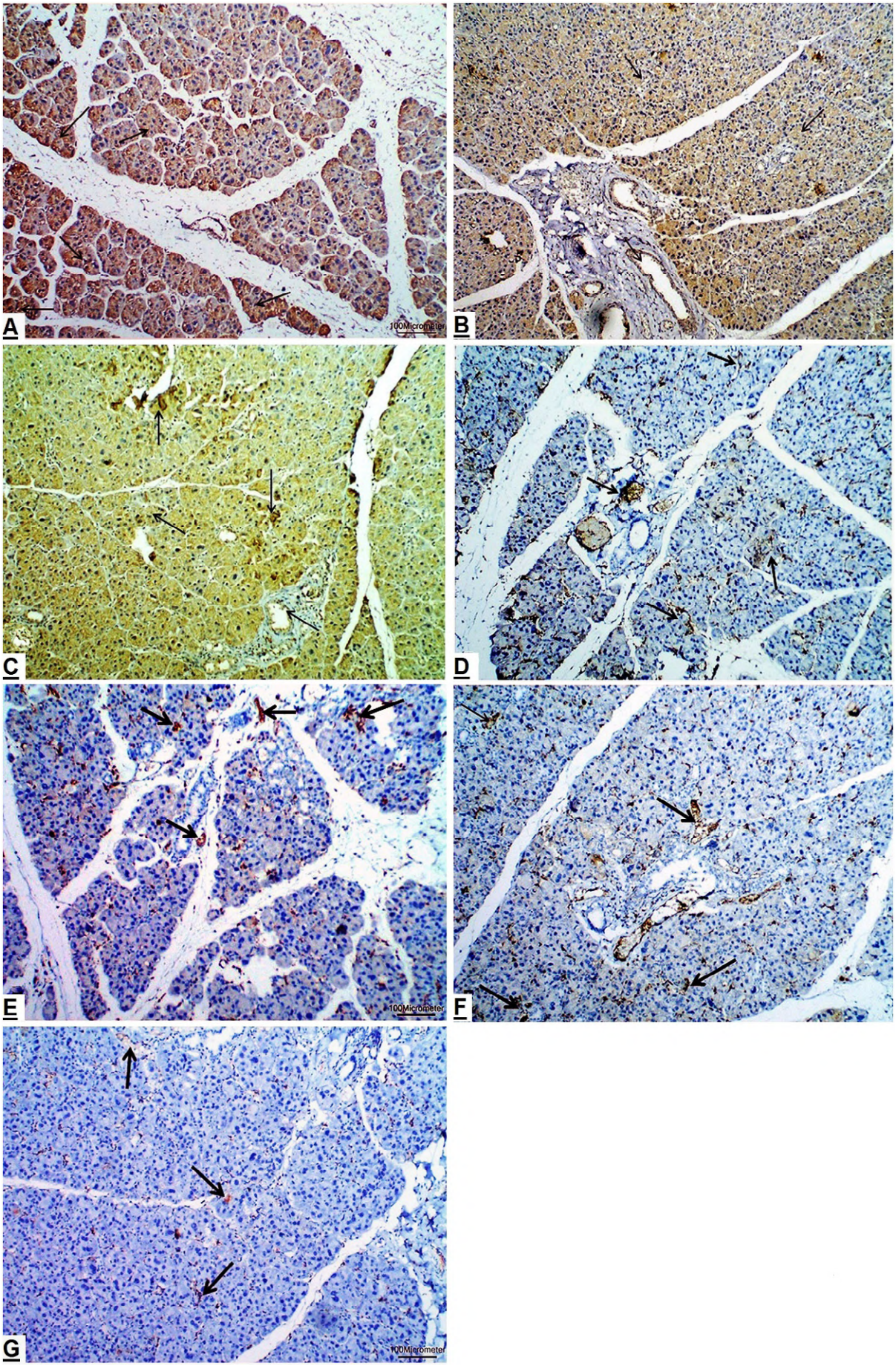

Fig. 3.- Sections of the parotid gland. **A.** intense expression of Bcl-2 protein in the cytoplasm of parotid gland cells (arrows). **B.** intense expression of Bcl-2 protein in the cytoplasm of parotid gland cells and ducts (arrows).; **C**. moderate expression. showing moderate expression; **D**. moderate expression of Bcl-2 protein in the cytoplasm of parotid gland cells and ducts (arrows). **E**. showing mild expression; **F**. moderate expression and **G.** weak expression of Bcl-2 protein in the cytoplasm of parotid gland cells and ducts (arrows). Immunohistochemistry, x100.

examination showed that some acinar cells had multiple cytoplasmic vacuolations. Other cells showed apoptotic pyknotic nuclei (Fig. 4D). Group IIIc: Histological sections revealed an apparently normal parotid architecture with normal serous acini and ducts and the interstitial spaces were filled with hemorrhagic exudate indicating recovery stage of the parotid gland after stoppage of taking the drugs (Fig. 1E). Mallory's trichrome stained sections showed minimal collagen fibers deposition around blood vessels and striated ducts (Fig. 2E), indicating recovery stage. Immunohistochemical stained sections showed mild expression of Bcl-2 protein in the cytoplasm of parotid gland cells and ducts (Fig. 3E), indicating that the parotid gland still healing. Electron microscopic study showed regaining of normal parenchymal architecture of the serous acini. Some of the acinar cells were apparently normal, with euchromatic nuclei and prominent nucleoli, while others still had pyknotic nuclei. The cytoplasm contained minimal cytoplasmic vacuoles. Others showed apparently normal rough endoplasmic reticulum with multiple electron lucent secretory granules. Normal mitochondria with intact membrane and cristae (Fig. 4E).

Group IVb: Histological sections revealed an improvement in the parenchymal architecture of the parotid gland. The structure of the duct system did not show any discernable change when compared with the control. The striated and the excretory ducts appeared with regular walls and narrow lumina (Fig. 1F). Mallory's trichrome stained sections showed collagen fibers were apparently decreased in comparison to group IIIa and IIIb around blood vessels and striated ducts (Fig. 2F), indicating starting recovery. Immunohistochemical stained sections showed moderate expression of Bcl-2 protein in the cytoplasm of parotid gland cells and ducts (Fig. 3F), indicating recovery. Electron microscopic examination showed that most of acini were apparently normal with euchromatic nuclei surrounded with normal rough endoplasmic reticulum; the mitochondria appeared normal, with intact membrane. The cytoplasm contained few cytoplasmic vacuoles; multiple electron lucent and electron dense secretory granules could be seen (Fig. 4F). Group IVc: histological sections revealed an apparently normal parotid architecture (Fig. 1G). Mallory's trichrome stained sections showed apparently decreased in collagen fibers deposition mainly around blood vessels (Fig. 2G), indicating recovery. Immunohistochemical stained sections showed variable degrees of recovery; weak expression (Fig. 3G) of Bcl-2 protein in the cytoplasm of parotid gland cells and ducts. Electron microscopic study showed preserved parenchymal architecture of the serous acini; the nuclei of the cells were basal euchromatic with prominent nucleoli. Regular intact nuclear envelope. The intercellular desmosomes were narrow and intact. Normal rough endoplasmic reticulum and electron lucent secretory granules could be seen (Fig. 4G).

Histomorphometric results

A - *Mean percentage area of collagen fibers deposition* (Fig. 5A - Table 1): Statistical analysis of data showed that there was no statistically significant difference in the mean area percent of collagen fibers between the control group I and sham control group II. Highly statistically significant increase in the mean area percent of collagen fibers of the parotid gland was detected in group III as compared to the control group and group IV. Group IIIb was highly significantly different compared to the control groups and IIIc, indicating more destruction. There was no statistically significant difference between group IV and control groups, but was significantly different compared to group III, indicating recovery. **B** – *Mean optical density of Bcl-2* (Fig. 5B - Table 2): Statistical evaluation of the mean values of the Bcl-2 optical density in the different experimental groups showed no statistically significant difference between the control group I and sham control group II. Statistical evaluation showed highly significant decrease in mean optical density in group III compared to control groups. The difference in group IIIb was statistically lower as compared to the control groups, group IIIa and IIIc, while the mean values in group IV showed no significant difference compared to control groups. **C** – *Statistical analysis of the mean T3, T4, TSH* (Figs. 5C, D, E - Tables 3, 4, 5): Statistical evaluation of the

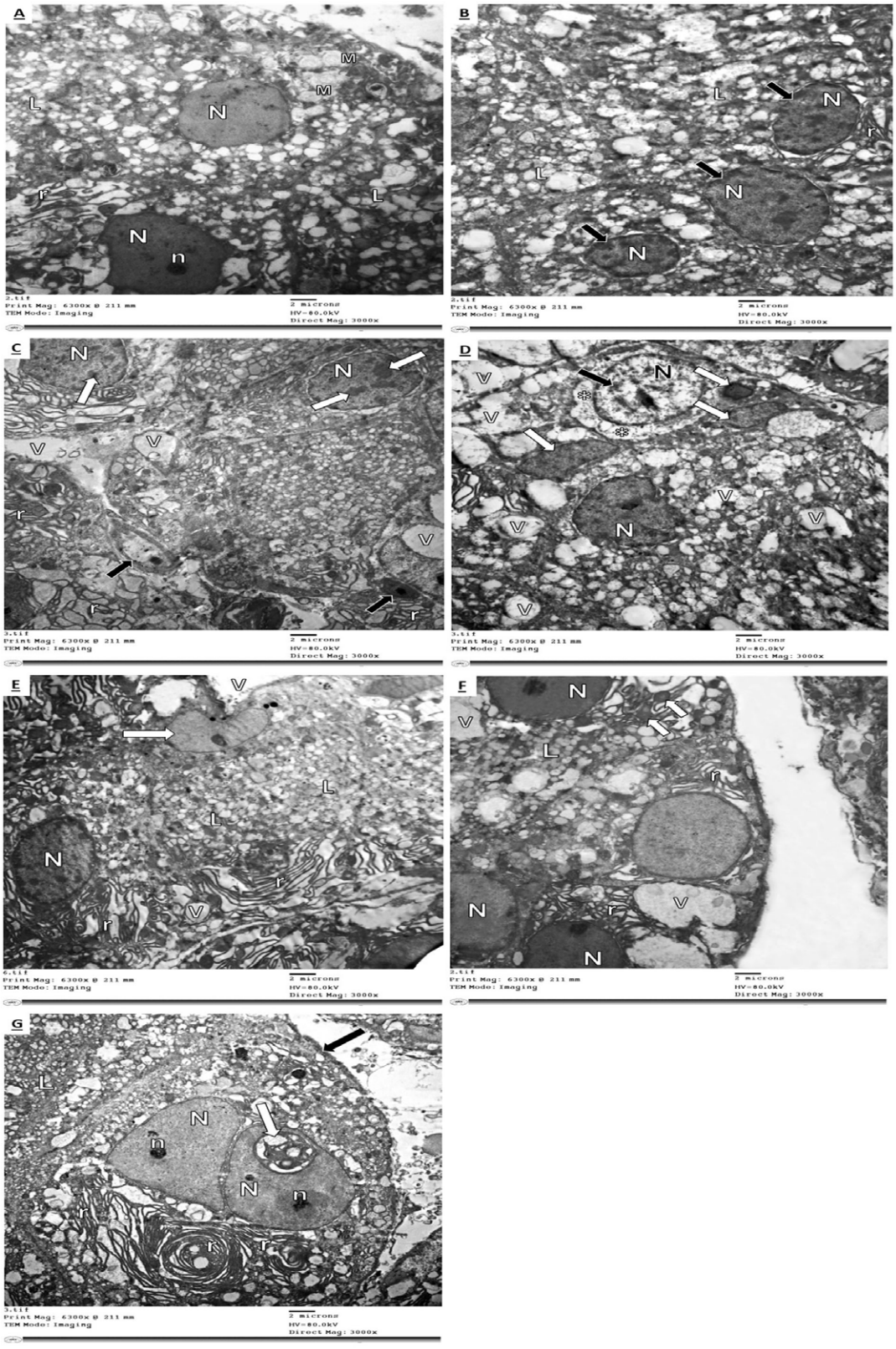

Fig. 4.- Electron micrographs of the parotid gland. **A.** an acinar cell with euchromatic nucleus (N) and prominent nucleolus (n), abundant rough endoplasmic reticulum (r) and many electron-lucent (L) secretory granules. Intact and prominent mitochondria (M) are present; **B.** acinar cell with euchromatic nucleus (N), intact nuclear membranes (arrows) and many electron-lucent (L) secretory granules. The cell cytoplasm is rich in mitochondria (M); **C**. acinar cells containing irregular heterochromatic nuclei (N) with chromatin clumps (white arrows). Shrunken condensed nuclei (black arrow) surrounded by dilated rough endoplasmic reticulum (r). Cytoplasmic vacuoles (V) are also seen; **D.** acinar cells with irregular heterochromatic nucleus (white N), some nuclei (black N) containing clumped chromatin material (black arrow) surrounded by rarified cytoplasm (*), other nuclei are condensed and shrunken (white arrows). Multiple cytoplasmic vacuoles (V) are seen; **E**. acinar cell with shrunken irregular nucleus (white arrow), other one heterochromatic nucleus (N), extensive electron-lucent secretory granules (L), apparently normal rough endoplasmic reticulum (r) and few vacuoles (V) could be detected. **F**. normal euchromatic nuclei (N) surrounded by normal rough endoplasmic reticulum (r), normal mitochondria (white arrows) and multiple electron-lucent (L) secretory granules. Few vacuoles could be detected (V); **G** apparently normal basal nuclei (N) with prominent nucleolus (n), but vacuolation within the nucleus could be detected (white arrow), surrounded by normal rough endoplasmic reticulum (r) with electron-lucent granules (L). The cell membrane is well defined (black arrows). Scale bars = 2 µm, x5000.

mean values of the T3, T4, and TSH in the different experimental groups showed no statistically significant difference between the control group I and sham control group II. Highly statistically significant decrease in the mean values of total T3 and total T4 and increase in the mean values of TSH was detected in the hypothyroid group (G III) compared to the control groups. Significant increase in the mean values of total T3 and total T4 and significant decrease in the mean values of TSH in L-Thyroxin supplemented group (G VI) were observable when compared to those of hypothyroid group (G III). However, there was no statistically significant difference in the mean values of the T3, T4, and TSH between group IV and control groups.

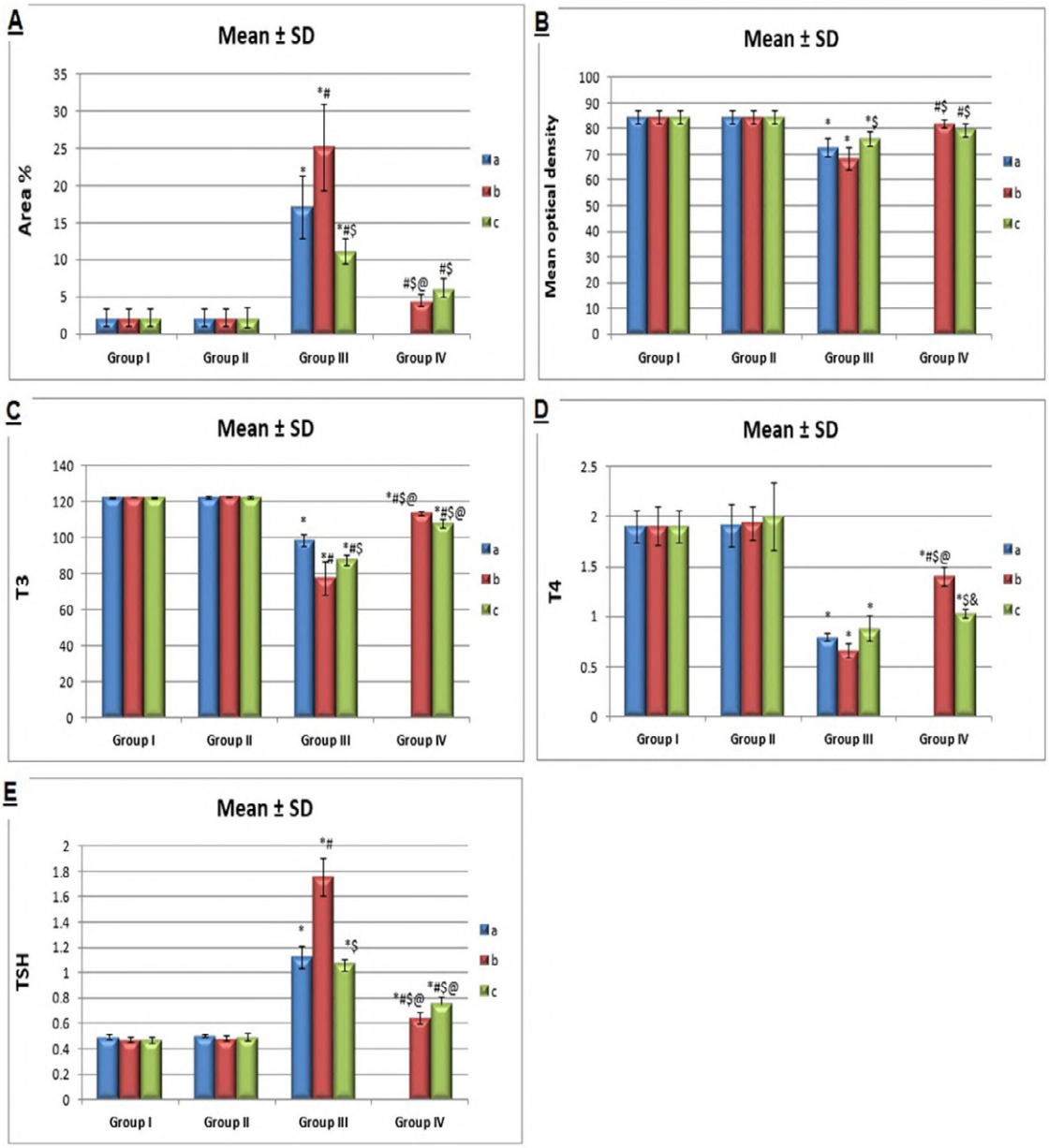

Fig. 5.- Histograms displaying: **A**: no statistically significant difference in the mean area percent of collagen fibers between the control group I and sham control group II. Highly statistically significant increase in the mean area percent of collagen fibers of the parotid gland was detected in group III as compared to the control group and group IV. Group IIIb was highly significant different compared to the control groups IIIa and IIIc; indicating more destruction. No statistically significant difference between group IV and control groups but was significant different compared to group III, indicating recovery; **B**: Statistical evaluation of the mean values of the Bcl-2 optical density showed no statistically significant difference between the control and sham control group. Statistical evaluation showed high significant decrease in mean optical density in group III compared to control groups. The difference in group IIIb was statistically lower as compared to the control groups, group IIIa and IIIc, while the mean values in group IV showed no significant difference compared to control groups; **C, D** and **E**: Statistical evaluation of the mean values of the T3, T4, and TSH showed no statistically significant difference between the control and sham control group. Highly statistically significant decrease in the mean values of total T3 and total T4 and increase in the mean values of TSH was detected in group III as compared to the control groups. Significant increase in the mean values of total T3 and total T4 and significant decrease in the mean values of TSH in group VI when compared to those of group III. However, there was no statistically significant difference in the mean values of the T3, T4, and TSH between group IV and control groups.

Table 1. The mean area percent of collagen fibers in all groups using ANOVA test: p-value is significant ≤ 0.05.

Area %	Group I	Group II	Group III	Group IV
a	2.13 ± 1.18	2.13 ± 1.19	**16.99 ± 4.23**	
b	2.09 ± 1.17	2.11 ± 1.18	**25.08 ± 5.81**	4.54 ± 0.84
c	2.19 ± 1.22	2.21 ± 1.31	**11.18 ± 1.66**	6.2 ± 1.19
P-values				
G IIIa vs. G IIIb			**<0.0001**	
G IIIb vs. G IIIc			**<0.0001**	
G IIIa vs. G IVb				**<0.0001**
G IIIb vs. G IVc				**<0.0001**
G IIIc vs. G IVc				0.075

Table 2. The mean Bcl-2 optical density in all groups using ANOVA test: p-value is significant ≤ 0.05 p-value is highly significant ≤ 0.01

Mean Opt Density	Group I	Group II	Group III	Group IV
a	84.27 ± 2.38	84.26 ± 2.37	**72.52 ± 3.44**	
b	84.27 ± 2.41	84.27 ± 2.42	**68.21 ± 4.4**	81.72 ± 1.57
c	84.27 ± 2.44	84.28 ± 2.44	**75.86 ± 2.78**	79.35 ± 2.56
P-values				
G IIIa vs. G IIIb			0.343	
G IIIb vs. G IIIc			**0.003**	
G IIIa vs. G IVb				**<0.0001**
G IIIb vs. G Ivc				**<0.0001**
G IIIc vs. G Ivc				0.64

Table 3. The mean T3 in all groups using ANOVA test: p- Value is significant ≤ 0.05 p-value is highly significant ≤ 0.01

T3	Group I	Group II	Group III	Group IV
a	122.28 ± 0.42	122.34 ±0.48	98.36 ± 3.26	
b	122.34 ± 0.27	122.4 ± 0.16	77.36 ± 9.05	113.46 ± 1.1
c	122.32 ± 0.33	122.18 ± 0.65	87.36 ± 2.86	107.6 ± 2.47
P-values				
G IIIa vs. G IIIb			**<0.0001**	
G IIIa vs. G IVb				**<0.0001**
G IIIb vs. G IVc				**<0.0001**
G IIIc vs. G IVc				**<0.0001**
G IVb vs. G IVc				0.143
G IIIb vs. G IVc				<0.0001

Table 4. The mean T4 in all groups using ANOVA test: p-value is significant ≤ 0.05 p-value is highly significant ≤ 0.01

T4	Group I	Group II	Group III	Group IV
a	1.9 ± 0.16	1.91 ± 0.21	0.79 ± 0.04	
b	1.9 ± 0.19	1.93 ± 0.16	0.66 ± 0.07	1.4 ± 0.1
c	1.9 ± 0.16	2 ± 0.34	0.88 ± 0.13	1.03 ± 0.04
P-values				
G IIIa vs. G IIIb			0.969	
G IIIa vs. G IVb				**<0.0001**
G IIIb vs. G IVc				**0.035**
G IIIc vs. G IVc				0.941
G IVb vs. G IVc				**0.039**
G IIIb vs. G IVc				0.035

Table 5. The mean TSH in all groups using ANOVA test: p-value is significant ≤ 0.05 p-value is highly significant ≤ 0.01

TSH	Group I	Group II	Group III	Group IV
a	0.49 ± 0.02	0.5 ± 0.01	1.12 ± 0.09	
b	0.47 ± 0.02	0.48 ± 0.02	1.75 ± 0.15	0.64 ± 0.05
c	0.47 ± 0.02	0.49 ± 0.03	1.07 ± 0.03	0.75 ± 0.06
P-values				
G IIIa vs. G IIIb			<0.0001	
G IIIa vs. G IVb				**<0.0001**
G IIIb vs. G IVc				**<0.0001**
G IIIc vs. G IVc				**<0.0001**
G IIIb vs. G IIIc			<0.0001	

DISCUSSION

THs have wide range of effects on multi organ systems of the human body. They are responsible for control of normal functions of nearly all tissues with prominent effects on thermogenesis, lipogenesis and oxygen consumption (Shi et al., 2002). Also, an association between thyroid dysfunction and a significant decrease in salivary parameters such as flow rate and buffering capacity had been confirmed (Muralidharan et al., 2013). It had also been reported that lack of THs provoked physiological and histological changes in the submandibular, sublingual and parotid glands respectively (Noorafshan, 2001). Previous studies proved that thyroid gland rendered hypofunctional when treated with hypothyroid drugs (Hayat et al., 2010). It was postulated that the hypothyroid drug acts as a false substrate for thyroid peroxidase, thus blocking the iodination of tyrosine residues within thyroglobulin (Čakić-Milošević et al., 2004).

In our experimental model, development of hypothyroidism was confirmed both by histological changes in the parotid gland and estimation of serum levels of T3, T4 and TSH. Significant decrease in T3, T4 and increase in TSH serum levels were indicative that the quantity and duration of treatment was sufficient to induce hypothyroid status in the experimental group of rats. Examination of the medical Hypothyroidism, short duration group showed that most of the serous acini had irregular outlines and were widely separated. Some acinar cells contained darkly stained and hyperchromatic nuclei, with narrow lumen and cytoplasmic vacuoles. Extravasated blood, dilatation of the duct system and cellular

infiltration were seen in the interstitial space; these were in line with the results of Abd Elazeem et al. (2016), who found that parotid parenchyma contained many serous acini and most of them had irregular outlines. The salivary glands atrophy observed in this study could explain the decreased salivary flow rate that was previously documented in hypothyroid rats in the study of Rodriguez et al., (2009), who stated that hypothyroidism was caused by propylthiouracil, a thyroperoxidase activity inhibitor, consequently inhibiting thyroid hormone biosynthesis and reduced the salivary flow in injected rats, in comparison with the euthyroid control rats. In our present study, the nuclei of parotid gland cells were darkly stained in the experimental animals of the hypothyroid groups. The same results were obtained by Ashour (1998), who reported that the amount of euchromatin was used as an indicator of the metabolic activity of cells; conversely a high proportion of heterochromatin indicates a cell with low metabolic activity.

Increased collagen fibers deposition in the parotid gland of the hypothyroid groups were observed in the present study around congested blood vessels compared to the control group in Mallory's trichrome stained sections. Those results were online with Hayat et al. (2010) and Abd Elazeem et al. (2016), who clarified the presence of extensive collagen fibers in between lobules, around blood vessels and interlobular ducts in parotid gland of hypothyroid rats for short duration. Examination of the medical hypothyroidism, long duration showed more destruction, atrophic serous acini with irregular arrangement. The acini were divided by connective tissue septa, which were markedly thick. During examination of the medical hypothyroidism, group III c and group IV showed apparently normal parotid architecture with normal serous acini and ducts. The same results were in line with Abd Elazeem et al. (2016), who found sections of parotid gland of thyroid hormone supplemented group for short duration, showing that most of acini and ducts were apparently normal, while some acini had an irregular outline. Some acinar cells still contained vacuolated cytoplasm.

Microscopic findings of the parotid glands of hypothyroid rat showed atrophy of acini and partial replacement of the parenchyma with a connective tissue component. The same results were obtained by Oncu et al. (2004) in the sublingual gland of rats after thyroidectomy, in addition to cytoplasmic vacuolization of the epithelial cells, enlargement and dilatation of lumina in most of the gland. This is probably due to severe hypothyroidism, increased mucous secretion, lipid tissue mass surrounding the parenchyma and mononuclear cell infiltration. Markitziu et al. (1993) reported that thyroidectomy caused hypercholesterolemia and fatty degeneration of the parotid parenchyma, which was in line with our findings in the parotid of hypothyroid groups.

In the current work, Mallory's trichrome stained sections clarified the presence of extensive collagen fibers in parotid glands of group IIIb more than in IIIa, indicating more destruction with increased duration, while collagen fibers were apparently decreased in group IIIc and group VI in comparison to group IIIa and IIIb. These finding were in agreement with Abd Elazeem et al. (2016), who showed amelioration of most degenerative changes that occurred in the parotid gland after treatment with L-Thyroxin.

ROS are by-products of normal metabolism in all aerobic cells. Most of the oxygen consumed by the cells is reduced to water during mitochondrial respiration. A sensitive balance exists between ROS production and the antioxidant defenses that protect the cells in vivo (Halliwell and Gutteridge, 2015). It has been observed that a change in thyroid gland function affects production of ROS in rats (Venditti and Di Meo, 2006). It has also been reported that hypothyroidism alters the antioxidant defense system in various tissues (Cattani et al., 2013) and thyroid dysfunction appears to be closely related to ROS formation as reported by Ahmed et al. (2012). In support to our results, some of the studies reported that hypothyroidism conditions change the activity of the antioxidant status in several tissues including the brain (Jena et al., 2012). The same results were obtained by Abou-Elghaita et al. (2011), who stated that thyroid deprivation causes changes in the levels of lipid peroxidation and antioxidant enzyme activities which were determined in different tissues of hypothyroid rats, causing

the functional disorder of these tissues. Pan et al. (2017) found that lipid peroxidation level was elevated while antioxidant defense enzymes levels were decreased in the hippocampus of hypothyroid rats. These findings and the results of the present study may suggest an imbalance between oxidant and antioxidant system as a leading factor to the parotid gland's oxidative damage in hypothyroidism.

Examination of ultrathin sections of the hypothyroid group showed acinar cells with irregular heterochromatic nuclei, dilated rough endoplasmic reticulum, degenerated mitochondria and cytoplasmic vacuoles, with more destructive changes in group IIIb than in IIIa. These structural changes were consistent with Yang et al. (2015), who found similar changes in the hippocampus of hypothyroid rats induced by propylthiouracil for 4 weeks: there were margination of nuclear chromatins; a lot of mitochondria were swollen, the cristae broke and showed significant vacuolar degeneration; the rough endoplasmic reticulum and ribosomes were obviously sparse. While the T4 injected group for 2 weeks exhibited clear nuclear membranes, the organelles were relatively sparse and a small amount of mitochondria exhibited vacuolation; rough endoplasmic reticulum was mildly dilated and in line with Abd Elazeem et al. (2016), who found that some acinar cells had irregular heterochromatic nuclei. Their cytoplasm contained markedly dilated rough endoplasmic reticulum. Some acinar cells showed variably sized vacuoles in their cytoplasm. Other cells showed apoptotic nuclei in parotid gland of hypothyroid rats after treatment with Carbimazole for successive 3 weeks. These changes were improved after induction of L-Thyroxin and in recovery group, which showed an apparently normal parotid architecture with normal serous acini and ducts.

Other areas showed acini with irregular walls and few cytoplasmic vacuoles, the interstitial spaces were wide, edematous and filled with hemorrhagic exudate, indicating healing of the parotid gland after stoppage taking the drugs. These results were in agreement with Abd Elazeem et al. (2016), after treatment with L-Thyroxin for successive 3 weeks. Cell apoptosis is orderly death of the cell by genes controlled, which control the stability of the internal environment. Recent studies (Pan et al., 2017) have found that apoptosis is closely related to the occurrence and development of many diseases. Bcl-2 family proteins play an important role in cell apoptosis (Hardwick and Soane, 2013). This hypothyroidism-induced acinar cell death was assumed to be due to apoptosis, which was supported in our study by the presence of shrunken dark irregular acinar nuclei in addition to chromatin clumping in some acinar nuclei (Takahashi et al., 2005).

In the current work, immunohistochemical examination for Bcl-2 was performed. In the control groups, immunohistochemical stained sections showed strong immune reaction for Bcl-2 in the cytoplasm of parotid cells and within the ducts. Concerning hypothyroid groups, weak immune reaction for Bcl-2 in the cytoplasm of parotid cells was detected. While immunohistochemical examination for Bcl-2 of L-Thyroxin-supplemented groups and recovery group revealed moderate reaction in the cytoplasm of parotid cells and ducts. These finding were in agreement with Abd Elazeem et al. (2016) in control, hypothyroid group and L-Thyroxin-supplemented group for short duration on parotid gland. The same results were obtained by Muller et al. (1995), who suggested that THs deficiency results in delayed proliferation and migration of cerebellar granule cells. They evaluated the effect of hypothyroidism on Bcl-2 family gene expression in the developing rat cerebellum. Muller et al. (1995) suggested that normal levels of THs prevent cerebellar apoptosis to a large extent, whereas hypothyroidism not only increases the extent but also the duration of apoptosis by downregulating the anti-apoptotic genes Bcl-2 and maintaining a high level of the pro-apoptotic gene Bax (Liu et al., 2017). Several researchers have suggested that the THs are important in the maintenance of normal salivary gland function and histology (Oncu et al., 2004).

In our study, supplementation of thyroid hormone in the form of exogenous T4 significantly improved the histological changes that occurred in the parotid gland, which was in agreement with

Abd Elazeem et al. (2016), who found improvement in Carbimazole induced hypothyroidism in rats' parotid glands treated with L-Thyroxin. From the collective data of the present study, it can be concluded that hypothyroidism exerts adverse effects on the rat's parotid gland, which can be ameliorated by administration of thyroid drugs (Muralidharan et al., 2013). The beneficial effects of thyroid hormones in the parotid gland became more obvious with increased duration.

ACKNOWLEDGEMENTS

I would like to express my deepest gratitude to Prof. Dr. Abd- Elwakeel Elsayed Essawy, Professor of Anatomy and Embryology, Faculty of Medicine, Cairo University, for his continuous encouragement and helpful advice, which contributed so much to bringing out this paper degree in an elegant and scientific form. It is my great honor to express my profound appreciation and sincere gratefulness to Dr. Gamal Hosny Mohammed, Assistant Professor of Anatomy and Embryology, Faculty of Medicine, Cairo University, for his valuable supervision and generous support. I would like to convey my discerning feeling of indebtedness to *Dr. Ramadan Moustafa Elsayed*, Lecturer of Anatomy and Embryology, Faculty of Medicine, Fayoum University and Dr. Ahmed Hamed Bayoumi, Lecturer of Anatomy and Embryology, Faculty of Medicine, Cairo University, for their continuous support and guidance.

REFERENCES

ABD ELAZEEM A, MOHAMMED MZ, HASSAN EZ (2016) Effect of experimentally induced hypothyroidism on the parotid gland of adult male albino rats and the possible role of thyroid hormone supplementation. *Brit J Sci*, 14(1): 19-36.

ABOU-ELGHAITA AT, RATEBB A, MAHMOUDB FY, GALAL O (2011) Effect of experimentally induced hypothyroidism during pregnancy and lactation on the retina of juvenile and adult albino rats and the possible role of thyroid hormone supplementation. *Egypt J Hist*, 34(1): 28-45.

AHMED OM, AHMED RG, EL-GAREIB AW, EL-BAKRY AM, ABD EL-TAWAB SM (2012) Effects of experimentally induced maternal hypothyroidism and hyperthyroidism on the development of rat offspring: II- The developmental pattern of neurons in relation to oxidative stress and antioxidant defense system. *Int J Dev Neurosci*, 30(6): 517-537.

ASHOUR MA (1998) Long-term effect of melatonin on submandibular salivary glands in old rats. *Eastern Med Health J*, 4(2): 324-331.

AVWIORO OG (2010) Histochemistry and tissue pathology, principles and techniques. *North Am J Med Sci*, 2(5): 561-568.

BANCROFT J, GAMBLE M (2008) Hematoxylins and Eosin. In: Bancroft J, Gamble M (eds). *Theory and Practice of Histological Techniques*. Churchill Livingstone, 6th edition, pp 121-134.

BASAÑEZ G, HARDWICK JM (2008) Unravelling the Bcl-2 apoptosis code with a simple model system. *PLoS Biol*, 6(6): 154.

BHANJA S, CHAINY GBN (2010) PTU-induced hypothyroidism modulates antioxidant defense status in the developing cerebellum. *Int J Dev Neurosci*, 28(3): 251-262.

ČAKIĆ-MILOŠEVIĆ M, KORAĆ A, DAVIDOVIĆ V (2004) Methimazole-induced hypothyroidism in rats: Effects on body weight and histological characteristics of thyroid gland. *Jugoslovenska medicinska biohemija J*, 23(2): 143-147.

CATTANI D, GOULART PB, CAVALLI VL (2013) Congenital hypothyroidism alters the oxidative status, enzyme activities and morphological parameters in the hippocampus of developing rats. *Mol Cell Endocrinol*, 375(1-2): 14-26.

DAKINE N, OLIVER C, GRINO M (2000) Effects of experimental hypothyroidism on the development of the hypothalamo-pituitary-adrenal axis in the rat. *Life Sci*, 67(23): 2827-2844.

DONG BJ (2004) Thyroid and anti-thyroid drugs. In: Green SFS, Dong BJ (eds). *Basic and clinical pharmacology*, 9th edition, pp 625-640.

EL-BASSOUNY DR (2012) Ultrastructural study of the adult albino rat parotid gland with special reference to the role of stromal telocytes. *Egypt J Hist*, 35(4): 761-772.

EL-WAKF AM, HASSAN HA, ELSAID FG, EL-SAID A (2009) Hypothyroidism in male rats of different ages exposed to nitrate polluted drinking water. *Res J Med Med Sci*, 4(2): 160-164.

FULOP M (1989) Pouting sublingual: enlarged salivary glands in myxedema. *Lancet*, 2(2): 550-551.

HALLIWELL B, GUTTERIDGE JMC (2015) Ageing, nutrition, disease and therapy: a role for antioxidants. In: Halliwell B, Gutteridge JMC (eds). *Free Radicals in Biology and Medicine*, 5th edition, pp 861-871.

HARDWICK JM, SOANE L (2013) Multiple functions of Bcl-2 family proteins. *Cold Spring Harb Perspect Biol*, (2): 1-5.

HAYAT NQ, TAHIR M, MUNIR B, SAMI W (2010) Effect of methimazole-induced hypothyroidism on histological characteristics of parotid gland of albino rat. *J Ayub Med Coll Abbottabad*, 22(3): 22-27.

JENA S, CHAINY GBN, DANDAPAT J (2012) Hypothyroidism modulates renal antioxidant gene expression during postnatal development and maturation in rat. *Gen Comp Endocrinol*, 178(1): 8-18.

KHALAWI AA, AL-ROBAI AA, KHOJA SM, ALI SS (2013) Can Nigella Sativa Oil (NSO) reverses hypothyroid status induced by PTU in rat? Biochemical and histological studies. *Life Sci J*, 10(2): 802-811.

KIERNAN JA (2015) Theory and Practice. In: Kiernan JA (ed). *Histological and Histochemical Methods*. Scion, 5th edition, pp 571-591.

LAMFON HA (2014) Effect of selenium on chlorpyrifos-induced thyroid toxicity in albino rats. *IBIMA*, 33(3): 441-450.

LIU Y, LIU YL, CHENG W, YIN XM, JIANG B (2017) The expression of SIRT3 in primary hepatocellular carcinoma and the mechanism of its tumor suppressing effects. *Eur Rev Med Pharmacol Sci*, 21: 978-998.

MARKITZIU A, LUSTMANN J, UZIELI B, KRAUSZ Y, CHISIN R (1993) Salivary and lacrimal gland involvement in a patient who had undergone a thyroidectomy and was treated with radioiodine for thyroid cancer. *Oral Surg Oral Med Oral Pathol*, 75(3): 318-322.

MULLER Y, ROCCHI E, LAZARO JB, CLOS J (1995) Thyroid hormone promotes Bcl-2 expression and prevents the apoptosis of early differentiating cerebellar granular neurons. *Int J Dev Neurosci*, 13(8): 871-885.

MURALIDHARAN D, FAREED N, PRADEEP PV, MARGABANDHU S, RAMALINGAM K, AJITH KBV (2013) Qualitative and quantitative changes in saliva among patients with thyroid dysfunction prior to and following the treatment of the dysfunction. *Oral Surg Oral Med Oral Pathol Oral Radiol*, 115(5): 617-623.

NOORAFSHAN A (2001) Stereological study on the submandibular gland in hypothyroid rats. *APMIS*, 109(3): 223-227.

ONCU M, KANTER M, GOKCIMEN A, KAVAKLI D (2004) Effect of thyroidectomy on the histology of rat sublingual gland. *APMIS*, 112(2): 119-122.

PAN LJ, WANG X, LING Y, GONG H (2017) MiR-24 alleviates cardiomyocyte apoptosis after myocardial infarction via targeting BIM. *Eur Rev Med Pharmacol Sci*, 21(13): 3088-3097.

PETRULEA MS, DUNCEA I, MURESAN A (2009) Thyroid hormones in excess induce oxidative stress in rats. *Acta Endocrinologica*, 5(2): 155-164.

PORTH CM, GASPARD K, GUVEN S, KUENZI JA, MATFIN (2004) Alterations in pituitary, thyroid, parathyroid and adrenal function. In: Porth CM, Grossman SC (eds). *Porth's pathophysiology, concept of altered health states*. Lippincott Williams & Wilkins, 9th edition, pp 538-559.

PUCCI E, CHIOVATO L, PINCHERA A (2000) Thyroid and lipid metabolism. *Int J Obes Relat Metab Disord*, 24(2): 109-112.

SHI YB, RITCHIE JWA, TAYLOR PM (2002) Complex regulation of thyroid hormone action: multiple opportunities for pharmacological intervention. *Pharmacol Ther*, 94(3): 235-251.

TAKAHASHI S, NAKAMURA S, DOMON T, YAMAMOTO T, WAKITA M (2005) Active participation of apoptosis and mitosis in sublingual gland regeneration of the rat following release from duct ligation. *J Mol Histol*, 36(3): 199-205.

RAJAB NMA, UKROPINA M, MILOSEVIC MC (2017) Histological and ultrastructural alterations of rat thyroid gland after short term treatment with high doses of thyroid hormones. *Saudi J Biol Sci*, 24(6): 1117-1125.

RODRIGUEZ TT, DANTAS VTA, RAMALHO MJP (2009) Participation of nitric oxide synthase and cyclooxygenase-2 in the salivary secretion of hypothyroid endotoxemic rats. *J Dental Sci*, 24(4): 383-388.

ROSS MH, PAWLINA W (2011) Digestive system I: oral cavity and associated structures- In: Ross MH, Pawlina W (eds). *Histology. A Text and Atlas with correlated cell and molecular biology*. Wolters Kluwer/Lippincott Williams & Wilkins Health, 6th edition, pp 327-330, 402-407.

VAIDYA B, PEARCE SH (2008) Management of hypothyroidism in adults. *BMJ*, 337: 284-289.

VENDITTI P, DI MEO S (2006) Thyroid hormone-induced oxidative stress. *Cell Mol Life Sci*, 63(4): 414-434.

YANG H, ZHA X, CAI Y, WANG F, WU Z, WU B, JIA X, ZHU D (2015) Impacts of thyroxine combined with donepezil on hippocampal ultrastructures and expressions of synaptotagmin-1 and SNAP-25 in adult rats with hypothyroidism. *Int J Clin Exp Med*, 8(10): 17922-17931.

Impact of a multimodal anatomy CPD course on intravenous cannulation skills – An Irish radiographers and radiation therapists' perspective

Mutahira Lone[1], Ahmad H. Sheikh[1], Andreea Factor[1], Niamh Moore[2], Muhammad A. Javaid[3]

[1] Department of Anatomy, University College Cork, Cork, Ireland

[2] Department of Radiography, University College Cork, Cork, Ireland

[3] Department of Anatomy, Anglia Ruskin University, Chelmsford, United Kingdom

SUMMARY

Radiographers and radiation therapists continually upgrade their knowledge to remain informed and competent in modern radiological imaging techniques. Despite the generally agreed upon significance of anatomy for successful interpretation of imaging modalities, its link with clinical performance of radiographers and radiation therapists has not been highlighted before.

The above-stated gap in the literature was addressed by employing an anatomy-based CPD course and investigating its influence on intravenous cannulation and administration skills of 10 radiographers and 4 radiation therapists. The course comprised interactive anatomy tutorials (employing vascular histology e-modules and vascular prosections), lectures and simulation sessions to practice IV cannulation. Likert questionnaires were employed to gauge attitudes and interests, prior to and after the course.

At the end of the course, participants perceived anatomy prosections/dissection more useful compared to other learning modalities, including social media, textbooks, e-learning, plastic models and lectures. This corresponded with a significant increase in their perceived level of anatomy knowledge and confidence in identifying structures on prosections, and tracing vessels on radiographs and body surface. Anatomy-based CPD course was valued with regards to their career progression and enhancement of anatomical knowledge. Furthermore, the use of prosections and hands-on practical sessions was highly commended and a desire to attend similar future courses was expressed. Lastly, participants identified factors facilitating or hindering course attendance and offered advice to improve efficacy of future courses.

We conclude that an interactive anatomy-based CPD—employing multimodal pedagogies—can be effective in enhancing anatomy knowledge and clinical competence of radiographers and radiation therapists.

Corresponding author:
Muhammad Asim Javaid MD, PhD, Senior Lecturer. Department of Anatomy, School of Medicine, Anglia Ruskin University, Bishops Hall Lane, Chelmsford, United Kingdom. Phone: +353-21-4205494. E-mail: Muhammad.javaid@aru.ac.uk

Submitted: February 14, 2021. **Accepted:** November 17, 2021

https://doi.org/10.52083/QPAW2060

Key words: Continuous professional development (CPD) – Radiographers – Radiation therapists – Anatomy – IV cannulation – Human prosections

INTRODUCTION

Anatomy has long been considered an essential part of medical education (McLachlan and Patten, 2006; Patel and Moxham, 2006; Drake et al., 2009). The significance of the link between a deep-rooted understanding of human anatomy and enhanced clinical interpretation and patient-management skills of healthcare professionals has been widely recognized (Turney, 2007; Arraez-Aybar et al., 2010; Martin et al., 2014). The practice of various allied healthcare professions, including radiography and radiation therapy, is heavily patient-centered. Hence, anatomy education—in integration with radiography and radiation therapy—has an important role to play in ensuring professional competence and provision of the highest standard of patient care in these fields (Heptonstall et al., 2016). Moreover, amidst increasing demands on healthcare professionals, there is a critical need for radiographers and radiation therapists to continually update their clinical and professional knowledge, in alignment with the requirements of their rapidly evolving profession, and to become increasingly competent in using and interpreting radiological imaging and modalities (Wareing et al., 2017).

A deeper understanding of anatomical concepts is important in interpreting various imaging modalities (Sugand et al., 2010). However, despite its established value in medical education, a decline in the anatomy knowledge of both students and health practitioners has been documented over the course of their academic and clinical years (Waterson and Stewart, 2005; Turney, 2007; Hall and Durward, 2009; Craft et al., 2017). Although anatomy is taught in sufficient detail during undergraduate courses, a need for radiographers and radiation therapists to revisit regional and cross-sectional anatomy and correlate it with their radiological image-interpretation skills, still exists (Hall and Durward, 2009).

Continuous Professional Development (CPD) is essential to maintain and improve the skills and knowledge necessary to provide the best of care for the patients (Henwood et al., 1998; Marshall et al. 2008; Wareing et al., 2017). A recent survey showed that the Irish Radiation Therapy departments are routinely employing intravenous contrast (IVC) during radiation therapy (RT) planning, thus necessitating the acquisition of this skill (Minogue et al., 2019). Furthermore, the Health and Social Care Professionals Council has introduced a regulatory body (CORU) for the registration of radiographers and radiation therapists since 2013. As a regulatory body, CORU has exercised its role to protect the public by promoting high standards of professional conduct, education, training and competence through statutory registration of health and social care professionals (CORU, 2019). While CPD courses can be organized in numerous ways, three main models have been highlighted in the literature (Wallace and May, 2016; Grehan et al., 2018). These include an 'input-based' CPD that involves a traditional but passive approach of attending workshops, conferences, symposia without any assessment of the learning, which has taken place (Wallace and May, 2016; Grehan et al., 2018). On the contrary, an 'output-based' CPD focuses on the learning outcomes and its impact on an individual's clinical practice, to maintain and improve professional competencies (Wallace and May, 2016; Grehan et al., 2018). 'Hybrid' variant of CPDs lies somewhere in the middle and exercises a combination of input and output-based approaches (Doughty and Hodgson, 2009; Grehan et al., 2018).

Research studies have investigated various CPD outcomes for radiographers and radiation therapists; including the motivational instigators and barriers linked with radiography CPD courses (Grehan et al., 2018), relevant aspects of CPD for radiographers (Marshall et al., 2008) and rationale affecting the radiographers and radiation therapists' participation in CPD courses (Walsh and Craig, 2016). While previous studies explored barriers affecting CPD courses, including IV cannulation (De Boo et al., 2020), the novelty of this study is that it investigates the association

between an anatomy teaching and learning CPD course and the cannulation skills of the course participants. It is our understanding that a link between basic anatomical knowledge and clinical performance of radiographers and radiation therapists has not been highlighted before.

The aim of the study was to investigate, via a questionnaire, the impact of a novel teaching and learning anatomy CPD course for radiographers and radiation therapists. The course was highly interactive and stimulated the active involvement of the participants. Moreover, they were encouraged to reflect and were provided ample opportunity to apply and practice their skills. The hands-on design of the course helped participants to identify and address any gaps in their clinical practice. In this study, an effective hybrid CPD model was used by employing multimodal pedagogical tools including prosections and modern pedagogies (TEL) and its association with the personal and professional development of the participants was explored.

MATERIALS AND METHODS

A CPD course pertaining to intravenous cannulation and administration was designed for radiographers and radiation therapists at University College Cork (UCC), Ireland. 14 participants (10 radiographers, 4 radiation therapists) attended the course. The CPD course was advertised on the website of UCC's Centre for CPD. In addition, advertising emails were distributed to the Radiography Service Managers and Radiation Therapy Service Managers nationally.

Design of the CPD course

The CPD course spanned over one and half days and comprised interactive anatomy tutorials, followed by didactic lectures and practical simulated training sessions pertaining to IV cannulation and administration.

Interactive anatomy tutorials

Day 1 of the CPD course commenced with 2-hours of anatomy tutorials on the circulatory system. The tutorials were conducted using human prosections, supplemented by plastic models and computer-assisted learning software (anatomy and physiology revealed®). The tutorials were hosted in the Anatomy FLAME laboratory at UCC and were facilitated by senior anatomy demonstrators. Participants rotated through four interactive thirty-minute tutorial stations.

At the first station, the demonstrators helped the participants to recognize the histological appearances of the different types of blood vessels; elastic and muscular arteries, veins and capillaries. The underlying structural variations were linked with the functional specifications of different types of vessels and the modulation of the flow of blood in them. An online e-learning resource entitled the 'Blue Histology' (http://bit.ly/neurohistology) was used for teaching with participants asking questions throughout.

The learning sessions over the next three stations were conducted using formalin-preserved prosections of the human body. All participants wore gloves and manually manipulated the structures under supervision, to identify and appreciate anatomical relationships in a three-dimensional haptic learning environment. A general overview of the human circulatory system was provided on the second station with participants identifying the major blood vessels of the trunk and the heart, and their features. Next, in the third station, participants identified the course of the arteries and veins—superficial and deep, in the shoulder, arm and forearm. They identified common sites of venous access. Moreover, the importance of arterial anastomoses in the shoulder and the upper limb and the significance of the flow of venous blood from the superficial to the deep veins was discussed with the demonstrators. Lastly, on reaching the fourth station, the participants were given a detailed overview of the vasculature of the pelvic region and the lower limb. The participants identified the principal arteries and veins within the hip, thigh, leg, ankle and foot regions. The tutorial facilitators demonstrated the localization of femoral, popliteal, dorsalis pedis and posterior tibial pulses, and described the accessible venous sites for emergency 'venous cutdown' procedures. In addition, the functional significance of arterial

anastomoses in the hip and knee, the role of the perforator venous connections between the superficial and deep veins and the function of the 'soleus muscle pump' for venous return to the heart were also mentioned.

Didactic lectures

Following the 2-hour anatomy tutorial, the remainder of day 1 of the CPD course comprised a series of didactic lectures delivered by radiographers, nurses and radiologists experienced in IV cannulation and administration of agents. During these educational sessions, participants were familiarized with the following theoretical underpinnings of intravenous cannulation:

1. Pharmacological and physiological principles underlying a) safe administration of intravenous preparations (radiopharmaceuticals and contrast agents) in diagnostic and therapeutic imaging, and b) recognition and management of adverse reactions or anaphylaxis associated with intravenous administration of contrast media;
2. Undertaking of patient safety and infection control precautions associated with intravenous cannulations;
3. Establishment and implementation of departmental protocols for the administration of intravenous injections and the role of the radiographer and radiation therapist in this context;
4. Safe usage of power pump injectors;
5. Medico legal issues associated with IV cannulation and administration of contrast agents.

Practical training session for intravenous cannulation and administration

Day 2 was aimed towards providing practical training to the radiographers and radiation therapists regarding administering intravenous cannulation and injecting contrast media and radiopharmaceuticals during imaging procedures. The teaching reflected the general principles of the IIRRT guidelines of best practice. The half-day long practical training took place in the Advanced Clinical Skills Department of the university.

At the start, the candidates attended a 1-hour simulation session on the safe preparation-technique for undertaking intravenous cannulations. This session was provided by an expert nurse in IV cannulation and was supervised by radiographers with at least 10 years' experience in IV cannulation. It involved the participants simulating the preparation of the cannulation equipment using all the appropriate infection control measures. Following the simulation, participants carried out several supervised IV cannulations on artificial training arms. There was 1 supervisor to 3 participants in these sessions, which lasted for 2 hours. The candidates learned the pathways that should be undertaken while carrying out cannulations, using a variety of cannulae and butterfly needles.

Questionnaire design

Questionnaires (1 and 2) were compiled to inquire about the opinion of radiographers and radiation therapists regarding the significance of anatomy teaching and learning for enhancing their clinical performance and their opinion regarding what they preferred in future CPD courses (Table 1). The questionnaires were modified versions of those employed earlier by Marshall and colleagues (2008) and Grehan and colleagues (2018), imparting validity to their design. The questionnaire design was further informed by piloting the questions across a group of radiographers and radiation therapists during the previous year (2018). The feedback acquired from the pilot study informed the adequacy of the final questionnaires and research design. However, the pilot data was not incorporated into the main study.

Questionnaire 1 was administered prior to the commencement of the CPD course on day 1. It inquired about the participants' demographics, their work experience and their anatomy teaching and learning experience (Table 1; part A).

Questionnaire 2 was administered at the end of the practical IV cannulation course on day 2 and inquired about participants' anatomy

teaching and learning experience, their opinion about both the anatomical component and the IV cannulation segment of the CPD course, specific areas where they would like to see further taught anatomy content employed and their satisfaction level at the end of the course (Table 1; part B).

Ethical approval

The study received approval from the Institutional Social Research Ethics Committee (Log 2019-118).

Statistical analysis

All statistical analysis was carried out using Excel® and the Statistical Package for Social Sciences, SPSS®, version 22 (IBM Corp., Armonk, NY). Descriptive statistics (mean, SD and percentages) were provided for explaining participants' demographics (Table 2), their prior experience with regards to using various imaging modalities, exposure to anatomy pedagogies during undergraduate years, factors facilitating or hindering course attendance, participants' perceived importance of anatomy-based CPD for career progression, preference for various learning modalities (prosections, e-learning, etc.) and topics preferred in future CPD courses.

Since the opinion of participants regarding various elements in the questionnaire (Table 1) was gauged using Likert scales (ordinal data), hence non-parametric tests, such as, Friedman's paired ranking and Wilcoxon's signed ranking tests were employed. Friedman's paired ranking test followed by post-hoc Wilcoxon ranking tests for paired comparisons were used in order to analyse potential differences in participants' opinion pertaining to their perceived usefulness of various anatomy-learning modalities, and differences in their confidence in being able to identify anatomical structures using various pedagogical modalities (prosections, radiographs, images, unlabeled diagrams). The latter (Wilcoxon ranking) test was also employed to compare participants' change in confidence in identifying anatomical vessels on radiographs vs body surface marking at the end of the CPD course.

Table 1. Design of the questionnaires.

A. Questionnaire 1 (administered prior to the CPD course) [a]
A1. Participants' characteristics: ①Gender ②Age ③Nationality ④Radiographer/radiation therapist ⑤Graduation (institute, year) ⑥Additional qualification.
A2. Work experience: ①Practicing County ②Type of institute ③Number of people in the department ④Time since in practice ⑤Area of specialization ⑥Career break taken ⑦Experience working with imaging modalities.
A3. Anatomy teaching/learning experience: ①Teaching pedagogies employed during undergraduate training ②Perceived level of anatomy knowledge ③Current usage of anatomy learning tools ④Perceived usefulness of anatomy learning modalities ⑤Perceived confidence of identifying (a-anatomical structures on various pedagogical modalities, b-specific vessels on radiographs and on human body).
B. Questionnaire 2 (administered after the CPD course) [a]
B1. Anatomy teaching/learning experience: ①Perceived level of anatomy knowledge ②Perceived usefulness of anatomy learning modalities ③Perceived confidence of identifying (a-anatomical structures on various pedagogical modalities, b-specific vessels on radiographs and on human body).
B2. Questions about the anatomy CPD course: ①Importance for career progression? ②Value added to knowledge of anatomy? ③Willingness to (a-attend additional CPD courses? b-spend time on anatomy CPD?) ④Beneficial aspects of the course for learning anatomy? ⑤Areas which need more focus in the future? ⑥Preferred learning materials in anatomy CPD? ⑦When attending the CPD what were (a-underlying reasons? b-barriers encountered?) ⑧Where did they hear about the course, their expectations and how to improve in the future?
B3. Earlier involvement and attendance in IV cannulation course earlier (Yes/No)
B4. Three specific topics or imaging modalities where the participants would welcome anatomy study materials in future CPD courses.
B5. Participants' course satisfaction.

[a] Questionnaires employed to gauge the attitudes and interests of radiographers and radiation therapists regarding an anatomy CPD course for IV cannulation, CPD = continuous professional development.

Table 2. Demographics.

Participants' characteristics
Gender Males = 3 (2 radiographers, 1 radiation therapist) Females = 11 (8 radiographers, 3 radiation therapists)
Age (±SD) 29 (±6.2) years
Nationality Irish = 12, Non-Irish = 2
Radiographers = 10/14 participants (71.4%), **Radiation therapists** = 4/14 participants (28.6%)
Graduation year (no. of participants), (Work experience ±SD) years
< 2000 (zero)
2000–2010 (2 participants), (15.5) years
2011–2020 (12 participants), (2.6 ±1.3) years
Graduation country (no. of participants)
United Kingdom (7), Ireland (5), non-EU country (2)[a]
Workplace type (no. of participants)
University hospital (9), Local hospital (2), Regional hospital (1), Clinic (2)

SD = Standard deviation, EU = European union, [a] = 2 participants (from Zimbabwe and India).

RESULTS

Participants' characteristics

The participants included 10 radiographers (2 males, 8 females) and 4 radiation therapists (1 male, 3 females), with a mean age of 29 ± 6.2 years (males = 28 ± 5.3 years, females = 29 ± 6.6 years) (Table 2). These were mainly Irish nationals (12/14 participants), who had graduated from Ireland and the United Kingdom. At the time of the study, all the participants were working in various counties of Ireland, with the majority (64.3%) working within university-hospital-based settings (Table 2). Most participants (85.7%) had graduated recently— within the last 10 years, with an average work experience of 2.6 ± 1.3 years (Table 2). Only two participants had graduated in 2001 and 2006, and possessed 18 and 13 years of experience practicing as a radiation therapist and a radiographer, respectively. In addition, the results revealed that 5 participants had previously taken a career break— two practitioners had taken a break for 3 months each, the other two for 12 months each, while one undertook a break for a time duration of 18 months. The career break was not influenced by the gender distribution of the participants (2 males, 3 females). Out of all the participants, 34.7% had been involved in performing intravenous cannulation prior to the course, while 21.4% had attended a similar CPD course earlier (Table 1-B3).

Work focus

The majority of participants (4 out of 14) specialized in working in CT. Several had worked in a variety of imaging modalities, including MRI, PET and the Cardiac catheterization laboratory (Table 1-A2-point 5). When inquired about the imaging modalities (Table 1-A2-point 7, Fig. 1), >70% of participants had worked with fluoroscopy (78.6%), plain film radiographs (78.6%), pediatric imaging (71.4%) and CT scanning (71.4%). A lesser percentage of radiographers and radiation therapists had experience of working with trauma imaging (64.3%), angiography and interventional imaging (50%), GI studies (42.9%), contrast agents (42.9%), radiotherapy (28.6%), mammography (14.3%), MRI (14.3%), nuclear medicine (7.1%), ultrasonography (7.1%) and PET imaging (7.1%) (Fig. 1).

Anatomy teaching and learning experience

When inquired about how anatomy was taught to the participants during undergraduate years (Table 1-A3-point 1), the results demonstrate that 93% of participants (13 out of 14) had been taught anatomy using PowerPoint lectures, with 64.3% been taught using dissection and plastic models, while prosections had been employed to teach the anatomy in only 7.1% of cases (1 participant) (Fig. 2). The data is not all-exclusive, with some participants having been taught using a combination of pedagogies during undergraduate years.

The results revealed a significant difference between the perceived usefulness of various modalities for learning anatomy, both before the CPD course (Table 1-A3-point 4, Fig. 3A, Friedman test; $\chi2(5) = 30.787$, $P < 0.001$) and after the CPD course (Table 1-B1-point 2, Fig. 3B, Friedman test; $\chi2(5) = 28.633$, $P < 0.001$). Additional analysis showed that before the CPD course, the usefulness of newer modalities, such as social media was rated significantly lower compared to all other modalities (Wilcoxon-signed rank test; $P < 0.05$ for social media vs. plastic models, $P < 0.01$ for social media vs. e-learning, prosections/dissection, textbooks and lectures). None of these mean perceived usefulness values correlated significantly with the age of the participants (Pearson correlation; $P > 0.05$). The perceived usefulness of social media continued to rank lower even after the CPD course (Wilcoxon-signed rank test; $P < 0.01$ for social media vs. lectures and prosections/dissection, $P < 0.05$ for social media vs. e-learning, plastic models and textbooks). However, the perceived usefulness of prosections/dissection increased significantly compared to all other anatomy learning modalities (Wilcoxon-signed rank test; $P < 0.01$ for prosection/dissection vs. social media and textbooks, $P < 0.05$ for prosection/dissection vs. e-learning, plastic models and lectures).

When inquired if practitioners were using any learning tools prior to the CPD course to enhance their knowledge of anatomy (Table 1-A3-point 3), only 3 participants mentioned employing e-learning and textbooks, while others did not report using any learning resource at all.

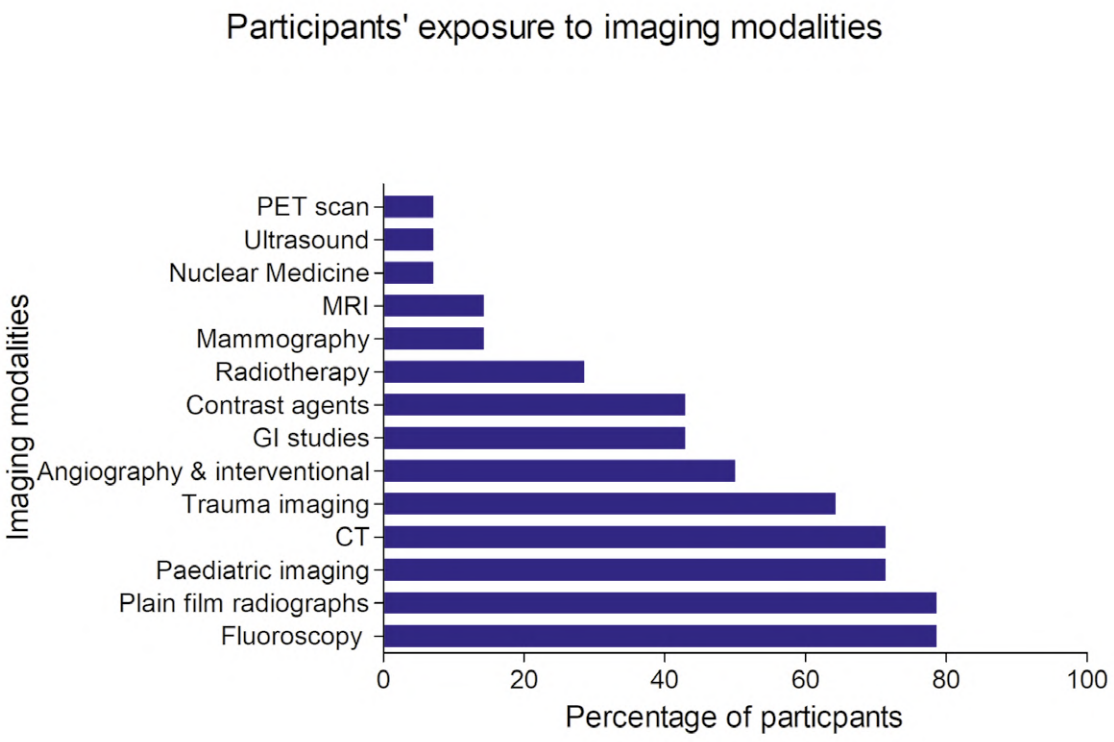

Fig. 1.- Percentage of participants (radiographers and radiation therapists) exposed to various imaging modalities. The greatest proportion of participants had worked with plain film radiographs and fluoroscopy, while the least proportion of participants were exposed to PET scan, ultrasound and nuclear medicine imaging modalities during their work experience. CT=contrast tomography, MRI=magnetic resonance imaging, PET=positron emission tomography, GI=gastrointestinal.

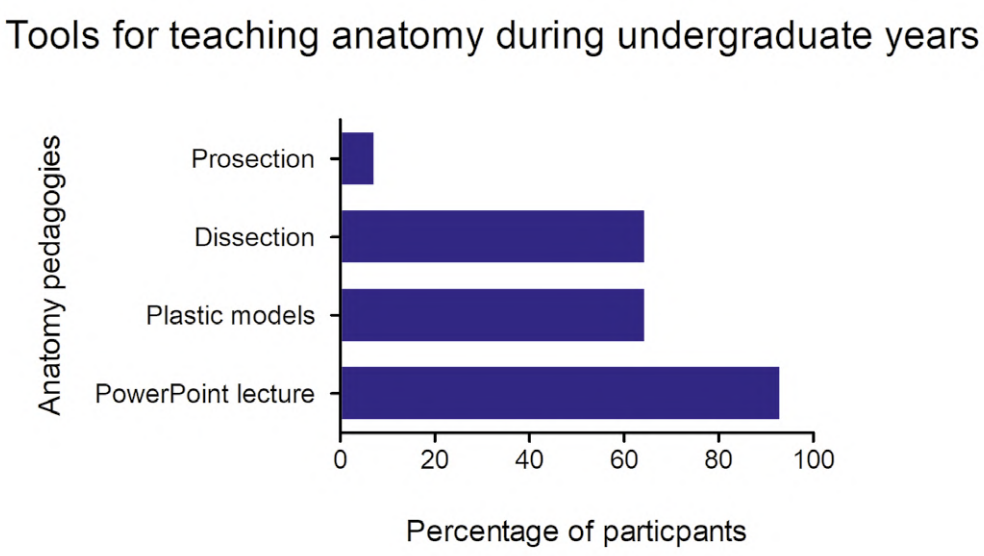

Fig. 2.- How were you taught anatomy during undergraduate years? Majority participants had been taught anatomy using PowerPoint lectures, followed by plastic models, dissection, and prosections.

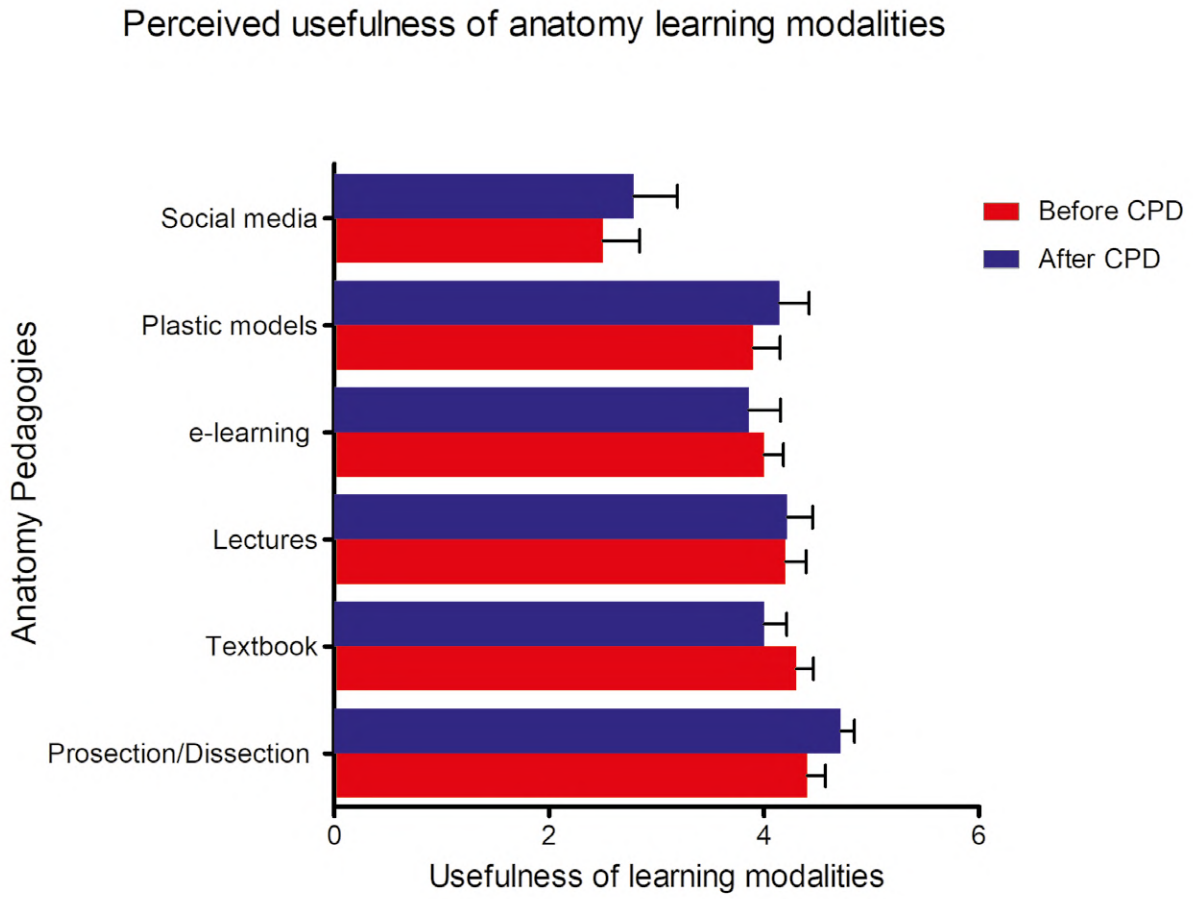

Fig. 3.- How would you rate the usefulness of following modalities for learning anatomy? (1=least useful, 5=most useful). The horizontal bars represent the participants' perceived usefulness of various modalities for learning anatomy, before (red bars) and after the CPD course (blue bars). The data demonstrates that social media was ranked significantly lower compared to all other modalities, before and after the CPD course. However, the perceived usefulness of the dissection/prosections increased significantly after the CPD course as compared to all other learning modalities ($P < 0.05$). The error bars signify the standard error of means (SEM).

Perceived level of anatomy knowledge and confidence in identifying anatomical structures

Prior to the commencement of the CPD course, the participants' average perceived level of anatomy knowledge was 3.3 (±0.27 SEM); on a scale of 1 to 5 (lowest to highest) (Table 1-A3-point 2). While the work experience and the year of graduation of the participants were strongly correlated with each other (r = 0.969, P < 0.01), neither of these two characteristic-features were significantly linked with the perceived level of anatomy knowledge (work experience; r = 0.317, P > 0.05, year of graduation; r = 0.226, P > 0.05). At the end of the CPD course, the participants seemed more confident regarding their level of anatomy knowledge (4.2 ±0.19 SEM), with the paired sample t-test results eliciting a significant increase in the mean perceived level of anatomy knowledge (T (13) = -2.738, P < 0.05) (Table 1-B1-point 1).

Prior to the CPD course, the participants showed a significant difference in their confidence in being able to identify structures between various pedagogical modalities (Table 1-A3-point 5a, Fig. 4A, Friedman test; $\chi2(4)$ = 33.809, P < 0.001). The confidence level was highest for the radiographs (Wilcoxon's signed rank test; P < 0.05 for comparisons of radiographs vs. prosections, plastic models, unlabelled diagrams and images), and lowest for the prosections (Wilcoxon's signed rank test; P < 0.05 for comparisons of prosections vs. images, unlabelled diagrams and prosections). The confidence levels for prosections (mean 2.8 ± 0.9 SEM) were not related to their earlier use of prosections (r = -0.186, P > 0.05) or dissection pedagogies (r = 0.069, P > 0.05) for learning anatomy during the undergraduate years.

Following the CPD course, the participants were equally confident in identifying anatomical structures on all pedagogical modalities (Table 1-B1-point 3a, Fig. 4B, Friedman test; $\chi2(4)$ = 8.254, P > 0.05). When compared with their confidence with the pedagogies prior to the CPD course, the results revealed that participants' confidence in identifying anatomical structures significantly increased across several pedagogies— including prosections (P < 0.01), plastic models (P < 0.05) and

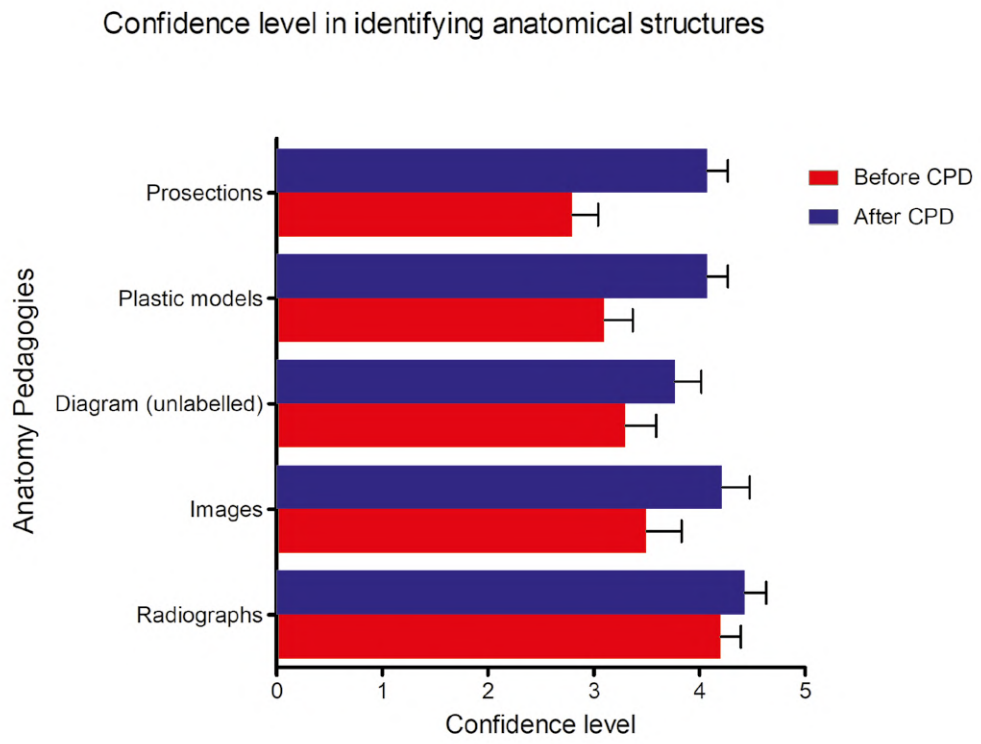

Fig. 4.- How would you rate your confidence at identifying anatomical structures in the following modalities/tools? (1=least confident, 5=highly confident). The horizontal bars represent the mean perceived level of confidence of the participants in identifying anatomical structures on various pedagogical modalities, before (red bars) and after the end of the course (blue bars). The error bars represent the SEM (standard error of mean). Results signify that participants' confidence in identifying anatomical structures increased at the end of the course, across all anatomical pedagogies.

images ($P < 0.05$), but not for radiographs ($P > 0.05$) and unlabelled diagrams ($P > 0.05$) (Fig. 4A, B).

Identification of specific anatomical vessels on the radiographs and on the human body

The results did not reveal any significant difference in the confidence level of participants when identifying anatomical vessels on the radiographs as compared to surface-marking them on the human body (Fig. 5, Wilcoxon's signed rank tests for all vessels $P > 0.05$).

The confidence level increased significantly by the end of the CPD course for most vessels, both in terms of identifying them on the radiographs (Fig. 5A) and surface-marking them on the human body (Fig. 5B). However, when compared against each other (post CPD, radiographs Vs. surface marking), the rise in confidence level was higher for surface marking for four vessels, namely cephalic, median cubital, popliteal and femoral veins, when compared to identifying them on the radiographs (Wilcoxon's signed rank test, $P < 0.05$).

Importance of the anatomy CPD course

The radiographers and radiation therapists were asked about the importance of an anatomy-based CPD for their career (Table 1-B2-point 1), 57.1 % were of the view that an anatomy-based CPD is very important for their career and 42.9% perceived it to be important, while none considered it to be unimportant for their career progression. All participants reported that the course added to their knowledge of anatomy, with 4 participants believing that it provided an opportunity for them to review anatomy (Table 1-B2-point 2). In addition, everyone expressed their desire to attend additional similar CPD courses (Table 1-B2-point 3a), with 50% willing to spend 1-5 hours, 35.7% willing to spend 5-10 hours and remaining willing to dedicate >10 hours each year to attending similar CPD courses in the future (Table 1-B2-point 3b).

The participants had an equal preference for prosections/cadaver-based material (12 participants) and e-learning (11 participants) within an anatomy CPD course (Table 1-B2-point 6). When inquired specifically about the beneficial aspects of the course (Table 1-B2-point 4), 7 out of 14 participants highly favoured the prosection-based anatomy teaching sessions and the practical sessions as part of the CPD course.

For the future CPD courses, a heavier focus was recommended on cross-sectional views of anatomy by 11 participants, vasculature by 7 participants and gross anatomy by 6 participants (Table 1-B2-point 5). When asked to pick three topics in which they would welcome anatomy

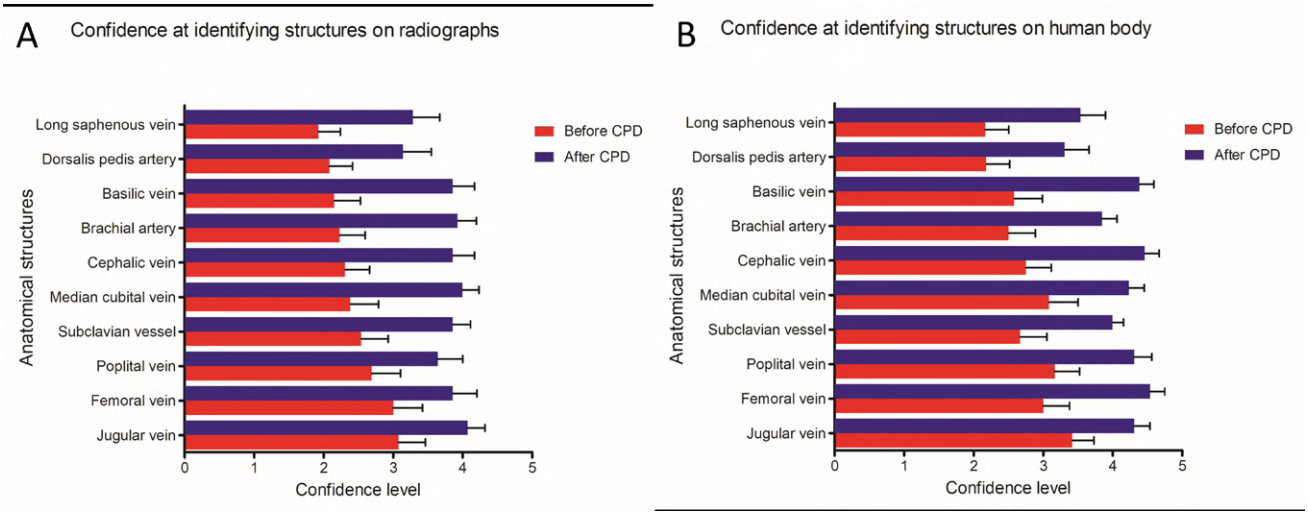

Fig. 5.- How would you rate your confidence at identifying the specific anatomical structures on radiographs and on patients (i.e., surface marking)? (1=least confident, 5=highly confident). The horizontal bars represent the mean perceived level of confidence of the participants in identifying various arteries and veins (enlisted along the y-axis), before and after the CPD course – on the radiographs (A) and on the human body (B). The error bars signify the SEM (standard error of mean). Results reveal that participants' confidence in identifying anatomical vessels increased significantly for most vessels at the end of the CPD course, both on the radiographs and upon surface marking them on the human body. Note: *= P < 0.05, **= P < 0.01.

study materials during future CPD courses, CT was selected by 13 (out of 14) participants, MRI by 5 participants and cross-sectional anatomy and radiotherapy by 4 participants (Table 1-B5).

When inquired about the reasons for undertaking the CPD course (Table 1-B2-point 7a), developing new knowledge (11/14 participants), fulfilling the mandatory requirement (8/14 participants) and skill enhancement (12/14 participants) were considered equally important factors by the participants for attending the course. Funding, time allocation, location and staffing issues, management and employer attitude or support were highlighted as potential barriers for attending the CPD course (Table 1-B2-point 7b). Most participants heard about the course from their employer or at their workplace and attended it with the expectations of learning the skill of intravenous cannulation. Only 1 discovered the course online, while 1 participant attended the course with the expectation of acquiring the complete knowledge of vasculature of the upper and lower limbs (Table 1-B2-point 8).

DISCUSSION

Both radiographers and radiation therapists are highly motivated professionals who aim to provide the highest and safest standards of care for the patients. Therefore, it is important for these professionals to continue enhancing their knowledge by participating in CPDs relevant to their field of practice. This study is novel, as it provides an Irish perspective of radiographers and radiation therapists on the significance of anatomy teaching and learning during a CPD course on IV cannulation and administration. The participants came from various locations across the country, and had been working in different parts of Ireland, providing a homogenous perspective of Irish radiographers and radiation therapists, with opinion not being biased by any specific region. The participants attended an on-site IV cannulation CPD course for one and a half days, and were encouraged to actively engage and enhance their learning process using various interactive teaching approaches.

An overwhelming proportion of participants were from university-based hospitals, which could potentially reflect the greater inclination of faculty involved in teaching and training towards fulfilling their CPD requirements. A previous study by Marshall and colleagues (2008) also showed a higher participation of university-based participants in CPD courses. Although their sample size was larger and encompassed 12 European countries, they did not include any Irish participants (Marshall et al., 2008). Hence, our study is novel, as it provides an Irish perspective on the significance of anatomy learning in an IV cannulation course.

An anatomy-based CPD was considered important by most Irish radiographers and radiation therapists for their career progression, in the context of enhancing their clinical IV cannulation skills. The key instigators were their interest in acquiring new knowledge and developing or enhancing their cannulation skills. All the participants agreed that the course added to their knowledge of anatomy, and agreed to attending similar courses in the future. Similar to other studies, funding, time allocation, location and staffing issues, management, and employed support were highlighted as potential barriers (Grehan et al., 2018).

The advent and rapid progression of the various cross-sectional medical imaging modalities (Marshall et al., 2008; Gore, 2020) were also reflected in our study by the fact that most participants' preferences for future CPD was an increased focus on cross-sectional views of anatomy. The continuous improvement of knowledge in cross-sectional imaging is important for radiographers and radiation therapists (Marshall et al., 2008; Hardy and Snaith, 2009). Moreover, a heavier focus was recommended by participants on cross-sectional views of anatomy and greater incorporation of CT images in the future, similar to results reported by Marshall and colleagues. The results suggest that there is an appetite amongst the majority to undertake CPD, and therefore resources should be redirected to address these limiting concerns. Participants' suggestions should be incorporated into future

courses for further enhancing the course quality standards and better meeting the radiographer's professional requirements.

Previously, Marshall and colleagues (2008) provided a general perspective of the Irish radiographers about the importance of CPD. However, the significance of anatomy learning in the specific context of the development or the enhancement of their IV cannulation skill had not been explored. One must remain mindful of the fact that most of the study participants were at an early stage of their career, with only approximately one third having prior cannulation experience, or having previously attended a similar CPD cannulation course. Moreover, the majority of participants were working in university-based settings, with a potential greater interaction with the university academic staff members. This lack of experience and interaction with the academic staff members might have inclined them to having a positive opinion about the CPD course, and possibly added bias to the results. The latter is also supported by the fact that majority of study participants heard about the course at their workplace. Hence, while the study provided a novel Irish perspective, a larger-scale study with increasing number of participants across the country needs to be conducted to validate the results further.

Survey results from Grehan and colleagues (2018) showed that most radiographers believed that their CPD was self-directed, with most departments having yet to set up structured internal CPD programs. Our CPD course was sequentially well-structured in a manner where participants were taught the basic anatomy of the human vasculature, followed by didactic lectures, and then providing opportunity to the participants to practice their IV cannulation skills. Apart from the lack of structure, previous studies have also shown that formal didactic approaches which had been commonly employed for CPD learning, might not necessarily suit people with varying learning styles (Waterston and Stewart, 2005; Grehan et al., 2018). Some people learn better through hands-on experience and/or visual interaction with the study material or even observation of practice (Grehan et al., 2018). Previously, it was reported that traditional CPDs have little impact in enhancing professional practice (Davis et al., 1999; Bloom, 2005; Wallace and May, 2016). The current study offers valuable results to steer the discussion on this viewpoint by supporting the validity of the hands-on experience and clinical work, while the significance of formal didactic lectures is not undermined. The instructional design of our CPD incorporated hands-on teaching and learning of anatomy, using prosections where participants acquired a haptic feedback as they reviewed their anatomy knowledge of human vasculature. Moreover, a simulation course for practicing their IV cannulation skills was provided using artificial training arms, which participants could hold in their hands to acquire haptic feedback. The results suggest that it enhanced their knowledge of vascular anatomy, and participants had a positive opinion of the course and were interested in attending similar courses and considered it important for their career progression (Shanahan, 2016).

Currently, there is a gap in the literature on the use of social media within postgraduate radiography education (Sterling et al., 2017) with a lack of evidence on the benefits of radiographers using social media as a constructive, positive tool for ongoing CPD. Grehan et al. (2018) showed that although most radiographers were comfortable with using social media in general, more than 25% of study participants were unwilling to use social media as a mechanism of obtaining CPD, especially the older age group being more reluctant to use social media for CPD purposes (Grehan et al., 2018). Our results further reinforce these findings by showing a lack of perceived usefulness of social media for learning vascular anatomy for enhancing their IV cannulation skills.

Previously, in a large-scale study conducted across 12 European countries, Marshall and colleagues (2008) showed that most radiographers (67%) prefer a combination of paper-based and e-learning methodologies as part of the pedagogical construct of the CPD courses, suggesting that they are receptive to creative ways for CPD delivery. However, the

data on the provision of human cadaver material for CPD for radiographers was missing in the literature. The current study employed the use of human prosections to help radiographers and radiation therapists to learn the 3D anatomical relationships of vascular anatomy. And our results show that the participants' appreciation of the usefulness of prosections was significantly higher than that of social media and the former increased significantly after the course, compared to all other pedagogical tools, including lectures, videos, animations and models, etc. While these results highlight the educational efficacy of employing prosections (never done before) for radiography CPD, it also highlights the usefulness of multimodal pedagogies employed in a structured fashion to enhance the knowledge and practical IV cannulation skills of the radiographers and radiation therapists. The results are useful in order to inform the instructional and experimental design of the future CPD courses for allied health professionals.

Our initial feedback suggests that the hybrid model of CPD is an excellent way to enhance the anatomy knowledge of radiographers and radiation therapists relevant to their field of practice.We consider that our CPD model is important, as the participants can integrate the anatomy knowledge achieved in their clinical practice. Ultimately, supporting and encouraging the radiographers and radiation therapists to engage and improve their continuous professional development is key in order to provide the best of care for the patients.

Limitations of the study

1. Small sample size

The results from the current study provide a novel Irish perspective on importance of anatomy learning and IV cannulation CPD. The sample size is limited; however, the results still hold paramount importance as they provide an Irish perspective, which is previously missing in the literature. We intend to continue the study for several years to increase our sample size and to follow the opinion of radiographers and radiation therapists in a prospective fashion.

2. Triangulation of data-acquisition methods

Data acquisition should be better triangulated by incorporating interviews and open-ended questionnaires, coupled with a qualitative analysis of the results acquired.

CONCLUSION

We conclude that the participants perceived anatomy prosections/dissection useful compared to other learning modalities. This corresponded with a significant increase in their perceived level of anatomy knowledge and confidence in identifying structures on prosections, and vessels on radiographs and body surface. The use of prosections and hands-on practical sessions was highly commended and a desire to attend similar future courses was expressed.

We conclude that an interactive anatomy-based CPD—employing multimodal pedagogies—is effective in enhancing anatomy knowledge, and can effectively contribute towards enhancing clinical competence of radiographers and radiation therapists.

NOTES ON CONTRIBUTORS

Dr Mutahira Lone, BDS. PhD is a lecturer and program coordinator for the MSc in Human Anatomy in the Department of Anatomy and Neuroscience at University College Cork. She also teaches gross anatomy to the MSc students and oral anatomy and histology to the dental students. Her research interest is focused on innovative and research-based pedagogies for anatomy students.

Ahmad H. Sheikh, MBBS, MRCS, MD is a Senior Medical Demonstrator in the Department of Anatomy and Neuroscience at the University College Cork, Ireland. He teaches Gross Anatomy and Neuroanatomy to a wide cohort of medical and health sciences' students using cadaver dissection, prosection, and a variety of modern anatomical teaching modalities. He devised a novel cadaver-based surgical skills and procedures workshop for medical students, as a new signature pedagogy in anatomical education.

Andreea Factor, M.D., MSc is a College Lecturer in the Department of Anatomy and Neuroscience, University College Cork, Ireland. She teaches in a number of programs in Medicine and Health as well as Biomedical Engineering. Her research interests include anatomy education, neurology and cardiology.

Niamh Moore, MSc is a diagnostic radiographer who holds an MSc in Computed Tomography. Niamh worked as a clinical radiographer for many years in advance of working in her current role as a lecturer on the MSc Diagnostic Radiography program in UCC. Niamh led in the development and running of the IV cannulation and administration course for Radiographers and Radiation Therapists in UCC.

Muhammad Asim Javaid, M.D., Ph.D is a senior lecturer in the Department of Anatomy at Anglia Ruskin University,

Chelmsford, United Kingdom. He is the Year 2 academic lead for the MBCHB program in Anglia Ruskin. He teaches anatomy to medical and health science students using cadaver-dissection, prosections and a variety of modern technological pedagogies. His research interests are focused on technology-enhanced learning in anatomy education.

REFERENCES

ARRAEZ-AYBAR LA, SANCHEZ-MONTESINOS I, MIRAPEIX RM, MOMPEO-CORREDERA B, SANUDO-TEJERO JR (2010) Relevance of human anatomy in daily clinical practice. *Ann Anat,* 192(6): 341-348.

BLOOM BS (2005) Effects of continuing medical education in improving physician clinical care and patient health: a review of systematic reviews. *Int J Technol Assess Health Care,* 21: 380-385.

CORU (2019) Guidance on Continuing Professional Development. Available from: https://coru.ie/files-education/cpd/rrb-guidance-on-continuing-professional-development.pdf [Accessed online 27th Apr 2021].

CRAFT JA, HUDSON PB, PLENDERLEITH MB, GORDON CJ (2017) Registered nurses' reflections on bioscience courses during the undergraduate nursing programme: an exploratory study. *J Clin Nurs,* 26(11-12): 1669-1680.

DAVIS D, O'BRIEN MAT, FREEMANTLE N, WOLF FM, MAZMANIAN P, TAYLOR-VAISEY A (1999) Impact of formal continuing medical education: do conferences, rounds, and other traditional continuing education activities change physician behaviour or health care outcomes? *JAMA,* 282: 867-874.

DE BOO DW, MARSHALL E, ERSKINE B, KOUKOUNARAS J, KAVNOUDIAS H, THOMSON KR (2020) Evaluation of a radiographer-led peripherally inserted central catheter insertion service. *J Med Imaging Radiat Oncol,* 64(4): 471-476.

DRAKE RL, MCBRIDE JM, LACHMAN N, PAWLINA W (2009) Medical education in the anatomical sciences: The winds of change continue to blow. *Anat Sci Ed,* 2(6): 253-259.

DOUGHTY J, HODGSON D (2009) Evaluation of a new clinical support model in radiotherapy practice. *Nurse Educ Pract*, 9(1): 28-35.

GORE JC (2020) Artificial intelligence in medical imaging. *Magn Reson Imaging*, 68: A1-A4.

GREHAN J, BUTLER ML, LAST J, RAINFORD L (2018) The introduction of mandatory CPD for newly state registered diagnostic radiographers: An Irish perspective. *Radiography,* 24(2): 115-121.

HALL AS, DURWARD BR (2009) Retention of anatomy knowledge by student radiographers. *Radiography*, 15(3): e22-e28.

HARDY M, SNAITH B (2009) Radiographer interpretation of trauma radiographs: Issues for radiography education providers. *Radiography*, 15(2): 101-105.

HENWOOD S, EDIE J, FLINTON D, SIMPSON R (1998) Continuing professional development – a re-examination of the facts. *Radiography*, 4(1): 5-8.

HEPTONSTALL NB, ALI T, MANKAD K (2016) Integrating radiology and anatomy teaching in medical education in the UK—the evidence, current trends, and future scope. *Acad Radiol*, 23(4): 521-526.

MARSHALL G, PUNYS V, SYKES A (2008) The continuous professional development (CPD) requirements of radiographers in Europe: An initial survey. *Radiography*, 14(4): 332-342.

MARTIN K, BESSELL NJ, SCHOLTEN I (2014) The perceived importance of anatomy and neuroanatomy in the practice of speech—Language pathology. *Anat Sci Educ*, 7(1): 28-37.

MCLACHLAN JC, PATTEN D (2006) Anatomy teaching: ghosts of the past, present and future. *Med Educ,* 40(3): 243-253.

MINOGUE S, GILLHAM C, KEARNEY M, MULLANEY L (2019) Intravenous contrast media in radiation therapy planning computed tomography scans – Current practice in Ireland. *Tech Innov Patient Support Radiat Oncol,* 1(12): 3-15.

PATEL KM, MOXHAM BJ (2006) Attitudes of professional anatomists to curricular change. *Clin Anat,* 19(2): 132-141.

SHANAHAN M (2016) Student perspective on using a virtual radiography simulation. *Radiography,* 22(3): 217-222.

STERLING M, LEUNG P, WRIGHT D, BISHOP TF (2017) The use of social media in Graduate Medical Education: A systematic review. *Acad Med*, 92(7): 1043-1056.

SUGAND K, ABRAHAMS P, KHURANA A (2010) The anatomy of anatomy: A review for its modernization. *Anat Sci Educ,* 3(2): 83-93.

TURNEY BW (2007) Anatomy in a Modern Medical Curriculum. *Ann R Coll Surg Engl,* 89(2): 104-107.

WALLACE S, MAY SA (2016) Assessing and enhancing quality through outcomes-based continuing professional development (CPD): a review of current practice. *Veterinary Rec,* 179(20): 515-520.

WALSH R, CRAIG A (2016) Radiation Therapists' and Diagnostic Radiographers' participation in continuing professional development and knowledge of regulatory body registration. *J Radiother Pract*, 15(2): 150-160.

WAREING A, BUISSINK C, HARPER D, OLESEN MG, SOTO M, BRAICO S, VAN LAER P, GREMION I, RAINFORD L (2017) Continuing professional development (CPD) in radiography: A collaborative European meta-ethnography literature review. *Radiography*, 23(Suppl.1): S58-S63.

WATERSTON S, STEWART I (2005) Survey of clinicians' attitudes to the anatomical teaching and knowledge of medical students. *Clin Anat,* 18(5): 380-384.

Effects of omega-3 fatty acids and CoQ10 on gross morphology of intervertebral discs subjected to immobilization

Fareeha Mushtaq[1], Abdullah Qamar[2], Muhammad S. Abdullah[3], Humaira Ali[4], Maimoona Ali[5], Kishwar Naheed[6]

[1] Mohterma Benazir Bhutto Shaheed Medical College, Mirpur, AJK

[2] Department of Anatomy, Army Medical College, Rawalpindi

[3] CMH Kharian Medical College, Kharian Cantt

[4] Swat Medical College, Saidu Sharif, Swat.

[5] Mohiuddin Islamic Medical College, Mirpur, AJK

[6] Watim Medical and Dental College, Rawalpindi

SUMMARY

The aim of the study was to determine the effects of immobilization on the gross morphology of rats' intervertebral disc (IVD) and observe the ameliorating effects of Omega 3 fatty acids and Co-enzyme Q 10 (CoQ10). Forty Sprague Dawley rats weighing 250-300 g were procured from NIH Islamabad. The animals were randomly selected and were divided into four groups of 10 animals in each. Group-A rats served as control group. Each rat of Group B was disc immobilized by using an Illizarov-type apparatus, which was applied for 60 days. Group-C and -D rats after disc immobilization were administrated with Omega 3 fatty acids (260 mg/kg/day) and CoQ10 (150mg/kg/day) through oral gavage respectively. Gross examination of IVD was done using the Thompson grading scale and the disc alterations were scored from grade 1 to 5 in increasing order of IVD alterations.

Gross examination of the sections of IVD's of the control group showed normal healthy morphology, falling in Thompson grade I degeneration. The frequency of disc alteration was statistically significant in disc-immobilized group B when compared to control group A (p-value=0.000), group C (p-value=0.000) and group D (p value=0.002). Group C in which n-3 fatty acid was given along with disc immobilization, showed significant improvement in disc degenerative changes. On comparison with group B, p-value<0.001 was statistically significant. In experimental Group D, where CoQ10 was given along with disc immobilization, the degenerative changes were significantly reduced as compared to Group B (p = 0.002). In this study, gross morphological changes were induced by immobilization in IVDs of the experimental rats and its reversal by omega 3 and CoQ10 was proven. Co-administration of Omega 3 and CoQ10 significantly minimized degenerative changes in IVDs induced by immobilization.

Key words: Intervertebral disc degeneration – Immobilization – Thompson Grade scoring –

Corresponding author:
Dr Fareeha Mushtaq. Mohterma Benazir Bhutto Shaheed Medical College, Mirpur, AJK. E-mail: dr.fareeha.shan@gmail.com

Submitted: September 11, 2021. **Accepted:** November 22, 2021

https://doi.org/10.52083/SBJZ3901

Nucleus pulposus – Annulus fibrosus – CoQ10 – Omega 3 fatty acid

INTRODUCTION

An intervertebral disc (IVD) is a cartilaginous structure in which progressive degenerative and ageing changes appear earlier than any other connective tissue in the body. Clinically it is considered very important because there is strong association of disc degeneration with disability and devastating backache (Urban and Roberts, 2003). Back pain is a common community health problem and a leading cause of disability that causes suffering and distress to patients and their families. There is a decreased incidence of low back pain in people who are physically fit and active, whereas a sedentary lifestyle with reduced physical activity is related to an increased risk for low back pain (James et al., 1999). An IVD is composed of three components: in the centre nucleus pulposus (NP), gelatinous core which is surrounded by 15-20 thick fibrous rings forming annulus fibrosus (AF), and the upper and lower end plates. Significant changes occur in these components that are indicative of disc degeneration. These include the destruction of extracellular matrix, the injury to the cells. Major morphological changes are observed in degenerated discs, where the annular lamellae become disorganized and irregular. In the NP, frequent cleft and fissure formation is seen (Buck Walter, 1995). An effective proteoglycan, Aggregan, is destroyed in degenerated discs, which lead to loss of hydration, and fragments of NP bulge into AF (Hayes et al., 2001).

Nerlich studied that oxidative stress is a cellular state where raised levels of reactive oxygen species (ROS) may contribute to destruction of extracellular matrix and cell apoptosis, which eventually results in disc degeneration (Nerlich et al., 2007). Disc degeneration is a form of chronic inflammation which leads to an upregulation of pro-inflammatory markers that shift homeostasis towards the extracellular matrix degeneration, with successive breakdown of its components (Burke et al., 2002). We hypothesize that the potent antioxidant property of Co Q 10, as well as the ability of omega 3 fatty acids to inhibit a number of aspects of inflammation, present them as good therapeutic candidates to treat disc degeneration (Sohal and Forster, 2007) (Wall et al., 2010).

MATERIALS AND METHODS

Forty Sprague-Dawley rats 3 to 4 months of age, with an average weight of 250-300 grams, were used in the experiment and were kept in controlled environment of animal house of NIH, Islamabad. The study was carried out in the Department of Anatomy, Army Medical College Rawalpindi, in collaboration with National Institute of Health (NIH), Islamabad and Armed Force Institute of Pathology (AFIP), Rawalpindi. It was a laboratory-based experimental control trial that spanned for two months.

Rats were randomly divided into four groups (n =10 animals in each group). Animals were raised on NIH laboratory standard diet and water ad libitum for two months in separate cages (Fig. 1A). Rats in group A served as control and were given standard lab diet and water ad libitum for

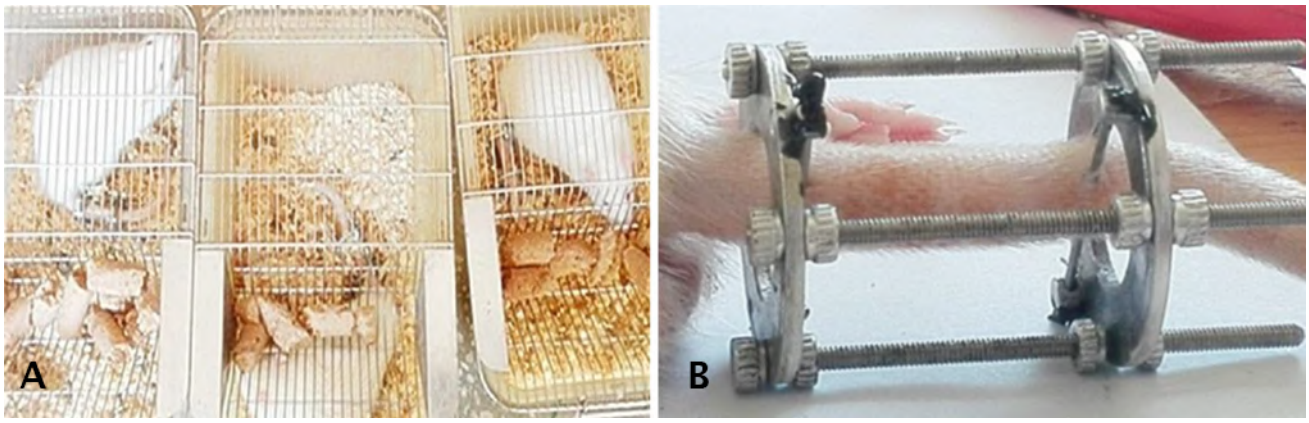

Fig. 1.- A. Rats placed in separate cages after apparatus was applied. **B.** Illazrov apparatus applied to immobilize the rat tail segment.

two months. Rats in group B were subjected to disc immobilization by using an Ilizarov-type apparatus (James et al., 1999). No medication was given to this group. They were given standard lab diet and water for two months. Rats in group C were subjected to disc immobilization using an Ilizarov type apparatus (Fig. 1B). They were administered omega 3FA through oral gavage at a dose of 260 mg/kg body weight (Abdou et al., 2014). In group D, rats were subjected to disc immobilization and were given Co-enzyme Q10 through oral gavage at a dose of 150 mg/kg/day (Kwong et al., 2002). At the end of 60 days, the animals were sacrificed.

The whole discs with the vertebrae adjacent to the immobilized segments (Co8-9 and Co10) were removed and dissected. The removed part of the vertebral column was sectioned in a sagittal plane 5 mm from the mid-line. The lateral cut surface was washed briefly under running tap water while brushing the bone lightly with soft toothbrush to remove debris. The cleaned surface was photographed and observed under dissecting microscope (Fig. 2). For the macroscopic analysis of these disc alterations, the Thompson grading scale (Table 1) was used, which attributes a grade of 1 to 5, in increasing order of intervertebral disc alterations (Thompson et al., 1990). A Sony digital camera (16 megapixel) was used through the ocular of the Olympus DP21 light microscope. The images were corrected and adjusted with respect to contrast, brightness, sharpness, and color balance by Photoscape software. IBM-SPSS version 21 was used for data analysis. Qualitative variables were presented by frequency and percentages. Chi square test was applied for comparison of qualitative variables.

RESULTS

Gross examination of IVD was done using the Thompson grading scale and the disc alterations were scored from grade 1 to 5 in increasing order of IVD alterations. On gross examination of specimens of Control Group A, intervertebral discs had soft central nucleus pulposus (NP) with well-

Fig. 2.- Rat tail under the dissecting microscope.

organized annulus fibrosus (AF) lamellae. They did not have any fissures in NP or any disruption of AF (Table 1, Fig. 3, Bar chart 1). Ten (100%) rats of the control group A showed Thompson grade I degeneration.

In disc-immobilized group B, 30% of the specimens showed Thompson III degeneration with loss of NP/AF distinction and fissures in NP and 50% of the specimens were lying in Thompson IV with fissures in NP and few points of focal sclerosis while 20% of the rats had flat discs and showed Thompson V degeneration. The frequency of disc alteration was statistically significant in disc-immobilized group B when compared to control group A (p-value=0.000), group C (p-value=0.000) and group D (p value=0.002) (Table 2, Fig. 4 and Bar chart 1).

Group C in which n-3 fatty acid is given along with disc immobilization, 40% of the rats were lying in Thompson I grade, 50% in Thompson II grade and 10% in Thompson III grade. On comparison with group B, p-value < 0.001, and this was statistically significant. When compared with experimental group D with p-value=0.450, the difference was statistically not significant (Table 2 and Bar chart 1).

Table 1. Thompson's macroscopic degeneration scale (Thompson et al., 1990).

Thompson Grade	Description
Thompson I	Nucleus pulposus of gelatinous appearance and annulus fibrosus with organized lamellae.
Thompson II	Nucleus pulposus with whitened fibrous tissue and mucinous material between the lamellae of the annulus fibrosus, note small fissure in the NP.
Thompson III	Loss of AF/NP distinction, focal defects in end-plate, sees dehydration of nucleus pulposus and longitudinal and vertical fissure.
Thompson IV	Fissures in the nucleus pulposus and parallel to the end-plate, with presence of focal sclerosis at this point.
Thompson V	Total sclerosis and flattening of the disc.

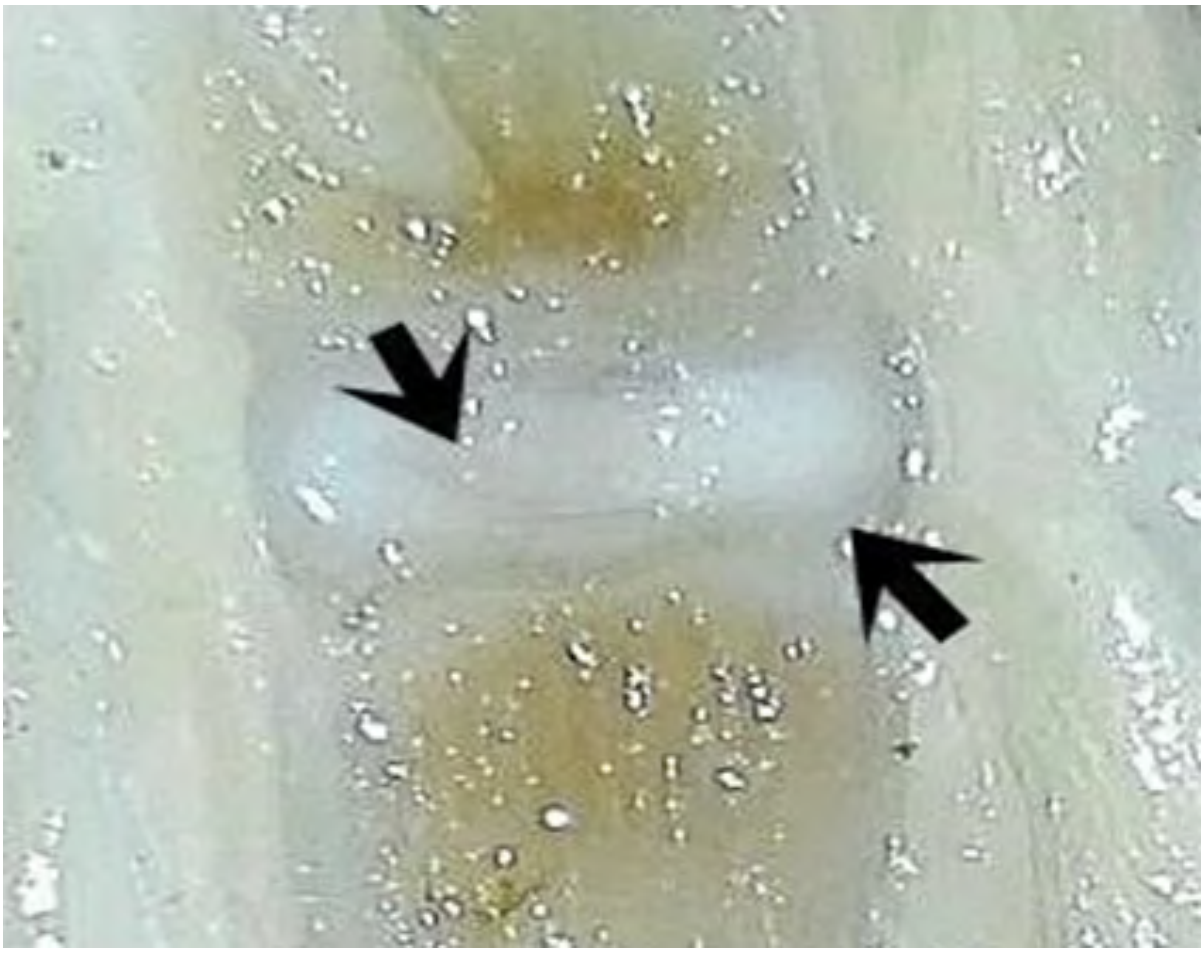

Fig. 3.- Normal healthy disc with central, gelatinous NP and well-organized AF in A6 rat of control group (Grade 1).

Table 2. Comparison of Thompson's scoring and p values for macroscopic degeneration between the control Group A and the experimental Groups B, C and D.

Thompson's scale for macroscopic degeneration	Group A (n=10)	Group B (n=10)	Group C (n=10)	Group D (n=10)	Group A/B	Group A/C	Group A/D	Group B/C	Group B/D	Group C/D
Thompson I	10(0%)	0(0%)	4(40%)	2(20%)	0.000*	0.011*	0.001*	0.000*	0.002*	0.450
Thompson II	0(0%)	0(0%)	5(50%)	5(50%)						
Thompson III	0(0%)	3(30%)	1(10%)	3(30%)						
Thompson IV	0(0%)	5(50%)	0(10%)	0(0%)						
Thompson V	0(0%)	2(20%)	0(0%)	0(0%)						

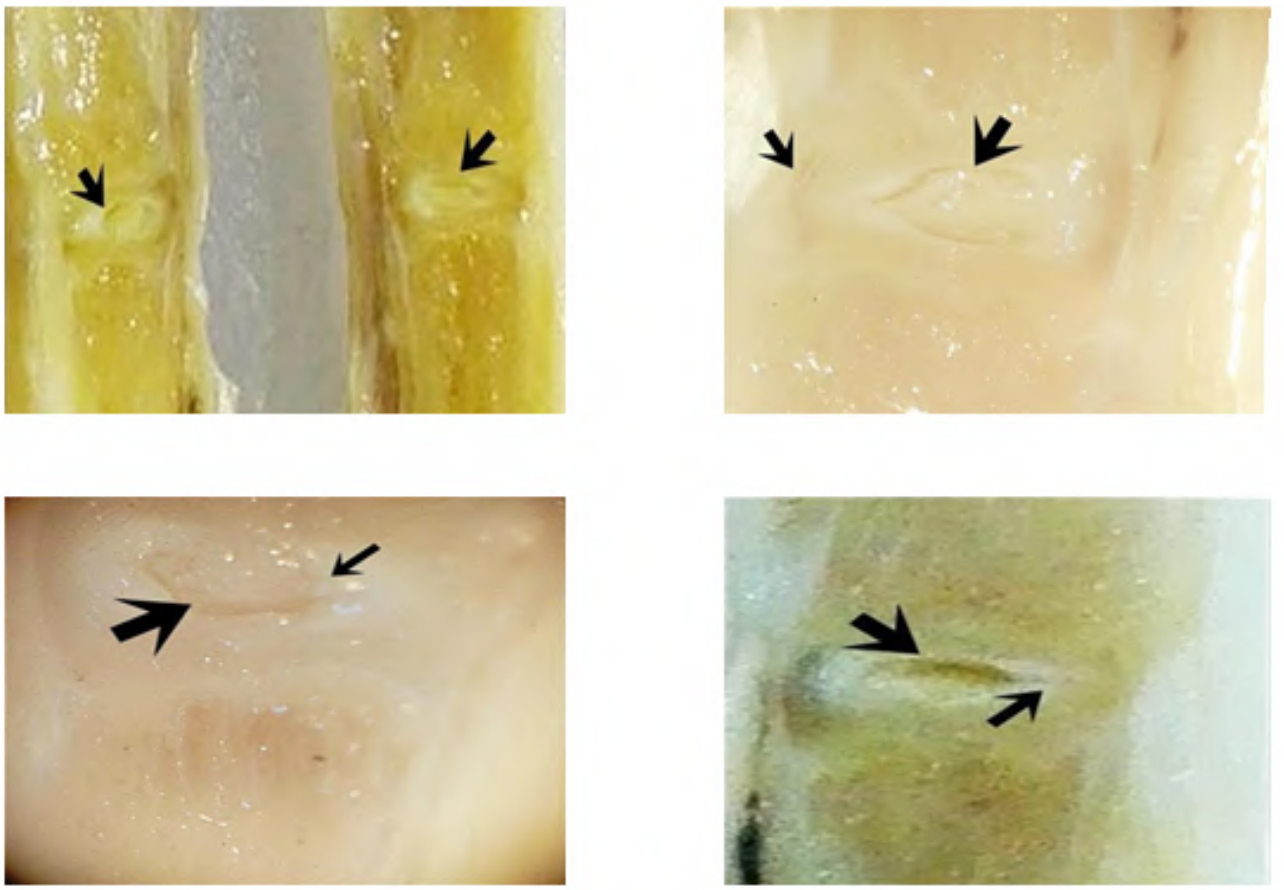

Fig. 4.- Different grades of gross morphological changes observed in intervertebral discs of rats of group B under dissecting microscope.

Whereas in experimental Group D, where CoQ10 is given along with disc immobilization, 20% of specimens showed Thompson I disc alterations, 50% showed Thompson II grade and 30% had Thompson III disc degeneration. On intergroup comparison it was found to be statistically significant with Group B (p = 0.002) (Table 2 and Bar chart 1).

DISCUSSION

This study indicated that immobilization induced in rats resulted in IVD degeneration. The causes for IVD degeneration are multifactorial and risk factors include heritability, ageing, rapid increase in weight, obesity, and physical activity levels. Effects of immobilization on IVD have been researched comprehensively; the main aim of this study was to appraise the beneficial effects

of nutraceuticals having anti-inflammatory and antioxidant properties in treating spinal pathologies.

Gross morphology of intervertebral discs was observed and graded with the help of two pathologists using Thompson's scale. All the animals in control group A showed healthy discs with no signs of degeneration. Gross morphological changes were significant and the severity (score) of disc degeneration was found to be significantly more in the disc-immobilized group B, and this validated the findings of the previous researchers, who established the adverse effects of prolong immobilization on disc morphology (Scholten et al., 2014; Che et al., 2018). Pro-inflammatory cytokines including interleukin-1β, interleukin-6, interleukin-8, interleukin-10, bFGF (basic fibroblast growth factor), phospholipase A2, PGE2 (prostaglandin E2) and TNF-α are released because of the destruction of ECM in IVD (Podichetty, 2007). It is established that these mechanisms lead to densification and disruption of the fibers constituting the annulus fibrosus (AF), progressive loss of distinction between annulus and nucleus, the formation of chondrocyte clusters in the deep part of the disc, the appearance of horizontal or vertical fissures in the disc, anterior and posterior herniation (with total or partial rupture of the fibers of AF) and flattening of disc (Baptista et al., 2015). Decreased cytokine-mediated ECM degeneration can be a more potent approach, since it interfered with an earlier phase in the pathway of IVD degeneration. The degenerative changes observed on gross morphology were reduced in frequency in group where omega 3 fatty acids were used. This is due to the fact that omega 3 fatty acids, when consumed in sufficient quantities, result in decreased leukocyte chemotaxis and decreased pro-inflammatory cytokines, and decreased adhesion molecule expression (Maroon and Bost, 2006), thus reducing damage to the intervertebral disc morphology. These results are in agreement

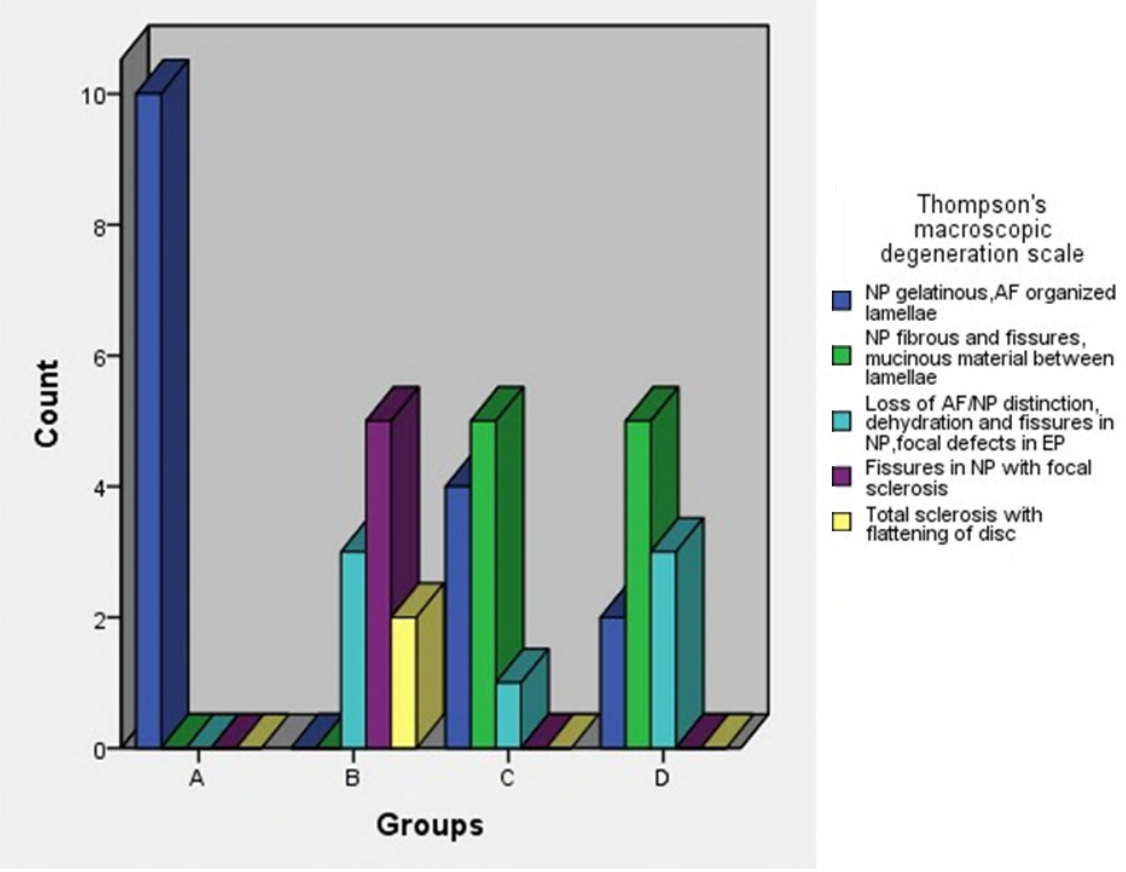

Bar chart 1. Clustered bar chart showing count of intervertebral discs (IVD) with scoring of macroscopic degeneration (Thompson's scale) among the control group A, disc immobilized group B, disc immobilized+Omg3 administrated group C and disc immobilized+CoQ10 administrated group D.

with the findings of Calder (2006). In recent years, numerous studies have demonstrated that oxidative stress plays an important role in the initiation and progression of disc degeneration (Suzuki et al., 2015).These reports led us to see an anti-oxidative therapy for alleviating oxidative stress on cells that may allow a slow but controlled regeneration of disc. Co Q10 is widely consumed by humans as dietary supplement and acts as a quencher of ROS. This motivated us to study the long term effects of Co Q10 on IVD degenerative process. The incidence of degenerative morphological changes was reduced in group D, given Co Q10, as compared to group B. These results are in accordance with those previously reported studies that have shown substantial reduction in oxidative stress and improvement in long-term degenerative diseases with oral Co Q10 supplementation (Sanoobar et al., 2013; Santoro, 2020). This is in agreement with a study that argues that antioxidant therapy aids in stabilizing blood vessels and reduce oxidative damage caused from degeneration within the IVD (Zhang et al., 2020).

CONCLUSION

Immobilization induced the gross morphological changes in the intervertebral discs of the experimental rats by increasing inflammation and oxidative stress. Co-administration of omega 3 fatty acids and enzyme CoQ10 minimized the immobilization-induced degeneration and improved the gross morphology of IVD, scored by using Thomson Grading Scale.

REFERENCES

ABDOU HM, HASSAN MA (2014) Protective role of omega 3 polyunsaturated fatty acid against lead acetate-induced toxicity in liver and kidney of female rats. *BioMed Res*, 2014: 435857.

BAPTISTA JS, FONTES RB DE V, LIBERTI EA (2015) Aging and degeneration of the intervertebral disc: Review of basic science. *Coluna/ Columna*, 14(2): 144-148.

BUCKWALTER JA (1995) Aging and degeneration of the human intervertebral disc. *Spine*, 20(11): 1307-1314.

BURKE JG, WATSON RW, MCCORMACK D, DOWLING FE, WALSH MG, FITZPATRICK JM (2002) Intervertebral discs which cause low back pain secrete high levels of proinflammatory mediators. *J Bone Joint Surg Br*, 84(2): 196-201.

CHE YJ, LI HT, LIANG T, CHEN X, GUO JB, JIANG HY, LUO ZP, YANG HL (2018) Intervertebral disc degeneration induced by long-segment in-situ immobilization: a macro, micro, and nanoscale analysis. *BMC Musculoskelet Disord*, 19(1): 1-10.

FRYMOYER JW, POPE MH, CLEMENTS JH, WILDER DG, MACPHERSON B, ASHIKAGA T (1983) Risk factors in low-back pain. An epidemiological survey. *JBJS*, 65(2): 213-218.

JAMES CI, PETER LM, IAN AFS, DAVID DA, MAURO A (1999) Compression-induced changes in intervertebral disc properties in a rat tail model. *Spine*, 24(10): 996-1002.

KWONG LK, KAMZALOV S, REBRIN I, BAYNE ACV, JANA CK, MORRIS P (2002) Effects of coenzyme Q10 administration on its tissue concentrations, mitochondrial oxidant generation, and oxidative stress in the rat. *Free Radical Biol Med*, 33(5): 627-638.

MARCHAND F, AHMED AM (1990) Investigation of the laminate structure of lumbar disc anulus fibrosus. *Spine*, 15(5): 402-410.

MAROON JC, BOST JW (2006) Omega-3 fatty acids (fish oil) as an anti-inflammatory: an alternative to nonsteroidal anti-inflammatory drugs for discogenic pain. *Surg Neurol*, 65(4): 326-331.

NERLICH AG, BACHMEIER BE, SCHLEICHER E, ROHRBACH H, PAESOLD G, BOOS N (2007) Immunomorphological analysis of RAGE receptor expression and NF-κB activation in tissue samples from normal and degenerated intervertebral discs of various ages. *Ann New York Acad Sci*, 1096(1): 239-248.

PODICHETTY VK (2007) The aging spine: the role of inflammatory mediators in intervertebral disc degeneration. *Cell Mol Biol*, 53(5): 4-18.

SANOOBAR M, EGHTESADI S, AZIMI A, KHALILI M, JAZAYERI S, REZA GOHARI M (2013) Coenzyme Q10 supplementation reduces oxidative stress and increases antioxidant enzyme activity in patients with relapsing–remitting multiple sclerosis. *Int J Neurosci*, 123(11): 776-782.

SANTORO MM (2020) The antioxidant role of non-mitochondrial CoQ10: mystery solved! *Cell Metab*, 31(1): 13-15.

SCHOLTEN I, CUSTERS IM, MOOLENAAR LM, FLIERMAN PA, COX T, GIANOTTEN J, HOMPES PGA, VAN DER VEEN F, MOL BW (2014) Long-term follow up of couples initially randomized between immobilization and immediate mobilization subsequent to IUI. *Reprod Biomed Online*, 29(1): 125-130.

SOHAL RS, FORSTER MJ (2007) Coenzyme Q, oxidative stress and aging. *Mitochondrion*, 7 (Suppl): S103-S111. https://doi.org/10.1016/j.mito.2007.03.006

SUZUKI S, FUJITA N, HOSOGANE N, WATANABE K, ISHII K, TOYAMA Y, TAKUBO K, HORIUCHI K, MIYAMOTO T, NAKAMURA M, MATSUMOTO M (2015) Excessive reactive oxygen species are therapeutic targets for intervertebral disc degeneration. *Arthritis Res Ther*, 17: 316.

THOMPSON JP, PEARCE RH, SCHECHTER MT, ADAMS ME, TSANG IK, BISHOP PB (1990) Preliminary evaluation of a scheme for grading the gross morphology of the human intervertebral disc. *Spine*, 15(5): 411-415.

URBAN JP, ROBERTS S (2003) Arthritis research & therapy. *Arthritis Res Ther*, 5(3): 120-130.

WALL R, ROSS RP, FITZGERALD GF, STANTON C (2010) Fatty acids from fish: the anti-inflammatory potential of long-chain omega-3 fatty acids. *Nutr Rev*, 68(5): 280-289.

ZHANG Q, LI J, LI Y, CHE H, CHEN Y, DONG J, XIAN CJ, MIAO D, WANG L, REN Y (2020) Bmi deficiency causes oxidative stress and intervertebral disc degeneration which can be alleviated by antioxidant treatment. *J Cell Mol Med*, 24(16): 8950-8961.

Possible ameliorative effects of pentoxifylline on cisplatin-induced ototoxicity in rats: a study with hearing test, light, and scanning electron microscopy

Marwa A. Al-Gholam[1], Asmaa S. Moaty[2], Ahmed M. Zein-Elabedein[2], Asmaa S. Essawy[1,3]

[1] Human Anatomy and Embryology Department, Faculty of Medicine, Menoufia University, Menoufia, Egypt

[2] Audiovestibular unit, Otolaryngology Department, Faculty of Medicine, Menoufia University, Menoufia, Egypt

[3] Anatomy Department, Ibn Sina National College for Medical Studies, Jeddah, Saudi Arabia

SUMMARY

Cisplatin is an antineoplastic drug widely used to treat various types of cancer. Ototoxicity is still cisplatin's most critical side-effect. Some patients may experience dose limitations due to hearing loss. Pentoxifylline (PX) exhibits powerful antioxidant, anti-inflammatory, and immune-regulatory effects. Our study was designed to investigate the protective effects of pentoxifylline on cisplatin-induced ototoxicity. Forty adult male healthy Sprague-Dawley rats were used through the entire experiment. Four groups of animals were categorized: Group I (control group); Group II (PX group) received 25 mg/kg/day of oral PX by gavage for 8 consecutive days; Group III (Cisplatin group) received cisplatin single intraperitoneal dose of 10 mg/kg; Group IV (PX + Cisplatin group) received 25 mg/kg/day of oral PX by gavage for 8 successive days and a single intraperitoneal dose of 10 mg/kg cisplatin at the 4th day. First and 9th-day Distortiondistortion-product otoacoustic emissions (DPOAE) tests were conducted. An intracardiac blood sample was collected for total antioxidant capacity (TAC) measurement, and the cochleae of rats were examined histopathologically. A significant reduction in serum TAC value was detected in the cisplatin group, while PX treatment significantly reduced TAC. Cisplatin decreased the DPOAE amplitudes in rats; conversely, the PX+cisplatin group showed a significant increase at all frequencies. Upon histopathological examination, the Ciplastin group revealed perturbation of the normal architecture of the organ of Corti, increased collagen deposition and marked expression of caspase-3, while the PX+cisplatin group revealed preserved architecture of the organ of Corti, minimal collagen deposition and downregulation of Caspase-3 expression. As evidenced by our findings and results from DPOAE results, biochemical findings, histological and ultrastructural analyses, PX significantly protects rats against ototoxicity caused by cisplatin.

Key words: Pentoxifylline – Cisplatin – Ototoxicity – Rats

Corresponding author:
Asmaa S. Essawy. Dept. of Anatomy, Faculty of Medicine, Menoufia University, Menoufia, Egypt & Ibn Sina National College for medical Studies, Jeddah, Almahjar street, 21418 Jeddah, Saudi Arabia. Mobile: +966546637821. E-mail: doc_asmaa@hotmail.com

Submitted: November 8, 2021. **Accepted:** December 8, 2021

Not final proof's revision by the authors

https://doi.org/10.52083/DQJC4772

INTRODUCTION

The term ototoxicity alludes to cellular damage or functional disorders that develop in the inner ear associated with any therapeutic or chemical (Kara et al., 2016). Cisplatin (cis-diamminedichloroplatin II) is widely used for treatment of a number of tumors (testicular and ovarian carcinoma, squamous head and neck carcinoma, lung carcinoma, malignant gliomas, advanced bladder cancer, and metastatic cancers such as mesothelioma, melanoma, breast and prostate cancer). The treatment with cisplatin is associated with side effects, such as ototoxicity, nephrotoxicity, myelotoxicity, and toxicity to the gastrointestinal system. Even though hydration therapy can control nephrotoxicity, ototoxicity remains a serious concern with cancer treatment with cisplatin (Roldan-Fidalgo et al., 2016).

Bilateral, irreversible, progressive sensorineural loss of hearing at high frequencies as well as tinnitus are the hallmarks of ototoxicity caused by cisplatin. Some patients may experience dose limitations due to hearing loss. The outer hair cells of the cochlea are progressively damaged by Cisplatin. 60-80% of patients who receive cisplatin suffer bilateral, permanent, and progressive hearing loss (Salehi et al., 2014). The severity of deafness can vary greatly, and it does not pose a life-threatening challenge. However, hearing loss can significantly affect the quality of life and can result in communication problems. Molecular and cellular mechanisms determining cisplatin toxicity remain poorly understood and the reduction of cisplatin ototoxicity remains one of the major objectives of anti-tumor therapies (Yumusakhuylu et al., 2012).

Cisplatin ototoxicity is associated with the accumulation of reactive oxygen species (ROS), including hydroxyl radicals and superoxide ions, and inhibition of antioxidant enzymes; therefore, antioxidants are popular agents to mitigate its toxicity (Rybak, 2007). Exogenous antioxidants such as amifostine, erdosteine, lycopene, vitamins C and E, dexamethasone, sodium salicylate, aminoguanidine, methionine, and resveratrol have been shown to have protective benefits in several studies (Kalkanis et al., 2004; Erdem et al., 2012; Xie et al., 2011).

Pentoxifylline (PX) is an alkaloid created by adding a hexanone group to theobromine, which is extracted from cocoa beans (Gill et al., 2015). As a nonspecific phosphodiesterase inhibitor, it was originally considered to treat peripheral vascular diseases. PX has several pharmacologic effects, such as reducing blood viscosity, improving microcirculation, increasing erythrocyte deformability, inhibiting platelets from aggregating in addition to its anti-inflammatory, immunomodulatory and antiproliferative properties (Nasiri-Toosi et al., 2013). Furthermore, it has also been used as an antioxidant to heal various tissue damages (Stojiljkovic et al., 2009). Considering oxidants' role in cisplatin-induced ototoxicity and the useful properties of pentoxifylline, this study has evaluated the protective effects of pentoxifylline against cisplatin-induced ototoxicity and the potential mechanisms through which it works.

MATERIALS AND METHODS

Chemicals

Pentoxifylline (PX) used in the study was obtained in the form of film-coated tablets (Trental) produced by Sanofi-Aventis, Egypt under licence of Sanofi-Aventis, Germany, and cisplatin as solution vials was obtained from Mylan, Greece (1 mg/ml).

Experimental design

This study was performed at the department of Human Anatomy and Embryology, Faculty of Medicine, Menoufia University. Forty adult male Sprague-Dawley rats weighing 180-200 g, aged 10-12 weeks, were used in the study. Rats were bought from the Egyptian Organization for Biological Products and Vaccines (Cairo, Egypt). They were acclimatized for two weeks in stainless steel cages prior to starting the experiment. The rats were fed ad libitum on standard laboratory pellets and with tap water. The room was kept at an optimum temperature and humidity with a 12-hour light/12-hour dark cycle.

All experimental procedures and animal maintenance were carried out according to the guidelines and roles prescribed by the Research

Ethics Committee, Menoufia University, Faculty of Medicine with the ethical approval number 7/2020ANAT2.

After two weeks of acclimatization, animals were separated randomly into four groups (n= 10 per group):

- Group I (Control group): was subdivided into:

  GIa (plain control), where animals did not receive anything.

  GIb (sham control), where animals received 1 ml intraperitoneal saline solution/day for eight successive days.
- Group II (PX group): each rat received 25 mg/kg/day of oral pentoxifylline dissolved in 1 ml saline via gastric gavage for 8 consecutive days (El-Anwar et al., 2018).
- Group III (Cisplatin group): each rat received a single cisplatin intraperitoneal dose of 10 mg/kg on the 4th day of the experiment (De Araujo et al., 2019).
- Group IV (PX + Cisplatin group): Each rat received 25 mg/kg/day of oral pentoxifylline dissolved in 1 ml saline via gastric gavage for 8 consecutive days and a single intraperitoneal dose of 10 mg/kg cisplatin at the 4th day (De Araujo et al., 2019).

An otoscopic examination was performed on all rats prior to the delivery of all medications under 50 mg/kg ketamine hydrochloride and 5 mg/kg xylazine anesthesia according to Struck et al. (2011). Then, all rats were subjected to the Distortion Product Otoacoustic Emissions (DPOAE) test. Under the same anesthesia protocol, DPOAE was again performed on the 9th day of the study. Rats were anesthetized 24 hours after the end of the experiment. A sample of intracardiac blood was taken utilizing plain tubes from each animal following completion of the final auditory assessment. After blood collection, all rats were sacrificed, and the temporal bones were then dissected. The cochleae were extracted, and cochleae from the right ear were prepared for light microscopic examinatio,n while those from the left ear were enucleated and processed for scanning electron microscopy.

Biochemical study for measurement of total antioxidant capacity (TAC)

After collecting blood samples and centrifuging them at 3000 rpm for 15 min, serum was then collected and stored at 80°C until being analyzed. Total antioxidant capacity (TAC) (Biodiagnostic, CAT. NO TA2513, Egypt) was measured colorimetrically, according to Koracevic et al. (2001). Serum TAC was assessed by the reaction of antioxidants in the sample with a known amount of exogenously provided hydrogen peroxide. TAC is measured in (mM/l) for each plasma sample.

Otoacoustic Emission Measurements

Distortion-product otoacoustic emissions (DPOAE) levels were assessed on the first day of the study as a baseline assessment using Eclipse 25 device (Eclipse/EP25 system, Inter acoustics Inc., Middle fart, Denmark). The rats were anesthetized before the assessment and submitted to otoscopic examination. The OAE probe with neonatal ear tips was inserted in the external auditory canal of the ear of the animals; animals with abnormal DPOAE measurements denoting abnormal hearing were excluded from the study. The resulting otoacoustic emissions levels were assessed at 2, 4, 6, and 8 kHz through DP gram. 2 frequencies were used for assessment: F1 and F2 with F2/F1 ratio=1.22 at 65 dB SPL, and the DPOAE levels were assessed at the first day (D1) and day 9 (D9) after administration of the otoprotective agent.

Light microscopic examination

On the apex of the right cochlea, a small hole was induced. After 2 days of incubation in 10% neutral buffered formalin, the specimens were put into ethylenediaminetetraacetic acid (EDTA) at 4 °C for 20 days; the solution was changed every two days until softening occurred. Washing, dehydrating, clearing, and embedding in paraffin blocks were performed. The sections were cut at five-µm and stained with Hematoxylin and Eosin (H&E) and Masson Trichrome stains. Further deparaffinizing of the paraffin-embedded sections was performed in xylene, and rehydrating with graded concentrations of ethanol to be immunohistochemically stained

with primary anti-Caspase-3 antibodies, a marker for apoptosis (rabbit polyclonal, Abcam), with a concentration of 100 µl at 0.872 mg/ml (dilution 1/50). The primary antibodies were applied on the slides and incubated overnight at room temperature in humidity chamber. All procedures were performed following the instructions of manufacturer (Suvarna et al., 2012).

Scanning electron microscopic examination

A small hole has been made on the apex of the left cochlea, washed repeatedly using PBS, and carefully dissected under a dissection microscope (Olympus SZ×9) to reveal the organ of Corti. Following dehydration in graded ethanol series, the specimens were critical-point dried using a CP dryer (Balzers, Lichtenstein). They were attached to aluminum stubs using carbon glue (Planocarbon, Groepl, Austria), coated with a 10–15-nm layer of gold-palladium in a Baltech MED 020 coating system, and examined using a scanning electron microscope (JSM- 6510 LV) (JEOL, Japan) at the Electron MicroscopeU in the Faculty of Agriculture, EL-Mansoura University, El-Mansoura, Egypt. To understand the morphology of hair cells, several photomicrographs at different magnifications were taken (Amora et al., 2013).

Statistical analysis

SPSS (statistical package for social science) version 23.0 on an IBM compatible computer (SPSS Inc., Chicago, IL, USA) was used to analyze the data. For comparisons of the studied groups, we used one-way-ANOVA followed by post hoc Bonferroni tests. DPOAE values were compared before and after drug application in each group using Paired samples t-tests. Data were expressed as the mean ± standard deviation (SD). P-values less than 0.05 were considered statistically significant, whereas those more than 0.05 were declared non-significant.

RESULTS

Total antioxidant capacity results

Compared with the control group, cisplatin significantly reduced serum TAC (mM/l) ($P< 0.001$). In comparison with cisplatin, PX treatment significantly reduced serum TAC levels ($P< 0.01$) (Fig. 1).

DPOAE results

DPOAE values did not differ significantly in terms of amplitude between the right and left ears of the rats. In the rats of the cisplatin group, a significant decrease in DPOAE amplitude

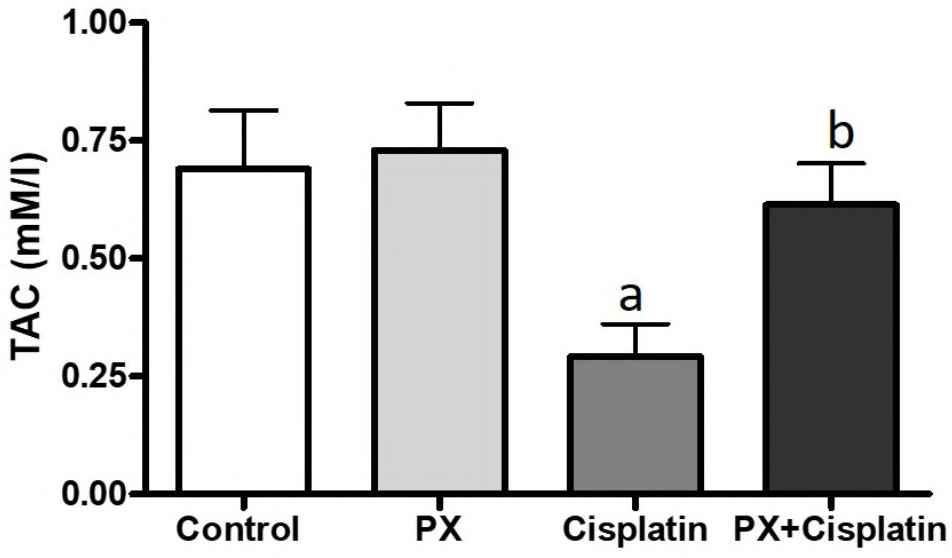

Fig. 1.- Total antioxidant capacity (TAC) results of different experimental groups. a, P<0.001 in comparison with the control group. b, P<0.001 based on cisplatin group comparison.

was observed on day 9 compared to day 1 at all frequencies ($p < 0.001$). DPOAE values did not differ significantly in terms of amplitude between control, PX and PX+cisplatin Groups compared to day 1 values. At all frequencies, there was marked decline in DPOAE amplitudes in the cisplatin group in comparison to the control group comparing the DPOAE amplitudes on day 9 ($p < 0.001$). Comparatively to the cisplatin group, the PX+cisplatin group exhibited greater DPOAE amplitudes values at all frequencies ($p < 0.001$) (Fig. 2).

Histopathological results

Control and PX groups had similar results for all the examined parameters. Therefore, they are regarded both as controls. On H&E-stained cochlear sections from the control group, the organ of Corti, stria vascularis, and spiral ganglion were visible. Among the organ of Corti's features are a spiral limbus, homogeneous tectorial membrane, three columnar outer hair cells, one columnar inner hair cell, outer and inner phalangeal cells, and outer and inner pillar cells (Fig. 3A). The stria vascularis was found to consist of three layers: a dark superficial marginal layer, a light intermediate layer, and a light basal layer attached to the spiral ligament (Fig. 3D). There were large cell bodies of pseudo-unipolar neurons with prominent central rounded nuclei enclosed in a capsule of satellite cells in spiral ganglia (Fig. 3G).

In the cisplatin group, the normal architecture of the organ of Corti was disrupted. All the hair cells, as well as their supporting cells, were fragmented and destroyed with a disrupted basement membrane (Fig. 3B). Vacuolation and degeneration of Stria vascularis marginal cells, the apparent increase in thickness, and vacuolation of CT underneath stria vascularis were detected (Fig. 3E). Vacuolation, hemorrhage and degeneration of the nuclei of the spiral ganglia were noted (Fig. 3H). The PX+cisplatin group showed preserved tectorial membrane architectures, intact outer and inner hair cells, and other supporting cells (Fig. 3C). Stria vascularis displayed intact layers with vacuolation of the underlying CT (Fig. 3F). Few vacuolated cells were present in the intact spiral ganglion neurons (Fig. 3I).

Minimal collagen fibers deposition in the basilar membrane and the area underlying stria vascularis in the control and PX+cisplatin groups. However, the cisplatin group shows increased collagen deposition (Fig. 4).

Immunohistochemical results

A faint brown reaction was detected in the organ of Corti, stria vascularis, and spiral ganglia in the

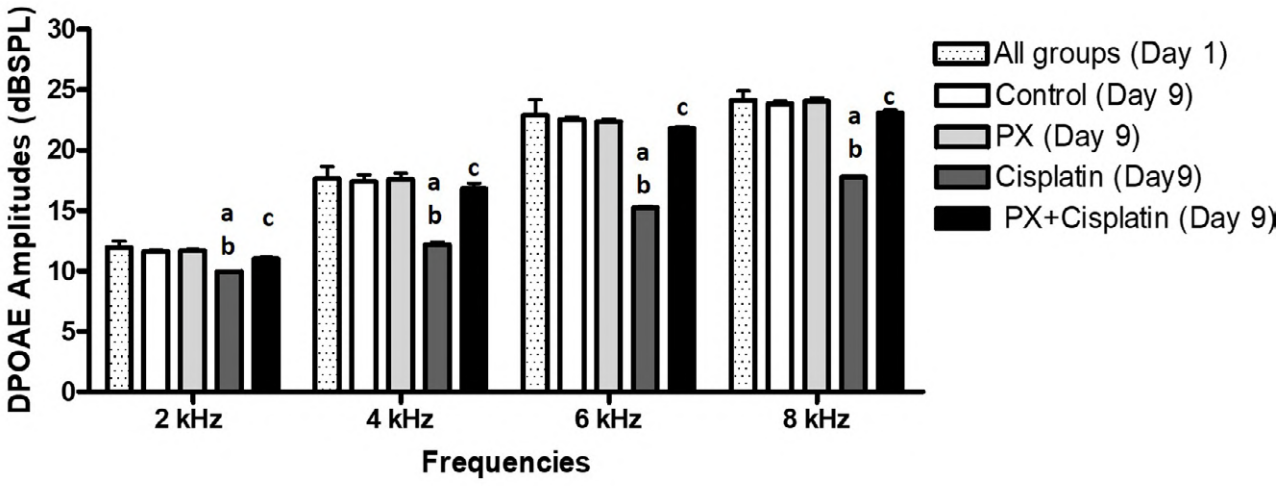

Fig. 2.- DPOAE results of different experimental groups. a, P<0.001 when compared to day 1. b, P<0.001 comparatively to the control group. c, P<0.001 comparatively to the cisplatin group.

control group when caspase-3 immunostained sections were examined (Fig. 5 A, D, G). In contrast, the cisplatin group showed marked expression in the organ of Corti, stria vascularis and spiral ganglia (Fig. 5 B, E, H). PX treatment showed downregulation of Caspase-3 expression (Fig. 5 C, F, I).

Scanning electron microscopic results

The control group cochlea was revealed to be a spiral tunnel by SEM. Three and a half turns could be seen in the tunnel from its base to its apex (Fig. 6A). A cast of cochlear normal vasculature was observed (Fig. 6B). The stereocilia on OHCs appeared to be arranged in three V-shaped rows, while the IHCs were arranged in a linear row. Both of them were regular, erect and well organized (Fig. 7 A, B, C).

Cochleae of cisplatin group showed collapsed cast of blood vessels (Fig. 6C). Stereocilia of outer and inner hair cells were destroyed, fragmented, merged, and disfigured;. cavitation was also revealed (Fig. 7 D, E, F).

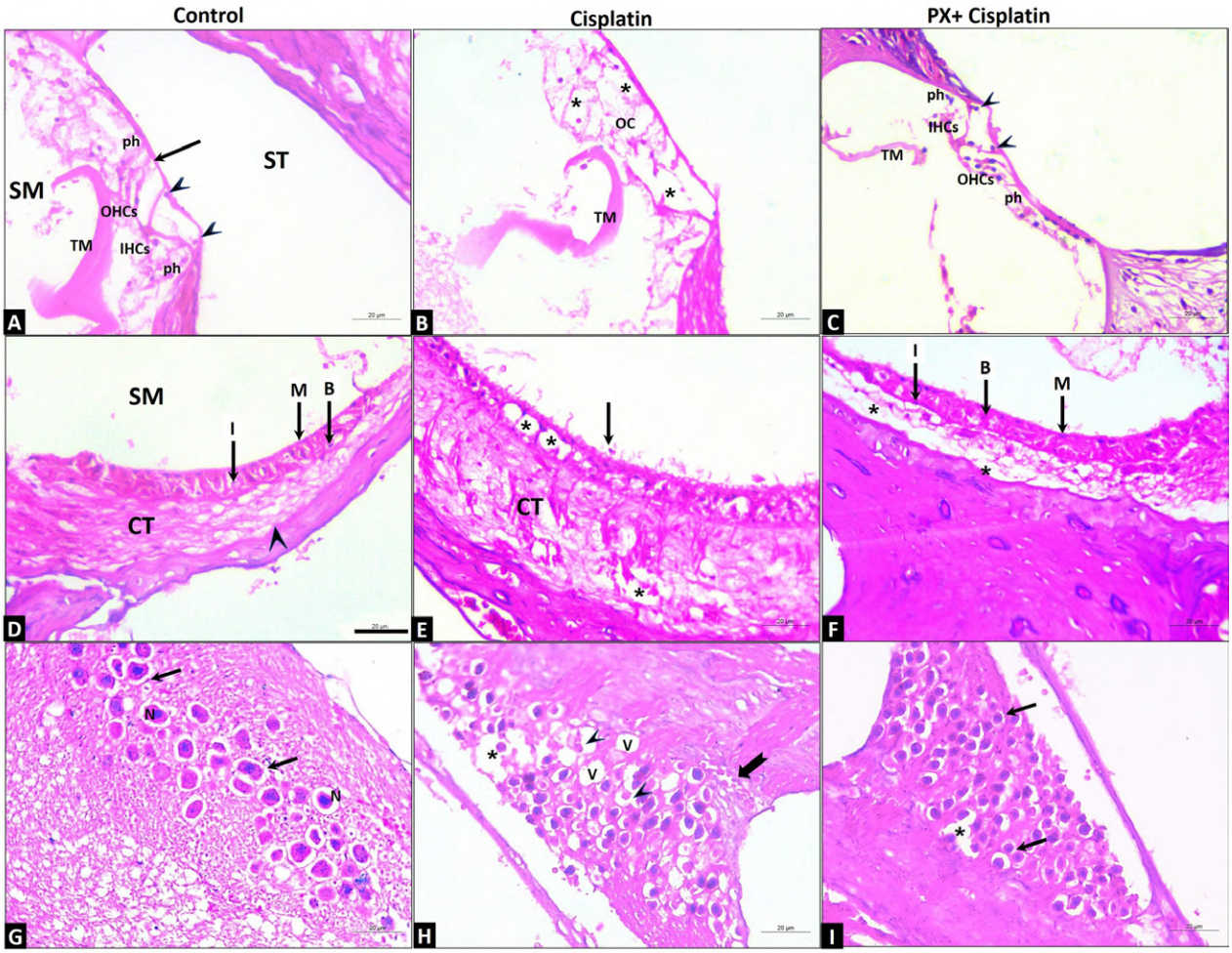

Fig. 3.- Photomicrographs of sections in the rat cochlea of different groups showing scala tympani (ST) and scala media (SM). The floor of the scala media (cochlear duct) is formed by basilar membrane (arrow), organ of Corti (OC) resting on this membrane. There are three rows of outer hair cells (OHC) and one row of inner hair cells (IHC) with their supporting Phalangeal cells (ph) in the organ of Corti. Pillar cells (arrowhead) can be seen (**A**). Cisplatin group exhibits damaged organ of Corti (OC) along with vacuolation (asterisks) (**B**) while PTX+Cis group showing homogenous basilar membrane (arrow), outer hair cells (OHC) and inner hair cells (IHC). Other supporting cells were preserved, including phalangeal cells (ph) and pillar cells (arrowhead) (**C**). Stria vascularis epithelium of control group is seen resting on basal lamina (arrowhead). It consists of three layers of cells, namely, marginal (M), intermediate (I) and basal (B) cells. It is facing the endolymph of the Scala media (cochlear duct) (SM) and vascular connective tissue underlying (CT) (**D**). An ill-defined stria vascularis, denuded marginal cells (arrow) and vacuolation (asterisks) are seen in the Cis group, also apparent increase in thickness of the underlying connective tissue layer (CT) is observed (**E**). The stria vascularis marginal (M), intermediate (I), and basal layers (S) are intact, but the connective tissue layer (CT) has some vacuolation (asterisks) in the PTX+Cisplatin group (**F**). The spiral ganglion of the control group consists of large central nuclei in pseudo-unipolar neurons (N) and satellite cells(arrow) surrounding it (**G**). Cisplatin group spiral ganglion exhibits hemorrhage (notched arrow), nuclear degeneration with perinuclear halo (arrowhead), and vacuolation (asterisk) (**H**). These spiral ganglion neuron bodies are well identified as pseudo-unipolar neurons in Cisplatin group (**I**) but some vacuolation (asterisk) is still detected. H&E, Scale bar = 20 µm, 40x.

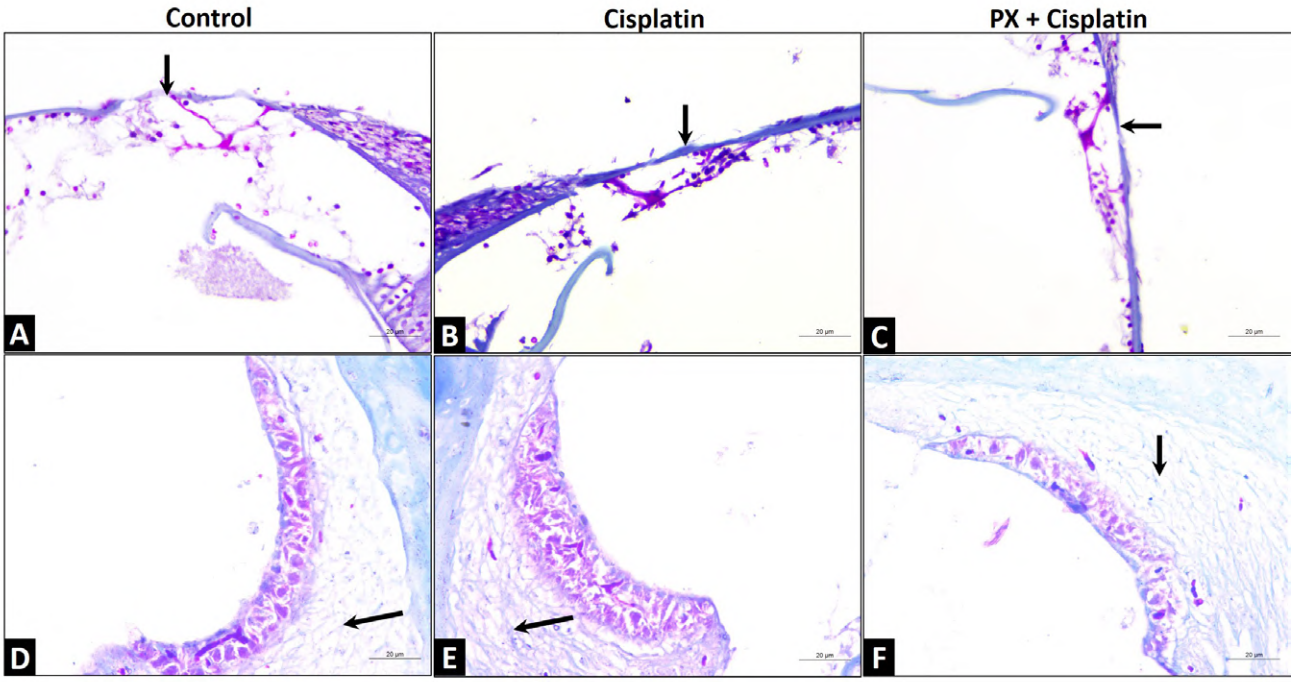

Fig. 4.- Photomicrographs of sections in the rat cochlea of different groups showing Control and PX+Cis groups have been deposited minimal collagen deposition in the basilar membrane (arrow) (**A** and **C,** respectively) and under the stria vascularis (**D**, **F**, respectively). In contrast, the Cis group exhibits an increased collagen deposit (**B**, **E**). Masson Trichrome, Scale bar = 20 µm, 40x).

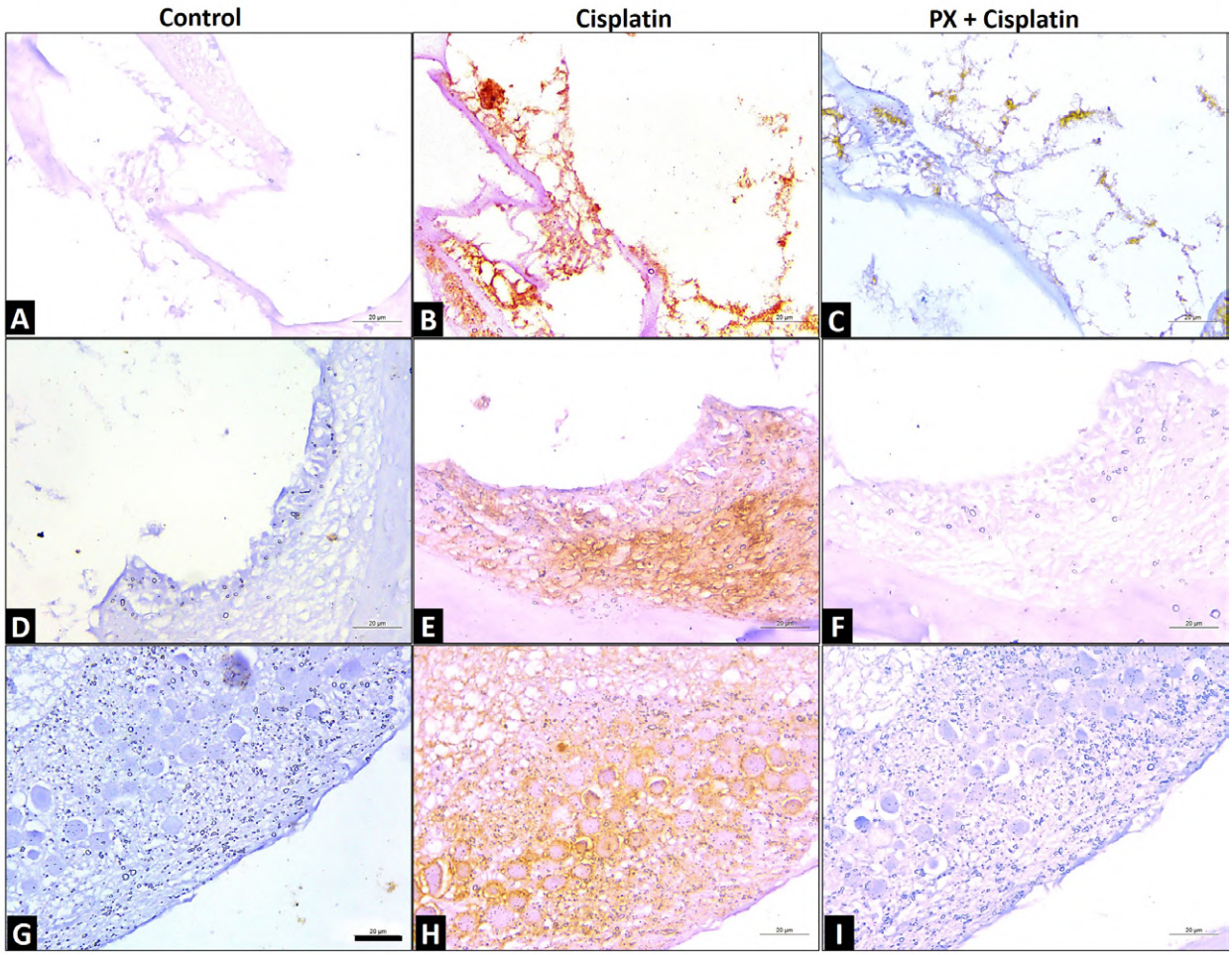

Fig. 5.- Photomicrographs of sections in the rat cochlea of different groups showing: **A, D, G)** A faint positive brown Caspases-3 reaction can be observed in the control group, organ of Corti, stria vascularis, and spiral ganglia. **B, E, H)** Cisplatin group exhibits marked expression in organ of Corti, stria vascularis and spiral ganglia. **C, F, I)** Caspase-3 reaction, however, is downregulated in the PX+Cis group. Caspase-3, Scale bar = 20 µm, 40x.

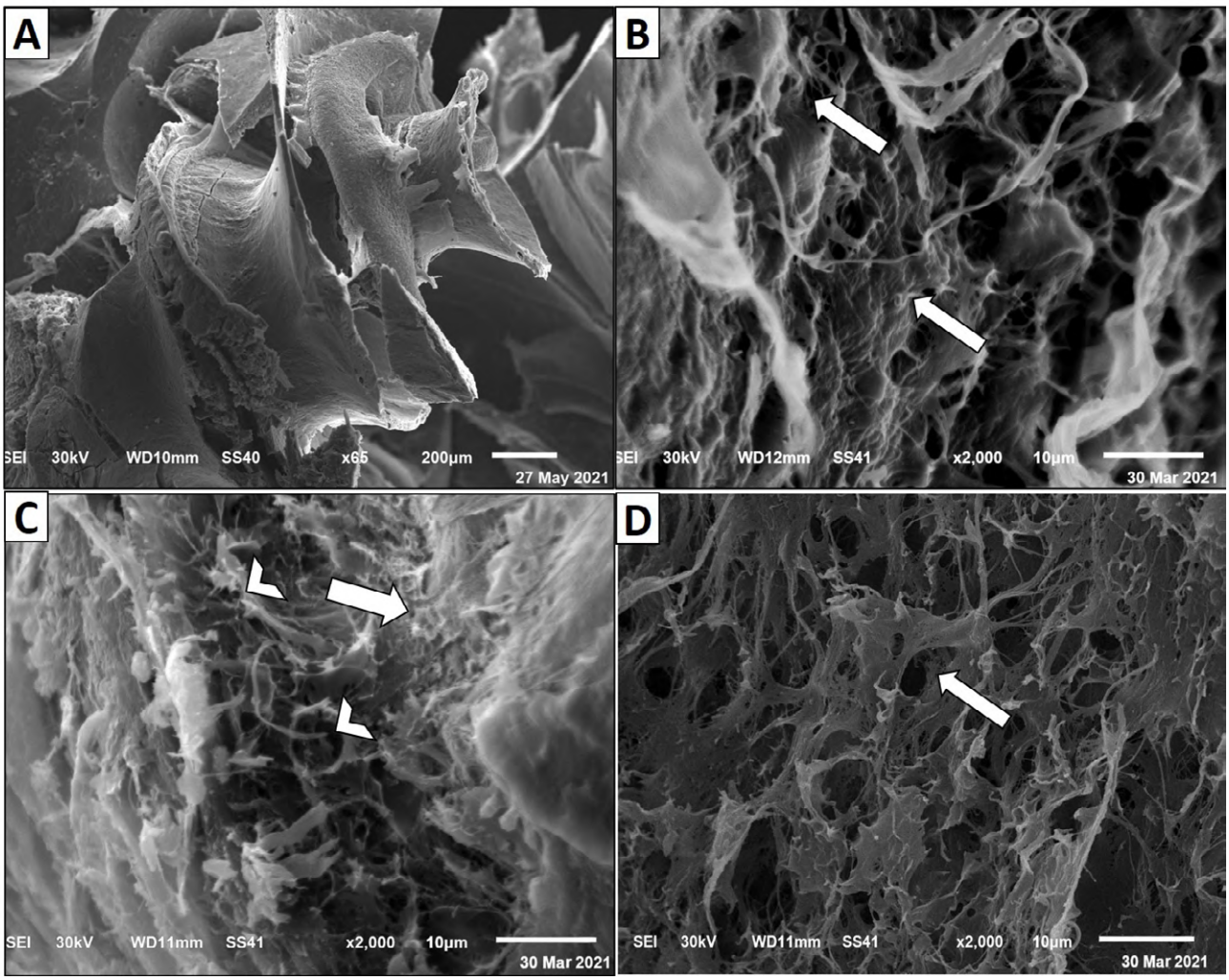

Fig. 6.- Scanning electron micrographs of rat cochlea of **A, B)** control group displays the spiral turn of the cochlea and cast of normal vasculature. **C)** Cisplatin group revealing a collapsed cast of cochlear vasculatures (arrow), disrupted veins and arteries can be seen (arrowhead). **D)** PX+Cis group normal cast of cochlear vasculatures (arrow). SEM, Scale bars: A = 200 µm, x65; B, C and D = 10 µm, x2000).

The cochlea of the PX+cisplatin group showed a normal cast of cochlear vasculatures (Fig. 6D). Cochlear hair cells were intact and arranged in a normal manner along with the normal architecture of stereocilia. However, areas of fusion of stereocilia of OHCs and cavitation were still detected (Fig. 7 G, H, I).

DISCUSSION

The antineoplastic drug cisplatin is widely used to treat a wide range of tumors. The most common side effects of this drug are nephrotoxicity, neurotoxicity, and ototoxicity. Ototoxicity is still cisplatin's most critical side-effect (Roldán-Fidalgo et al., 2016). Chemotherapy's powerful anti-tumor properties can be preserved by developing effective methods to reduce cisplatin ototoxicity (Soyalıç et al., 2016).

The results of our study clearly showed that pentoxifylline is protective against cisplatin-induced ototoxicity. It was found that pentoxifylline prevented oxidative stress from occurring in the cochlea both biochemically and histologically after administration of cisplatin. Also, DPOAE findings demonstrated that pentoxifylline protected against cisplatin-induced hearing loss.

There is a lack of understanding of the molecular and cellular mechanisms of ototoxicity. Cisplatin damages the outer hair cells of the cochlea, which can lead to excessive free oxygen radical production in the organ of Corti, stria vascularis, spiral ligament and spiral ganglion cells (Yumusakhuylu et al., 2012; Lee et al., 2003). Moreover, cisplatin treatment is associated with decreased expression of endogenous antioxidants,

thereby increasing oxidative damage. In addition, cisplatin can damage DNA and increase free radical production in the cochlea (Sagit et al., 2013).

The most prominent histopathological finding is hair cell degeneration. Furthermore, it results in the collapse of Reissner's membrane and atrophy of the support cells of the stria vascularis and the organ of Corti (Yumusakhuylu et al., 2012; Yazici et al., 2012).

In the current study, histopathological examination of the cochlea in the cisplatin group showed that the normal architecture of the organ of Corti was disrupted. All the hair cells, as well as their supporting cells, were fragmented and destroyed with a disrupted basement membrane, vacuolation and degeneration of stria vascularis marginal cells with an apparent increase in thickness and vacuolation of CT underneath stria vascularis. Similar findings have been reported by Soyalic et al. (2016), who demonstrated extreme histological damage to the organ of Corti in cisplatin-treated rats. Also, Akdemir et al. (2018) reported that cisplatin treatment reduced the number of outer hair cells in the organ of Corti of rats, and caused desquamation and erosion of vessels in the stria vascularis.

Although oxidative stress is thought to be the primary cause of this damage at the cellular level, the exact molecules and pathology responsible are unknown. Numerous studies have suggested that cisplatin can cause ototoxicity by causing an increase in free oxygen radicals within cellular structures in the cochlea. Furthermore, cisplatin has also been reported to reduce levels of antioxidant enzymes in the cochlea. In cochlear tissues, cisplatin causes the creation

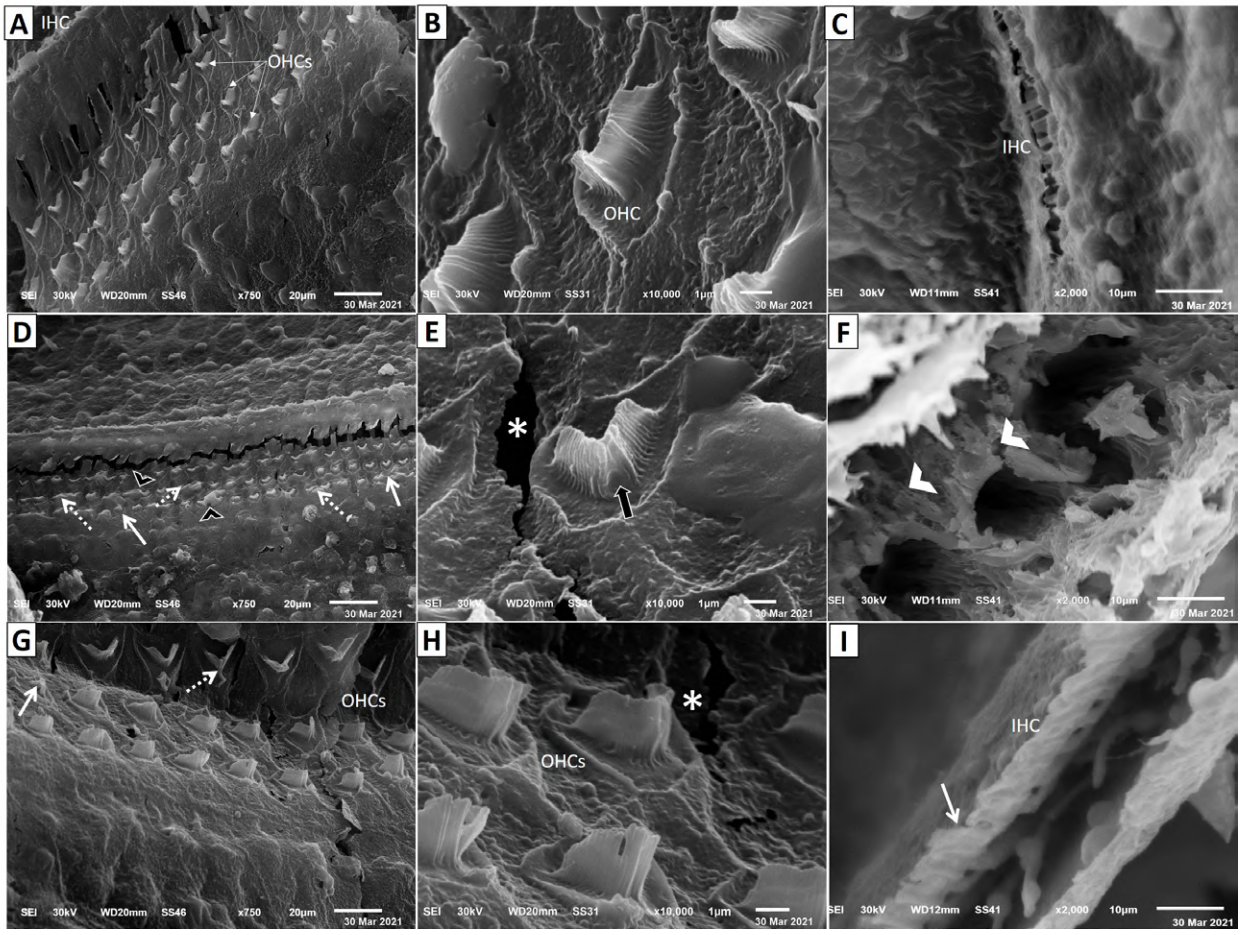

Fig. 7.- Scanning electron micrographs of rat cochlea of **A, B, C)** control group exhibits three rows of outer hair cells (OHCs) stereocilia and one row of inner hair cells (IHC) stereocilia. The regular arrangement of most of the stereocilia of the outer (OHCs) and inner hair cells (IHCs) is observed; Cis group **(D, E, F)** showing destructed (thin arrows), fused (dashed arrows), distorted (black arrowhead) and fragmented outer hair cells stereocilia (black arrow) and cavitation (asterisk). Loss of all stereocilia in the inner hair cells (white arrowheads). PX+Cis group **(G, H, I)** display intact stereocilia of both outer and inner hair cells (OHCs and IHC respectively) but areas destructed stereocilia (arrows) of OHC and IHC, fused stereocilia of OHCS (dashed arrow), outer hair cells and cavitation is still detected. SEM, Scale bars: A, D, G = 20µm, x750; B, E, H = 1 µm, x10,000; C, F, I = 10µm , x2,000.

of dysfunctional proteins and enzymes by impairing DNA synthesis. This will increase free oxygen radicals and reduce the antioxidant enzyme system. Increased ROS and a reduced antioxidant system result in oxidative stress, a cytotoxic condition. Oxidative stress damages cochlear cells and causes cell death (Doğan et al., 2016).

The measurement of total antioxidant capacity (TAC) is a reasonable and accurate method to evaluate changes related to oxidative stress. By using the TAC, we can assess how various conditions affect oxidative statuses in vivo, such as ROS exposure and supplementation with galenic antioxidants. Additionally, plasma TAC values may provide information about antioxidant supplement absorption and bioavailability (Ghiselli et al., 2000).

The measurements of TAC in our study revealed that pentoxifylline wielded its effect on circulation. Levels of TAC did not differ between the control and cisplatin + pentoxifylline groups (P > .05.), although the cisplatin group had significantly lower levels than the other groups. This was in agreement with Kınal et al. (2021), who found that cisplatin-treated rats had significantly lower TAC value than controls. It has been shown that pentoxifylline could prevent cisplatin from decreasing the TAC level when administered with it.

As a result of the present study, the expression of Caspase-3 was significantly up-regulated in the cisplatin-treated rats' cochleae, confirming apoptotic changes. The results were consistent with the observation made by Kilic et al. (2019), who noticed high immunopositivity of Caspase-3 in the outer hair cells of cochleae of rats receiving cisplatin. Furthermore, Wang et al. (2004) found that cisplatin treatment activated caspase-3 and caspase-9 in pigmented guinea-pig cochlear hair cells. In summary, Sheth et al. (2017) explained that caspases are involved in cisplatin-induced apoptosis of auditory cells, which is triggered by several upstream pathways. Inhibiting some or all of these pathways could be enough to rescue hair cells and hearing could be restored.

As is well known, drug toxicity mostly affects the outer hair cells in the organ of Corti. Normal otoacoustic emissions indicate healthy outer hair cells; however, diminished otoacoustic emissions reflect damaged hair cells. DPOAE and transient evoked otoacoustic emission (TEOAE) is used most commonly in clinical practice. Based on the studies conducted, DPOAE was shown to be more sensitive than TEOAE in detecting cisplatin-induced hearing loss (American Academy of Audiology, 2009). Using DPOAE as an audiologist monitoring procedure for ototoxicity, we emphasized that a single dose of cisplatin (10 mg/kg) decreased the DPOAE amplitudes in rats. There have been similar findings reported by Kilic et al. (2019), De Araujo et al. (2019), Eryilmaz et al. (2016) and Soyalic et al. (2016). There is a wide range of possible frequencies that can be studied through DPOAE depending on the type of animal. Lopez-Gonzalez et al. (2000) identified them between 1 and 6 kHz in Wistar rats; Sockalingan et al. (2000), between 2 and 8 kHz for a signal/noise ratio ≥ 3 dB SPL in albino rats.

The use of various approaches to treat cisplatin ototoxicity has increased over the past two decades. These include the administration of antioxidants or drugs that promote endogenous antioxidants. By activating the mitochondrial pathway, cisplatin induces apoptosis in hair cells. It is possible to prevent this by targeting the mitochondrial pathway. In addition, anti-inflammatory agents can also be used in order to treat the pro-inflammatory mechanisms accompanying cisplatin therapy of the cochlea. Understanding the cisplatin entry process in hair cells and other cochlear cells might boost the development of drugs that prevent cisplatin from entering these cells without affecting the entrance of cisplatin into cancer cells (Sheth et al., 2017).

In light of these pathophysiologic processes, reduction of reactive oxygen species levels and an increase in antioxidant enzyme levels are thought to protect against ototoxicity caused by cisplatin. Numerous antioxidant agents have been studied for this purpose in ototoxicity. In our study, we explored the protective effect of PX, a powerful antioxidant agent, on cisplatin-induced ototoxicity.

The methylxanthine phosphodiesterase inhibitor PX exhibits powerful antioxidant, anti-inflammatory and immune-regulatory effects

(Shan et al., 2012). In the present work, the beneficial effect of PX against ototoxicity caused by cisplatin was examined based on histological, ultrastructural and immunohistochemical assessment. The coadministration of cisplatin with PX significantly ameliorated cochlear damage. It has been reported that PX can alleviate gentamicin effects (Stojiljkovic et al., 2009), cisplatin (Kim et al., 2003), glycerol (Akpolat et al., 2000) and cyclosporine-induced nephrotoxicity (Brunner et al., 1989). Moreover, Garcia et al. (2014) showed that PX significantly reduced blood glucose levels, fructosamine, HbA1c levels, and iNOS, COX-2, and TNF-alpha immunoreactivity in the diabetic pancreas, liver, and kidney tissue.

Our results are also in line with those of Stojiljkovic et al. (2009), who suggested that pentoxifylline might have renoprotective effects as a result of its vascular decongestant effects, and Ozer et al. (2009), who exhibited that tumor necrosis factor-alpha (TNF- α) and other cytokines are inhibited by pentoxifylline. Pentoxifylline has been demonstrated to protect against chemotherapy- and amikacin-induced nephrotoxicity in several studies (Shifow et al., 2000). Pentoxifylline may provide otorenoprotection by inhibiting arachidonic acid metabolism and reducing pro-inflammatory mediators such as TNF-α. In addition to activating macrophages, TNF-α also stimulates neutrophil proinflammatory secretion, causing apoptosis. This result in cell death, leading to necrosis of target organs. In addition, Aviado et al. (1984) stated that, in addition to scavenging free radicals, pentoxifylline also inhibits nitric oxide synthase.

CONCLUSION

As evidenced by our findings and results from DPOAE, biochemical findings, histological and ultrastructural analyses, PX significantly protects rats against cisplatin-induced ototoxicity. PX should be studied further in order to determine the appropriate dosages and indications to be used against cisplatin-induced ototoxicity before clinical use.

REFERENCES

AKDEMIR FNE, GOZELER MS, YILDIRIM S, ASKIN S, DORTBUDAK MB, KIZILTUNC A (2018) The effect of ferulic acid against cisplatin-induced ototoxicity. *Med-Science Int Medical J*, 7(3): 528-531.

AKPOLAT T, AKPOLAT I, OZTURK H, SARIKAYA S, COŞAR A M, BEDIR A, KANDEMIR B (2000) Effect of vitamin E and pentoxifylline on glycerol-induced acute renal failure. *Nephron*, 84: 243-247.

AMERICAN ACADEMY OF AUDIOLOGY POSITION STATEMENT AND CLINICAL PRACTICE GUIDELINES (2009): Ototoxicity Monitoring. Reston, Virginia: American Academy of Audiology.

AMORA LDAS, MURASHIMA ADAB, ROSSATO M, MOREIRA MB, HYPPOLITO MA, FAGUNDES DJ (2013) The effects of hyperbaric oxygen therapy upon ototoxic injuries produced by amikacin in guinea pigs. *Braz J Otorhinol*, 79(3): 342-348.

AVIADO DM, PORTER JM (1984) Pentoxifylline: A new drug for the treatment of intermittent claudication. Mechanism of action, pharmacokinetics, clinical efficacy and adverse effects. *Pharmacotherapy*, 4(6): 297-307.

BRUNNER LJ, VADIEI K, IYER LV, LUKE DR (1989) Prevention of cyclosporine-induced nephrotoxicity with pentoxifylline. *Ren Fail*, 11: 97-104.

DE ARAUJO JG, SERRA LSM, LAUAND L, KÜCKELHAUS SAS, SAMPAIO ALL (2019) Protective effect of melatonin on cisplatin-induced ototoxicity in rats. *Anticancer Res*, 39(5): 2453-2458.

DOĞAN M, POLAT H, YAŞAR M, KAYA A, BAYRAM A, ŞENEL F, ÖZCAN I (2016) Protective role of misoprostol against cisplatin-induced ototoxicity. *Eur Arch Otorhinolaryngol*, 273: 3685-3692.

EL-ANWAR MW, ABDELMONEM S, NADA E, GALHOOM D, ABDELSAMEEA AA (2018) Protective effect of pentoxifylline on amikacin-induced ototoxicity. *Ear Nose Throat J*, 97(8): E8-E12.

ERDEM T, BAYINDIR T, FILIZ A, IRAZ M, SELIMOGLU E (2012) The effect of resveratrol on the prevention of cisplatin ototoxicity. *Eur Arch Otorhinolaryngol*, 269: 2185-2188.

ERYILMAZ A, ELIYATKIN N, DEMIRCI B, BASAL Y, KURT OMURLU I, GUNEL C, BASAK S (2016) Protective effect of Pycnogenol on cisplatin-induced ototoxicity in rats. *Pharm Biol*, 54(11): 2777-2781.

GARCIA FA, PINTO SF, CAVALCANTE AF, LUCETTI LT, MENEZES SM, FELIPE CF, ALVES AP, BRITO GA, CERQUEIRA GS, VIANA GS (2014) Pentoxifylline decreases glycemia levels and TNF-alpha, iNOS and COX-2 expressions in diabetic rat pancreas. *Springerplus*, 3: 283.

GHISELLI A, SERAFINI M, NATELLA F, SCACCINI C (2000) Total antioxidant capacity as a tool to assess redox status: critical view and experimental data. *Free Radic Biol Med*, 29(11): 1106-1114.

GILL SE, ROHAN M, MEHTA S (2015) Role of pulmonary microvascular endothelial cell apoptosis in murine sepsis-induced lung injury in vivo. *Respir Res*, 16: 109.

KALKANIS JG, WHITWORTH C, RYBAK LP (2004) Vitamin E reduces cisplatin ototoxicity. *Laryngoscope*, 114: 538-542.

KARA M, TÜRKÖN H, KARACA T, GÜÇLÜ O, UYSAL S, TÜRKYILMAZ M, DEMIRTAŞ S, DEREKÖY FS (2016) Evaluation of the protective effects of hesperetin against cisplatin- induced ototoxicity in a rat animal model. *Int J Pediatr Otorhinolaryngol*, 85:12-18.

KILIC K, SAKAT MS, AKDEMIR FNE, YILDIRIM S, SAGLAM YS, ASKIN S (2019) Protective effect of gallic acid against cisplatin-induced ototoxicity in rats. *Braz J Otorhinolaryngol,* 85(3): 267-274.

KIM YK, CHOI TR, KWON CH, KIM JH, WOO JS, JUNG JS (2003) Beneficial effect of pentoxifylline on cisplatin-induced acute renal failure in rabbits. *Ren Fail*, 25: 909-922.

KINAL ME, TATLIPINAR A, UZUN S, KESKIN S, TEKDEMIR E, OZBEYLI D, AKAKIN D (2021) Investigation of astaxanthin effect on cisplatin ototoxicity in rats by using otoacoustic emission, total antioxidant capacity, and histopathological methods. *Ear Nose Throat J*, 100(4): 198-205.

KORACEVIC D, KORACEVIC G, DJORDJEVIC V, ANDREJEVIC S, COSIC V (2001) Method for the measurement of antioxidant activity in human fluids. *J Clin Pathol*, 54(5): 356-361.

LEE JE, NAKAGAWA T, KIM TS, IGUCHI F, ENDO T, DONG Y, YUKI K, NAITO Y, LEE SH, ITO J (2003) A novel model for rapid induction of apoptosis in spiral ganglions of mice. *Laryngoscope*, 113: 994-999.

LOPEZ-GONZALEZ MA, GUERRERO JM, ROJAS F, DELGADO F (2000) Ototoxicity caused by cisplatin ameliorated by melatonin and other antioxidants. *J Pineal Res*, 28: 73-80.

NASIRI-TOOSI Z, DASHTI-KHAVIDAKI S, KHALILI H, LESSANPEZESHKI M (2013) A review of the potential protective effects of pentoxifylline against drug-induced nephrotoxicity. *Eur J Clin Pharmacol*, 69:1057-1073.

OZER MK, ASCI H, ONCU M, YESILOT S, SAVRAN M, BAYRAM D, CICEK E (2009) Effects of pentoxifylline on amikacin-induced nephrotoxicity in rats. *Ren Fail*, 31(2): 134-149.

ROLDAN-FIDALGO A, MARTÍN SALDANA S, TRINIDAD A, OLMEDILLA-ALONSO B, RODRÍGUEZ-VALIENTE A, GARCÍA-BERROCAL JR, RAMÍREZ-CAMACHO R (2016) In vitro and in vivo effects of lutein against cisplatin-induced ototoxicity. *Exp Toxicol Pathol*, 68: 197-204.

RYBAK LP (2007) Mechanisms of cisplatin ototoxicity and progress in otoprotection. *Curr Opin Otolaryngol Head Neck Surg*, 15: 364-369.

SAGIT M, KORKMAZ F, AKCADAG A, SOMDAS MA (2013) Protective effect of thymoquinone against cisplatin-induced ototoxicity. *Eur Arch Otorhinolaryngol*, 270: 2231-2237.

SALEHI P, AKINPELU OV, WAISSBLUTH S, PELEVA E, MEEHAN B, RAK J, DANIEL SJ (2014) Attenuation of cisplatin ototoxicity by otoprotective effects of nanoencapsulated curcumin and dexamethasone in a Guinea pig model. *Otol Neurotol*, 35: 1131-1139.

SHAN D, WU HM, YUAN QY, LI J, ZHOU RL, LIU GJ (2012) Pentoxifylline for diabetic kidney disease. *Cochrane Database Syst Rev*, 2: CD006800.

SHETH S, MUKHERJEA D, RYBAK LP, RAMKUMAR V (2017) Mechanisms of cisplatin-induced ototoxicity and otoprotection. *Front Cell Neurosci*, 11: 338.

SHIFOW AA, NAIDU MU, KUMAR KV, PRAYAG A, RATNAKAR K S (2000) Effect of pentoxifylline on cyclosporine-induced nephrotoxicity in rats. *Indian J Exp Biol*, 38(4): 347-352.

SOCKALINGAM R, FREEMAN S, CHERNY L, SOHMER H (2000) Effect of high-dose cisplatin on auditory brainstem responses and otoacoustic emissions in laboratory animals. *Am J Otol*, 21: 521-527.

SOYALIÇ H, GEVREK F, KOÇ S, AVCU M, METIN M, ALADAG I (2016) Intraperitoneal curcumin and vitamin E combination for the treatment of cisplatin-induced ototoxicity in rats. *Int J Pediatr Otorhinolaryngol*, 89: 173-178.

STOJILJKOVIC N, VELJKOVIC S, MIHAILOVIC D, STOILJKOVIC M, RADENKOVIC M, RANKOVIC G, RANDJELOVIC P (2009) Protective effects of pentoxifylline treatment on gentamicin-induced nephrotoxicity in rats. *Ren Fail*, 31:54-61.

STRUCK MB, ANDRUTIS KA, RAMIREZ HE, BATTLES AH (2011) Effect of a short-term fast on ketamine-xylazine anesthesia in rats. *J Am Assoc Lab Anim Sci*, 50(3): 344-348.

SUVARNA SK, BANCROFT JD, LAYTON C (2012) *Bancroft's Theory and Practice of Histological Techniques*, 7th ed. Churchill Livingstone Elsevier, Philadelphia, PA.

WANG GG, LU XH, LI W, ZHANG C (2011) Protective effects of luteolin on diabetic nephropathy in STZ-induced diabetic rats. *Evid based Complement Alternat Med*, 2011: 323171.

WANG J, LADRECH S, PUJOL R, BRABET P, WATER VD, T R, PUEL JL (2004) Caspase inhibitors, but not c-Jun NH2-terminal kinase inhibitor treatment, prevent cisplatin-induced hearing loss. *Cancer Res*, 64: 9217-9224.

XIE J, TALASKA AE, SCHACHT J (2011) New developments in aminoglycoside therapy and ototoxicity. *Hear Res*, 281: 28-37.

YAZICI ZM, MERIC A, MIDI A, ARINC YV, KAHYA V, HAFIZ G (2012) Reduction of cisplatin ototoxicity in rats by oral administration of pomegranate extract. *Eur Arch Otorhinolaryngol*, 269: 45-52.

YUMUSAKHUYLU AC, YAZICI M, SARI M, BINNETOGLU A, KOSEMIHAL E, AKDAS F, SIRVANCI S, YUKSEL M, UNERI C, TUTKUN A (2012) Protective role of resveratrol against cisplatin induced ototoxicity in Guinea pigs. *Int J Pediatr Otorhinolaryngol*, 76: 404-408.

Kahoot!'s contribution to immediate learning feedback for anatomy students

Daniel P.M. Barros[1], Diego A.C. Santana[1], Thaíse K.L. Costa[2], Ana K.F.T.C. Pereira[3], Amira R.C. Medeiros[3]

[1] *Medical Sciences Center, Federal University of Paraiba, João Pessoa, Brazil*
[2] *Department of Exact Sciences, Federal University of Paraiba, Rio Tinto, Brazil*
[3] *Department of Morphology, Federal University of Paraiba, João Pessoa, Brazil*

SUMMARY

Kahoot! is a popular game-based learning platform. This study aims to investigate whether there is a relationship between Kahoot! score and student's grade in the traditional examination (GTE), and to understand their perception about the use of this platform. A cross-sectional study was developed in the Human Anatomy course, which is divided into 5 topics of systemic anatomy (TSA). 5-question quizzes about the taught subject were given at the end of 66.7% of the lectures. 53 students who participated in at least one of the quizzes were included. In each TSA, students were subjected to a traditional examination (GTE, scale 0-10) and the mean of Kahoot! scores (MKS, scale 0-6000) was calculated, totalizing 190 independent observations. An opinion questionnaire was given at the course's end. Spearman's test analyzed the correlation between MKS and GTE; area under the ROC curve (AUC) evaluated MKS's ability to predict GTE; chi-square test verified the association between the categorical variables. There was a positive moderate correlation between MKS and GTE (rho=0.43, p<0.001). MKS performed regularly to predict GTE≥9 (AUC=0.734). 67.8% of the students in the MKS≥3000 group obtained GTE≥9, versus only 28.0% in the MKS<3000 group (p<0.001). Amongst the <20-year-old students, 83.3% agreed that Kahoot! was important to motivate them as they studied, versus 52.4% in the ≥20-year-old group (p=0.041). Kahoot!'s score can provide immediate feedback about the student's learning process, and it serves as a parameter to predict their final performance. The motivation to use Kahoot! can be influenced by the students' age.

Key words: Kahoot – Game-based learning – Anatomy – Teaching – Active learning

INTRODUCTION

Anatomy is an essential subject for medical training, as it introduces students to the medical language and the study of pathophysiology (Shaffer, 2004). Clinical doctors or surgeons use anatomical knowledge to carry out a good physical examination of the patient, form diagnostic hypotheses, interpret medical imaging and communicate the findings to the patient and other professionals involved in care (Turney, 2007). However, the teaching of Human Anatomy has been facing some challenges over the last decades, such as the progressive reduction of available

Corresponding author:
Daniel Pereira Maurício de Barros. Medical Sciences Center, Federal University of Paraiba, Cidade Universitária, João Pessoa, PB, 58051-900, Brazil. E-mail: daniel.barros@academico.ufpb.br Orcid no: 0000-0003-4587-9920

Submitted: November 8, 2021. **Accepted:** December 9, 2021

https://doi.org/10.52083/NCEH9192

time, the large amount of content, the increase in the number of students and the difficulty of access to cadaveric dissection (Guimarães et al., 2017). In addition, the new generation of students has demands such as connectivity, practical application of knowledge and innovation in the teaching-learning process (Ruzycki et al., 2019), in contrast to the shortage of anatomy professors in the labor market (Wilson et al., 2020). In the last few years, the perspective that the best way to deal with these difficulties is by combining several pedagogical resources that complement one another has grown, ranging from traditional dissection to new methods of active learning (Estai and Bunt, 2016).

Several active learning techniques have been used to overcome the challenges inherent in the teaching-learning process of anatomy, such as team-based learning, case-based learning and game-based learning (Singh et al., 2019; Aktekin et al., 2018; Zumwalt et al., 2010; Nieder et al., 2005). Associated with these new pedagogical practices, technological advances have shown that applications for smartphones can be useful tools in medical education (Payne et al., 2012; Fan et al., 2016). The use of smartphones for educational purposes (mobile learning) can enable a favorable environment for the construction and fixation of learning, which has generated an increasing mobilization to investigate how to implement, validate and improve these tools for teaching anatomy (Rondon et al., 2013; Pather et al., 2020; Küçük et al., 2016; Lall et al., 2019; Egarter et al., 2020).

In this context of constant innovation, tools such as the game-based student response system (GSRS) emerge, a new generation of "clickers", instruments used to provide greater interaction between professors and students in the classroom (Caldwell, 2007; Wang, 2015). Kahoot! is a GSRS launched in 2013 that allows the creation of interactive multi-choice questionnaires, the result of the Lecture Quiz prototype developed by the Norwegian University of Science and Technology (Wang, 2015). It is a user-centered tool based on behavioral design methodologies (Plump and LaRosa, 2017). In this sense, it can be used to review knowledge, assess students continuously and improve classroom dynamics, in order to increase student motivation, pleasure and concentration (Wang and Tahir, 2020).

Our hypothesis is that the Kahoot! score may generate useful feedback for the student to measure whether the taught content has been assimilated at the end of the lecture. Therefore, the objective of this study is to investigate the relationship between the Kahoot! score and the performance obtained in the traditional examination of the anatomy subject, as well as understanding the students' perception of the use of Kahoot! in teaching anatomy, according to their sociodemographic profile.

MATERIALS AND METHODS

Ethical Approval

The study was approved by the Research Ethics Committee of the Federal University of Paraiba's Health Sciences Center, under protocol number 2.617.483. All ethical and legal aspects for research with human beings were adopted and the participants signed the Free and Informed Consent Term, according to Resolution nº 466/2012 of the Brazilian National Health Council.

Study design

This is a quantitative cross-sectional study, developed in the Department of Morphology of the Federal University of Paraiba's Health Sciences Center, by the Human Anatomy professors and teaching assistants of the Medicine course. This subject is part of the integrated curriculum of the pre-clinical phase, which consists of lectures with theoretical exposition of the content and practical activities with human cadavers in the anatomy laboratory. The course content is divided into 5 topics of systemic anatomy (TSA): TSA1 - Cardiovascular System (6 lectures); TSA2 - Respiratory System (4 lectures); TSA3 - Digestive System (8 lectures); TSA4 - Endocrine and Reproductive Systems (4 lectures); and TSA5 - Urinary System (2 lectures). The data collection was conducted in the first semester of 2018, when students were invited to respond Kahoot! quizzes about the content taught, at the end of the lectures. At the completion of every TSA, the students were sent to a traditional examination. In

addition, an opinion questionnaire about Kahoot! platform was applied at the end of the course.

Participants' recruitment

Fifty-six first-year medical students enrolled in the Human Anatomy course were invited to participate in the study. The inclusion criteria adopted was to have participated in at least one Kahoot! quiz during the academic semester, and to have taken the traditional examination of this TSA. Fifty-three students (94.6%) who met these criteria were included and the student participation in each TSA was considered independently, totalizing 190 observations. Twenty-one students (39.6%) participated in the activities of all five TSAs; 9 (16.9%) participated in the activities of four different TSAs; 10 (18.8%) participated in the activities of three different TSAs; 6 (11.3%) participated in the activities of two different TSAs; and 7 (13.2%) participated in only one TSA. Thirty-nine (73.6%) students responded to the socio-demographic profile questionnaire. The participants' median age was 20 years, ranging from 18 to 26 years. 54.7% were men, 56.4% lived in their own family home, 89.7% were never employed, 97.4% were single and 97.4% had never attended another college before. Per capita family income was expressed in minimum wages (MW) in force at the time, with 1 MW equivalent to R$ 954.00 or U$ 261.40. The median of the per capita family income was 1.6 MW, ranging from 0.3 to 6.0 MW.

Kahoot! platform

Two experienced anatomy professors produced and reviewed 16 Kahoot! quizzes, containing questions that reflected the learning objectives of the respective lectures (Graham, 2015). Each quiz was composed of 5 multiple-choice questions with 4 alternatives of which students should choose a correct alternative regarding a concept or anatomical structure described through a text or an image. The parameters "question timer" and "points possible" were adjusted to 60 seconds and 1000 points, respectively.

At the end of the lectures, a Kahoot! quiz was shown from a computer connected to a projector and interested students participated through the Kahoot! app for smartphones (Aktekin et al., 2018). The students were instructed on the operating rules of the platform and were asked to identify themselves by a previously defined numerical code to enable data tabulation and ensure anonymity. The platform was programmed to display the question and only then present the alternatives and start the timing.

A ranking with the best scores for the sum of the 5 questions is displayed after the completion of the quiz. The score for each answer is calculated using the formula [(1 - (({response time} / {question timer}) / 2)) {points possible}]. The player can also receive 100, 200, 300 and 400 streak bonus points for 2, 3, 4 and 5 correct answers, respectively. Thus, the platform calculates the final score based on the number of correct answers and the speed with which the answers were given and, finally, provides a report of this data (Wang and Tahir, 2020). In every quiz applied, the maximum possible score was 6000 points.

The quizzes were given in 16 (66.7%) of the 24 lectures scheduled in the Human Anatomy course. Indeed, 4, 1, 5, 4 and 2 Kahoot! were conducted in TSA1, TSA2, TSA3, TSA4 and TSA5, respectively, which provided a frequency of quizzes for these TSAs of 66.7%, 25%, 62.5%, 100% and 100%. Student participation in each TSA was represented by the arithmetic mean of Kahoot! score (MKS) in the respective topic.

Traditional examination

The official assessment of the students was carried out at the end of every TSA, totaling five tests. This traditional examination was composed of two parts, one theoretical and one for the identification of anatomical structures in cadavers. Every theoretical test included 10 multiple-choice questions compatible with the content taught. The identification test consisted of 20 anatomical elements discussed in the lecture. The student's grade in the traditional examination (GTE) of each TSA was represented by the arithmetic mean of the scores of the theoretical test and the identification test on anatomical structures in the cadaver, ranging from 0 to 10. GTE greater than or equal to 7, 8 and 9 were considered as sufficient, regular, and excellent performance, respectively.

Student feedback

A questionnaire developed by the authors and based on the Likert scale was used to assess the students' opinions about the use of Kahoot!, considering the following sentences: 'I had fun using Kahoot!'; 'I would recommend Kahoot! to assist in learning of other subjects'; 'I would use Kahoot outside of the university'; 'Kahoot was important for me to learn anatomical terms taught in the lecture'; 'Kahoot! contributed to my performance in the Human Anatomy tests'; and 'Kahoot! was important to keep me motivated in the study of Human Anatomy'.

Statistical analysis

The statistical analysis was performed using R version 3.6.3 (R Core Team, Vienna, Austria) and RStudio version 1.2.5033 (RStudio Inc., Boston, MA, USA). The internal consistency of the opinion questionnaire was evaluated by Cronbach's alpha coefficient. The data normality was verified by the Kolmogorov-Smirnov test with Lilliefors adjustment. Due to the non-parametric distribution, the Kruskal-Wallis test was used to assess whether there was a variation in MKS and GTE between the different TSAs. Spearman's correlation coefficient was calculated to assess whether there is an association between MKS and GTE. Area under the ROC curve (AUC) was used to evaluate the performance of MKS in predicting GTE (score greater than or equal to 7, 8 and 9). The parameters sensitivity, specificity, positive predictive value, negative predictive value, and accuracy were also calculated using as MKS cut-off point ≥ 3000. The Chi-square test was used to assess the association between MKS in categories and the student's performance in the traditional examination, as well as to identify the association between sociodemographic variables and the students' opinion about the use of Kahoot!. All tests were applied considering a 95% confidence interval.

RESULTS

Relationship between Kahoot! score and the grade in the traditional examination

Both MKS and GTE varied according to TSA ($p < 0.001$), and, except for TSA2, these scores increased as the subject progressed. Detailed descriptive statistics are shown in Table 1. There was a significant positive and moderate

Table 1. Descriptive analysis of the Kahoot! score and grade in the traditional examination according to the topics of systemic anatomy course (n=190).

Parameter	TSA	n	Minimum	Maximum	Mean	SD	Median	IQR	Normality
MKS	1	48	843.0	4721.8	2354.5	827.5	2348.1	1173.5	**0.200**
	2	34	775.0	4355.0	2158.4	997.1	1796.0	1308.0	0.020
	3	41	1721.0	5146.5	3344.7	828.2	3470.5	1217.8	**0.200**
	4	39	932.0	4999.3	3578.7	890.2	3680.0	1077.5	**0.200**
	5	28	969.0	5601.5	3643.1	1382.9	3916.0	2484.1	**0.200**
	Total	190	775.0	5601.5	2974.3	1144.7	2950.8	1690.3	**0.200**
GTE	1	48	3.9	10.0	8.2	1.2	8.2	1.4	**0.200**
	2	34	3.5	9.3	7.6	1.4	7.9	1.7	0.040
	3	41	3.9	10.0	8.5	1.4	9.1	1.8	0.004
	4	39	4.3	10.0	8.8	1.4	9.3	1.4	<0.001
	5	28	8.5	10.0	9.6	0.4	9.8	0.5	<0.001
	Total	190	3.5	10.0	8.5	1.4	8.8	1.6	<0.001

TSA = topic of systemic anatomy; SD = Standard deviation; IQR = interquartile range; MKS = Mean of Kahoot! score; GTE = grade in the traditional examination

correlation between MKS and GTE (rho = 0.43, p <0.001). MKS showed regular performance to predict GTE ≥ 8 (AUC = 0.720, p <0.001) and GTE ≥ 9 (AUC = 0.734, p = 0.037), but performance was poor to predict GTE ≥ 7 (AUC = 0.655, p = 0.018), as shown in Fig. 1. The cut-off point MKS ≥ 3000 (half of the maximum possible score to be reached) was chosen to perform a detailed analysis, as shown in Table 2.

Considering the categories MKS < 3000 and MKS ≥ 3000, there was a significant association between the Kahoot! score and performance in the traditional examination (Fig. 2). A total of 94.4% of students in the MKS ≥ 3000 group achieved GTE ≥ 7, which was statistically different from the 83.0% of students who achieved this grade in the MKS < 3000 group (p = 0.014). While 85.6% of students in the MKS ≥ 3000 group reached GTE ≥ 8, this percentage was 61.0% in the MKS < 3000 group (p <0.001). Finally, 67.8% of students in the MKS ≥ 3000 group achieved GTE ≥ 9, versus only 28.0% in the MKS < 3000 group (p <0.001).

Student opinion about Kahoot!

Thirty-nine participants (73.6%) answered the opinion questionnaire. The questionnaire showed substantial internal consistency, with Cronbach's Alpha of 0.799. The level of agreement of the participants with the sentences is shown in Fig. 3. It was found that 83.3% of younger students, up to 19 years old, agreed that the use of Kahoot! was important in motivating the study of Human Anatomy, versus 52.4% in the group aged 20 or over (p = 0.041). There was no association between the students' opinion about the use of Kahoot! and other sociodemographic variables analyzed (gender, paid employment, marital status, previous education, housing type and family income per capita).

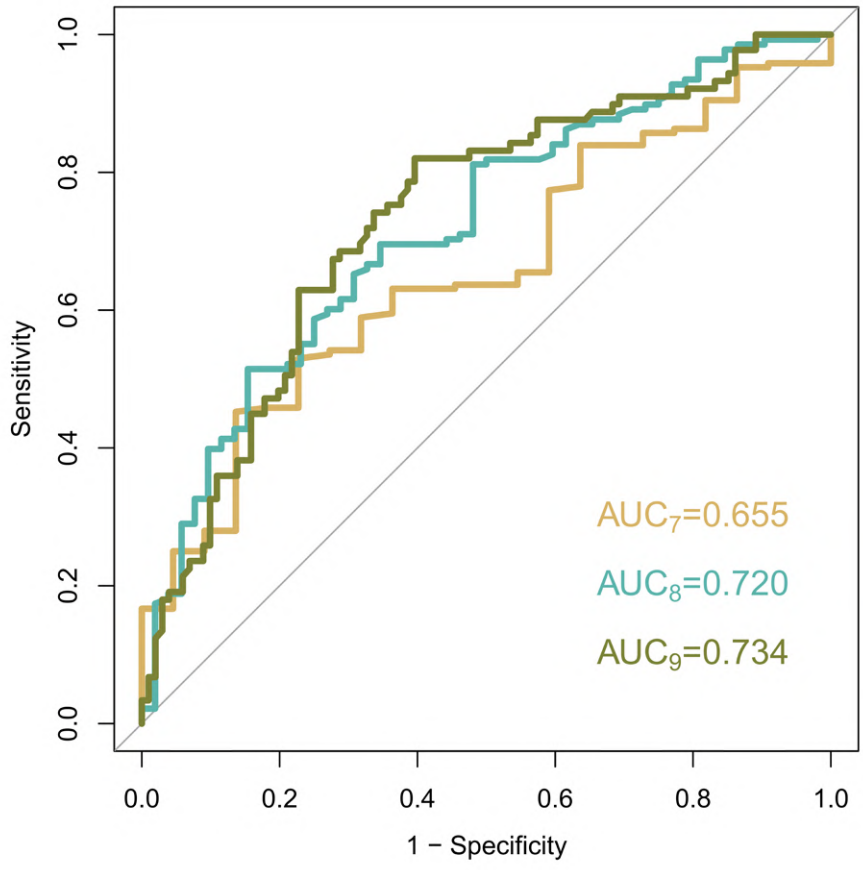

Fig. 1.- ROC curve using the Kahoot score as a predictor of grade in the traditional examinations (n = 190).

Table 2. Diagnostic test results to evaluate the ability of Kahoot! score (MKS) greater than or equal to 3000 to predict grade in the traditional examination (GTE) greater than or equal to 7, 8 and 9 (n=190).

MKS ≥ 3000	**GTE ≥ 7.0**		**GTE ≥ 8.0**		**GTE ≥ 9.0**	
Diagnostic tests	(%)	95%CI	(%)	95%CI	(%)	95%CI
Sensitivity	50.6	43.0 – 58.2	55.8	47.5 – 64.1	68.5	58.9 – 78.2
Specificity	77.3	59.8 – 94.8	75.0	63.2 – 86.8	71.3	62.5 – 80.1
Positive predictive value	94.4	89.7 – 99.2	85.6	78.3 – 92.8	67.8	58.1 – 77.4
Negative predictive value	17.0	9.6 – 24.4	39.0	29.4 – 48.6	72.0	63.2 – 80.8
Accuracy	53.7	46.6 – 60.8	61.1	54.1 – 68.0	70.0	63.5 – 76.5

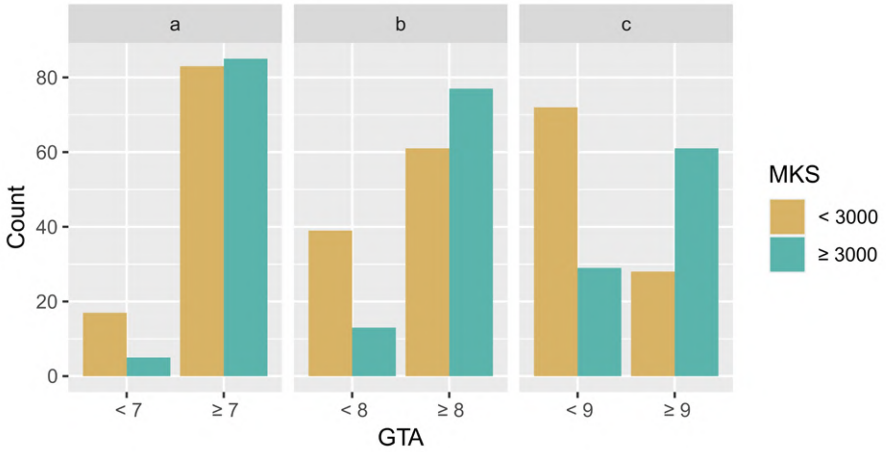

Fig. 2.- Distribution of the frequency of grades in the traditional examination (GTE) greater than or equal to 7 (a), 8 (b) and 9 (c), according to the mean Kahoot! score (MKS) (n = 190).

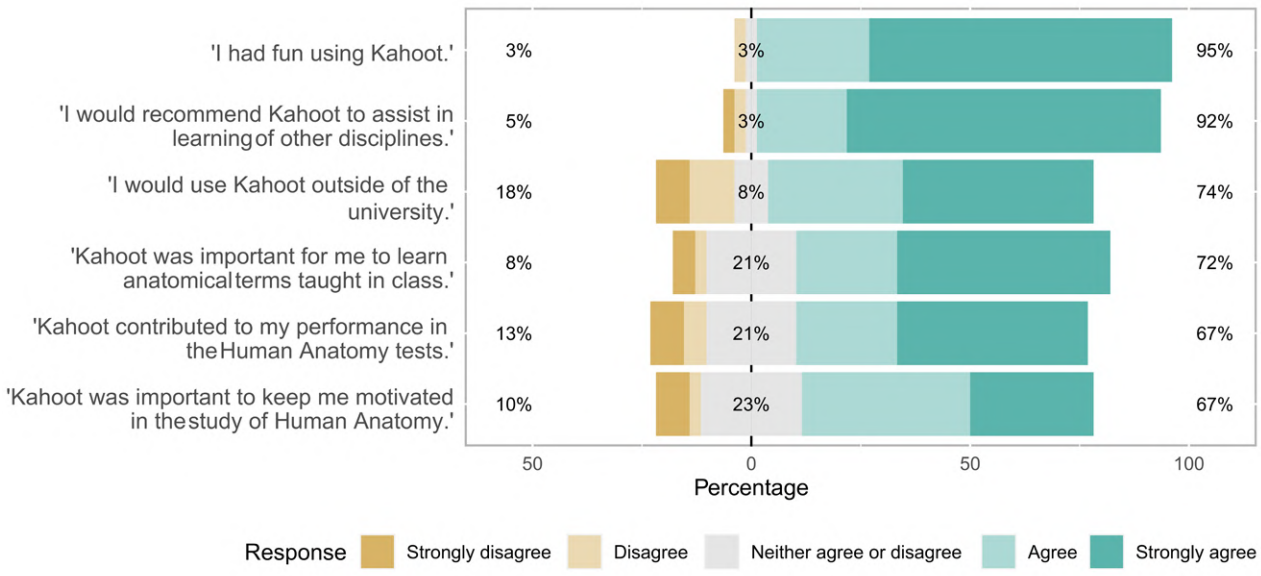

Fig. 3.- Student's opinion about the use of Kahoot! in the study of Human Anatomy, considering the level of agreement with the sentences (n = 39).

DISCUSSION

Kahoot! has gained prominence in the context of game-based learning (Wang, 2015; Plump and LaRosa, 2017; Wang and Tahir, 2020). This study raises the hypothesis that the Kahoot! can generate useful feedback for the student to measure the assimilation of the content taught in the lecture. This led us to investigate whether there is a relationship between the Kahoot! score and the grade in the traditional examination, as well as understanding the students' perception of the platform according to the sociodemographic characteristics. Our data shows that the performance in Kahoot! was associated with performance in the traditional examination. In addition, students were receptive to using Kahoot! in the classroom and the motivation was correlated with their age.

The parameters MKS and GTE varied in a peculiar way during the Human Anatomy course. Except for TSA2, the mean and median of MKS and GTE increased as the subject progressed, and this may be associated with the participants' natural adaptation process to Kahoot! quiz format and traditional examination throughout the course. The characteristics of TSA2 may have triggered the measurement of a smaller MKS, because in this topic the MKS represents the application of a single quiz, with non-normal distribution and low number of participants. Knowing that the TSA2 GTE was also lower compared to the others, it is possible that both scores are actually reflecting less knowledge retention in the short and medium term in that specific TSA, due to factors not controlled in this study. The correlation between MKS and GTE has already been identified in previous studies, as in a study that evaluated Kahoot! as a method to review concepts at the end of the course (Dell and Chudow, 2019). Our study is a pioneer in proposing the application of Kahoot! at the end of each lecture, in order to compare the MKS and GTE across the various topics in the course. The correlation found in this study indicates that MKS can be used as a predictor of good performance in the subject of Human Anatomy.

The ROC curve with the best AUC was the one that used score 9 as a goal in the traditional examination. This was because the overall performance of the students was high (general median of 8.8), which means that 50% of the students achieved performance in the traditional examination above 8.8. As for grade 7 in the traditional examination, the minimum parameter for approval in the subject, there was a low AUC. This may be related to the different aspects really evaluated by Kahoot! and by traditional examination, since the cognitive levels of the educational objectives of both tests were not fully equivalent. While the questions elaborated for Kahoot! involved the dimensions of the cognitive process of levels 1 (remember) and 2 (understand), the traditional examination presented questions where the student should be able to perform applications (level 3), analyses (level 4) and examinations (level 5) (Krathwohl, 2002). Thus, it was expected that it would not be completely possible to demonstrate a strong correlation between the two examination methods.

Although the global analysis of the ROC curves shows low accuracy, when considering the predictive values, interpretation from the individual aspect can be important for each student. Those with MKS ≥ 3000 had a 94.4%, 85.6% and 67.8% probability of obtaining a grade equal to or greater than 7, 8 and 9, respectively, according to the positive predictive value found. When it comes to the subject pass parameter (GTE ≥ 7), obtaining MKS < 3000 revealed a very low negative predictive value (17.0%), i.e., even reaching a low Kahoot! score, the student can perform well in the traditional examination. This is justified because Kahoot! evaluates the moment immediately after the lecture. The association between the categorized MKS and GTE values highlights that Kahoot! can serve as an alert for students with low MKS, demonstrating that more dedication may be needed to study the respective content for traditional summative examination.

The use of Kahoot! in the classroom can contribute to motivation, focus on the most relevant concepts and reflection on what has been assimilated (Ismail et al., 2019; Licorish et al., 2018; Ismail and Mohammad, 2017). Apart from successful prior use, the main reason for choosing the Kahoot! platform as a GSRS was to

keep students simultaneously focused on the same question and then discuss the answers together. Other advantages were the user-friendly interface of the platform, the possibility to add media of different formats and the quickness to apply the quiz. Furthermore, the Kahoot! quiz provides the learner with real-time feedback and does not require prior training to be implemented. The number of questions in each Kahoot! quiz was adequate for the objectives of the lecture and for the time dedicated to the execution of the activity. The sections ranged from 10 to 15 minutes, including students' connection time to the Kahoot! application, reading, answering, discussing each question, viewing the score on each question, and the final podium, which was compatible with the limited time available for teaching Human Anatomy.

Systematic reviews show moderate evidence of the effect of game-based learning on students' overall performance (Gorbanev et al., 2018; All et al., 2016; Abdulmajed et al., 2015). Specifically, Kahoot! has been associated with positive effects on learning performance and classroom dynamics, although there are studies that indicate little or no effect (Wang and Tahir, 2020; Sumanasekera et al., 2020). Our results demonstrate good feedback from students on Kahoot!, which in itself would justify its use as a complementary method. It is interesting to note that the participants have fun with Kahoot! and would indicate it in other subjects. However, there was less agreement on the importance of Kahoot! for content fixing, motivation, and final performance, which maintains that students understand Kahoot! as a method that improves classroom dynamics but has less influence on their learning process. Regarding the age group, it is known that age is a factor that influences the receptivity to the use of applications and online platforms as a pedagogical practice (Fan et al., 2016). Our results show that the motivation for the study linked to the emotional connection generated by using the Kahoot! platform has suffered from age factor, being more intense among younger individuals.

Finally, Kahoot! presents some peculiarities from the pedagogical point of view. In fact, game-based learning is not restricted to a specific learning theory and uses elements of constructivism, humanism, cognitivism and behaviorism (Wu et al., 2012). Kahoot! sessions bring aspects of stimulus and reinforcement seen in behaviorism, through the typical dynamics of games, but there is no aspect of repetition of behavior to generate learning. The game sessions involve humanistic characteristics such as trust, freedom to participate and student self-knowledge, however the pace is not determined by the student. Thus, the authors consider that the most striking principles of Kahoot! sessions are related to constructivist cognitivism, since students are challenged, and given the difficulties of assimilation by the professor's proposal, they undergo a process of modification, adaptation, and restoration of balance. Therefore, the student adapts to the process, and is educated to learn.

Limitations

This study has several limitations. First, the sample was restricted to students of only one course, which prevented the presentation of reproducibility of results in another group. Second, there was no rigor regarding the participation of the students in the Kahoot! sessions. This may have contributed to a greater participation of those who liked the subject and eventually had better results, as it was a voluntary activity that required the student to remain in the classroom for a longer period. The use of codes to maintain the anonymity of students was an alternative employed to minimize the lack of adherence by the fear of exposure. Thirdly, there were also technical limitations regarding the applicability of the method, such as the need for the student to have smartphone and internet access at the time of the quiz. It was therefore not uncommon for some students to just attend the sessions without participating in the game. Furthermore, the demand for digital resources such as a computer and an image projector or TV was also a limiting factor, especially in the TSA2, as most classes on this topic were taught in the anatomy laboratory. The lack of these devices in the laboratory prevented the application of

Kahoot! at the end of some of the lectures. Lastly, the quality of internet access may also have been a source of bias in the quiz result, as Kahoot! counts the response time to generate the score obtained, which may have benefited students that had a smartphone with a better processor and internet data provider.

CONCLUSION

The performance in the Kahoot! quiz is associated with performance in the traditional examination, which can provide the student with immediate feedback on the retention of the exposed content, and can serve as a predictor of final performance, although the two processes have differences in the dimension of the assessed cognitive process. Students understand that this instrument makes classroom dynamics more interactive and assists in content fixation, motivation, and academic performance. The motivation generated using technologies such as the Kahoot! platform in the classroom can be influenced by the age of students.

REFERENCES

ABDULMAJED H, PARK YS, TEKIAN A (2015) Assessment of educational games for health professions: A systematic review of trends and outcomes. *Med Teach*, 37(S1): S27-S32.

AKTEKIN NÇ, ÇELEBI H, AKTEKIN M (2018) Let's kahoot! Anatomy. *Int J Morphol*, 36(2): 716-721.

ALL A, CASTELLAR EPN, LOOY JV (2016) Assessing the effectiveness of digital game-based learning: Best practices. *Comput Educ*, 92: 90-103.

CALDWELL JE (2007) Clickers in the large classroom: Current research and best-practice tips. *CBE Life Sci Educ*, 6(1) :9-20.

DELL KA, CHUDOW MB (2019) A web-based review game as a measure of overall course knowledge in pharmacotherapeutics. *Curr Pharm Teach Learn*, 11(8): 838-842.

EGARTER S, MUTSCHLER A, TEKIAN A, NORCINI J, BRASS K (2020) Medical assessment in the age of digitalisation. *BMC Med Educ*, 20(1): 101.

ESTAI M, BUNT S (2016) Best teaching practices in anatomy education: A critical review. *Ann Anat*, 208: 151-157.

FAN S, RADFORD J, FABIAN D (2016) A mixed-method research to investigate the adoption of mobile devices and Web2.0 technologies among medical students and educators. *BMC Med Inform Decis Mak*, 16(1): 43.

GORBANEV I, AGUDELO-LONDOÑO S, GONZÁLEZ RA, CORTES A, POMARES A, DELGADILLO V, YEPES FJ, MUÑOZ Ó (2018) A systematic review of serious games in medical education: quality of evidence and pedagogical strategy. *Med Educ Online*, 23(1): 1-9.

GRAHAM K (2015) TechMatters: Getting into Kahoot!(s): Exploring a game-based learning system to enhance student learning. *Loex Q*, 42(3): 6-7.

GUIMARÃES B, DOURADO L, TSISAR S, DINIZ JM, MADEIRA MD, FERREIRA MA (2017) Repensar a anatomia: Como superar os desafios da evolução da educação médica. *Acta Med Port*, 30(2): 134-140.

ISMAIL MAA, AHMAD A, MOHAMMAD JAM, FAKRI NMRM, NOR MZM, PA MNM (2019) Using Kahoot! as a formative assessment tool in medical education: A phenomenological study. *BMC Med Educ*, 19(1): 230.

ISMAIL MAA, MOHAMMAD JAM (2017) Kahoot: A promising tool for formative assessment in medical education. *Educ Med J*, 9(2): 19-26.

KRATHWOHL DR (2002) A revision of bloom's taxonomy: An overview. *Theory Pract*, 41(4): 212-218.

KÜÇÜK S, KAPAKIN S, GÖKTAŞ Y (2016) Learning anatomy via mobile augmented reality: Effects on achievement and cognitive load. *Anat Sci Educ*, 9(5): 411-421.

LALL P, REES R, YI LAW GC, DUNLEAVY G, COTIČ Ž, CAR J (2019) Influences on the implementation of mobile learning for medical and nursing education: Qualitative systematic review by the digital health education collaboration. *J Med Internet Res*, 21(2): e12895.

LICORISH SA, OWEN HE, DANIEL B, GEORGE JL (2018) Students' perception of Kahoot!'s influence on teaching and learning. *Res Pract Technol Enhanc Learn*, 13(1): 1-23.

NIEDER GL, PARMELEE DX, STOLFI A, HUDES PD (2005) Team-based learning in a medical gross anatomy and embryology course. *Clin Anat*, 18(1): 56-63.

PATHER N, BLYTH P, CHAPMAN JA, DAYAL MR, FLACK NAMS, FOGG QA, GREEN RA, HULME AK, JOHNSON IP, MEYER AJ, MORLEY JW, SHORTLAND PJ, ŠTRKALJ G, ŠTRKALJ M, VALTER K, WEBB AL, WOODLEY SJ, LAZARUS MD (2020) Forced disruption of Anatomy Education in Australia and New Zealand: An acute response to the Covid-19 pandemic. *Anat Sci Educ*, 13(3): 284-300.

PAYNE KFB, WHARRAD H, WATTS K (2012) Smartphone and medical related App use among medical students and junior doctors in the United Kingdom (UK): A regional survey. *BMC Med Inform Decis Mak*, 12(1): 121.

PLUMP CM, LAROSA J (2017) Using Kahoot! in the classroom to create engagement and active learning: a game-based technology solution for eLearning novices. *Manag Teach Rev*, 2(2): 151-158.

RONDON S, SASSI FC, FURQUIM DE ANDRADE CR (2013) Computer game-based and traditional learning method: A comparison regarding students' knowledge retention. *BMC Med Educ*, 13(1): 30.

RUZYCKI SM, DESY JR, LACHMAN N, WOLANSKYJ-SPINNER AP (2019) Medical education for millennials: How anatomists are doing it right. *Clin Anat*, 32(1): 20-25.

SHAFFER K (2004) Teaching anatomy in the digital world. *N Engl J Med*, 351(13): 1279-1281.

SINGH K, BHARATHA A, SA B, ADAMS OP, MAJUMDER MAA (2019) Teaching anatomy using an active and engaging learning strategy. *BMC Med Educ*, 19(1): 149.

SUMANASEKERA W, TURNER C, LY K, HOANG P, JENT T, SUMANASEKERA T (2020) Evaluation of multiple active learning strategies in a pharmacology course. *Curr Pharm Teach Learn*, 12(1): 88-94.

TURNEY BW (2007) Anatomy in a modern medical curriculum. *Ann R Coll Surg Engl*, 89(2): 104-107.

WANG AI (2015) The wear out effect of a game-based student response system. *Comput Educ*, 82: 217-227.

WANG AI, TAHIR R (2020) The effect of using Kahoot! for learning – A literature review. *Comput Educ*, 149: 103818.

WILSON AB, NOTEBAERT AJ, SCHAEFER AF, MOXHAM BJ, STEPHENS S, MUELLER C, LAZARUS MD, KATRIKH AZ, BROOKS WS (2020) A look at the Anatomy Educator job market: anatomists remain in short supply. *Anat Sci Educ*, 13(1): 91-101.

WU WH, HSIAO HC, WU PL, LIN CH, HUANG SH (2012) Investigating the learning-theory foundations of game-based learning: A meta-analysis. *J Comput Assist Learn*, 28(3): 265-279.

ZUMWALT AC, LUEFLER RS, MONTEIRO J, SHAFFER K (2010) Building the body: Active learning laboratories that emphasize practical aspects of anatomy and integration with radiology. *Anat Sci Educ*, 3(3): 134.140.

An unusual case of quadruple polyorchidism in a human cadaver mimicking bilateral lipoma

Ernest F. Talarico, Jr.[1AB], Joseph G. Castaneda[2B], Sana M. Wahab[2B], Katelyn M. Paulus[2B], Jack D. Walsh[2B], Amy E. Stromberg[2B], Victoria N. Olson[2B], Paul J. Janus[2B], Nicholas R. Rocco[3C]

[1] *Department of Anatomy*

[2] *Department of Biology*

[3] *Department of Urology*

[A] *Tan Tao University School of Medicine, Long An Province, Việt Nam*

[B] *North Park University, Chicago, Illinois, USA*

[C] *United States Naval Medical Center, San Diego, California, USA*

SUMMARY

Polyorchidism is a rare congenital disorder defined as the presence of more than two testicles for which the underlying etiology is unknown. This report examines a novel case, correlates findings to the literature, and discusses potential mechanisms of dysgenesis. This study was conducted on a 96-year-old male cadaver. Meticulous skilled dissection was done with careful attention to the pelvis, the inguinal region, the scrotum and testes. Measurements of the scrotal testes (STs), supernumerary testes (SNTs), scrotal epididymides (SEs), supernumerary epididymides (SNEs), ductus deferens (DD) and supernumerary ductus deferens (SDD) were taken, and testicular volume was calculated. Sagittal sectioning of STs, SNTs, SEs and SNEs was performed and, using standard histologic protocol, tissues were processed, stained with H&E, and examined. Histological findings supported the anatomical suspicion of high, bilateral inguinal polyorchdism, or tetraorchdism, in this patient. STs and SNTs have normal, gross morphological features. The left SNT was supplied by the testicular artery, and the right SNT by the inferior epigastric artery. Both SNTs and SNEs were infiltrated with adipose tissue, whereas the scrotal homologues were histologically normal. Testicular volumes were 26.5 cm^3 and 23.7 cm^3, and 12.3 cm^3 and 0.55 cm^3, for the left and right STs and SNTs, respectively. The left and right SEs measured 7.2 cm and 7.0 cm; the left and right SNEs measured 4.7 cm and 1.7 cm, respectively. The left DD measured 40.2 cm from the scrotum. The SDD from the left SNT measured 5.9 cm and joined the main ductus 16 cm proximal to its origin. The right main DD measured 39.2 cm, and the SDD from the right SNT was 3.2 cm and joined the main DD 17.4 cm

Corresponding author:
Ernest F. Talarico, Jr., Ph.D., Department of Anatomy, Tan Tao University School of Medicine, Tân Đức, Đức Hòa, E. City Đức Hòa Long An, Việt Nam; Adjunct Professor of Anatomy, North Park University. E-mail: talaricojrernest@gmail.com
Paul J. Janus, Ed.D., Anatomy and Biology Instructor, Department of Biology, North Park University, 3225 West Foster Avenue, Chicago, Illinois 60625-4895 USA. E-mail: pjjanus@northpark.edu

Submitted: November 15, 2021. **Accepted:** December 6, 2021

https://doi.org/10.52083/VKMZ1059

proximal to its origin. The current work suggests a novel classification for polyorchidism of Type 3, Subgroup B, or SNT attached to the draining epididymis and vas deferens without reproductive potential and SNT located outside the scrotal sac. Clinicians must correlate anatomical and histological findings in suspected polyorchids to avoid misdiagnosis of SNTs as benign lipomas.

Key words: Anatomy – Congenital disorder – Polyorchid – Polyorchidism – Supernumerary – Testes – Testicle – Tetraorchidism

ABBREVIATIONS

Anterior-Posterior (AP)
Centimeter(s) (cm)
Ductus (vas) Deferens (DD)
Embalming mixture (EB mix)
Epididymis (E)
Height (H)
Inferior Epigastric Artery/Vein (IEA/IEV)
Left (Lt)
Length (L)
Length-sagittal (L-SAG)
Pampiniform Plexus (PP)
Right (Rt)
Scrotal Epididymis/Epididymides (SE/SEs)
Scrotal Testis/Testes (ST/STs)
Spermatic Cord (SC)
Supernumerary Ductus (vas) Deferens (SDD)
Supernumerary Epididymis/Epididymides (SNE/SNEs)
Supernumerary Testis/Testes (SNT/SNTs)
Testicular artery (Ta)
Testicular vein (Tv)
Transverse left-right (TR)
Width (W)

INTRODUCTION

Polyorchidism or supernumerary testes (SNTs) is a rare congenital disorder defined as the presence of more than two testicles (Bergholz et al., 2007; Bergholz, 2009). A male who has polyorchidism is known as a polyorchid. The first histologically confirmed example of polyorchidism was in 1880 (Ahlfeld 1880; Danrad et al., 2004); however, the first clinical case was reported in 1895 by Lane, as an incidental discovery during exploration of the groin (Lane, 1895; Artul and Habib, 2014; Hassan et al., 2008; Hassan et al., 2014). A survey shows fewer than 200 cases reported in the medical literature (Bergholz and Wenke, 2009; Artul and Habib, 2014; Cohen et al., 2017), with the majority of cases being detected in patients ranging from 4 weeks to 75-years-old and a median age of 17-years-old (Mathur et al., 2002; Bergholz, 2009; Mittal et al., 2018). Further, there are only seven documented cases in the animal kingdom: two horses, two dogs, two cats, and a single hummingbird (Roca-Ferrer et al., 2015; Tamminen et al., 2012; Witt and Bautista, 2011; Aziz et al., 2016).

Polyorchidism often has no symptoms outside the extra testis. When symptoms are present, they may include pain in the scrotum or lower abdomen, or an obvious mass within the scrotum detected upon palpation (i.e., testicular examination) (Dollard, 2011; Sakamoto et al., 2007; Mittal et al., 2018; Otero, 2016). Associated inguinal hernia or undescended testis are not uncommon findings (Artul and Habib, 2014). Because undescended testes are not uncommon in polyorchids, there is also an increased risk or association between polyorchidsm and testicular cancer (Talarico et al., 2018; Avargues et al., 2015). However, symptoms of polyorchidism may be similar to a paratesticular lesion that may derive from a number of structures that surround the testicle within the scrotum; most commonly, they derive from the spermatic cord (Hassan et al., 2014; Hassan et al., 2008). To differentiate polyorchidism from a paratesticular lesion, an ultrasound and magnetic resonance imaging may be done (Arslanoglu, 2013). Aside from paratesticular lesions, there are some commonly associated abnormalities that are associated with polyorchidism. These abnormalities include testicular maldescent (40%), inguinal hernia (30%), testicular torsion (13%), hydrocele (9%), and malignancy (6%) (Mathur et al., 2002; Tonape et al., 2012). These abnormalities may draw attention and lead to eventual diagnosis of polyorchidism.

Usually, the additional testis or testes are on the left side (Artul & Habib, 2014; Cohen et al, 2017). SNTs are typically not as large as the two normal testes, making polyorchidism more likely to go undetected for a long time. There are four types of polyorchidism (Table 1 and Table 2; Haddock and Burns, 1987; Bergholz 2007; Friedman, 2015). The most common clinical presentation of triorchidism (i.e., presence of a single extra testicle) is painless swelling (Abduljabbar, 2015; Gune and Gune, 2021). The literature shows left-sided triorchidism as compared to the right-sided variant occurs at a 3:1 ratio (Sheah et al., 2004). Even more rare is a polyorchid with the tetraorchidism (4 testes) type, where only 9 cases are cited in the scientific literature (Ibrahim, 2016; Duymus et al., 2016). There are only two reported cases of a polyorchid with five testicles, where in one case all SNTs were located high in the left inguinal canal and in the second case location of SNTs varied between abdomen and left inguinal canal (Zahirian Moghadam et al., 2020).

It has been hypothesized that polyorchidism is a result of duplication or malformation of the gonadal ridge during embryological development (Mittal, 2020; Bergholz 2009; Ellet, 2015). During the division of the gonadal ridge, the primordial testes may be transversely or longitudinally divided. Some investigators suggest that a transverse division results in the duplication of both the epididymis and testis, while longitudinal division results in only duplication of the testis (Méndez-Gallart et al., 2012). Otero (2016) suggested that the mechanism underlying division of the gonadal ridge is the malformation of peritoneal bands over the gonadal ridge, thereby transversely dividing the gonadal ridge. However, Otero's approach only explains transversal division, and not longitudinal division. When only the testis is duplicated, that organ has no reproductive potential and an increased malignant potential (Danrad et al., 2004). A more common finding in polyorchids is duplication of the epididymis and vas deferens, rather than SNTs sharing a single epididymis or vas deferens (Akbar et al., 2003). In contrast, Sheah (2004) suggests that, depending upon the segmentation plane and the site of segmentation along the gonadal ridge, SNTs may develop with a common or single epididymis and vas deferens, and that in most cases the epididymis and vas deferens are shared or missing. Another theory for polyorchidism focuses on the degeneration of parts of the mesonephric duct. After a transverse division of the primordial gonadal ridge, there is

Table 1. Anatomical Classification Scheme of Polyorchidism.

TYPE	DESCRIPTION	THEORETICAL ORIGIN
I	SNT lacks an epididymis or vas deferens and has no attachment to the usual testis.	Division of genital ridge.
II	SNT drain into the epididymis of the usual testis and they share a common vas deferens.	Division of genital ridge occurs in the region where the primordial gonads are attached to the metanephric ducts, although the mesonephros and metanephric ducts are not divided (i.e., incomplete division).
III	SNT have their own epididymis and both epididymis of the ipsilateral testes drain into one vas deferens.	Complete transverse division of the mesonephros as well as of genital ridge.
IV	Complete duplication of testes, epididymis and vas deferens.	Vertical division of genital ridge and mesonephros.

Table 2. Anatomical - Functional Classification Scheme of Polyorchidism.

TYPE	ANATOMICO-FUNCTIONAL DESCRIPTION	SUBGROUP
1	SNT attached to the draining epididymis and vas deferens with reproductive potential (i.e., Types II, III and IV).	**Type 1 - Subgroup A.** SNT located within the scrotum (ortho-topic) **Type 1 - Subgroup B.** SNT located outside the scrotal sac (ectopic)
2	SNT with lack of such an attachment without having any reproductive potential (i.e., Type I).	**Type 2 - Subgroup A.** SNT located within the scrotum (ortho-topic) **Type 2 - Subgroup B.** SNT located outside the scrotal sac (ectopic)

an attachment to part of the mesonephric duct. The attachment may induce testicular duplication. Support for this model arises from the observation that the gonadal ridge and the mesonephric duct both need to be duplicated in order for there to be a complete separation of the drainage system and testes (Wolf et al., 1998). However, none of these embryological theories is singularly sufficient to explain polyorchidism pathogenesis (Zahirian Moghadam et al., 2020). Interestingly, in only 3% of cases were chromosomal abnormalities reported in a patient with polyorchidism (Artul and Habib, 2014; Spranger et al., 2002; Vasaiya et al., 2021). Yet, a review of medical literature on the subject shows a lack of research into potential genetic factors that might lead to polyorchidism.

This symposium presents the case of a polyorchid discovered in the normal course of undergraduate, gross anatomical dissection of a male cadaver. This case is unique, because of the advanced age of the polyorchid, the Type IV or tetraorchidism variant, SNTs bilaterally located, and one SNT being supplied by the ipsilateral, inferior epigastric artery. Findings are correlated to a survey of the current literature, and potential mechanisms are discussed.

MATERIALS AND METHODS

Cadaveric Specimen

This study was conducted on a 96-year-old male cadaver as part of the Advanced Human Cadaver Laboratory at North Park University (Chicago, Illinois, USA), and with consent of the Anatomical Gift Association of Illinois (Chicago, Illinois, USA). Medical and hospital records, and secondary medical history were unavailable. All federal and state guidelines were followed regarding the use and care of cadaveric materials, as well as all regulations set forth by the Anatomical Gift Association of Illinois and North Park University.

The embalming procedure is a 2-phase procedure beginning within the first 24 hours after death. The embalming mixture (EB mix) is 128 oz of Dodge Funeral Home Fixative (*The Dodge Company*, Batavia, Illinois USA) and 256 oz of water. The first phase of the embalming procedure is a three-step infusion via the carotid artery of three (separate) tanks of EB mix with a Mark V embalming machine (*Mortech Manufacturing*, Azusa, California, USA). This is followed in phase 2 with single tank of EB mix via gravity flow. The specimen is stored in a body bag that is placed onto a stainless-steel tray and into the cadaver rack at 62 ºF, and then allowed to cure for a minimum of 4 weeks. With respect to the present work, this anatomical donor was embalmed on October 18, 2019, and prosection began August 27, 2020. Thus, this was approximately 10 months cure time, during which the specimen was re-wet, 2-3 times per week with Restorative Solution (*The Dodge Company*).

Gross Examination and Photography

Detailed physical examination was performed utilizing a “donor report” (i.e., similar to an autopsy report), where gross observations and quantitative data were collected. Digital photography of the external features and viscera was done using a NIKON D3100 SLR Camera (*B&H Foto & Electronic Corporation*, NY USA) equipped with an 18-55 mm VR NIKKOR Macro lens and a Nikon 40 mm f/2.8G AF-S DX NIKKOR 2200 VR Micro lens.

Dissection

Dissection of the inguinal canals, scrotum, spermatic cords, epididymides and testes were done in the standard fashion. Briefly, with the cadaver in supine position, the integument and superficial fascia were removed from the anterior and lateral abdominal wall. Each of the anatomical structures contributing to the inguinal canal were identified (i.e., oblique, internal oblique, and transversus abdominus muscles, lateral and medial crus, intercrural fibers and Poupart’s Ligament (i.e., the inguinal ligament). The external oblique aponeurosis was carefully incised to expose the full length of the spermatic cord. This approach was taken because the following anatomical structures contribute to the inguinal canal: inguinal ligament (lateral wall), internal oblique (medial wall), transversus abdominus and the transversalis fascia (floor of the canal). This was done on both left and right sides.

Bilaterally, the spermatic cord was carefully freed from the surrounding fascia and adipose tissue with blunt dissection. An incision was made in the proximal scrotum, through the integument, dartos and superficial fascia, and was carried down to the distal region. The scrotal spermatic cord was exposed, the gubernaculum testis was cut and the testis freed from surrounding areolar tissue. Next, the spermatic cord was incised and the coverings (i.e., external spermatic fascia, cremaster and internal spermatic fascia) removed to expose the ductus deferens (DD), testicular artery (Ta), and the pampiniform plexus of veins. This was continued proximally and superiorly along the cord and through the deep inguinal ring.

For both scrotal testes (STs) and SNTs, structures attached to the spermatic cord were isolated and cleaned of remaining areolar tissue. The tunica vaginalis was opened, the epididymis was identified, and the testis oriented along a longitudinal axis; allowing for a sagittal cut creating lateral and medial halves (of testis with epididymis). Gross identification included tunica vaginalis, tunica albuginea, epididymis (head, body and tail), DD and testicular vessels, seminiferous tubules and the region of the rete testis.

When masses were identified (i.e., suspected SNTs) along the tract of the inguinal canal or near to the superficial/deep inguinal ring, the same protocol was done with respect to testicular dissection, and a reasonable attempt was made to identify anatomical structures. In a similar fashion, the same was done with components of the spermatic cord attached to the SNTs, and these structures were traced back to their origin.

Measurements

Measurements of the STs and SNTs, scrotal epididymides (SEs), supernumerary epididymides (SNEs), and DD were taken in centimeters. Three measurements of each testis were taken: Anterior-Posterior (AP); Transverse left-right (TR); Length-sagittal (L-SAG).

Because testicular size and volume change in boys/men from childhood through adulthood and an orchidometer was unavailable, testicular volume was calculated using the formula for an ellipsoid: length (L) × width (W) × height (H) × 0.52 (Sakamoto et al., 2006). The measurements for the length of the DD and epididymides were taken using the method previously described by Van Lee and Talarico (Van Lee and Talarico, 2020). This method was modified for epididymides, where the thread was placed mid-sagittal (or length-wise) along each epididymis from the superior most point of the anatomical caput (or head) to the inferior most point of the anatomical cauda (or tail).

Tissue Preparation

STs and SNTs were removed from the cadaver and placed into trays. Sagittal sections of the left and right ST, SNTs, SEs, and SNEs were obtained in 5 x 5 mm increments using a No. 22 scalpel blade and placed into a labeled tissue cassette. Tissues and cassettes were placed into containers with Formal Fixx (Thermo Scientific Shandon, Hampton, NH, USA). After 24 hours, each specimen was transferred to a container with 70% EtOH for 72 hours. Next, each specimen was paraffin-embedded, sectioned and processed with the standard protocol for H&E at the University of Chicago Tissue Processing Center (University of Chicago, Chicago, IL, USA).

RESULTS

Case Report

The cadaver (i.e., patient) is a 96-year-old, white male, with a cause of death listed as congestive heart failure. No medical records, or other history, was available.

Topographical examination was consistent with a moderately overweighted male without any evidence of cancer or other disease. The glabella and supraorbital margins, the external genitalia, nipples/breast and body hair distribution were normal for age and did not indicate any pituitary or other endocrine disorder, nor androgenetic alopecia. The penis was of normal caliber. Testicles were palpable within the scrotum bilaterally. There was no visual or evidence of hernia or mass in the abdomen or inguinal region.

Cadaveric dissection documented a total of 4 testicles present in this patient. Two grossly mature testicles were located, one each, in the left and right scrotal sacs separated by the scrotal septum (i.e., scrotal testes (STs)) (Fig. 1A-C). The volumes of the left and right STs were 26.5 cm^3 and 23.7 cm^3, respectively. Each ST had an epididymis (i.e., SE) that measured 7.2 cm (left - length) and 7.0 cm (right - length). The right spermatic cord had a complex and dilated pampiniform plexus that encompassed the testicular artery (Fig. 1A, Fig. 1C) and coursed superiorly from the right testicle within the right, hemi-scrotum to the superficial and deep inguinal rings. The left pampiniform plexus was only slightly dilated in contrast to the contralateral homologous structure, and had an identical, but left-sided, anatomical course (Fig. 1 A-C).

Two mases were identified, one each bilaterally, high up in the inguinal canal and near to the superficial inguinal ring. Each was first thought to be a fatty lipoma because of "fatty-like" appearance and amorphous consistency. However, closer inspection documented a gross morphology of a testis and epididymis for each mass (Fig. 1A, Fig. 1 D-E), and thus these masses were then suspected to be SNTs with SNEs. The left SNT appeared grossly mature, with epididymis and testis proper, and with adhesions to the superficial inguinal ring. The volume of the left SNT was 12.3 cm^3, and the length of the left SNE was 4.7 cm^3. The left SNT had its own branch from the main spermatic cord extending down into the scrotum, and this branch had a testicular artery, sparce pampiniform plexus and a DD. In contrast, the right SNT appeared more atrophied, surrounded by adipose tissue, and was located high within the right inguinal canal and near to the deep inguinal ring (Fig. 1E). The volume of the right SNT was 0.55 cm. Further, the right SNE appeared malformed (and atrophic), and was only 1.8 cm in length. The right SNT received its blood supply from the right inferior epigastric artery (Fig. 2). The right ST and the left ST and SNT were supplied by the right and left testicular arteries, respectively. Both the right and left testicular arteries originated at the abdominal aorta and followed the usual course through the pelvic cavity into the inguinal canal.

The left and right ilioinguinal nerves and the genital and femoral branches of the left and right genitofemoral nerves followed the usual anatomical course through the inguinal canal. The ilioinguinal nerves course through the inguinal canal superficial to the spermatic cord and to the mons pubis. The genital branch of the genitofemoral nerve entered the inguinal canal through the deep inguinal ring and accompanied the spermatic cord in the usual fashion on both left and right sides. In contrast, no accessory branches of the left and right ilioinguinal nerves and the left and right genitofemoral nerves coursing along/with the spermatic cord of SNTs were grossly identified.

The DD on the left is joined 16 cm proximal to its origin by a 5.9 cm supernumerary ductus deferens (SDD) arising from the left SNT, then the main branch followed the normal course through the inguinal canal to the posterior-inferior urinary bladder. The total length of the DD arising from the left SE was 40.2 cm. The DD from the right ST also followed the normal anatomical pathway. However, the SDD from the right SNT was 3.2 cm (visible) and did not join that DD arising from the right ST until approximately 17.4 cm proximal to the origin at the epididymis. The total length of the main right DD was 39.2 cm. These measurements are summarized in Table 3.

Histological Evaluation

Histological examination of the left and right STs (Fig. 3A and Fig. 3B - main panel) documents that the seminiferous tubules show a clear lumen. Spermatogonia, Sertoli nuclei, spermatocytes, and spermatids can all be observed. The tubular basement membrane is seen, and the interstitium contains a few Leydig cells, blood vessels and fibrous components. The tubules of the left and right SEs (Fig. 3C and Fig 3D - insert) are lined with tall ciliated pseudostratified columnar epithelium. Cilia are stereocilia type. Spermatozoa and debris are seen in the lumen of the tubules. Smooth muscle is identified around the tubules. Photomicrographs of the SNTs (Fig. 3C and Fig. 3D - main panel) and SNEs (Fig. 3C and Fig. 3D - insert) lack the normal histologic morphology, and instead show adipose tissue.

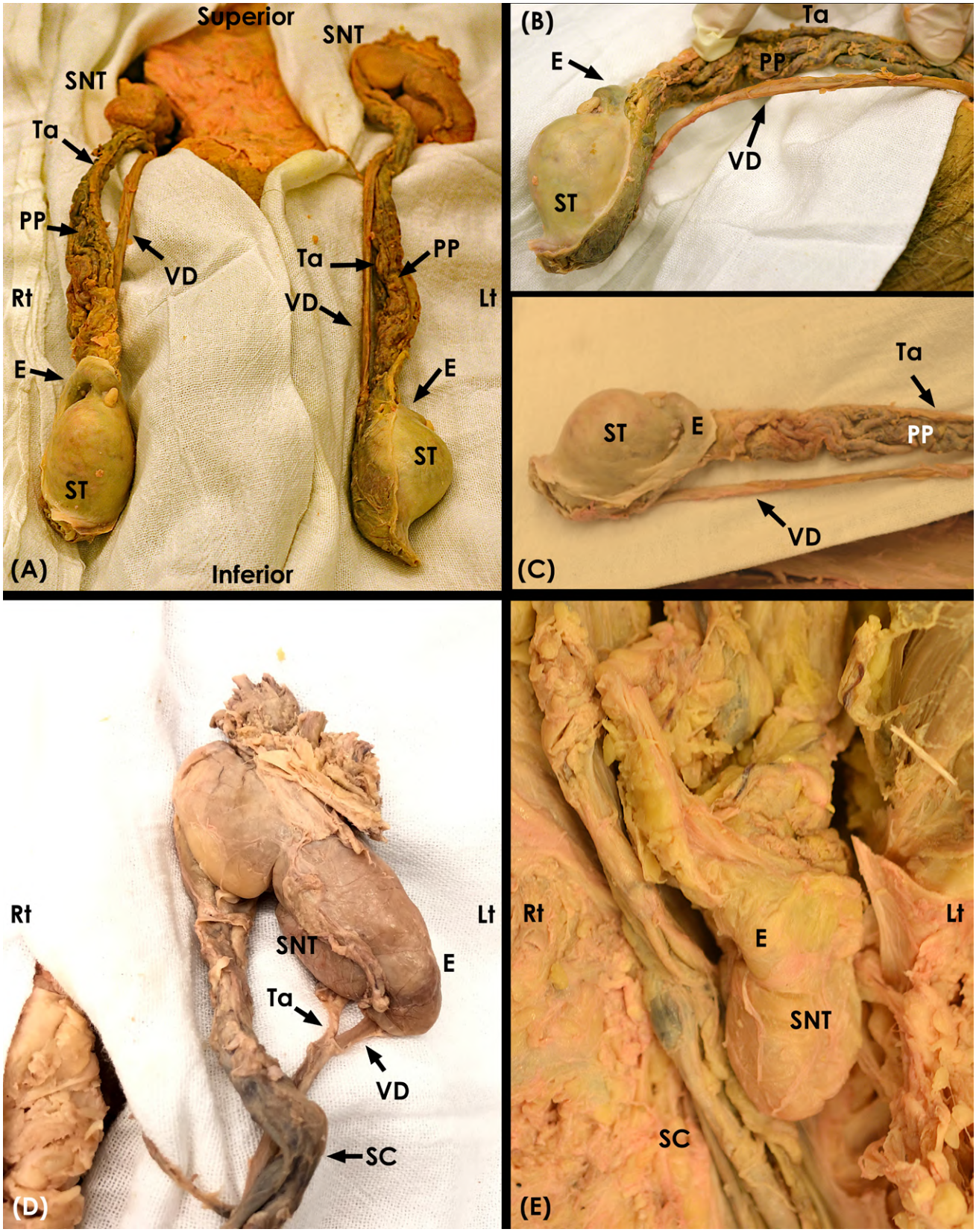

Fig. 1.- Gross Prosection of Testes. **(A)** Survey view. **(B)** Left scrotal testis with components of the spermatic cord and epididymis. **(C)** Right scrotal testis with spermatic cord and epididymis. **(D)** Left supernumerary testis (SNT). The left SNT has its own testicular artery and ductus deferens that branch from the main (scrotal) spermatic cord (SC). **(E)** Right supernumerary testis (SNT). The right SNT is more atrophied that the left SNT, and it is also higher up in the inguinal canal near to the deep inguinal ring. [The color on some of the labels in figure panels was changed from "black" to "white" to better visualize the indicated structures. **Abbreviations:** Ductus (vas) Deferens (VD), Epididymis (E), Left (Lt), Pampiniform plexus (PP), Right (Rt), Scrotal Testis (ST), Supernumerary Testis (SNT), Testicular artery (Ta)].

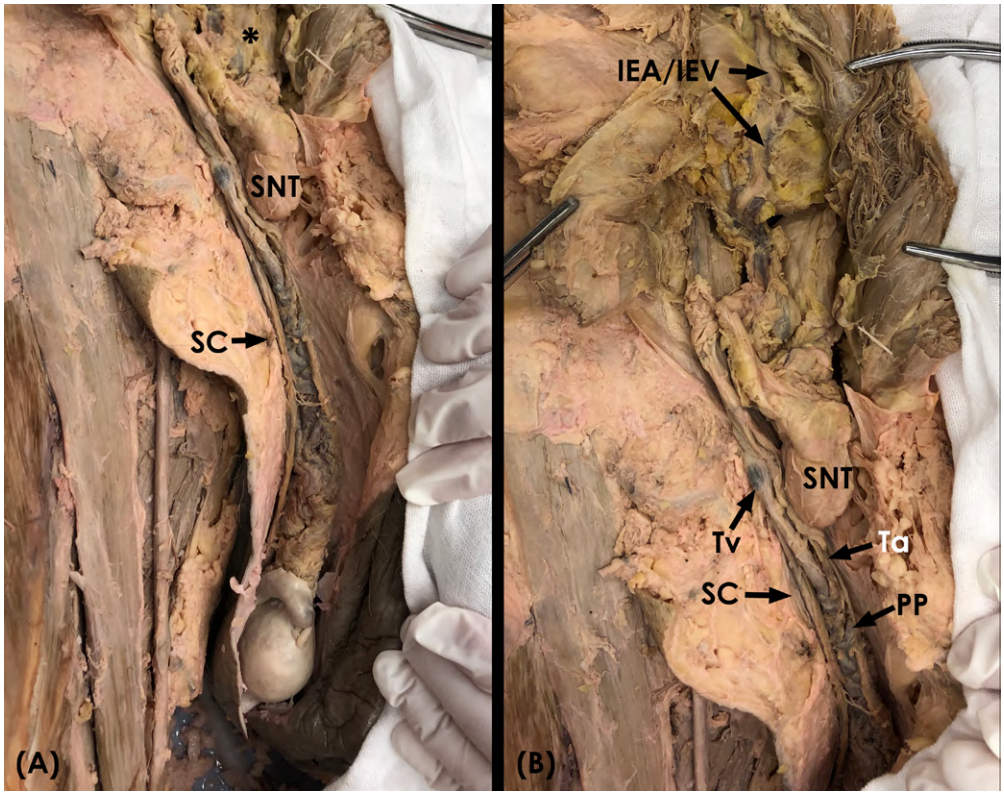

Fig. 2.- Vascular Support to Right Supernumerary Testis. **(A)** Survey view with right scrotal testis and spermatic cord. The Supernumerary Testis can be observed high in the right inguinal canal. The vessels (i.e., artery and vein) are indicated by the asterisk. **(B)** This prosected view shows the inferior epigastric vessels (artery is pink; vein is blue) that can be traced down to the right supernumerary testis. The testicular artery (Ta) and vein (Tv) to the right scrotal testis can be seen independent from the inferior epigastric vessels. [The color on some of the labels in figure panels was changed from "black" to "white" to better visualize the indicated structures. **Abbreviations:** inferior epigastric artery (IEA), inferior epigastric vein (IEV), spermatic cord (SC - testicular artery, pampiniform plexus (PP) and ductus deferens), supernumerary testis (SNT)].

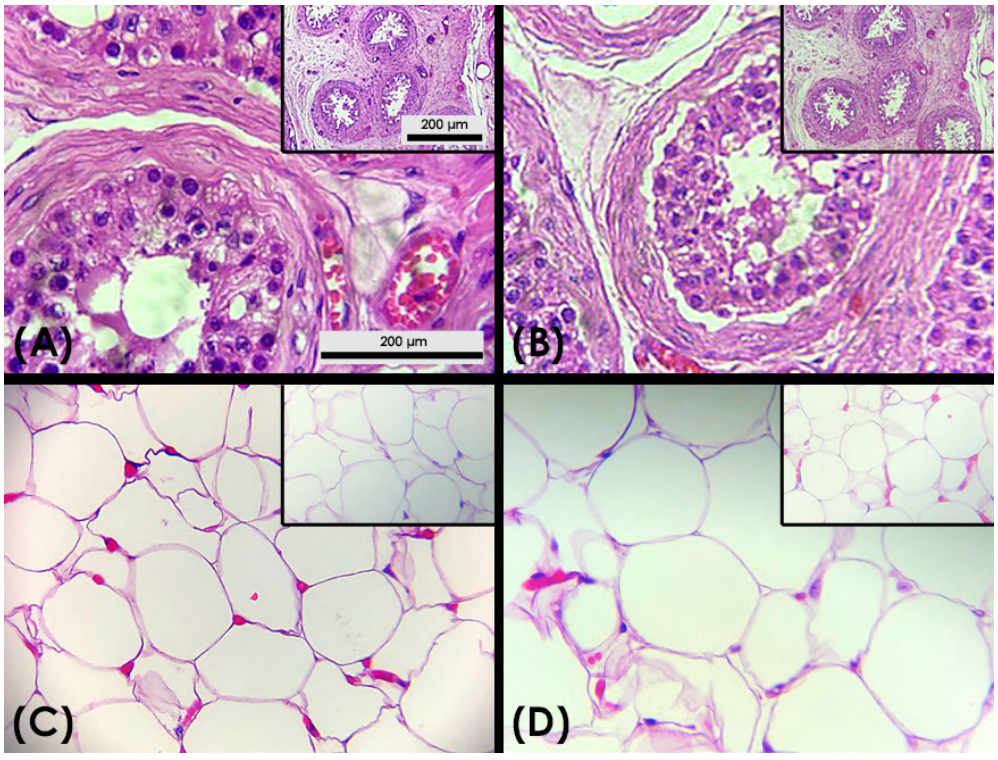

Fig. 3.- H&E-Stained Slides of Cadaveric Gonadal Tissue Sections. **(A)** Left scrotal testis and epididymis (insert) with normal morphology. **(B)** Right scrotal testis and epididymis (insert) with normal morphology. **(C)** Left supernumerary testis and supernumerary epididymis (insert). Gonadal tissue has been almost totally replaced by adipose tissue infiltrate. **(D)** Right supernumerary testis and supernumerary epididymis (insert). Similar to the left SNT and epididymis, gonadal tissue has been replaced by adipose tissue infiltrate. Yet, gross photographs document morphologically outlined structures (i.e., testis and epididymis) that appear atrophied and fat-like. [The calibration bars in (A) apply to all images and inserts.]

Table 3. Measurements.

STRUCTURE	MEASUREMENT (cm)*	VOLUME (cm^3)[T]	REFERENCE VALUE (cm)
LEFT Testicle	3.5 AP	26.5	3
	2.8 TR		3 - 4
	5.2 L-SAG		3 - 5
LEFT Epididymis	7.2		6 - 7
LEFT Ductus Deferens	40.2		20 - 40
LEFT SUPERNUMERARY Testicle	2.9 AP	12.3	3
	1.8 TR		3 - 4
	4.7 L-SAG		3 - 5
LEFT SUPERNUMERARY Epididymis	4.7		6 - 7
LEFT SUPERNUMERARY Ductus Deferens	5.9 (joining the main ductus deferens 16 cm proximal to its origin at the epididymis)		20 - 40
RIGHT Testicle	3.2 AP	23.7	3
	2.9 TR		3 - 4
	5.1 L-SAG		3 - 5
RIGHT Epididymis	7.0		6 - 7
RIGHT Ductus Deferens	39.2		20 - 40
RIGHT SUPERNUMERARY Testicle	1.2 AP	0.55	3
	0.5 TR		3 - 4
	3.0 L-SAG		3 - 5
RIGHT SUPERNUMERARY Epididymis	1.8		6 - 7
RIGHT SUPERNUMERARY Ductus Deferens	3.2 (joining main ductus deferens 17.4 cm proximal to its origin at the epididymis)		20 - 40

*Anterior-Posterior (AP); Transverse left-right (TR); Length-sagittal (L-SAG).
[T]**Testicular volume** was calculated using the formula for an ellipsoid: length (L) × width (W) × height (H) × 0.52.

DISCUSSION

Overall Summary of Results

In most cases, polyorchidism is incidentally discovered early in life by ultrasonography or surgery when another condition is present, such as inguinal hernia or pain, testicular torsion, mal-descent, malignancy, hydroceles and varicoceles, and treated via orchiectomy or orichidopexy. This was not the situation in the current research. There are several aspects of this case that make it unique and different from any discussed in the published literature. These are:

The patient's age at the time polyorchidism was detected was 96-years. Nearly all the existing literature has been on living patients ranging from infants to middle-aged males.

The patient presents with very high, bilateral inguinal polyorchidism, or tetraorchidism. Few cases of tetraorchidism are recorded in the

published literature, and none are recorded in an elderly polyorchid (Ibrahim, 2016; Duymus et al., 2016; Sheah et al., 2004).

The left SNT (Fig. 1D) also bears a structure resembling a fully formed epididymis, in contrast to the right SNT (Fig. 1E) in which the suggested epididymis appears with an increased degree of atrophy and adipose infiltration.

The high-degree of adipose infiltration into the SNTs. It is reasonable to suggest that due to the specimen's age that the right SNT atrophied and became fatty since it was not functioning, and both SNTs were infiltrated with fatty tissue resembling lipomas secondary to non-descent and age at time of detection (Hanes and Rosenbloom, 1911; Tasian et al., 2009; Nistal, et al., 2017).

Each SNT had a gross anatomically identifiable (by observation of structure, anatomical relationships and anatomical course) SDD. This is also supportive evidence that the identified masses are not lipomas or testicular nubbins but are SNTs (i.e., lipomas would lack an anatomic DD, and the present SNTs lack fibrosis, calcifications and giant cells).

The right SNT is being supplied blood from the inferior epigastric artery, which usually supplies the abdominal wall and rectus abdominus muscle and not the testis (Fig. 2), in contrast to the left SNT receiving blood in the usual fashion from the left Ta. A survey of the literature reveals no documented case with the branch from the inferior epigastric artery supplying the SNTs or STs.

The anatomical presentation does not fit within the current classification schemes for polyorchidism.

Histology

Prior literature describes the presence of SNTs; however, few studies supply histological evidence. In some cases, sonography and magnetic resonance imaging are used to confirm the existence of SNTs (Di Cosmo et al., 2016; Abduljabbar, 2015; Artul and Habib, 2014; Arslanoglu, 2013; Baker et al., 1987). In this paper, to confirm that these structures were SNTs, samples were prepared from the left and right SNTs and compared with tissue samples from both the left and right STs. Histological study with H&E staining confirmed that the STs contained seminiferous tubules and interstitial cells. This is similar to findings of STs in other studies focusing on polyorchids. In contrast to prior studies in the present work, histological evidence of both SNTs revealed extensive infiltration with adipose tissue, the right greater than left. Prior studies have documented shortening and wall thickening of the seminiferous tubules occurs, as well as a decrease in number of Sertoli cells with an accumulation of abundant lipids (Nistal et al, 2017). Further, other investigations have shown that the morphological findings in adult cryptorchid patients are that (1) testes are much smaller than normal, (2) the tubules are atrophic, (3) the germinal epithelium is generally largely absent, and (4) Leydig-cells are vacuolated and loaded with lipids (Nistal et al., 2017). It is suggested in the present case that because of this polyorchids age and due to SNT non-descent, that components of the undetected SNTs were replaced with fatty tissue (Nistal et al., 2017; Tasian et al., 2009; Hanes and Rosenbloom, 1911). Thus, it is possible that there are more cases of undiagnosed polyorchidism in elderly patients that are *misdiagnosed* as lipomas, a benign tumor of adipose tissue. Therefore, the findings in the present work suggest that histological study is encouraged to be correlated with gross anatomic findings and anatomical relationships (i.e., arterial supply, DD, etc.) in the confirmational workup of a suspected polyorchid.

A Novel Classification

Current classification models for polyorchidism are organized under anatomical (Table 1) and anatomical-functional (Table 2) descriptions (Haddock and Burns, 1987; Bergholz et al., 2007). In the patient reported herein, the left SNT and right SNT fit the description of Type IV anatomical (Table 1) but does not fit in any category of the anatomical-functional scheme secondary to lack of reproductive potential. Reproductive potential of the SNTs in this case may have been present early in life and into late teens, however, polyorchidism discovered at 96-years of age showed appropriate and attached anatomical structures with adipose

infiltration into the testes. Further, the SNTs in the present research are not testicular nubbins. A testicular nubbin is the residual tissue of the human testis after a supposed perinatal vascular accident involving the testicular blood supply. They differ from testicular nubbins because in nubbins there is fibrosis, hemosiderin, giant cells and calcifications (Emir et al., 2007; Cendron et al., 1998). Thus, it is suggested to add a novel Type 3 with Subgroups A and B to the anatomical-function classification scheme; making the classification in this patient Type 3, Subgroup B, or SNT attached to the draining epididymis and vas deferens without having any reproductive potential (i.e., Type 3) and SNT located outside the scrotal sac (ectopic) (i.e., Subgroup B).

Inguinodynia and Possible Correlation to SNTs

Inguinodynia (i.e., chronic post-herniorrhaphy pain), defined as pain lasting longer than 3 months after open inguinal hernia repair, has become the most important complication after inguinal surgery and therefore compromises quality of life (Konchake et al., 2020). Frequently, males complain of inguinal pain before and after surgery for polyorchidism, inguinal lipomas, or inguinal hernias (Mathur et al., 2002; Tonape et al., 2012; Dollard, 2011; Sakamoto et al., 2007; Mittal et al., 2018; Otero, 2016; Artul and Habib, 2014; Hassan et al., 2014; Hassan et al., 2008). Yet, a survey of the literature does not reveal the documented presence of peripheral (or accessory) inguinal or genitofemoral nerves associated with SNTs or inguinal lipomas. This is consistent with the present work, as well as all other published studies on human polyorchids, that relied on gross anatomical dissection and not microscopic analysis of the spermatic cord. It is possible that microscopic branches of these nerves may be present along the spermatic cords coursing to the SNTs. If so, this is clinically significant in that these nerve fibers may contribute to complaints of pain. Still further, accessory nerve fibers may be clinically significant in the management of chronic groin pain, post operative inguinal pain, or testicular pain following inguinal hernia repair or excision of SNTs (Amid and Chen, 2011; Hue and Chen, 2018; Lange et al., 2015). Thus, a major reason for inguinodynia might be the lack of neuroanatomical knowledge and suboptimal management of the nerves during such surgeries (Konchake et al., 2020).

Embryology and a Possible Genetic Basis for Polyorchidism

Polyorchidism and the concurrent failure of the SNT to descend into the scrotum may be the result of defective gonadal embryogenesis. Normal development of testes occurs at the genital ridge with subsequent cell differentiation and proliferation (Titi-Lartey and Khan, 2021). Testicular function and development are both dependent on normal Sertoli cell differentiation (Makela et al., 2018). However, the descent of the testes into the scrotum occurs in two stages. The first stage is transabdominal and occurs during weeks 10 - 15 of gestation (Hutson et al, 2013; Titi-Lartey and Khan, 2021). The testes are moving from the abdomen into the inguinal canal. The gubernaculum enlarges during 16 - 24 weeks of gestation (Favorito et al., 2014). The second stage, or the inguinoscrotal stage, occurs during weeks 25 - 35 of gestation (Favorito et al., 2014). During this phase, the gubernaculum connects the epididymis and the gonad to the forthcoming inguinal canal, eventually pulling (or migrating) the developing testes down into the scrotum. During sexual differentiation, the testes become more attached to the gubernaculum while testosterone causes the mesonephric (Wolffian) duct to form the epididymis and vas deferens (Hutson et al., 2013).

The anatomy of the normal testes is oval shaped and located in the left and right hemi-scrotum separated by the scrotal septum. In the present research, the polyorchid had two mature STs and two SNTs discovered *abnormally proximal in the inguinal canals*. The left SNT appeared further developed with epididymis and testis proper in comparison to the right SNT, which appeared to be more atrophied and maldeveloped. The left SNT was observed to have adhesions that were attached to the superficial inguinal ring. The left SNT was supplied by its own branch from the left main spermatic cord and included a testicular artery, sparce pampiniform plexus

and vas deferens. In contrast, the right SNT was supplied by the inferior right epigastric artery but was atrophied and surrounded by adipose tissue. The above results suggest some factor(s) affecting "duplicity" and "migration" of the developing gonads.

A survey of the literature focused on polyorchidism shows little to no mention of genetic factors that may play a role in the development of this condition. It has been hypothesized that polyorchidism is caused by the division of the genital ridge during embryological development (Lawrentschuk and MacGregor, 2004; Friedman, 2015; Satoh, 1991). Based on this theory, it can be suggested that in individuals with polyorchidism there may be a genetic factor that has led to the increased likelihood that anomalous division may occur. Cell-cell adhesion proteins have been identified that play roles in the developing and adult testis in normal testicular development in rats as a model organism (Pipreck et al, 2019). All of these genes for these proteins belong to the Cadherin family of genes: CDH1, CDH2 and CDH3, encode for the proteins E-Cadherin, N-Cadherin and P-Cadherin, respectively. N-Cadherin is proposed to be the most likely candidate, because CDH2 gene knockout mutants in gonadal germ cells showed significant loss of normal gonadal structure (Pipreck et al, 2019). Therefore, a mutation that reduces the effectiveness of this tissue adhesion molecule could potentially play a role in aberrant division of the genital ridge and the development of polyorchidism. The present work set the stage to explore this potential link between the Cadherin gene family and polyorchidism using full exome sequencing.

Significance of the Current Work

There are approximately 200 cases of polyorchidsm reported in the literature; the most common variant having three testicles (i.e., left SNT), and only 9 cases of tetraorchidism (i.e., left and right SNTs), and none in an elderly male (Ibrahim 2016). The current research describes an additional and unique case of tetraorchidism with data from gross anatomical and histological perspectives that suggest (1) a novel classification and (2) a hidden presentation mimicking lipoma. This suggests that some SNTs may be clinically misdiagnosed as lipomas, and therefore are more prevalent than previously recorded. Further, the current work sets that stage for molecular and genetic studies focused on the mechanistic basis of the new classification.

Limitations

The research was conducted on a postmortem anatomical donor. Access to the comprehensive medical, social and occupational histories of the donor were not available. It is unknown if the donor was aware of the condition, if he had a family history of polyorchidism or reproductive challenges.

CONCLUSION

This investigation has described a novel case of polyorchidism in an adult male with a cause of death determined as congestive heart failure. This case is interesting because: (1) it differs from the usual time of discovery of polyorchidism, here in a 96-year-old (vs. young) male; (2) it is only the 10th case of tetraorchidism to be discovered; (3) it documents that SNTs may have arterial supply that has not been previously described in the literature (i.e., the inferior epigastric artery); (4) it suggests that lipomas of the inguinal canal may be misdiagnosed and actually be SNTs, and (5) this research proposes a reasonable, *novel* classification of polyorchidism not presented in the current literature, but supported by gross anatomical data. Although multiple conditions may be associated with polyorchidism, the underlying developmental mechanism has yet to be determined. Further, the present work establishes the foundation for genetic/molecular investigation into this condition. Most commonly, polyorchidism is highly curable with orchiectomy or orchidopexy (for preservation of reproductive potential reproductive function), but an increased risk of testicular cancer remains. To achieve accurate diagnosis and optimal patient outcomes, a multidisciplinary approach is needed with expert knowledge of anatomical and histological correlations.

ACKNOWLEDGEMENTS

The authors wish to express their sincere gratitude to the patient and his family, who donated his remains to medical research and education. We also wish to thank the director and staff of Anatomical Gift Association of Illinois (Chicago, Illinois, USA) for their expertise in preparing this anatomical donor's remains for the present study. We also express our sincere appreciation to the team at the University of Chicago Tissue Processing Center (University of Chicago, Chicago, IL, USA).

NOTES ON CONTRIBUTORS

ERNEST F. TALARICO, JR., serves in the appointments of Adjunct Professor of Anatomy (North Park University, Chicago, Illinois USA); Visiting Professor of Anatomy and Radiology, Medical Student Academic Adviser, and Research Adviser at Tan Tao University School of Medicine (Long An, Việt Nam). He is a founding member of the medical advisory board and founder of the Center for Medical Education and Research at the new Nam Can Tho University Hospital (Can Tho, Việt Nam). Dr. Talarico is a consultant and lead prosector for the Anatomical Gift Association of Illinois (Chicago, Illinois USA), and senior research consultant in the Cardiovascular Research Laboratories, Methodist Hospital (Merrillville, Indiana USA). He created and served as director for the International Human Cadaver Prosection Program, which in 2008 received the award for most outstanding and innovative program in undergraduate and continuing medical education from the AAMC Central Group on Educational Affairs. He is creator of the "Talarico Protocol for Human Gross Anatomy" and is the 2008 recipient of the Partnership Matters Award from the Northwest Indiana Area Health Education Center. In recognition of his work and innovations in anatomical education, in October 2010, Dr. Talarico was inducted as a fellow into the Northwest Indiana Society of Innovators.

JOSEPH G. CASTANEDA is currently a junior, undergraduate student at North Park University (Chicago, Illinois USA) working on a B.S. in Biomedical Sciences. He has served as a prosector in the human gross anatomy laboratory and has created a multi-media presentation focused on aneurysms of brachial plexus that is used to educate other students and prosectors. Mr. Castaneda plans to attend medical school.

SANA M. WAHAB is a 2021 graduate from North Park University (Chicago, Illinois USA). She graduated with a B.S. in Biomedical Sciences. Ms. Wahab was involved in various academic groups including Women in STEM, the American Medical Student Association, the *Tri Beta* Honor Society, as well as cadaveric exploration groups. She also served as a teaching assistant and supplemental instructor for human anatomy.

KATELYN M. PAULUS is a sophomore, undergraduate student in the Pre-Nursing program at North Park University (Chicago, Illinois USA). Ms. Paulus has served in the cadaver prosection laboratory, and she created a multi-media presentation that is used to educate students about the brachial plexus and the muscles innervated.

JACK D. WALSH is an undergraduate student studying Molecular Biology and Biotechnology at North Park University (Chicago, Illinois USA). He holds active memberships in the Tri Beta Biological Honors Society, the American Society for Cell Biology, and the American Society for Biochemistry and Molecular Biology. Mr. Walsh serves in the Biology Department at North Park University, where he participates in many projects to improve the laboratories as well as maintaining equipment and preparing labs for various classes. He is also involved in multiple research opportunities on campus, where he takes initiative and leadership in preforming directed research and teaching underclassmen so they may continue his research once he graduates this coming May. Currently, Mr. Walsh is in the process of applying to graduate programs in pursuit of his Ph.D. in the fields of Molecular Biology and Biochemistry.

AMY E. STROMBERG graduated from North Park University (Chicago, Illinois USA) in 2021 with a B.S in Biomedical Sciences and a minor in Psychology. She has served as a teaching assistant for anatomy and zoology and has worked as the animal care coordinator for the zoology laboratory. Ms. Stromberg's prior student research focused on the roles of melanism in urban pigeons. She is currently obtaining certification as an emergency medical technician and plans to go on to medical school.

VICTORIA N. OLSON graduated in 2021 from North Park University (Chicago, Illinois USA), Summa Cum Laude with a B.A. in Biomedical Sciences and a minor in Chemistry. She served as an anatomy teaching assistant and an undergraduate learning assistant for advanced physiology, as well as Treasurer of the *Beta Beta Beta* Honor Society. Ms. Olson created a human cadaver imaging atlas that is being implemented as a learning tool at North Park University. She is a member of the American Medical Student Association and is currently applying to medical school.

PAUL J. JANUS received his Ed.D. in Higher Education and Adult Learning from Walden University (Minneapolis, Minnesota USA). Dr. Janus serves as the Laboratory Manager for the Department of Biology, the Director of Anatomical Research, and a Professor of Biology and Chemistry at North Park University (Chicago, Illinois USA).

NICHOLAS R. ROCCO is a doctor of allopathic medicine; Dr. Rocco graduated from Uniformed Services University of Health Sciences School of Medicine (Bethesda, Maryland USA). Dr. Rocco has completed extensive training in urology, and he serves as a reconstructive surgeon in urology as a member of the Naval Medical Center - San Diego in the Department of Urology (San Diego, California USA).

REFERENCES

ABDULJABBAR AH (2015) A case report: triorchidism; is a rare mistaken cause for extra testicular neoplasm. *Urol Case Rep*, 3(3): 89-91.

AHLFELD F (1880) Die Missbildungen des Menschen. Leipzig, Germany: Grunow, 126.

AKBAR SA, SAYYED TA, JAFRI SZ, HASTEH F, NEILL JS (2003) Multimodality imaging of paratesticular neoplasms and their rare mimics. *Radiographic*s, 23(6): 1461-1476.

AMID PK, CHEN DC (2011) Surgical treatment of chronic groin and testicular pain after laparoscopic and open preperitoneal inguinal hernia repair. *J Am Coll Surg*, 13(4): 531-536.

ARTUL S, HABIB G (2014) Polyorchidism: two case reports and a review of the literature. *J Med Case Rep*, 8: 464-468.

ARSLANOGLU, A, TUNCEL SA, HAMARAT M (2013) Polyorchidism: Color doppler ultrasonography and magnetic resonance imaging findings. *Clin Imaging*, 37(1): 189-191.

AVARGUES A, ROGEL R, BROSETA E, LUJÁN S, BETANCOURT JA, MORALES G, BORONAT F (2015) Polyorchidism: the case in a young male and review of the literature. *Asian J Androl*, 17(3): 511-512.

AZIZ W, REHMAN KU, RAFIQUE MZ (2016) Doppler ultrasound findings in a patient with primary infertility and triorchidism. *BMJ Case Rep*, 215346, doi: 10.1136/bcr-2016-21534.

BAKER LL, HAJEK PC, BURKHARD TK, MATTREY RF (1987) Polyorchidism: evaluation by MR. *AJR Am J Roentgenol*, 148(2): 305-306.

BERGHOLZ R, KOCH B, SPIEKER T, LOHSE K (2007) Polyorchidism: a case report and classification. *J Ped Surg*, 42(11): 1933-1935.

BERGHOZ R, WENKE K (2009) Polyorchidism: a meta-analysis. *J Urol*, 182(2): 2422-2427.

CENDRON M, SCHNED AR, ELLSWORTH PI (1998) Histological evaluation of the testicular nubbin in the vanishing testis syndrome. *J Urol*, 160(3 Pt 2): 1161-1163.

COHEN T, AGARD H, PAREKH N, CLARK C (2017) Management of bilateral undescended bilobed testes and review of the literature. *Urology*, 110: 213-215.

DANRAD R, ASHKER L, SMITH W (2004) Polyorchidsim: imaging may denote reproductive potential of accessory testicle. *Pediatr Radiol*, 34(6): 492-494.

DI COSMO, SILVESTRI T, BUCCI S, BERTOLOTTO M, TROMBETETA C (2016) A singular case of polyorchidism, *Archivio italiano di urologia, andrologia: organo ufficiale [di] Societa italiana di ecografia urologica e nefrologica, 88(4): 333-334.*

DOLLARD DJ, FOBIA JB (2011) Extra scrotal spermatocele causing lower abdominal pain: a first case report. *Am J Emerg Med*, 29(3): 358.37-39.

DUYMUŞ M, MENZILCIOĞLU MS, ÇETINÇAKMAK M, AVCU S (2016) A rare case of polyorchidism: four testes. *Pol J Radi,* 81: 39-41.

ELLETT JD, ROSOFF JS, PRASAD MM (2015) Three testicles in one hemiscrotum: an unusual presentation of polyorchidism. *BMJ Case Rep*, doi: 10.1136/bcr-2014-206033

EMIR H, AYIK B, ELIÇEVIK M, BÜYÜKÜNAL C, DANIŞMEND N, DERVIŞOĞLU S, SÖYLET Y (2007) Histological evaluation of the testicular nubbins in patients with nonpalpable testis: assessment of etiology and surgical approach. *Pediatr Surg Int*, 23(1): 41-44.

FAVORITO LA, COSTA SF, JULIO-JUNIOR HR, SAMPAIO FJ (2014) The importance of the gubernaculum in testicular migration during the human fetal period. *Int Braz J Urol*, 40(6): 722-729.

FRIEDMAN, DAVID (2015) Polyorchidism: a case of supernumerary testes. *Sonography*, 2(1): 14-16.

GUNE AR, GUNE RP (2021) Triorchidism: a rare case report. *Afr J Urol*, 27:15:1-3.

HADDOCK G, BURNS HJG (1987) Polyorchidism. *Postgrad Med J*, 63: 703-705.

HANES FM, ROSENBLOOM J (1911) A histological and chemical study of the fatty matter of normal and cryptorchid testes. *J Exp Med*, 13(3): 355-364.

HASSAN A, EL-MOGY MS, MOSTAFA T (2008) Triorchidism: a case report and review of similar conditions. *Andrologia*, 40(4) :265-269.

HASSAN A, ELHANBLY S, EL-MOGY MS, MOSTAFA T (2014) Triorchidism: two case reports. *Andrologia*, 46(9): 1073-1077.

HUTSON JM, SOUTHWELL BR, LI R, LIE G, ISMAIL K, HARISIS G, CHEN N (2013) The regulation of testicular descent and the effects of cryptorchidism. *Endocr Rev*, 34(5): 725-752.

HU QL, CHEN DC (2018) Approach to the patient with chronic groin pain. *Surg Clin North Am*, 98(3): 651-665.

IBRAHIM H, ROBERTS MJ, HUSSEY D (2016) Quadruple orchidopexy for torsion testis in an adolescent with polyorchidism: a case report. *Urology*, 87: 196-199.

KONSCHAKE M, ZWIERZINA M, MORIGGL B, FÜGGER R, MAYER F, BRUNNER W, SCHMID T, CHEN DC, FORTELNY R (2020) The inguinal region revisited: the surgical point of view: An anatomical-surgical mapping and sonographic approach regarding postoperative chronic groin pain following open hernia repair. *Hernia*, 24(4): 883-894.

LANE WA (1895) A case of supernumerary testis. *Trans Clin Soc Lond*, 28: 59-60.

LANGE JF, KAUFMANN R, WIJSMULLER AR, PIERIE JP, PLOEG RJ, CHEN DC, AMID PK (2015) An international consensus algorithm for management of chronic postoperative inguinal pain. *Hernia*, 19(1): 33-43.

LAWRENTSCHUK N, MACGREGOR RJ (2004) Polyorchidism: A case report and review of the literature. *ANZ J Surg*, 74(12):1130-1132.

MÄKELÄ JA, KOSKENNIEMI JJ, VIRTANEN HE, TOPPARI J (2019) Testis Development. *Endocr Rev*, 40(4): 857-905.

MATHUR P, PRABHU K, KHAMERSRA HL (2002) Polyorchidism revisited. *Pediatr Surg Int*, 18(5-6): 499-450.

MÉNDEZ-GALLART R, ESTEVEZ-MARTÍNEZ E, RODRÍGUEZ-BARCA P, GARCÍA-PALACIOS M, BAUTISTA-CASASNOVAS A (2012) Incomplete unilateral polyorchidism (bilobed testicle) mimicking testicular tumour. *J Pediatr Surg*, 47(11): 2140-2142.

MITTAL PK, ABDALLA AS, CHATTERJEE A, BAUMGARTEN DA, HARRI PA, PATEL J, MORENO CC, GABRIEL H, MILLER FH (2018) Spectrum of extratesticular and testicular pathologic conditions at scrotal MR imaging. *Radiographics*, 38(3): 806-830.

MITTAL PG, PETERS NJ, MALIK MA, SAMUJH R (2020) Intraoperative dilemmas in polyorchidism: to pex or not to pex!! *J Indian Assoc Pediatr Surg*, 25(3): 175-177.

NISTAL M, GONZÁLEZ-PERAMATO P, SERRANO Á (2017) Clues in the Diagnosis of Non-tumoral Testicular Pathology. 1st Edition, *Springer Nature*, Switzerland AG.

OTERO J, BEN-YAKAR N, ALEMAYEHU B, KOZUSKO SD, BORAO F, VATES III TS (2016) A unique case of intraabdominal polyorchidism: a case study. *Case Rep Urol*, Epub doi: 10.1155/2016/2729614

PIPREK RP, KOLASA M, PODKOWA D, KLOC M, KUBIAK JZ (2019) N-cadherin is critical for the survival of germ cells, the formation of steroidogenic cells, and the architecture of developing mouse gonads. *Cells*, 8(12): 1620:1-24.

ROCA-FERRER J, RODRIGUZ E, RAMIREZ GA, MORAGAS C, SALA M (2015) A rare case of polyorchidism in a cat with four intra-abdominal testes. *Reprod Domest Animi*, 50(1): 172-176.

SAKAMOTO H, SAITO K, OOHTA M, INOUE K, OGAWA Y, YOSHIDA H (2007) Testicular volume measurement: comparison of ultrasonography, orchidometry, and water displacement. *Urology*, 69(1): 152-157.

SATOH M (1991) Histogenesis and organogenesis of the gonad in human embryos. *J Anat*, 177: 85-107.

SHEAH K, TEH HS, PEH OH (2004) Supernumerary testicle in a case of polyorchidism. *Ann Acad Med Singap*, 33(3): 368-370.

SPRANGER R, GUNST M, KÜHN M (2002) Polyorchidism: a strange anomaly with unsuspected properties. *J Urol*, 168(1): 198.

SINGER BR, DONALDSON JG, JACKSON DS (1992) Polyorchidism: functional classification and management strategy. *Ped Urol*, 39(4): 384-388.

TALARICO JR EF, MAS JL, JONES JA (2018) A comprehensive anatomical characterization and radiographic study of stage III testicular cancer in a 31-year-old male patient. *Eur J Anat*, 22(3): 241-256.

TAMMINEN TM, LEINONEN MR, KACK H, ANDERSSON M (2012) A polyorchid dog. *Reprod Domests Anim*, 47(2): e26-28.

TASIAN GE, HITTELMAN AB, KIM GE, DISANDRO MJ, BASKIN LS (2009) Age at orchiopexy and testis palpability predict germ and Leydig cell loss: clinical predictors of adverse histological features of cryptorchidism. *J Urol*, 182(2): 704-709.

TITI-LARTEY OA, KHAN YS (2021) Embryology, Testicle. In: StatPearls, *StatPearls Publishing*; Available from: https://www.ncbi.nlm.nih.gov/books/NBK557763/

TONAPE T, SINGH G, KOUSHIK P, TUMEPALLI T (2012) Triorchidism: a rare genitourinary abnormality. *J Surg Tech Case Rep*, 4(2): 126-128.

VAN LE C, TALARICO JR. EF, TRUONG NGUYEN K (2020) The size of intestines in Vietnamese adults. *Eur J Anat*, 24(3): 169-178.

VASAIYA, MK, SHAH, SM, GOHIL VB (2021) Polyorchidism: A rare case report. *Int Surg J*, 8(1): 398-400.

WITT CC, BAUTISTA E (2011) Triorchidism in a Hummingbird. *Wilson J Ornithol*, 123(3): 632-635.

WOLF B, YOUNGSON GG (1998) Polyorchidism. *Pediatr Surg Int*, 13(1): 65-66.

ZAHIRIAN MOGHADAM T, MOHSENI RAD H, ZANDIAN H, HOSSEINKHANI A (2020) Five testicles in the genital area of a thirteen-month-old baby: a case report. *BMC Urol*, 20(1): 128-130.

A new student-led dissection approach to the glenohumeral joint

Robert J. Leigh[1], Deborah Merrick[2]

[1]*School of Medicine, Faculty of Medicine and Health Sciences, University of Nottingham, United Kingdom*
[2]*School of Life Sciences, Faculty of Medicine and Health Sciences, University of Nottingham, United Kingdom*

SUMMARY

Modern day anatomy educators face many educational challenges associated with changes in curriculum, institutional reorganization and reduced teaching hours—all alongside criticism that medical students' anatomical knowledge at graduation is insufficient. At the University of Nottingham in the United Kingdom, a traditional approach to full body cadaveric dissection is carried out in the undergraduate medical curriculum, using dissection manuals based on long- published dissector guides. First-year medical students dissect the shoulder region in a superficial manner allowing good visualization of musculature and surrounding neurovascular structures, although observation of the internal joint is significantly limited. This study reports a student-led adaption to a novel dissection approach of the glenohumeral joint, which involves splitting the humeral head to expose the internal joint capsule in exceptional detail. The prosection generated was incorporated into an on-line teaching package for first-year medical students. Students' knowledge of the region was assessed before and after accessing the on-line teaching material, and results highlighted a significant improvement in anatomical knowledge after completion of the package (P = 0.013). First-year medical students who view the novel dissection also out-performed second-year medical students who had experienced traditional teaching of this region (P = 0.002). This study has demonstrated that a novel dissection of the glenohumeral joint can provide educational benefit by increasing anatomical knowledge of the region. Furthermore, student-led innovations may act as a powerful means of achieving much-needed reform in the field of musculoskeletal anatomy education.

Key words: Gross anatomy education – Medical education – Undergraduate education – Musculoskeletal medicine – Glenohumeral joint – Cadaveric dissection

INTRODUCTION

Future clinicians need a proficient understanding of core anatomy as a backbone of their clinical practice (Lazarus et al., 2012). In recent decades, the medical curriculum has seen a decrease in time devoted to a range of basic medical sciences, including anatomy, to allow for much wider teaching within modern medicine (McKeown et al., 2003; Turney, 2007; Rockarts et al., 2020). Alongside these implemented changes, there is growing concern by many newly qualified doctors and senior clinicians that graduates sim-

Corresponding author:
Dr. Deborah Merrick. School of Life Sciences, University of Nottingham Medical School, Queen's Medical Centre, Nottingham, NG7 2UH, United Kingdom. E-mail: deborah.merrick@nottingham.ac.uk

Submitted: November 8, 2021. **Accepted:** December 3, 2021

https://doi.org/10.52083/FYKJ4035

ply do not possess sufficient anatomical knowledge for their first clinical placement (Waterson and Stewart, 2005; Fitzgerald et al., 2008). Deficits in medical students' knowledge (Day et al., 2007; Al-Nammari et al., 2015) and lack of confidence in performing and interpreting the findings of musculoskeletal examinations are often cited in the literature (Skelley et al., 2012; Peitzman and Cuddy, 2015). Further evidence suggests that the current approach to preclinical musculoskeletal medicine provides no improvement to clinical competency post-graduation (Khorsand et al. 2018). The deficit in the musculoskeletal field of teaching has been observed in institutions across the world, which has led to attempts at improvement by adaptation of the curriculum (Murphy et al., 2014; Hose et al., 2017). Curricular reform, via multidisciplinary collaboration, student-run musculoskeletal (MSK) clinic (McQuillan et al., 2017) and novel approaches to dissection (Hlavac et al., 2017; Cotofana et al., 2021) have been cited in the literature as potential routes to improve education in this field (Murphy et al., 2014). A solid foundation of musculoskeletal anatomy is clinically very important, as musculoskeletal disorders and complaints are commonly observed within the clinical setting (Huisstede et al., 2006: Buchbinder et al., 2013). It is therefore essential that medical students receive appropriate teaching of these regions, within the confines of the time allocated in the curriculum. The mode of teaching and its effectiveness is therefore an important consideration of all anatomy educators.

First-hand cadaveric dissection is often referred to as the gold standard for teaching anatomy, which, many would argue, has seen little development or change over many preceding decades, if not centuries (Elizondo-Omaña et al., 2005; Memon, 2018). Cadaveric dissection serves to provide a unique and authentic three-dimensional view of the organization of the human body, illustrating anatomical variation and pathology (often representative of the local population), alongside reinforcing compassion and respect (Konschake and Brenner, 2014; Dissabandara et al., 2015;). Although numerous reported benefits are associated with full body cadaveric dissection, many universities are moving away from this teaching practice, cited reasons including a shortage of qualified anatomists (Wilson et al., 2019), lack of cadaveric material (Chen et al., 2018) and the financial and time-consuming nature of the teaching modality (Patel et al., 2015; Estai and Bunt, 2016; Ghazanfar et al., 2018;). This, coupled with recent advancements in technological media to learn anatomy, has resulted in some medical schools' revision of their anatomical curricula with less emphasis, or completely without any emphasis at all, on the features of cadaveric dissection (Parker, 2002; Davis et al., 2014; Memon, 2018; Birbara et al., 2020). The improvement in technology, alongside the need to adapt teaching to the Covid-19 pandemic, means that online learning or a blended approach is now commonplace for anatomy teaching (Evans et al., 2020; Franchi, 2020; Pather et al., 2020). Recent findings suggest that these new approaches can provide students with greater knowledge of gross anatomy, provided there is sufficient student engagement (Green and Whitburn, 2016; Green et al., 2018).

The University of Nottingham in the United Kingdom (UK) runs an undergraduate-entry Medicine BMBS program where students experience 98 hours of gross anatomy teaching during their preclinical (years 1-3) training (Pratten et al., 2014). Teaching takes the form of lectures, workshops and practical cadaveric dissection classes that are largely based on the approach described in Hansen dissector (Hansen, 2002). Students carry out full body cadaveric dissection, alongside having access to pre-dissected (prosected) material, osteology specimens, a digital imaging library, anatomical models and on-line computer aided learning packages to help support their learning within the dissecting room (Turmezei et al., 2009). Assessment of gross anatomical knowledge forms the basis of an end-of-year Objective Structured Practical Examination, and application of this knowledge is incorporated into theory-based end-of-year summative exams. The musculoskeletal gross anatomical component of the medical course is taught primarily in year 1, and comprises a total of 28 teaching contact hours (7 one-hour lectures and 21 hours of dissection). This approach is

consistent with other UK Medical Schools in both the delivery method and devoted teaching time (Gogalniceanu et al., 2009). A very small number of students have the chance to dissect again as part of a second-year anatomy optional module (8-10/300), or as part of a third-year dissertation project (14-16/300). As student enter the clinical phase of the medical course (years 4 and 5), they receive ad hoc informal musculoskeletal teaching within the clinical setting, although the exact amount of this teaching is difficult to determine and will vary widely. Formal teaching does occur in the final clinical year during their Musculoskeletal Disorders and Disability module.

At the University of Nottingham, the educational approach utilized in gross anatomy teaching is reevaluated annually. This ensures that the anatomical content and its delivery is clinically relevant and effective for teaching clinicians of the future (Leveritt et al., 2016; Marino et al., 2018). Students play an important role in this reevaluation process by identifying common anatomical difficulties before subsequently designing, implementing and evaluating new dissection protocols. This study presents an example of a shoulder dissection reevaluation, adapted from a study by Fabrizio et al. (2017), to be carried out by first-year medical students with limited dissection experience and within a short timeframe. The educational value and effectiveness of this approach are discussed. The findings suggest that there is real potential to empower medical students to help improve their own anatomy education, at a time when [arguably] reform of this age-old medical teaching is needed more than ever before.

MATERIALS AND METHODS

Undergraduate medical students at the University of Nottingham (UK) carry out an optional module during their second year. Students rank optional modules in order of preference and an algorithm is applied to provide allocations. “Advanced Anatomical Sciences” is one optional module available for a small number of medical students (8-10/300) each year led by an Anatomist. The aim of this module is for students to gain a greater insight into an anatomical region of interest. In doing so, students explore clinical relevance through the process of cadaveric dissection. The module incorporates lectures (2 hours), practical dissection classes (10 hours) and workshops (5 hours), all supported by the lead Anatomist. Students are asked to reflect on personal dissection experience, current dissection methodology (including Hansen, 2002; Tank, 2005; Clemente, 2007), clinical significance of the region and explore difficult concepts associated with the area of study. Students then design and implement a dissection approach based on their findings. Finally, they produce a portfolio in which they reflect on their experience leading their own dissection, in comparison to group dissections performed earlier in the medical course. Reflective discussion was emphasized as a key learning objective and marking criterion in the final portfolio produced in this module. Three elements of the module are assessed to provide a summative module mark; the quality of dissection/prosection generated, an oral presentation and a reflective portfolio. One student’s approach in this module led to the adaptation of a recently described novel dissection method of the glenohumeral joint (Fabrizio et al., 2017), which had only ever been performed by professional dissectors. The students’ adaptation devised a method that could be performed by students/novices, suggesting that the novel dissection method is suitable for introduction into medical school curriculum.

Student adaptation of a novel dissection approach of the glenohumeral joint

Dissector manuals routinely used by undergraduate medical students direct a superficial approach focusing mostly on preservation and identification of neuromuscular structures surrounding the glenohumeral joint (Zuckerman, 1981; Hansen, 2002; Tank, 2005; Clemente, 2007). Although this is a good approach to visualize the brachial plexus, musculature and superficial osteology, observation of internal joint structure is limited. A novel approach to the glenohumeral joint dissection detailed below (steps 1-3) allowed the internal joint capsule to be observed in detail, whilst maintaining the integrity

to the head of the humerus and its associated musculature (approach adapted from Fabrizio et al., 2017).

1. Skin and subcutaneous fascia surrounding the upper two thirds of the arm was reflected, continuing superiorly to the furthest lateral projection of the clavicle. The anterior part of the deltoid was reflected by cutting its proximal attachment. Trapezius and infraspinatus fascia were removed, and the posterior part of the deltoid reflected by cutting its medial attachment (Fig. 1).
2. The proximal humerus was cut twice with an oscillating 16,000/min cast saw (CC4 cast saw system; de Soutter Medical Ltd., Buckinghamshire, UK). The first cut was a longitudinal cut along the shaft of the humerus. The cut extended along the lateral aspect of the proximal one third of the humerus, commencing anterior to the greater tubercle and posterior to the lesser tubercle of the humerus. The second cut, perpendicular to the first, extended posteriorly from the distal end of cut one (Fig. 2A). Care was taken to ensure that the cuts did not damage any nearby structures, including rotator cuff musculatures and tendon of the long head of the biceps muscle.
3. The head of the humerus was opened to view the internal structures using a 23mm postmortem chisel (Surgical Holdings, Southend-on-Sea, UK) to view internal joint structures. The integrity of the muscles in this region was maintained throughout the dissection procedure (Fig. 2B). Further detailed dissection allowed the identification of the long head of biceps brachii tendon, glenoid labrum and the subscapularis tendon (Fig. 2C-D).

The novel glenohumeral joint dissection approach was successfully completed in its entirety by one second-year medical student.

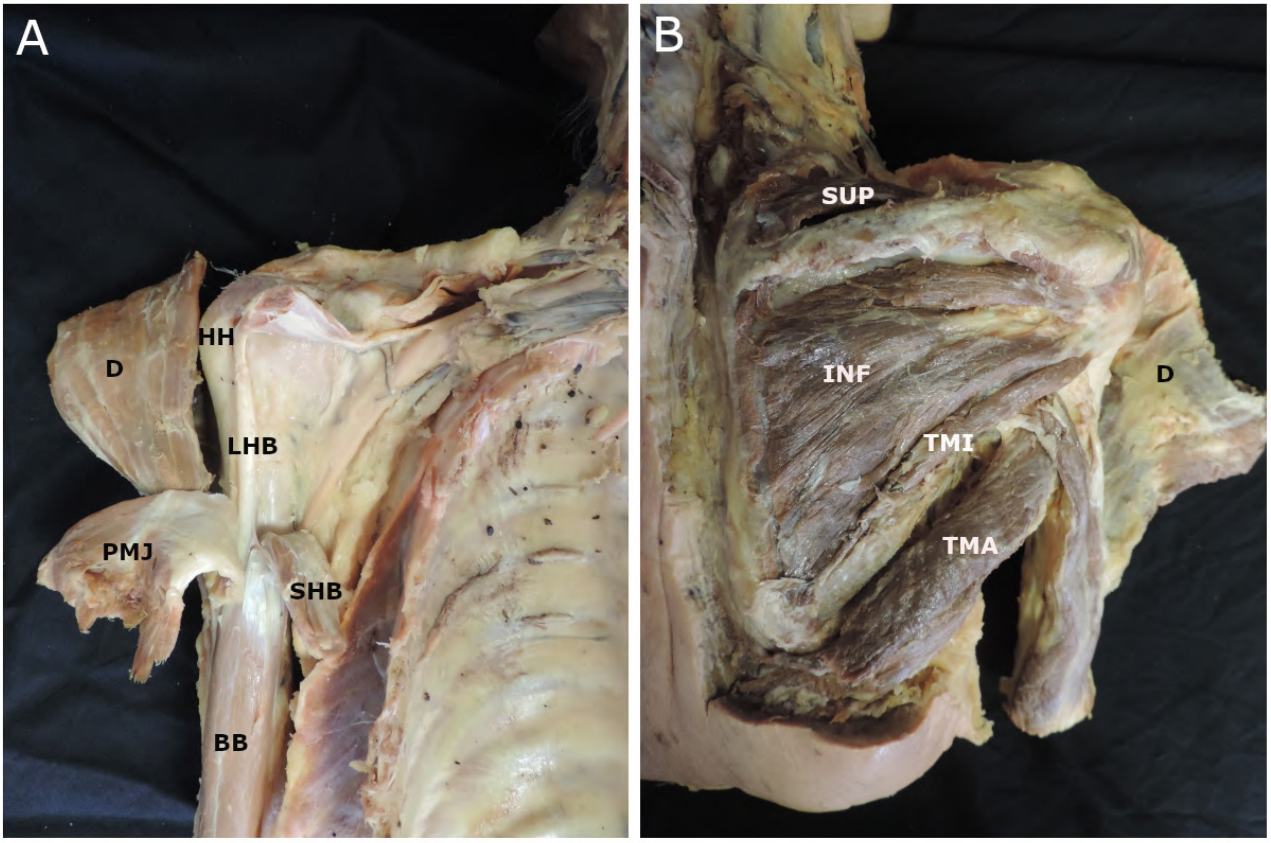

Fig. 1.- Standard undergraduate medical students dissection approach of the glenohumeral joint. A: Anterior view of proximal humerus with deltoid (D) and short head of biceps brachii reflected. B: Posterior view of the shoulder illustrating associated rotator cuff musculature. The dissection was carried out on an elderly female cadaver by the lead author within the anatomy suite (BB – biceps brachii, D – deltoid, HH – humeral head; INF – infraspinatus, LHB – long head of biceps brachii; PMJ – pectoralis major, SHB – short head of biceps brachii, SUP – supraspinatus, TMA – teres major, TMI – teres minor).

The generation of the prosection took 8 student dissection hours in total. This approach started with skin reflection, identification and preservation, where possible, of musculature and neurovascular structures surrounding the shoulder. The time taken incorporated meticulous dissection, detailed imaging and documentation of the dissection stages. The final stage of this novel prosection approach, which encompassed the splitting of the humeral head, took approximately 10 minutes (an anatomy technician helped stabilize and hold the prosection during this final stage). The cadaveric protocols carried out were in line with Human Tissue Act 2004 regulations, and carried out in a designated laboratory.

On-line learning package to illustrate the novel dissection

First-year medical students were then given the opportunity to view the new glenohumeral joint prosection on-line teaching package (it was

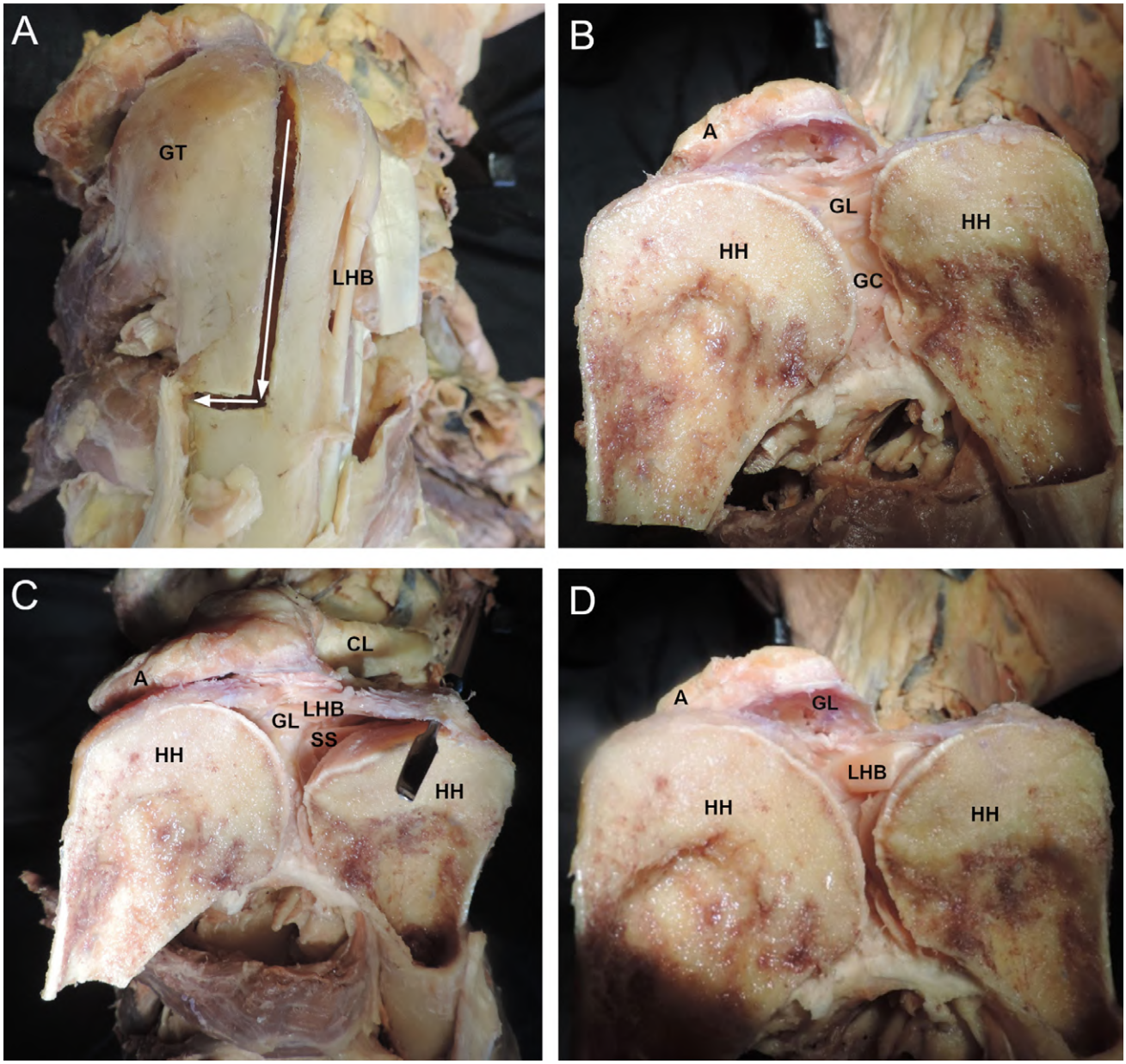

Fig. 2.- Novel undergraduate medical student dissection approach of the glenohumeral joint. **A**: Proximal humerus viewed from the lateral aspect highlighting the direction of saw cuts made. **B**: View of joint capsule upon initial opening. **C-D:** Joint capsule as viewed following minimal dissection of the region to highlight the long head of biceps brachii insertion into the glenoid labrum. The dissection was carried out on an elderly female cadaver by the lead author within the anatomy suite (A – acromion; CL – clavicle; GC – glenoid cavity; GL – glenoid labrum; GT – greater tubercle of humerus; HH – humeral head; LHB – long head of biceps brachii; SS – subscapularis muscle).

initially planned that all students would view the prosection within the anatomy suite; however, due to the unprecedented impact of Covid-19, this was not feasible). The teaching package was created by a second-year medical student (author R.J.L.) using PowerPoint software, version 16.31 (Microsoft Corp., Redmond, WA) and made accessible to students via Moodle course management system, version 3.7.5 (Moodle, West Perth, WA, Australia), the University of Nottingham on-line teaching platform. Anatomical accuracy of the package was checked and verified by the lead Anatomist (author D.M.). The teaching package began with a five-minute introduction to the shoulder region, which consisted of commonly seen anatomical drawings and still images of shoulder anatomy, accompanied by audio to aid learning. The teaching package then introduced the methodology of the new dissection method, comparing and contrasting to standard dissection in the medical course. Still images/photographs (taken on a Panasonic Lumix DMC-G7 digital camera (Panasonic UK & Ireland, Bracknell, UK) were used, which demonstrated the process of the novel dissection, accompanied by audio files describing method of dissection. This package took an average of 30 minutes to complete.

Effectiveness of novel dissection approach (quantitative cohort analysis)

A series of questions were designed by the authors to explore the first-year undergraduate medical students' knowledge of the glenohumeral joint, which were then verified by an additional anatomist for appropriate level and accuracy. Applying the principles of Bloom's taxonomy to the quizzes, the questions were identified to be aimed at knowledge, comprehension and application levels of learning deemed appropriate for first year undergraduate students (Bloom, 1956). Questions were piloted and validated with a cohort of second-year medical students (n = 122) who had already completed teaching, learning and assessment of this region in the previous academic year. The second-year students did not access the on-line teaching package; however, the pilot study allowed the series of questions to be grouped based on question type (cadaveric or non-cadaveric-based) and on difficulty levels. The questions were then randomly allocated to two comparable quizzes, each containing eight questions (herein named quiz A and quiz B; see Appendix A for examples of knowledge-based questions). First-year medical student completed quiz A prior to accessing the on-line package and quiz B following completion of the package. Quizzes were delivered in survey monkey (SNMK Inc., San Mateo, CA) and data extracted into Excel spreadsheet program, version 16.31 (Microsoft Corp., Redmond, WA). Quiz A was made available to all first-year medical students (*n = 298*) to complete on-line three weeks after they had been taught the anatomy of the glenohumeral joint through dissection following a standard dissection approach (outlined in Hansen, 2002). As the first- and second-year medical students were taught using the same dissection approach, Cronbach alpha and Kendall's Tau statistical tests were carried out to judge the consistency and validity of each cohort's performance on Quiz A (i.e., the students' performance prior to seeing the novel dissection).

All first-year medical students were encouraged to access the package and then complete a second quiz (quiz B). All elements of this study (on-line package and quizzes) were optional throughout and therefore students were able to choose their level of engagement. Ethical approval of this project was obtained by the School of Life Sciences Ethics Committee, University of Nottingham, UK (Ref no. C110320DM). A paired t-test was used to statistically compare results from quiz A and B. A paired t-test was also performed to statistically compare results between the pilot group (second-year medical students) and first year medical students: this compared performance in quiz-A questions when neither cohort had seen the novel dissection, and in quiz-B questions when only the first-year medical students had seen the novel dissection (accessed teaching package).

RESULTS

The on-line teaching package presenting the novel glenohumeral joint prosection was accessed by 144 first-year medical students (48.3% of year cohort) following staff making

on-line announcements of its presence. Of the students who accessed the package, 22.2 % (n = 32) completed quiz A, and 18.1% (n = 26) quiz B between April-May 2020.

Cohort performance before viewing novel dissection on-line package

No statistical difference in overall initial quiz (A) performance was observed between first- and second-year medical students (P = 0.38; Fig. 3). Both cohorts of students performed better on non-cadaveric questions (year 1, 57.5% ± 1.6 SD; year 2, 34.2% ± 4.4 SD) compared with questions requiring interpretation of cadaveric images (year 1, 31.3% ± 18.7 SD; year 2, 31.7% ±13.3 SD). However, the increased performance of both cohorts on non-cadaveric questions compared to cadaveric questions was insignificant (P = 0.34). Cronbach's alpha statistical test showed high internal consistency (0.79) for quiz A, with Kendall's tau-b test showing an insignificant correlation (0.57, P = 0.064).

Cohort performance after viewing novel dissection on-line package

First-year medical students showed a statistically significant increase in the number of correct responses after completing the on-line package, compared with their initial quiz (p = 0.013; Fig. 4). The mean score for students taking the initial quiz (A) before viewing the on-line teaching package was 40.3% (±17.3 SD), whereas the mean score after viewing the resource (quiz B) was 76.0% (±17.6 SD). First-year medical students' ability to correctly identify structures on images of cadaveric specimen increased from 31.3% (±18.7 SD) to 76.3% (±15.8 SD) following visualization of the novel glenohumeral joint prosection. A similar increase was observed for non-cadaveric questions without any associated imagery (49.3% ±9.39 SD to 75.8% ±19.6 SD). Looking at performance based on question type, after completing the on-line teaching package, students now scored equally well on cadaveric compared with non-cadaveric questions (76.3% ±15.8 SD and 75.8% ±19.6 SD respectively, p

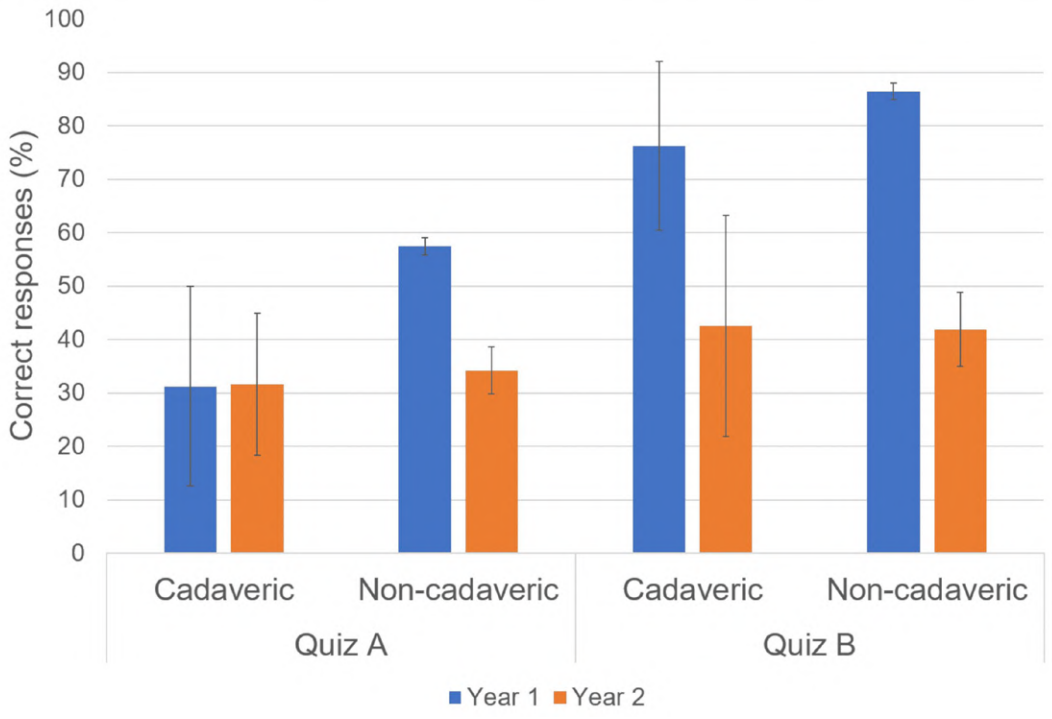

Fig. 3.- First-year and second-year undergraduate medical students' performance on a series of anatomical questions based around the shoulder region. Questions in each quiz were themed as being cadaveric or non-cadaveric knowledge-based questions. Quiz A relates to questions asked prior to first-year medical students viewing the novel prosection, quiz B relates to questions asked after first-year students viewed the on-line teaching package. Note the second-year medical students did not view the teaching package illustrating the novel glenohumeral dissection at any point during this study (error bars = standard deviation).

= 0.15). Second-year students did not view the teaching package but did answer questions associated with the second quiz (quiz B). Across all question types, second-year medical students were outperformed by those first-year medical students who had viewed the on-line teaching package (P = 0.002; Fig. 3).

DISCUSSION

Shoulder pain is a common and disabling complaint with a lifetime prevalence of up to 70% (Luime et al., 2004); with glenohumeral joint disorders (e.g., problems associated with the subacromial bursa) being one of the most common causes of shoulder pain in primary care (Mitchell et al., 2005; Greenberg, 2014). Clinical diagnosis in primary care is principally achieved through careful history taking and physical examination. Therefore, clinical knowledge and experience are essential in accurate diagnosis and establishing the appropriate management (Mitchell et al., 2005; Artus et al., 2017). However, global data suggest that there is low confidence in primary healthcare practitioners' ability to diagnose and appropriately manage shoulder pain (Glazier et al., 1998; Loebenberg et al., 2006; Buchbinder et al., 2013). This, coupled with the growing evidence that musculoskeletal knowledge (Day et al., 2007; Al-Nammari et al., 2015), and confidence in applying this knowledge (Peitzman and Cuddy, 2015; Marino et al., 2018), is often inadequate in medical students, illustrates the importance of establishing optimal teaching of this region (Skelley et al., 2012). This study has shown how first-year medical students' performance improved on a series of cadaveric and non-cadaveric knowledge-based questions (an increase of 45.0% and 26.5% respectively) after viewing images of the novel glenohumeral joint dissection (p = 0.013). These students also out-performed second-year medical students who had been taught and assessed on this region of anatomy in the previous academic year, but who did not view the on-line teaching package (p = 0.002). These results suggest that a blended approach to anatomy teaching is effective and can provide students with greater knowledge. These results are in line with other published studies (Green and Whitburn, 2016; Green et al., 2018). Combining such approaches with exposure to a clinical setting may have optimal educational benefit (Newcomer et al., 2013; Sayma and Williams, 2016; Khorsand et al., 2018). Therefore, it will be important to establish where in the curriculum this teaching should ideally take place.

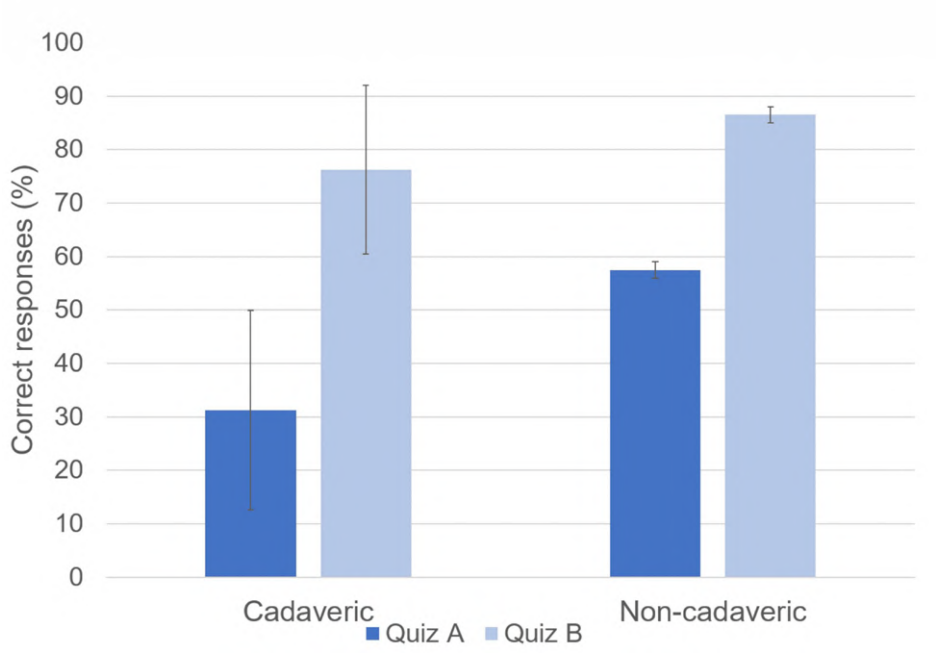

Fig. 4.- First-year undergraduate medical students' performance on a series of anatomical questions based around the shoulder region before (quiz A; n = 32) and after (quiz B; n = 26) viewing a novel prosection of the glenohumeral joint on-line. Questions in each quiz were themed as being cadaveric or non-cadaveric knowledge-based questions (error bars = standard deviation).

There is a growing body of literature describing novel dissection approaches to a variety of different anatomical regions, including the orbit (Cotofana et al., 2006), knee (Clemente et al., 2009), brain (Hlavac et al., 2017) and sinoatrial node of the heart (Nooma et al., 2020). Many of these novel dissections have been carried out by skilled surgeons, anatomists, or postgraduate medical students with extensive dissection experience (Mattioli et al., 2017; Cotofana et al., 2021). If a novel dissection approach requires the skill and time of a clinician or anatomist to carry out, the impact it can have in a medical curriculum setting may be very limited. However, this study reports for the first time that a novel dissection of the glenohumeral joint can be carried out by a novice dissector using standard dissection tools, typically available to undergraduate students within practical dissection classes. This is being championed at the University of Nottingham (UK), and in this academic year (2021-22) the new glenohumeral dissection approach will be incorporated into all first-year student-led dissection classes. Finally, it is of note that the appraisal of the current dissection approaches and execution of the novel glenohumeral dissection approach were carried out within an optional module setting. Optional modules within a medical curriculum inherently have more autonomy and may serve as an opportunity to empower students to drive reform and make innovations (Novak et al., 2011; Cantwell et al., 2015; Georgetti et al., 2021).

Limitations of the Study

The internal consistency of the quiz (A) was found to be consistent with other classifications as "high/acceptable" (Tavakol and Dennick, 2011; Taber, 2018), and suggests that the quizzes were consistent in their ability to assess the same areas of knowledge in both first- and second-year students. No relationship could be identified between performances on quiz (A) questions between first- and second-year medical students (as ascertained by Kendall's tau-b). However, this insignificance may be attributed to the small amount of data in this correlation, given that only quiz-A questions were included (quiz-B questions were excluded as, unlike first-year students, second-year students did not see the novel dissection when answering these questions). Just under half of the first-year medicine cohort (48.3%) accessed the optional on-line resource, and only a proportion of these carried out the associated quizzes (18.1-22.2%). The uptake may have been limited due to the fact that the end-of-year Objective Structured Practical Examination was cancelled because of the restrictions imposed by the Covid-19 pandemic. Therefore, although only speculative, the cancelling of the gross anatomy practical exam may have influenced the time that students devoted to revising this discipline. This study utilized cohorts of medical students at the University of Nottingham (UK) through an unprecedented time where anatomy teaching was moved on-line in a rapid and tight timeframe. Therefore, it is acknowledged that findings from this study may not be generalized to other institutional settings and other student populations.

CONCLUSIONS

Medical students' knowledge of musculoskeletal anatomy is reported widely in the literature to be inadequate and not sufficient for clinical placement. This study looked at ways to utilize a novel student-led dissection approach to improve the knowledge of the glenohumeral joint in first-year medical students. Through creation of an anatomy blended on-line teaching package, students gained greater regional insight, illustrated by improved performance in knowledge-based questions. Novel cadaveric dissections are not a new concept, but novel approaches that can increase subject knowledge and be carried out by novice dissectors may have real educational benefit that is worthy of further exploration and, where successful, curriculum reform.

ACKNOWLEDGEMENTS

The authors sincerely thank those who donated their bodies to science so that anatomical research and teaching could be performed. Results from such research can potentially increase scientific knowledge and can improve patient

care. Therefore, these donors and their families deserve our highest respect. The authors would also like to thank all of the Anatomy Suite staff at the University of Nottingham for help during this study. In particular, thanks to Miss Leia Boote and Miss Jo Lockley for their technical support during the final stages of prosection generation.

NOTES ON CONTRIBUTORS

ROBERT J. LEIGH, BMedSci., is a fourth-year undergraduate medical student in the School of Medicine, Faculty of Medicine and Health Sciences at the University of Nottingham, Nottingham, United Kingdom.

DEBORAH MERRICK, B.Sc., Ph.D., S.F.H.E.A., is an assistant professor of anatomy in the School of Life Sciences, Faculty of Medicine and Health Sciences at the University of Nottingham, Nottingham, United Kingdom. She teaches anatomy and embryology to pre-clinical medical students and is a senior tutor for medicine. Her research interests include student engagement and assessment within anatomical education and student wellbeing.

REFERENCES

AL-NAMMARI SS, PENGAS I, ASOPA V, JAWAD A, RAFFERTY M, RAMACHANDRAN M (2015) The inadequacy of musculoskeletal knowledge in graduating medical students in the United Kingdom. *J Bone Joint Surg Am,* 97: e36.

ARTUS M, VAN DER WINDT DA, AFOLABI EK, BUCHBINDER R, CHESTERTON LS, HALL A, RODDY E, FOSTER NE (2017) Management of shoulder pain by UK general practitioners (GPs): a national survey. *BMJ Open*, 7: e015711.

BIRBARA NS, SAMMUT C, PATHER N (2020) Virtual reality in anatomy: A pilot study evaluating different delivery modalities. *Anat Sci Educ,* 13: 445-457.

BLOOM BS (1956) Taxonomy of Educational Objectives: The Classification of Educational Goals. *Handbook 1: Cognitive Domain*. 1st ed. David McKay Co, Inc, New York, pp 201.

BUCHBINDER R, STAPLES MP, SHANAHAN EM, ROOS JF (2013) General practitioner management of shoulder pain in comparison with rheumatologist expectation of care and best evidence: an Australian national survey. *PLoS One*, 8: e61243.

CANTWELL S, BONADURER GF, PAWLINA W, LACHMAN (2015) Near-peer driven dissection selective: A primer to the medical school anatomy course. *Clin Anat,* 28: 985-993.

CHEN D, ZHANG Q, DENG J, CAI Y, HUANG J, LI F, XIONG K (2018) A shortage of cadavers: The predicament of regional anatomy education in mainland China. *Anat Sci Educ*, 11: 397-402.

CLEMENTE CD (2007) Clemente's Anatomy Dissector. 2nd ed. Lippincott, Williams and Wilkins, Baltimore, MA, pp 65-68.

CLEMENTE FR, FABRIZIO PA, SHUMAKER M (2009) A novel approach to the dissection of the human knee. *Anat Sci Educ*, 2: 41-46.

COTOFANA S, GAVRIL DL, FRANK K, SCHENCK TL, PAWLINA W, LACHMAN N (2021) Revisit, reform, and redesign: A novel dissection approach for demonstrating anatomy of the orbit for continuing professional development education. *Anat Sci Educ,* 14: 505-512.

DAY CS, YEH AC, FRANKO O, RAMIREZ M, KRUPAT E (2007) Musculoskeletal medicine: An assessment of the attitudes and knowledge of medical students at Harvard Medical School. *Acad Med,* 82: 452-457.

DAVIS CR, BATES AS, ELLIS H, ROBERTS AM (2014) Human anatomy: Let the students tell us how to teach. *Anat Sci Educ,* 7: 262-272.

DISSABANDARA LO, NIRTHANAN SN, KHOO TK, TEDMAN R (2015) Role of cadaveric dissections in modern medical curricula: a study on student perceptions. *Anat Cell Biol,* 48: 205-212.

ELIZONDO-OMAÑA RE, GUZMÁN-LÓPEZ S, GARCÍA-RODRÍGUEZ MA (2005) Dissection as a teaching tool: Past, present, and future. *Anat Rec,* 285B: 11-15.

ESTAI M, BUNT S (2016) Best teaching practices in anatomy education: A critical review. *Ann Anat*, 208: 151-157.

EVANS D, BAY BH, WILSON TD, SMITH CF, LACHMAN N, PAWLINA W (2020) Going virtual to support Anatomy Education: A STOPGAP in the midst of the Covid-19 pandemic. *Anat Sci Educ*, 13: 279-283.

FABRIZIO P, TOPPING D, WOLFE K (2017) Glenohumeral joint dissection: A new protocol. *Anatomy,* 11: 37-41.

FITZGERALD JE, WHITE MJ, TANG SW, MAXWELL-ARMSTRONG CA, JAMES DK (2008) Are we teaching sufficient anatomy at medical school? The opinions of newly qualified doctors. *Clin Anat,* 21: 718-724.

FRANCHI T (2020) The impact of the Covid-19 pandemic on current Anatomy Education and future careers: a student's perspective. *Anat Sci Educ,* 13: 312-315.

GEORGETTI LJ, SIMS AC, FOCHT, ELCOCK JN, NIXON-CAVE K, AMABILE AH (2021) Participation in an advanced anatomy capstone project facilities student involvement in the development of an instructional tool for novel dissection. *Educ Res Int,* 2021: 6681994.

GHAZANFAR H, RASHID S, HUSSAIN A, GHAZANFAR M, GHAZANFAR A, JAVAID A (2018) Cadaveric dissection a thing of the past? The insight of consultants, fellows, and residents. *Cureus,* 10: e2418.

GLAZIER RH, DALBY DM, BADLEY EM, HAWKER GA, BELL MJ, BUCHBINDER, LINEKER SC (1998) Management of common musculoskeletal problems: a survey of Ontario primary care physicians. *CMAJ,* 158: 1037-1040.

GOGALNICEANU P, O'CONNOR EF, RAFTERY A (2009) Undergraduate anatomy teaching in the UK. *Bull Roy Coll Surg Engl,* 91: 102-106.

GREEN RA, WHITBURN LY (2016) Impact of introduction of blended learning in gross anatomy on student outcomes. *Anat Sci Educ,* 9: 422-430.

GREEN RA, WHITBURN LY, ZACHARIAS A, BYRNE G, HUGHES DL (2018) The relationship between student engagement with online content and achievement in a blended learning anatomy course. *Anat Sci Educ,* 11: 471-477.

HANSEN JT (2002) Essential Anatomy Dissector: following Grant's method. 2nd ed. Lippincott, Williams & Wilkins, Philadelphia, PA, pp 224.

HLAVAC RJ, KLAUS R, BETTS K, SMITH SM, STABIO ME (2017) Novel dissection of the central nervous system to bridge gross anatomy and neuroscience for an integrated medical curriculum. *Anat Sci Educ,* 11: 185-195.

HOSE MK, FONTANESI J, WOYTOWITZ M, JARRIN D, QUAN A (2017) Competency based clinical shoulder examination training improves physical exam, confidence, and knowledge in common shoulder conditions. *J Gen Intern Med,* 32: 1261-1265.

HUISSTEDE BM, BIERMA-ZEINSTRA SM, KOES BW, VERHAAR JA (2006) Incidence and prevalence of upper-extremity musculoskeletal disorders. A systematic appraisal of the literature. *BMC Musculoskelet Disord,* 7: 7.

KHORSAND D, KHWAJA A, SCHMALE GA (2018) Early musculoskeletal classroom education confers little advantage to medical student knowledge and competency in the absence of clinical experiences: A retrospective comparison study. *BMC Med Educ*, 18: 46.

KONSCHAKE M, BRENNER E (2014) "Mors auxilium vitae" – Causes of death of body donors in an Austrian anatomical department. *Ann Anat,* 196: 387-393.

LAZARUS MD, CHINCHILLI VM, LEONG SL, KAUFFMAN GL (2012) Perceptions of anatomy: critical components in clinical setting. *Anat Sci Educ,* 5: 187-199.

LEVERITT S, MCKNIGHT G, EDWARDS K, PRATTEN M, MERRICK D (2016) What anatomy is clinically useful and when should we be teaching it? *Anat Sci Educ,* 9: 468-745.

LOEBENBERG MI, ROSEN JE, ISHAK C, JAZAWI LM, ZUCKERMAN JD (2006) A survey of decision-making processes in the treatment of common shoulder ailments among primary care physicians. *Bull Hosp Jt Dis,* 63: 137-144.

LUIME JJ, KOES BW, HENDRIKSEN IJ, BURDORF A, VERHAGEN AP, MIEDEMA HS, VERHAAR JA (2004) Prevalence and incidence of shoulder pain in the general population; A systematic review. *Scand J Rheumatol,* 33: 73-81.

MARINO K, MERRICK D, EDWARDS K, PRATTEN M (2018) Musculoskeletal radiology teaching at a UK medical school: Do we need to improve? *Anat Sci Educ,* 12: 257-263.

MATTIOLO F, PRESUTTI L, CAVERSACCIO, BONALI, ANSCHUETZ L (2017) Novel dissection station for endolaryngeal microsurgery and laser surgery: Development and dissection course experience. *Otolaryngol Head Neck Surg,* 156: 1136-1141.

MCKEOWN PP, HEYLINGS DJ, STEVENSON M, MCKELVEY KJ, NIXON JR, MCCLUSKEY DR (2003) The impact of curricular change on medical students' knowledge of anatomy. *Med Educ,* 37: 954-961.

MCQUILLAN T, WILCOX-FOGEL N, KRAUS E, LADD A, FREDERICSON M (2017) Integrating musculoskeletal education and patient care at medical student-run free clinics. *PM R,* 9: 1117-1121.

MEMON I (2018) Cadaver dissection is obsolete in medical training! A misinterpreted notion. *Med Princ Pract,* 27: 201-210.

MITCHELL C, ADEBAJO A, HAY E, CARR A (2005) Shoulder pain: Diagnosis and management in primary care. *BMJ,* 331: 1124-1128.

MURPHY RF, LAPORTE DM, WADEY VM, AMERICAN ACADEMY OF ORTHOPAEDIC SURGEONS ORTHOPAEDIC EDUCATION STUDY GROUP (2014) Musculoskeletal education in medical school: Deficits in knowledge and strategies for improvement. *J Bone Joint Surg Am,* 96: 2009-2014.

NEWCOMER KL, LASKOWSKI ER, GRANDE JP, DYRBYE LN (2013) The physiatrists' crucial role in the development and implementation of a longitudinal musculoskeletal physical examination curriculum in a medical school. *Am J Phys Med Rehabil,* 92: 84-89.

NOOMA K, SAGA T, IWANAGA J, TABIRA Y, WATANABE K, TUBBS RS, YAMAKI K (2020) A novel method with which to visualize the human sinuatrial node: Application for a better understanding of the gross anatomy of this part of the conduction system. *Clin Anat,* 33: 232-236.

NOVAK S, QUINN M, CANAN T, METTEN S, WISCO JJ, WIMMERS PF, UIJTDEHAAGE S (2011) A new approach to how to teach: medical students as instructional designers. *Med Educ Online,* 16: 7525.

PARKER LM (2002) Anatomical dissection: Why are we cutting it out? Dissection in undergraduate teaching. *ANZ J Surg,* 72: 910-912.

PATEL SB, MAURO D, FENN J, SHARKEY DR, JONES C (2015) Is dissection the only way to learn anatomy? Thoughts from students at a non-dissecting based medical school. *Perspect Med Educ,* 4: 259-260.

PATHER N, BLYTH P, CHAPMAN JA, DAYAL MR, FLACK N, FOGG QA, GREEN RA, HULME AK, JOHNSON IP, MEYER AJ, MORLEY JW, SHORTLAND PJ, ŠTRKALJ G, ŠTRKALJ M, VALTER K, WEBB AL, WOODLEY SJ, LAZARUS MD (2020) Forced disruption of anatomy education in Australia and New Zealand: An acute response to the Covid- 19 pandemic. *Anat Sci Educ,* 13: 284-300.

PEITZMAN SJ, CUDDY MM (2015) Performance in physical examination on the USMLE Step 2 Clinical Skills Examination. *Acad Med,* 90: 209-213.

PRATTEN MK, MERRICK D, BURR SA (2014) Group in-course assessment promotes cooperative learning and increases performance. *Anat Sci Educ,* 7: 224-233.

ROCKARTS J, BREWER, DELUCE D, SHALI A, MOHIALDIN V, WAINMAN B (2020) National survey on Canadian undergraduate medical programs: The decline of the anatomical sciences in Canadian medical education. *Anat Sci Educ,* 13: 381-389.

SAYMA M, WILLIAMS HR (2016) A new method for teaching physical examination to junior medical students. *Adv Med Educ Pract,* 7: 91-97.

SKELLEY NW, TANAKA MJ, SKELLEY LM, LAPORTE DM (2012) Medical student musculoskeletal education: An institutional survey. *J Bone Joint Surg Am,* 94: e146.

TABER KS (2018) The use of Cronbach's alpha when developing and reporting research instruments in science education. *Res Sci Educ,* 48: 1273-1296.

TANK PW (2005) Grant's Dissector. 15th ed. Lippincott, Williams & Wilkins, Baltimore, MD, pp 57-60.

TAVAKOL M, DENNICK R (2011) Making sense of Cronbach's alpha. *Int J Med Educ,* 2: 53-55.

TURMEZEI TM, TAM M, LOUGHNA S (2009) A survey of medical students on the impact of a new digital imaging library in the dissection room. *Clin Anat,* 22: 761-769.

TURNEY BW (2007) Anatomy in a modern medical curriculum. *Ann Roy Coll Surg Engl*, 89: 104-107.

WATERSON SW, STEWART IJ (2005) Survey of clinicians' attitudes to the anatomical teaching and knowledge of medical students. *Clin Anat,* 18: 380-384.

WILSON AB, NOTEBAERT A, SCHAEFER A, MOXHAM BJ, STEPHENS A, MUELLER C, LAZARUS MD, KATRIKH AZ, BROOKS WS (2019) A look at the anatomy educator job market: Anatomists remain in short supply. *Anat Sci Educ,* 13: 91-101.

ZUCKERMAN SB (1981) A New System of Anatomy, a Dissector's Guide and Atlas. 2nd ed. Oxford University Press, Inc, Oxford, UK, pp 135-140.

Anatomy and the future: opportunities as translational science

Antonia Aránega

Department of Human Anatomy, University of Granada, E-mail: aranega@ugr.es
Spanish Association for the Advancement of Science

SUMMARY

Considerations are made on the development and future of Anatomy as a translational science, as well as the social impact it has had and has as a scientific discipline within the medical sciences. Throughout history, it has been possible to verify how Anatomy has been expanding its common borders with the rest of the medical disciplines, and how its scientific achievements show the close relationship between the development of society and scientific-technological progress. The progressive incorporation of modern study technologies into anatomical research has made it possible to broaden the field of exploration and diagnosis of diseases at the cellular, subcellular and macromolecular levels. With these considerations, I have also wanted to demonstrate the important work that translational anatomical research carries out in medical practice and, so that this work can be recognized in all its dimensions, including the social one.

Key words: Anatomical Research – Translational Research in Anatomy – Translational Science

COMMENTARY

Over time, anatomical research has shown an abundant legacy of important contributions in basic and translational research, contributing, with its scientific achievements, to the fundamental understanding of various pathologies and medical-surgical approaches. Knowledge in general must influence the resolution of complex problems and the creative expansion of the frontiers of science (Domínguez-Franco et al., 2012).

In the last two decades, different analyses have indicated that anatomists in general had lagged behind in updating basic research compared to other disciplines of medicine. But it is also true that recently this situation has clearly changed: the research groups of the Anatomy departments, in a high percentage, have internalized and assumed the relevance of the usefulness of scientific achievements, assuming that translational research becomes possible when basic scientific achievements also have a clinical utility. These requirements are the key to the progress of translational research (Álvarez et al., 2014).

Evidence of this is the appearance in the area of Anatomy of new scientific journals such as *Translational Research in Anatomy*. This journal prioritizes translational research articles, and aims to disseminate the knowledge acquired in

Corresponding author:
Antonia Aránega. Department of Human Anatomy, University of Granada, E-mail: aranega@ugr.es
Spanish Association for the Advancement of Science

Submitted: October 25, 2021. **Accepted:** November 12, 2021

https://doi.org/10.52083/WBCN5068

basic anatomical science to apply it to diagnosis and treatment of human pathology in order to improve the individual well-being of the patient. This new editorial strategy fosters the links between morphological research and medicine, so that they are strong and effective and that the collaboration between anatomical science and other areas is effective.

There are multiple pathologies that require different diagnostic and therapeutic solutions. These are demonstrative of the need for an interdisciplinary approach, where the role of anatomical knowledge is very important.

Basic researchers are paying much attention to translational approaches to their own research achievements to help, as far as possible, to overcome current and unresolved clinical problems.

Translational and interdisciplinary research is research that involves more than one discipline, where researchers from each area make contributions to a common research objective, integrating concepts and methodologies from their lines of research to reach new knowledge. This strategy has become an important component in shaping cutting-edge science and innovation (Arrizabalaga, 2021).

Advanced hospitals are based on multidisciplinary scientific and technical advances, because complex health care problems cannot be successfully addressed by a single discipline (Arguello et al., 2020).

For this reason, the strength of interdisciplinary research with strong and stable collaborations between the basic and clinical sciences and other disciplines, such as big data, physics and engineering, is an evident fact (Álvarez et al., 2021).

Even so, the training and professional qualification of physicians will continue to evolve, betting on much broader and more diverse interdisciplinary teams, focused on the value of sustained interdisciplinary research.

Throughout history, there are many examples of how anatomical knowledge has contributed effectively to advances in medical science: for example, the interface of the human prosthesis.

The human-prosthesis interface is one of the most complicated challenges facing the field of prosthetics. Its most important contributions are made in research and development by basic and clinical researchers around the world, Scientific achievements in the area of morphology have contributed to the understanding of the interface mechanics, favoring the design and evaluation of limb prostheses in general. It is high-quality, multidisciplinary research, much needed for advancements in the development of some bionic designs that have the potential for clinical application (Safari, 2020).

The contributions of different fields such as physics, materials sciences and mechanics are fundamental for the design of functional prostheses, although the researcher always requires an adequate qualification in anatomy, kinesiology, biomechanics and biology. The participations of engineering, artificial intelligence or electronics are contributing to a better understanding and manufacture of prosthetic mechanisms and pathomechanics.

Translational research has a bidirectional sense from basic research to patient-oriented research, and involves collaboration between scientists from multiple disciplines. Its current challenge is to find the relevant ways that allow to apply its research achievements to society (Rubio et al., 2010; Zarbin, 2020).

Modern regenerative medicine needs this translational concept of basic research, as it uses the principles and methods of basic science and engineering to promote the growth and regeneration of damaged tissues and viscera, or restore cell and tissue function.

Therefore, *Translational Research in Anatomy* should be useful not only to increase knowledge in general, but also as a communication and understanding platform between the discipline of anatomy and the rest of biomedical areas.

REFERENCES

ÁLVAREZ P, BOULAIZ H, VÉLEZ C, RODRÍGUEZ-SERRANO F, ORTIZ R, MELGUIZO C, PRADOS J (2014) Qualitative and quantitative analyses of anatomists' research: evaluation of multidisciplinarity and trends in scientific production. *Scientometrics,* 98(1): 447-456.

ÁLVAREZ P, REYES M, ARGÜELLO A (2021) The management of scientific achievement in life sciences: a perspective from the complexity. *Eur J Anat*, 25(5): 615-624.

ARGÜELLO A, SOLANA VH, JÜRGENS B, ARÁNEGA P (2020) Patent analysis and territorial development: Example in the Biosanitary field. *J Econ Bus Intellig*, 2: 13-19.

ARRIZABALAGA J (2021) The challenge of (re)emerging diseases, the limits of the biomedical response and the new paradigm of global health. *História, Ciências, Saúde-Manguinhos*, 28(1): 255-281.

DOMÍNGUEZ-FRANCO A, GONZÁLEZ FJ, RODRÍGUEZ-LOSADA N, MARCHAL JA, CABRERA-BUENO F, CARRILLO E, PERÁN M, JIMÉNEZ-NAVARRO MF, ARÁNEGA A (2012) Factors influencing mobilisation of endothelial progenitor cells and angiogenic cytokines after an extensive acute myocardial infarction. *Med Clin*, 138(10): 415-421.

RUBIO DM, SCHOENBAUM EE, LEE LS, SCHTEINGART DE, MARANTZ PR, ANDERSON KE, ESPOSITO K (2010) Defining translational research: implications for training. *Acad Med*, 85(3): 470.

SAFARI R (2020) Lower limb prosthetic interfaces: Clinical and technological advancement and potential future direction. *Prosthetics Orthotics Int*, 44(6): 384-401.

ZARBIN M (2020) What constitutes translational research? Implications for the scope of translational vision science and technology. *Transl Vis Sci Technol*, 9(8): 22.

European Journal of Anatomy